

Investigations into Tin- and Tantalum-Phosphorus Compounds for Low-Coordinate Moieties and Supramolecular Assemblies

Dissertation zur Erlangung des
Doktorgrades der Naturwissenschaften (Dr. rer. nat.)

der Naturwissenschaftlichen Fakultät IV – Chemie und Pharmazie
der Universität Regensburg



vorgelegt von
Brian P. Johnson
aus Gallatin, Tennessee, USA
2005

Promotionsgesuch eingereicht am: 05. Dezember 2005

Die Arbeit wurde angeleitet von: Prof. Dr. M. Scheer

Vorsitzender: Prof. Dr. R. Winter

Prüfungsausschuß: Prof. Dr. M. Scheer (1. Gutachter)

Prof. Dr. H. Brunner (2. Gutachter)

Prof. Dr. B. König (3. Prüfer)

Tag der Promotion: 11. Januar 2006

Dedicated to my family

Die vorliegende Arbeit wurde in der Zeit von September 2001 bis März 2004 am Institut für Anorganische Chemie der Universität Karlsruhe (TH) sowie in der Zeit von April 2004 bis November 2005 am Institut für Anorganische Chemie der Universität Regensburg unter Anleitung von Herrn Prof. Dr. M. Scheer angefertigt.

Table of Contents

1	Introduction	1
1.1	Phosphanyl compounds in main-group chemistry	2
1.1.1	Phosphanyl stannylenes	3
1.1.2	Multiple bonding in tin-phosphorus compounds	6
1.2	Stabilization of low-coordinate moieties with bulky terphenyl ligands	8
1.3	Novel phosphorus ligands in transition-metal complexes	10
1.3.1	Transition-metal phosphinidene complexes	11
1.3.2	P _n -ligand complexes	12
1.4	Supramolecular chemistry of P _n -ligand complexes	12
1.4.1	Polymeric networks	13
1.4.2	Fullerene-like 3D structures	14
2	Research Objectives	16
3	Results and Discussion	17
3.1	Stabilization of Sn/P compounds by transition-metal fragments	17
3.1.1	Background and research objective	17
3.1.2	Reactions of SnCl ₂ and Sn[N(SiMe ₃) ₂] ₂ with Li[H ₂ PW(CO) ₅] and [H ₃ PW(CO) ₅]	18
3.1.3	Reaction of [(CO) ₅ WSnCl ₂ (thf) ₂] with Li[H ₂ PBar ^F ₃]	19
3.1.4	Synthesis of [H(Me ₃ Si) ₂ PW(CO) ₅] (2)	20
3.1.5	Reactions of SnCl ₂ and Sn[N(SiMe ₃) ₂] ₂ with Li[(Me ₃ Si) ₂ PW(CO) ₅] and [H(Me ₃ Si) ₂ PW(CO) ₅]	21
3.1.6	Reaction of [Fp ₂ SnX ₂] (X = Cl, Br) with Li[H ₂ PW(CO) ₅]	23
3.1.7	Reaction of [Fp ₂ SnBr ₂] with LiP(SiMe ₃) ₂ ·1.8THF	29
3.1.8	Reaction of [Fp ₂ SnCl ₂] with LiP(H)Trip	32
3.2	Investigations into tin-phosphorus compounds supported by bulky aryl groups	36
3.2.1	Background and research objective	36
3.2.2	Preparation of Ph*SnCl	37

3.2.3	Reactions of Ph*SnCl with alkali-metal phosphanides	38
3.2.3.1	Synthesis of Ph*SnP(SiMe ₃) ₂ (7)	38
3.2.3.2	Reactivity of Ph*SnP(SiMe ₃) ₂ (7)	44
3.2.3.3	Reactions of Ph*SnCl with LiP(H)Ph, LiP(H)Trip, and Li ₂ PTrip	45
3.2.3.4	Reaction of Ph*SnCl with Li[H ₂ PW(CO) ₅]	50
3.2.4	Reactions of Ph*SnCl with PCl ₃ and Cp*PCl ₂	54
3.2.5	Oxidation of Ph*SnCl with Me ₃ SiOOSiMe ₃ and Me ₃ NO	56
3.2.5.1	Synthesis of Ph*Sn(OSiMe ₃) ₂ Cl (12)	56
3.2.5.2	Synthesis of [Ph*Sn(μ-O)Cl] ₂ (13)	56
3.2.6	Synthesis of Ph*SnCl ₃ (14a)	59
3.2.7	Reactions of Ph*SnCl ₃ (14a), Ph*Sn(OSiMe ₃) ₂ Cl (12), and [Ph*Sn(μ-O)Cl] ₂ (13) with [P(SiMe ₃) ₂] ⁻	62
3.3	Tris(aryloxy)amine tantalum complex for probing reactivity with phosphanide reagents	64
3.3.1	Background and research objective	64
3.3.2	Synthesis of [L*TaCl ₂] (15)	65
3.3.2.1	Route via lithiation of L*H ₃	65
3.3.2.2	Direct thermolysis of L*H ₃ with TaCl ₅	66
3.3.3	Synthesis of [L*Ta(Cl)E(SiMe ₃) ₂] (E = P (16a), As(16b))	70
3.3.4	Synthesis of [L*TaMe ₂] (17)	75
3.4	<i>cyclo</i> -P ₄ tantalum complex for formation of supramolecular assemblies	79
3.4.1	Background and research objective	79
3.4.2	Preparation of [Cp''Ta(CO) ₂ (η ⁴ -P ₄)] (18)	80
3.4.3	Synthesis of [{Cp''Ta(CO) ₂ (μ,η ⁴ :η ¹ :η ¹ :η ¹ :η ¹ -P ₄)} ₆ {CuCl} ₈] (19a)	81
3.4.4	Synthesis of [{Cp''Ta(CO) ₂ (μ,η ⁴ :η ¹ :η ¹ :η ¹ :η ¹ -P ₄)} ₆ {CuBr} ₈] (19b)	90
3.4.5	Reaction of [Cp''Ta(CO) ₂ (η ⁴ -P ₄)] (18) with CuI	94
4	Experimental Section	96
4.1	General remarks	96
4.1.1	Methods	96
4.1.2	Spectroscopy and analysis	96
4.2	Starting materials	97
4.2.1	Synthesis of [H(Me ₃ Si) ₂ PW(CO) ₅] (2)	97

4.2.2	Synthesis of 2,6-dichloro-1-iodobenzene	98
4.2.3	Synthesis of Ph*I	99
4.2.4	Synthesis of Ph*Li·OEt ₂	100
4.2.5	Synthesis of Ph*SnCl	101
4.3	Reactions starting from SnCl ₂ and Sn[N(SiMe ₃) ₂] ₂	102
4.3.1	Reaction of Sn[N(SiMe ₃) ₂] ₂ with [H(Me ₃ Si) ₂ PW(CO) ₅], isolation of [(Me ₃ Si) ₃ PW(CO) ₅] (3)	102
4.3.2	Reaction of SnCl ₂ with Li[(Me ₃ Si) ₂ PW(CO) ₅], isolation of [(Me ₃ Si) ₃ PW(CO) ₅] (3)	102
4.4	Reactions starting from [Fp ₂ SnX ₂] (X = Cl, Br)	102
4.4.1	Synthesis of [Fp ₂ Sn{PH ₂ W(CO) ₅ } ₂] (4)	102
4.4.2	Synthesis of [Fp ₂ Sn{P(SiMe ₃) ₂ } ₂] (5)	103
4.4.3	Reaction of [Fp ₂ SnCl ₂] with LiP(H)Trip in THF, synthesis of Fp ₄ Sn (6)	104
4.5	Reactions starting from Ph*SnCl	105
4.5.1	Synthesis of Ph*SnP(SiMe ₃) ₂ (7)	105
4.5.2	Reaction of Ph* SnP(SiMe ₃) ₂ with BrCH ₂ CH ₂ Br, formation of Ph*Br (8)	106
4.5.3	Reaction of Ph*SnCl with LiP(H)Ph (2 equivalents)	106
4.5.4	Reaction of Ph*SnCl with LiP(H)Ph (1 equivalent)	106
4.5.5	Reaction of Ph*SnCl with LiP(H)Trip, generation of Ph*SnP(H)Trip (9)	107
4.5.6	Reaction of Ph*SnCl with Li ₂ PTrip, generation of Li ⁺ [Ph*SnPTrip] ⁻ (10 , proposed)	107
4.5.7	Reaction of Ph*SnCl with Li[H ₂ PW(CO) ₅], formation of [Ph*Sn{W(CO) ₅ }(μ-O) ₂ SnPh*] (11)	108
4.5.8	Reaction of Ph*SnCl with Cp*PCl ₂	108
4.5.9	Synthesis of Ph*Sn(OSiMe ₃) ₂ Cl (12)	109
4.5.10	Synthesis of [Ph*Sn(μ-O)Cl] ₂ (13)	109
4.6	Reactions involving Ph*Sn(IV)-halides and pseudohalides	110
4.6.1	Synthesis of Ph*SnCl ₃ (14a)	110
4.6.2	Synthesis of Ph*SnBr ₃ (14b)	111
4.6.3	Reaction of Ph*SnCl ₃ , Ph*Sn(OSiMe ₃) ₂ Cl, and [Ph*Sn(μ-O)Cl] ₂ with LiP(SiMe ₃) ₂ ·1.8THF	112
4.7	Reactions involving tris(aryloxy)amine (L*)	112
4.7.1	Synthesis of Li ₃ L*	112
4.7.2	Synthesis of [L*TaCl ₂] (15)	113

4.7.3	Synthesis of $[L^*Ta(Cl)P(SiMe_3)_2]$ (16a) and $[L^*Ta(Cl)As(SiMe_3)_2]$ (16b)	114
4.7.4	Synthesis of $[L^*TaMe_2]$ (17)	115
4.8	Reactions involving $[Cp''Ta(CO)_2(\eta^4-P_4)]$	116
4.8.1	Synthesis of $Cp''H$	116
4.8.2	Preparation of $Cp''Sn(nBu)_3$	116
4.8.3	Preparation of $[Cp''TaCl_4]$	116
4.8.4	Preparation of $[Cp''Ta(CO)_4]$	117
4.8.5	Preparation of $[Cp''Ta(CO)_2(\eta^4-P_4)]$ (18)	117
4.8.6	Preparation of $[\{Cp''Ta(CO)_2(\mu, \eta^4: \eta^1: \eta^1: \eta^1: \eta^1-P_4)\}_6\{CuX\}_8]$ (X = Cl (19a), Br (19b), I (proposed, 19c))	118
5	Crystallographic Data	120
5.1	General remarks	120
5.2	$[(Me_3Si)_3PW(CO)_5]$ (3)	122
5.3	$[Fp_2Sn\{H_2PW(CO)_5\}_2]$ (4)	125
5.4	$[Fp_2Sn\{P(SiMe_3)_2\}_2]$ (5)	128
5.5	$[Fp_4Sn]$ (6)	131
5.6	$Ph^*SnP(SiMe_3)_2$ (7)	134
5.7	$[Ph^*Sn\{W(CO)_5\}(\mu-O)SnPh^*]$ (11)	137
5.8	$[Ph^*Sn(\mu-O)Cl]_2$ (13)	140
5.9	Ph^*SnCl_3 (14a)	143
5.10	$[L^*TaCl_2]$ (15)	146
5.11	$[L^*Ta(Cl)P(SiMe_3)_2]$ (16a)	149
5.12	$[L^*Ta(Cl)As(SiMe_3)_2]$ (16b)	152
5.13	$[L^*TaMe_2]$ (17)	155
5.14	$[\{Cp''Ta(CO)_2(\mu, \eta^4: \eta^1: \eta^1: \eta^1: \eta^1-P_4)\}_6\{CuCl\}_8]$ (19a)	158
5.15	$[\{Cp''Ta(CO)_2(\mu, \eta^4: \eta^1: \eta^1: \eta^1: \eta^1-P_4)\}_6\{CuBr\}_8]$ (19b)	161
6	Conclusion	168
6.1	Transition-metal supported tin-phosphorus compounds	168
6.2	Kinetically stabilized low-coordinate tin-phosphorus compounds	169
6.3	Survey of a tris(aryloxy)amine tantalum platform	171
6.4	Use of a <i>cyclo</i> -P ₄ tantalum complex for synthesis of spherical molecules	172

7	Appendices	174
A.1	Directory of abbreviations	174
A.1.1	NMR abbreviations	176
A.1.2	IR abbreviations	176
A.2	Directory of compounds	176
A.3	Literature cited	178

1 Introduction

Compounds possessing phosphorus atoms in unusual or reactive coordination environments have been the subject of intense exploration. [1] Current investigations related to this field include, but are not limited to, three principal classes: 1) compounds with low-coordinate phosphorus atoms both in free molecules and as complexed ligands; 2) phosphorus complexes with reactive P-Si or P-H bonds capable of further functionalization; and 3) complexes bearing substituent-free P_n ligands useful for further coordination to metal centers.

Phosphorus compounds in which the phosphorus atom is located in a low-coordination environment (generally, $CN \leq 2$) are of particular interest for their participation in phosphorus multiple bonding. [1] While purely organic species with P-C double bonds have been known for several decades, investigations involving organic triply bonded phosphorus species and phosphorus-metal multiply bonded systems have flourished just in the past two decades. Transition-metal complexes supporting P_1 ligands as triply bonded phosphido complexes or as multiply-bonded bridging species represent a dynamic field and have been the subject of recent reviews. [2] However, analogous compounds exhibiting multiple bonding between phosphorus and heavier main-group metals are relegated to a few doubly bonded species, while the corresponding triply bonded species constitute an area still in the early stages of development.

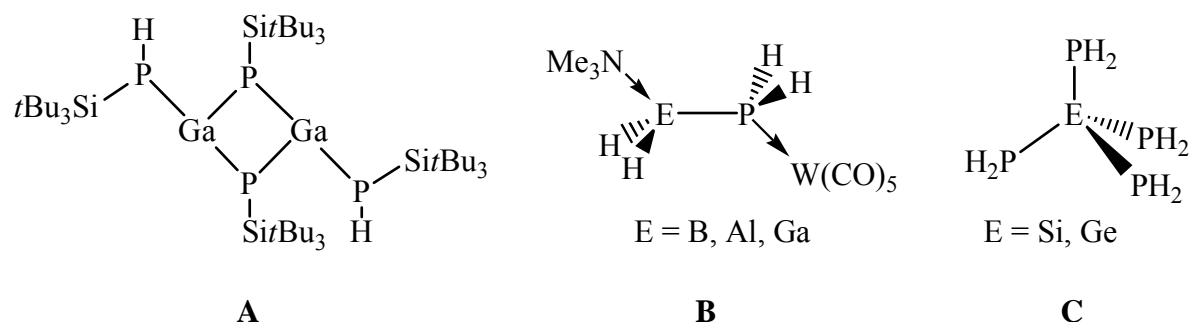
Ligands containing P-Si bonds have long been of interest in both transition-metal and main-group metal chemistry, whereby phosphorus with a protective trialkylsilyl group can readily be introduced into a metal system. The reactive P-Si bonds can then be cleaved selectively in many cases, for example by hydrolysis or halogenation resulting in P-H and P-Cl functionalities, respectively. Ligands containing P-H bonds, in particular, have received much interest, both for their high reactivity and potential for further functionalization. Such ligands have been used as a source of naked P_n -ligands and in precursor compounds capable of monomolecular elimination of primary phosphanes to generate multiply bonded species.

Complexes bearing substituent-free P_n -ligands have received considerable attention, both for their interesting bonding properties and for their rich diversity in reactivity and coordination modes, and the development of such ligand complexes has been detailed in the literature. [3,4] The ability of “naked” phosphorus to build coordinatively stabilized *cyclo*- P_n ligands similar to the carbon-based butadiene, cyclopentadiene, and benzene rings has often drawn allusion to the diagonal relationship between carbon and phosphorus. [5] However, in contrast to the relative inertness of ancillary carbon-based ring ligands, *cyclo*- P_n ligands have

shown a remarkable potential for further insertion, rearrangement, and coordination chemistry. The presence of multiple lone electron pairs on *cyclo*-P_n ligands and resulting potential for multi-dimensional coordination provide an entry into phosphorus-based polymeric networks and supramolecular assemblies.

1.1 Phosphanyl compounds in main-group chemistry

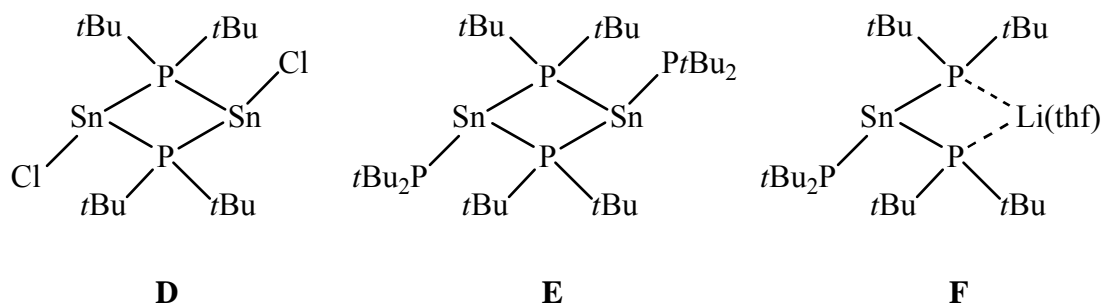
In recent years, interest has grown in main-group–phosphorus compounds that feature either a removable functionality on phosphorus (e.g. P-H or P-Si bonds) or hindrance of oligomerization via donation of the phosphorus lone pair, or both. An example of the former was recently synthesized by Westerhausen *et al.*, whereby the compound [(*t*Bu₃SiP(H)Ga(μ -PSi*t*Bu₃))₂] (**A**) was described. [6] Compound **A** was interpreted as consisting of a GaPGa heterallylic [RGa=PR'GaR]⁺ moiety bound to a (tris(*tert*-butyl)silyl)phosphandiyl fragment, and this view was supported by DFT calculations, thus demonstrating unexpected bonding properties in main-group phosphanyl/phosphandiyl compounds.



The concept of Lewis acid/base stabilization was recently applied in the Scheer group in preparing [(Me₃N·EH₂PH₂)W(CO)₅] (E = B, Al, Ga) (**B**), the donor/acceptor adducts of the previously experimentally inaccessible phosphanyltrielanes H₂EPH₂. [7] Through this method, oligomerization could be hindered and the reactivity of the P-E and P-H bonds could be studied. In the group of Driess, use of a phosphide transfer reagent, *i*Bu₂AlPH₂, has recently enabled the synthesis of Group 14 compounds with homoleptic phosphide ligands without Lewis-acid protection at the phosphorus atoms. Thus, reaction of *i*Bu₂AlPH₂ with ECl₄ (E = Si, Ge) resulted in the mild phosphide/chloride exchange and isolation of E(PH₂)₄ (**C**) [8] Formation of the germanium congener, Ge(PH₂)₄, is marked by disproportionation reactions to P₂H₄, HGe(PH₂)₃, H₂Ge(PH₂)₂, thus signifying a high reactivity of PH₂[−] ligands in connection with the heavier Group 14 elements.

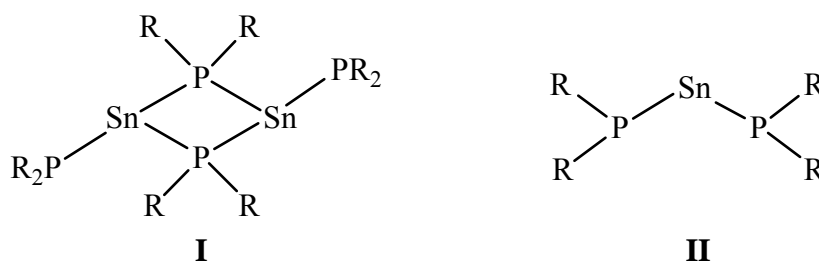
1.1.1 Phosphanyl stannylenes

The first phosphanyl stannylenes were synthesized by du Mont and co-workers by the salt-elimination reaction of SnCl_2 or $\text{Et}_3\text{P}\cdot\text{SnCl}_2$ with two equivalents of K^tBu_2 to afford the dimeric compound $[\text{Sn}(\text{P}^t\text{Bu}_2)_2]_2$ (**E**), which is composed of two bridging phosphanide ligands and two terminal phosphanides. [9] Nearly a decade later Cowley and co-workers showed that treating SnCl_2 with three equivalents of LiP^tBu_2 in THF afforded the ionic compound $\text{Li}(\text{thf})[\text{Sn}(\text{P}^t\text{Bu}_2)_3]$ (**F**), a novel stannate salt and heavier lithium-coordinated analogue of a carbanion. [10] Studies showed that the neutral phosphanide stannylenes could undergo redistribution reactions with SnCl_2 to give the heteroleptic chloro stannylene phosphide $[\text{Sn}(\mu\text{-P}^t\text{Bu}_2)\text{Cl}]_2$ (**D**) with bridging phosphanide ligands, [11] thus mimicking a behavior already established in the well-known stannylene amide and stannocene compounds. The position of the bridging phosphanide ligand demonstrates the superior bridging ability of phosphanide ligands over amides and stands in contrast to the heteroleptic compound $[\text{Sn}(\mu\text{-Cl})\text{N}(\text{SiMe}_3)_2]_2$, which is bridged through the chloride ligand. [12] The related compound Cp^*SnCl , though described as a monomer, shows distant intermolecular $\text{Sn}\cdots\text{Cl}$ contacts and can be described as having an asymmetric chloride bridge in the solid state. [13]

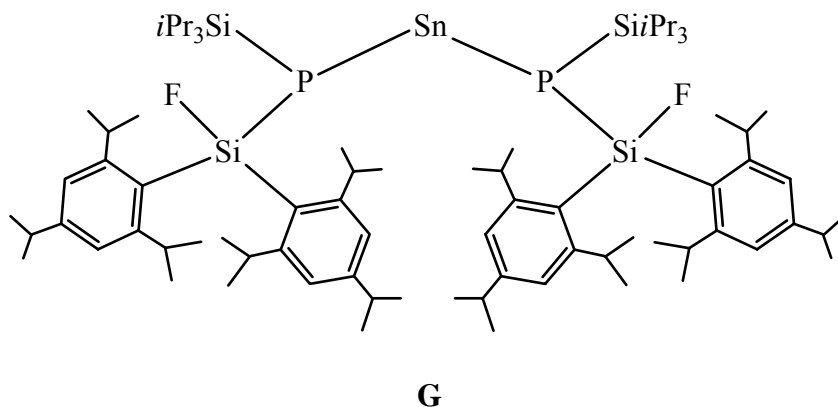


With the ultimate goal of developing solution-phase routes to precursors of inorganic phosphides, [14] the group of Buhro synthesized a series of bis(organosilyl)phosphido stannylene compounds. Instead of the usual tin(II) halides, the bis(trimethylsilyl)amido stannylene $\text{Sn}[\text{N}(\text{SiMe}_3)_2]_2$ was employed as starting material. [15] Reaction of $\text{Sn}[\text{N}(\text{SiMe}_3)_2]_2$ with $\text{HP}(\text{SiMe}_3)_2$ or $\text{LiP}(\text{SiPh}_3)_2$ afforded the dimeric compound $[\text{Sn}\{\text{P}(\text{SiMe}_3)_2\}_2]_2$ [16] and the monomeric compound $\text{Sn}[\text{P}(\text{SiPh}_3)_2]_2$, respectively. [17] The compound $[\text{Sn}\{\text{P}(\text{SiMe}_3)_2\}_2]_2$, as with $[\text{Sn}(\text{P}^t\text{Bu}_2)_2]_2$ above, exhibits the bridging mode (**I**), while $\text{Sn}[\text{P}(\text{SiPh}_3)_2]_2$, with the more sterically demanding triphenylsilyl groups adopts the non-bridging form (**II**). Isolation of the latter compound demonstrated the role of using

sterically encumbering ligands in stabilizing the first mononuclear phosphanido stannylene compound.

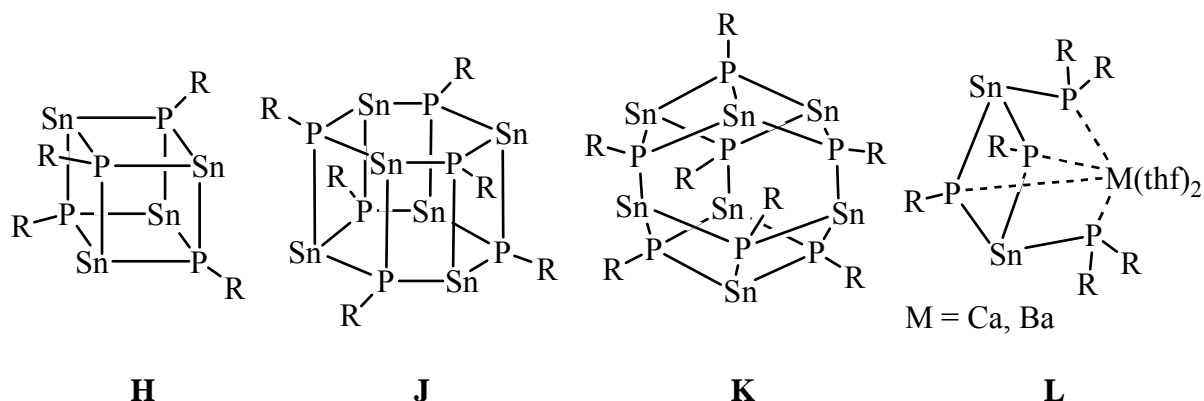


A fascinating monomeric phosphanido stannylene, $\text{Sn}[\text{P}(\text{Si}i\text{Pr}_3)(\text{Si}(\text{F})\text{Trip}_2)]_2$ (**G**) (of non-bridging form (**II**)), was later synthesized by Driess and co-workers, whereby the functional fluoride at one of the silane groups was incorporated for potential thermal fluorosilane elimination for anticipated production of a Sn/P/Si multiply bonded system. [18] However, this and the related germylene and plumbylene compounds were thermally stable up to 90°C and deposited the Group 14 metal at higher temperatures.

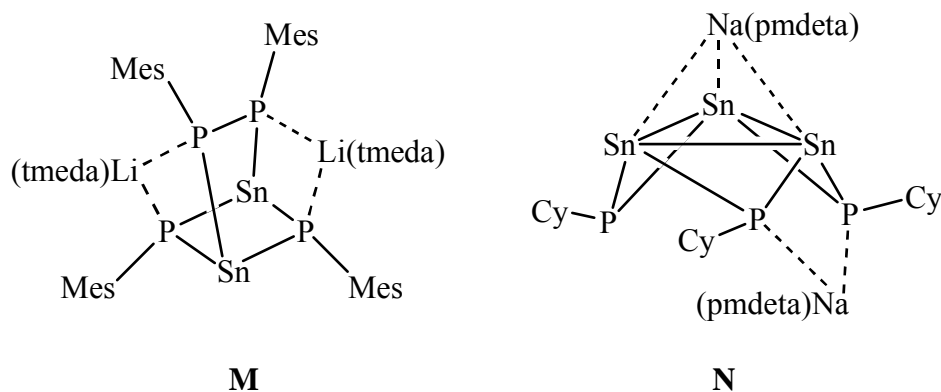


Though relatively few Sn/P cage compounds are known, a host of monosilylphosphanido stannylene clusters has been synthesized within the past decade by various methods. Routes incorporating the metalation of primary silylphosphanes R_3SiPH_2 ($\text{R} = i\text{Pr}, t\text{Bu}$) with $\text{Sn}[\text{N}(\text{SiMe}_3)_2]_2$ were employed in formation of the species $[\text{Sn}(\text{PSi}i\text{Pr}_3)]_6$ (**J**) and $[\text{Sn}(\text{PSi}t\text{Bu}_3)]_4$ (**H**). [19,20] A related heptameric cluster was synthesized recently in the von Hähnisch group by the salt-elimination route from $\text{Li}_2\text{PSi}i\text{Pr}_3$ and SnCl_2 , from which $[\text{Sn}(\text{PSi}i\text{Pr}_3)]_7$ (**K**) was isolated. [21] Such Sn/P clusters are characterized by Sn atoms and R_3SiP fragments each in trigonal pyramidal environments, whereby each Sn atom is bound to phosphorus by two σ -bonds and one $\text{P} \rightarrow \text{Sn}$ dative bond, all of which alternate throughout the cluster. Bimetallic systems such as $[(\text{thf})_2\text{MSn}_2\{\mu\text{-P}(\text{SiMe}_3)_2\}_2\{\mu_3\text{-P}(\text{SiMe}_3)_3\}_2]$ ($\text{M} = \text{Ca}, \text{Ba}$)

(**L**) were achieved by the three-component reactions of $M[N(SiMe_3)_2]_2$ with $Sn[N(SiMe_3)_2]_2$ and $HP(SiMe_3)_2$ with concomitant elimination of the disproportionation by-product $P(SiMe)_3$. [22]



The group of Wright has recently devised an approach to a class of novel heterometallic phosphanido stannates, in which the phosphorus atoms are supported by aryl or aliphatic groups. [23] This strategy makes use of phosphanide starting materials that possess one reactive P-bound proton, which is deprotonated during stannate formation by amine elimination from the employed main-group amide. Thus, reaction of $LiP(H)Mes$ with $Sn(NMe_2)_2$ in the presence of the bidentate donor ligand TMEDA resulted in P-P coupling and formation of $[(tmeda)_2Li_2\{Sn(\mu\text{-}PMes)\}_2(PMes)_2]$ (**M**), while reaction of $NaP(H)Cy$ with $Sn(NMe_2)_2$ in the presence of tridentate PMDETA resulted in Sn-Sn coupling to give $[(pmdeta)_2Na_2\{Sn(\mu\text{-}PCy)\}_3]$ (**N**) possessing a planar Sn_3 core. [24,25] The reactivity of the protons of the aryl group was also demonstrated in such systems, as C-H activations were observed in cluster formation in some reactions involving the mesityl phosphanide. [26]



1.1.2 Multiple bonding in tin-phosphorus compounds

For many decades it was thought that multiple bonds between heavier main-group elements (principal quantum number ≥ 3) were not possible, a principle often referred to as the double-bond rule. [27] The notorious reluctance of the heavier main-group elements to participate in multiple-bonding [28] is manifested in the dearth of examples in comparison to the 2p elements carbon, nitrogen, and oxygen. The current state of compounds possessing multiple bonds between Group 14 elements ($E = C, Si, Ge, Sn, Pb$) and heavier Group 15 elements ($E' = P, As, Sb, Bi$) is summarized in the grid below, with double-bonded imine analogues on the left side and triple-bonded nitrile analogues on the right side. Known compounds are represented as $R_2E=E'R$ or $RE\equiv E'$, where R is an alkyl, aryl, amido, or oxy group, and examples not yet isolated are represented as E/E' . All combinations involving Bi have been omitted, as no relevant examples are known.

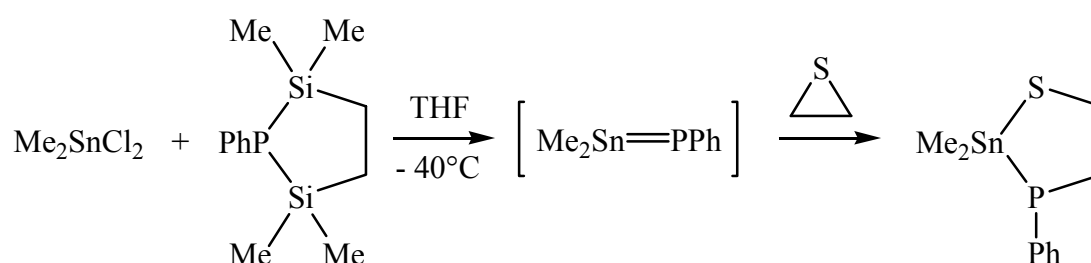
$\begin{array}{c} R \\ \diagdown \\ C \\ \diagup \\ R \end{array} = \begin{array}{c} R \\ \diagup \\ P \\ \diagdown \\ R \end{array}$	$\begin{array}{c} R \\ \diagdown \\ C \\ \diagup \\ R \end{array} = \begin{array}{c} R \\ \diagup \\ As \\ \diagdown \\ R \end{array}$	$\begin{array}{c} R \\ \diagdown \\ C \\ \diagup \\ R \end{array} = \begin{array}{c} R \\ \diagup \\ Sb \\ \diagdown \\ R \end{array}$	$R-C\equiv P$	$R-C\equiv As$	C/Sb
$\begin{array}{c} R \\ \diagdown \\ Si \\ \diagup \\ R \end{array} = \begin{array}{c} R \\ \diagup \\ P \\ \diagdown \\ R \end{array}$	$\begin{array}{c} R \\ \diagdown \\ Si \\ \diagup \\ R \end{array} = \begin{array}{c} R \\ \diagup \\ As \\ \diagdown \\ R \end{array}$	Si/Sb	Si/P	Si/As	Si/Sb
$\begin{array}{c} R \\ \diagdown \\ Ge \\ \diagup \\ R \end{array} = \begin{array}{c} R \\ \diagup \\ P \\ \diagdown \\ R \end{array}$	Ge/As	Ge/Sb	Ge/P	Ge/As	Ge/Sb
$\begin{array}{c} R \\ \diagdown \\ Sn \\ \diagup \\ R \end{array} = \begin{array}{c} R \\ \diagup \\ P \\ \diagdown \\ R \end{array}$	Sn/As	Sn/Sb	Sn/P	Sn/As	Sn/Sb
Pb/P	Pb/As	Pb/Sb	Pb/P	Pb/As	Pb/Sb

Well-defined and characterized phosphalkenes ($R_2C=PR$) have been known since 1976, [29] and an extensive amount of literature has since appeared on this class. Though arsaalkenes ($R_2C=AsR$) have been known nearly as long, since 1977, [30] they are much rarer. [31] Only very few examples of stibaalkenes with a $C=Sb$ double bond are known and have appeared only within the last decade, [32] and a stable arsasilene was also described one

decade ago. [33] Phosphaalkynes ($\text{RC}\equiv\text{P}$) have been isolable since 1981, and many representatives have since appeared. [34] However, arsaalkynes are in comparison extremely rare, with the first stable representative, $\text{Mes}^*\text{C}\equiv\text{As}$, reported in 1986. [35] A recent development in this class is represented by the description of borate derivatives of the types $[(\text{F}_3\text{C})_3\text{BC}\equiv\text{P}]^-$ and $[(\text{F}_3\text{C})_3\text{BC}\equiv\text{As}]^-$ possessing phosphaehtynyl and arsaethynyl ligands. [36]

Compounds of the type $\text{R}_2\text{E}=\text{PR}'$ with heavier group 14 elements have been isolated involving $\text{Si}=\text{P}$ [37] and $\text{Ge}=\text{P}$ [38] double bonds, generally kinetically stabilized by bulky aryl groups (Mes, Trip, or Mes^*) or bulky aliphatic groups ($t\text{Bu}$ or $\text{CH}(\text{SiMe}_3)_2$) at both phosphorus and the Group 14 atom. Additionally, *P*-silyl and *P*-phosphanyl derivatives have been successfully prepared in compounds of type $\text{R}_2\text{Si}=\text{PSiR}'_3$ and $\text{R}_2\text{Si}=\text{PPR}'_2$, respectively. [39] In these studies, it was deduced that a P-bound silyl group creates an additional degree of stability in such double-bond compounds. [40]

For tin-phosphorus compounds, multiple bonding was first speculated in intermediate compounds during reaction of Me_2SnX_2 ($\text{X} = \text{NEt}_2, \text{Cl}$) with 2,5-disilaphospholanes from which cyclic Sn/P rings of the type $[\text{Me}_2\text{Sn-PPh}]_3$ were isolated. [41] The identity of the proposed intermediate $[\text{Me}_2\text{Sn}=\text{PPh}]$ was verified via trapping reactions at low temperature by insertion with thiirane.

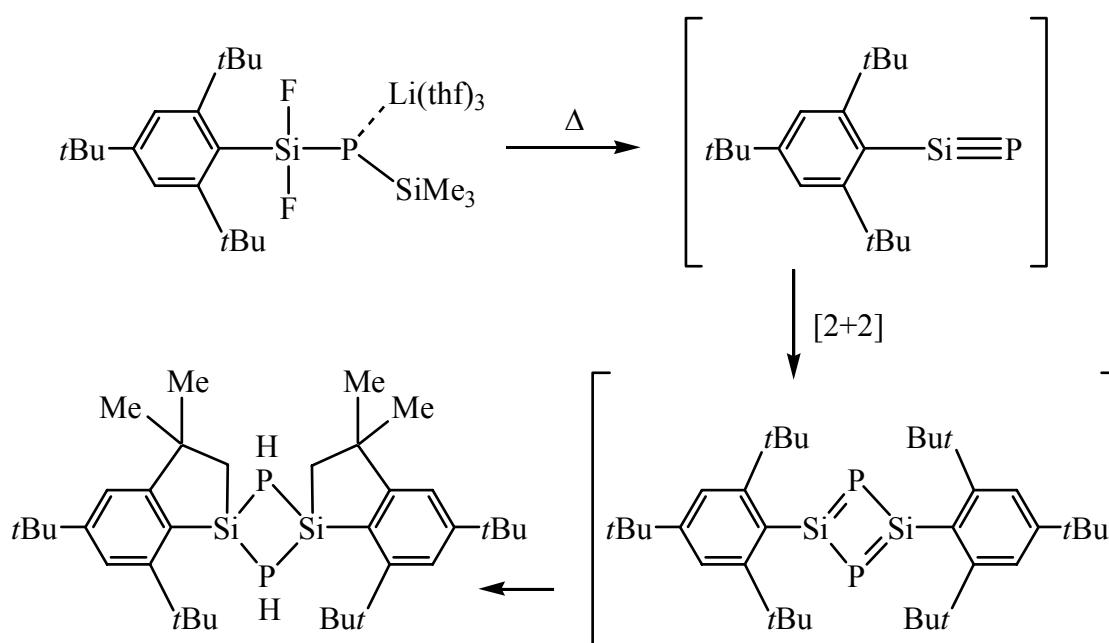


Scheme 1: Generation of stannaphosphene intermediate and trapping with thiirane.

The first stable compounds with $\text{Sn}=\text{P}$ double bonds were prepared by hydrohalogen elimination analogously to those of $\text{Si}=\text{P}$ and $\text{Ge}=\text{P}$ compounds. [42,43] The reactivity of two representatives, $[\text{R}_2\text{Sn}=\text{PMes}^*]$ ($\text{R} = \text{CH}(\text{SiMe}_3)_2$) and $[\text{Trip}_2\text{Sn}=\text{PMes}^*]$, has been studied and shows that the polar double bond undergoes the expected addition reactions with hydrides, organolithium reagents, inorganic acids (of type HX), alcohols, as well as small organic molecules such as *ortho*-benzoquinones, α -diketones, and α -ethylene aldehydes/ketones. [44]

Each compound containing an $\text{E}=\text{P}$ double bond for $\text{E} = \text{Si}, \text{Ge}, \text{Sn}$ exhibits a highly polarized bond due to differences in the E and P electronegativities. The doubly bonded

species can be easily identified in their reaction mixtures by way of the diagnostic ^{31}P -NMR signals, which appear in the area of $\delta = +200$ ppm for $\text{E} = \text{Sn}$, and by the large $^1J_{\text{PE}}$ coupling constants for $\text{E} = \text{Si}$, Sn , which indicate strong s-character in the $\text{E}=\text{P}$ double bond. Additionally, crystal structures have been reported for the silaphosphenes $\text{R}_2\text{Si}=\text{PR}'$ and germaphosphenes $\text{R}_2\text{Ge}=\text{PR}'$, but no structural data has been presented for the corresponding stannaphosphenes $\text{R}_2\text{Sn}=\text{PR}'$. Compounds featuring an $\text{E}\equiv\text{P}$ ($\text{E} = \text{Si}$, Ge , Sn , Pb) triple bond have yet to be detected directly or isolated; only a compound with a $\text{Si}\equiv\text{P}$ triple bond was tentatively proposed as an unobserved intermediate, the identity of which was suggested based solely on the nature of the isolated product (Scheme 2). [45]

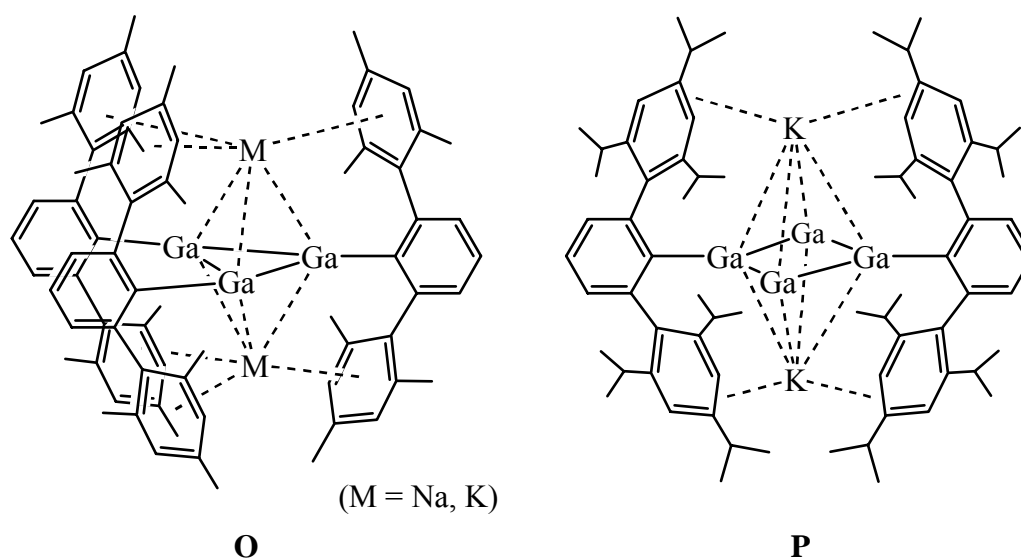


Scheme 2: Reaction pathway of thermolysis of $\text{Mes}^*\text{Si}(\text{F})_2\text{P}\{\text{Li}(\text{thf})_3\}\text{SiMe}_3$ and proposed generation of intermediate $\text{Mes}^*\text{Si}\equiv\text{P}$.

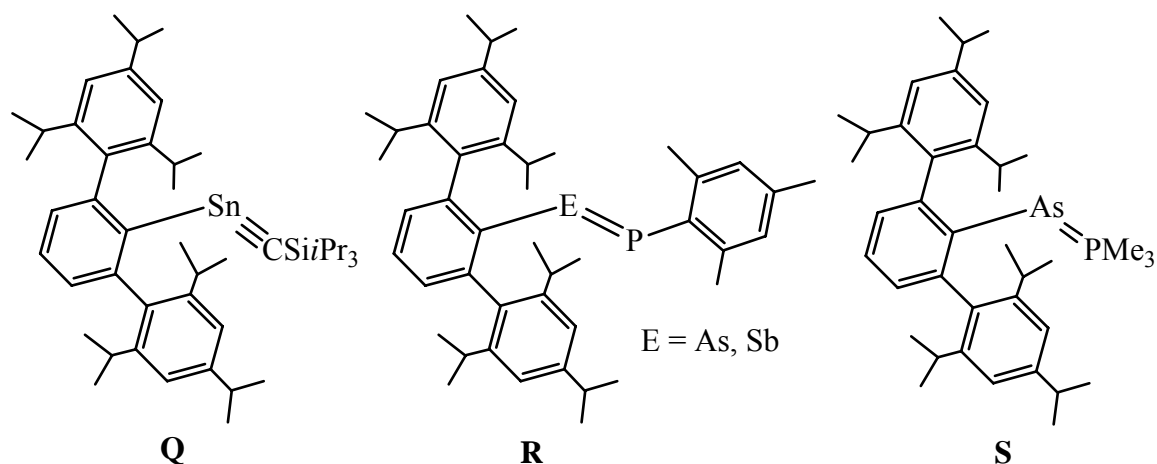
1.2 Stabilization of low-coordinate moieties with bulky terphenyl ligands

The use of bulky monodentate ligands has been shown to be advantageous in stabilizing a host of transition-metal and main-group compounds possessing atoms in novel bonding situations or oxidation states, [46] including a recent breakthrough involving isolation of a terphenyl-stabilized moiety exhibiting $\text{Cr}(\text{I})\text{-Cr}(\text{I})$ quintuple bonding. [47] It has been proposed that the stabilizing ability of terphenyl ligands in main-group compounds

comes as a result of both thermal and kinetic factors, especially in anionic compounds where aryl-metal interactions may offer thermodynamic stabilization of ion pairs. [48] In this respect, the Robinson and Power groups have succeeded in isolating a series of homonuclear Ga dianionic compounds, $\text{Na}_2[(\text{GaC}_6\text{H}_3\text{-2,6-Trip}_2)_2]$, $\text{M}_2[(\text{GaC}_6\text{H}_3\text{-2,6-Mes}_2)_3]$ ($\text{M} = \text{Na}, \text{K}$) (**O**), and $\text{K}_2[\text{Ga}_4(\text{C}_6\text{H}_3\text{-2,6-Trip}_2)_2]$ (**P**), where the latter two exhibit planar Ga_3 - and Ga_4 -rings, respectively, with delocalized electronic structures. [49,50] Additionally, the Power group has synthesized a series of terphenyl-supported heavier alkyne analogues (for Ge, Sn, Pb) and their various reduced species. [51]



While many novel homonuclear main-group compounds have been synthesized from reduction of terphenyl element halides (e.g. Ph^*GaCl_2 and Ph^*SnCl), the chemistry of terphenyl-supported, heteronuclear main-group compounds has received less attention, a situation presumably stemming from the extra synthetic steps required to access the heteronuclear compounds. A novel stannaacetylene, $2,6\text{-Trip}_2\text{-C}_6\text{H}_3\text{Sn}\equiv\text{CSiPr}_3$ (**Q**), has recently been proposed as a reactive intermediate [52], and the asymmetric dipnictenes $2,6\text{-Trip}_2\text{-C}_6\text{H}_3\text{E}=\text{PMes}$ ($\text{E} = \text{As}, \text{Sb}$) (**R**) were synthesized in the Power group. [53] The novel arsa-Wittig reagents $2,6\text{-Ar}_2\text{-C}_6\text{H}_3\text{As}=\text{PMe}_3$ ($\text{Ar} = \text{Mes}, \text{Trip}$) (**S**) have been developed by Protasiewicz and co-workers, whereby the phosphorus atom is in the +5 oxidation state. [54]



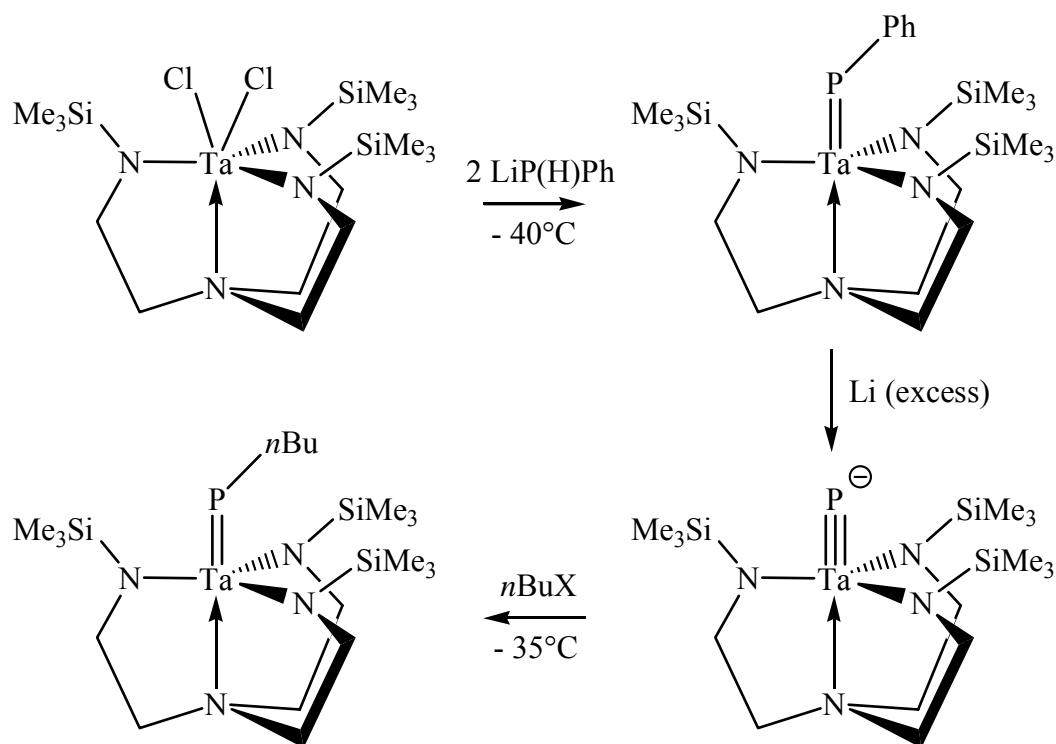
The field involving use of bulky terphenyl ligands to stabilize multiply bonded systems with atoms from two different p-block groups is still in its infancy, and representatives of such compounds have yet to be isolated and fully characterized. The stability of triply bonded $\text{R}\text{Sn}\equiv\text{P}$ systems was predicted by quantum chemical calculations only for examples in which R is a bulky terphenyl group. [55]

1.3 Novel phosphorus ligands in transition-metal complexes

Though complexes with generally non-reactive tertiary phosphines form the largest basis for complexes with phosphorus–metal bonds, a large number of functional phosphorus ligands has been synthesized and used for further reactions at the P atom. The Hey-Hawkins group has recently been active in preparing complexes with P-H functionalities that can be deprotonated and used for making M-P-M bridges formed exclusively by σ -bonding. [56] In bis- or tris-primary phosphinido complexes, such P-H functionalities have also shown interesting reactivity patterns, including intramolecular P-P bond formation, under thermal conditions. [57] Even more prevalent in phosphorus–transition-metal chemistry are ligands possessing P-Si bonds. Examples of the selective cleavage of one or more P-Si bonds in a transition-metal complex include the chlorination of $[\text{Cp}^x\text{M}(\text{CO})_2\text{P}(\text{SiMe}_3)_2]$ ($\text{Cp}^x = \text{Cp}, \text{Cp}^*$; $\text{M} = \text{Fe}, \text{Ru}$) with C_2Cl_6 to form $[\text{Cp}^x\text{M}(\text{CO})_2\text{PCl}_2]$ [58] and the hydrolysis of a series of complexes $[\text{L}_n\text{M}\{\mu\text{-P}(\text{SiMe}_3)_2\}\text{M}'\text{L}_n']$ with MeOH or MeCOOH to give $[\text{L}_n\text{M}(\mu\text{-PH}_2)\text{M}'\text{L}_n']$ [59]. The formation of M-P multiply bonded species is also possible through intermolecular fragmentation of silylphosphanide ligands, $-\text{P}(\text{SiMe}_3)_2$, via loss of $\text{P}(\text{SiMe}_3)_3$.

1.3.1 Transition-metal phosphinidene complexes

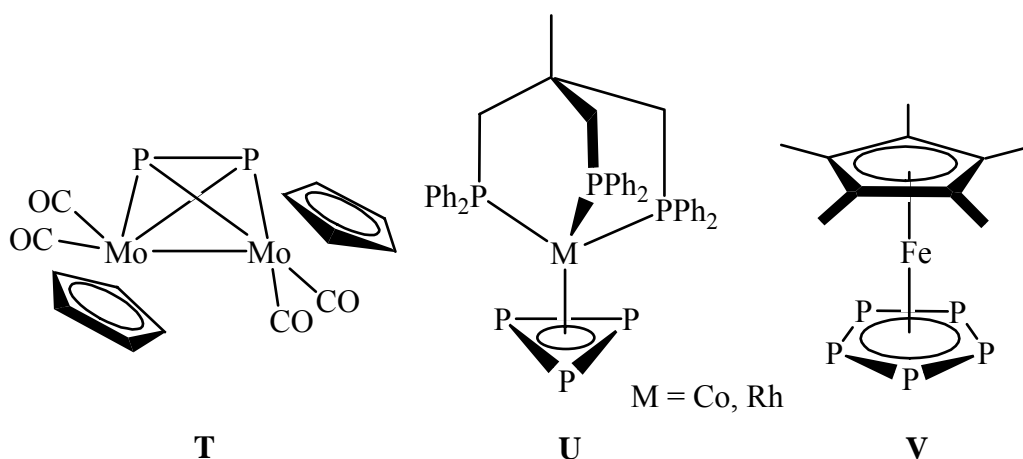
Transition-metal complexes with terminal phosphinidene ligands, $[L_nM=PR]$ were for years widely sought after [60] but remained elusive until Lappert and co-workers synthesized the first examples in 1987 with $[Cp_2M=PMes^*]$ ($M = Mo, W$), which possesses a bulky aryl group at phosphorus. [61] A few years later, the Wolczanski group isolated the tantalum phosphinidene complex $[(silox)_3Ta=PPh]$ ($silox = tBu_3SiO$) supported by sterically bulky siloxide ligands at the transition metal rather than possessing steric bulk at the main-group atom. [62] Using a bulky multidentate tris(silylamido)amine ligand, Schrock and co-workers developed a family of tantalum phosphinidene complexes by a singular approach. Thus, $[(N_3N)TaCl_2]$ ($N_3N = (Me_3SiNCH_2CH_2)_3N$) reacted with two equivalents of $LiP(H)R$ to form $[(N_3N)Ta=PR]$ ($R = Ph, Cy, tBu$) in moderate yields. [63] It was then demonstrated that the complexes with a phenyl substituent on phosphorus could be further functionalized. Reaction of $[(N_3N)Ta=PPh]$ with an excess of lithium metal resulted in solutions of $Li^+[(N_3N)Ta\equiv P]^-$, which could be characterized based only on its ^{31}P -NMR signal and through trapping reactions with RX to afford further phosphinidene complexes $[(N_3N)Ta=PR]$ ($R = Me, nBu, SiMe_3, SiMe_2Ph$). [64]



Scheme 3: Functionalization of $[(N_3N)TaCl_2]$ to complexes with Ta-P multiple bonds.

1.3.2 P_n-ligand complexes

Another strategy for producing novel phosphorus ligands in the coordination sphere of transition metals is by reaction of white phosphorus, P₄, with transition-metal fragments in low oxidation state. Rearrangements of the P₄ tetrahedron typically lead to P-rich ligands. Such reactions have formed a cornerstone of the research in the Scheer group [65], and the large breadth of possible transformations, especially reactions of P₄ with transition-metal hydrides, has been recently reviewed. [66] Of particular interest in this field is the degradation of P₄ to “naked” (i.e. unsubstituted) P_n-ligand complexes. [3,4] Three representatives of this class of compounds include the μ -P₂ complex [$\{\text{CpMo}(\text{CO})_2\}_2(\mu, \eta^2\text{-P}_2)$] (**T**), the *cyclo*-P₃ complexes [(triphos)M($\eta^3\text{-P}_3$)] (M = Co, Rh; triphos = 1,1,1-tris(diphenylphosphanylmethyl)ethane) (**U**), and the *cyclo*-P₅ complex [$\text{Cp}^*\text{Fe}(\eta^5\text{-P}_5)$] (**V**), each prepared by the thermal reaction of P₄ with the low-valent complexes [CpMo(CO)₂]₂, *in situ* generated [(triphos)MX] (M = Co, X = (BF₄)₂; M = Rh, X = Cl), and [Cp*Fe(CO)₂]₂, respectively. [67,68,69]



The reactivity of P_n-ligand complexes represents an area of active investigation, whereby reactions with Lewis-acidic transition-metal complexes have been studied for several years. Such reactions often yield binuclear or tetranuclear adduct formation or insertion of the transition-metal fragment into the P-P bonds of the P_n ligand. The coordination chemistry with late transition-metal halides and pseudohalides and their use for generating extended structures have remained largely unexplored.

1.4 Supramolecular chemistry of P_n-ligand complexes

The most common general synthetic strategy for forming coordination polymers and extended structures via self-assembly has been through the use of nitrogen donors and

nitrogen heterocycles as linking units. [70] Within the past few years, it has been shown in the Scheer group that P_n -ligand complexes are suitable for this purpose. In contrast to the mostly organic nitrogen-containing linkers, P_n -ligand complexes have the interesting characteristic of enabling the synthesis of purely inorganic polymeric and oligomeric frameworks while offering a wide array of novel multi-dimensional geometries. With such P_n -ligand complexes, no organic spacers are involved within the core of the structures, thus allowing more compact inorganic arrays.

1.4.1 Polymeric networks

Some of the first investigations of the coordination chemistry of P_n -ligand complexes were carried out by Stoppioni and co-workers and include the reactions of the *cyclo*- P_3 complexes $[(\text{triphos})M(\eta^3\text{-}P_3)]$ with Cu(I), Ag(I), and Au(I) salts, [71] from which one reaction with CuBr produced $[\{(\text{triphos})\text{Co}(\mu, \eta^3: \eta^1: \eta^1\text{-}P_3)\}_2\{\text{CuBr}\}_6]$, a cobalt multi-decker complex with a $(\text{CuBr})_6$ middle deck. [72] More recently the Scheer group has succeeded in employing the complex $[\{\text{CpMo}(\text{CO})_2\}_2(\mu, \eta^2\text{-}P_2)]$ in preparing dimeric and polymeric structures through coordination with Cu(I) and Ag(I) centers. Reaction of $[\{\text{CpMo}(\text{CO})_2\}_2(\mu, \eta^2\text{-}P_2)]$ with CuX (X = Cl, Br, I) results in the near quantitative formation of the linear (1D) polymers $[\text{CuX}\{\text{Cp}_2\text{Mo}_2(\text{CO})_4(\mu, \eta^2: \eta^1: \eta^1\text{-}P_2)\}]_\infty$. [73]

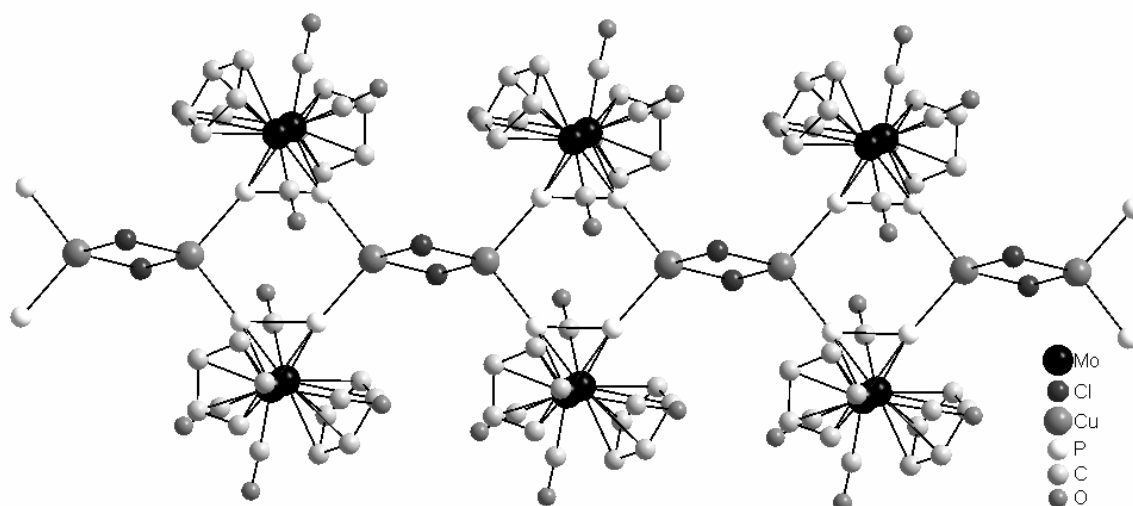


Figure 1: One-dimensional chain structure in $[\text{CuCl}\{\text{Cp}_2\text{Mo}_2(\text{CO})_4(\mu, \eta^2: \eta^1: \eta^1\text{-}P_2)\}]_\infty$.

Similarly, reaction of $[\text{Cp}^*\text{Fe}(\eta^5\text{-P}_5)]$ with CuCl resulted in the isolation of the linear (1D) chain $[\text{CuCl}\{\text{Cp}^*\text{Fe}(\mu, \eta^5: \eta^1: \eta^1\text{-P}_5)\}]_\infty$, albeit in only ca. 50% yield, in which only two of the five phosphorus atoms from each *cyclo*- P_5 ligand coordinate to Cu. In contrast, reactions of $[\text{Cp}^*\text{Fe}(\eta^5\text{-P}_5)]$ with CuBr and CuI resulted in the quantitative formation of novel 2D polymeric structures. [74]

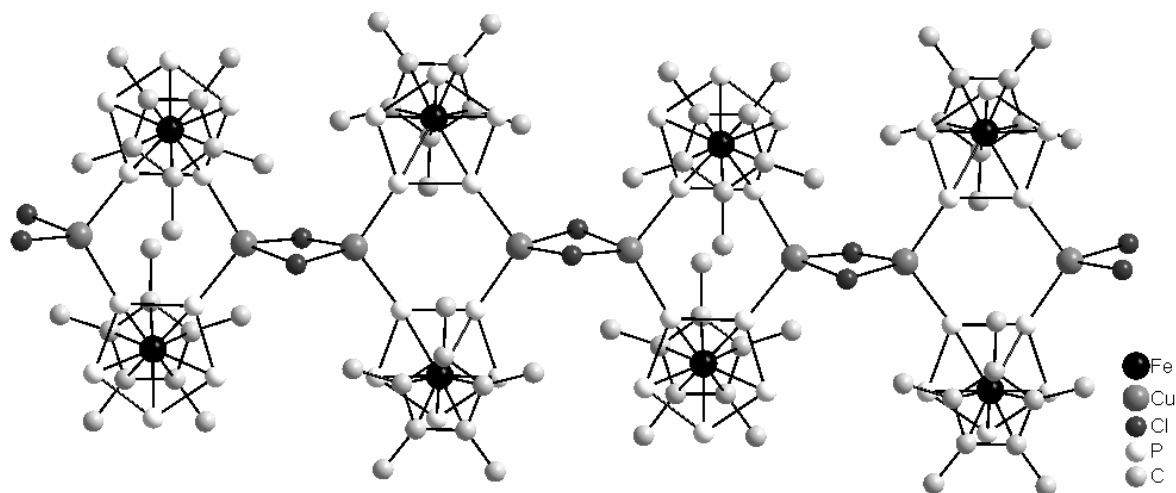


Figure 2: One-dimensional chain structure in $[\text{CuCl}\{\text{Cp}^*\text{Fe}(\mu, \eta^5: \eta^1: \eta^1\text{-P}_5)\}]_\infty$.

While the linear CuCl polymer exhibited *cyclo*- P_5 ligands bound to Cu in 1,2-coordination mode, the 2D polymers with CuBr and CuI possessed *cyclo*- P_5 ligands bound to Cu in 1,2,4-coordination mode. This was the first evidence that multiple coordination modes were possible for a single type of P_n -ligand complex.

1.4.2 Fullerene-like 3D structures

During investigations of the $[\text{Cp}^*\text{Fe}(\eta^5\text{-P}_5)]/\text{CuCl}$ system, it was found that in addition to the 1D polymer $[\text{CuCl}\{\text{Cp}^*\text{Fe}(\mu, \eta^5: \eta^1: \eta^1\text{-P}_5)\}]_\infty$, formed in about 50%, another species was present in the mother liquor. Further work-up and structural analysis revealed the formation of $[\{\text{Cp}^*\text{Fe}(\mu, \eta^5: \eta^1: \eta^1: \eta^1: \eta^1\text{-P}_5)\}_{12}\{\text{CuCl}\}_{10}\{\text{Cu}_2\text{Cl}_3\}_5\{\text{Cu}(\text{MeCN})_2\}_5]$, a spherical molecule with a fullerene-like mode of alternating 5- and 6-membered rings. The core is formed by two half-shells adjoined by Cu_2Cl_3 and $\text{Cu}(\text{MeCN})_2$ bridges and possesses a total of 90 inorganic atoms. [75]

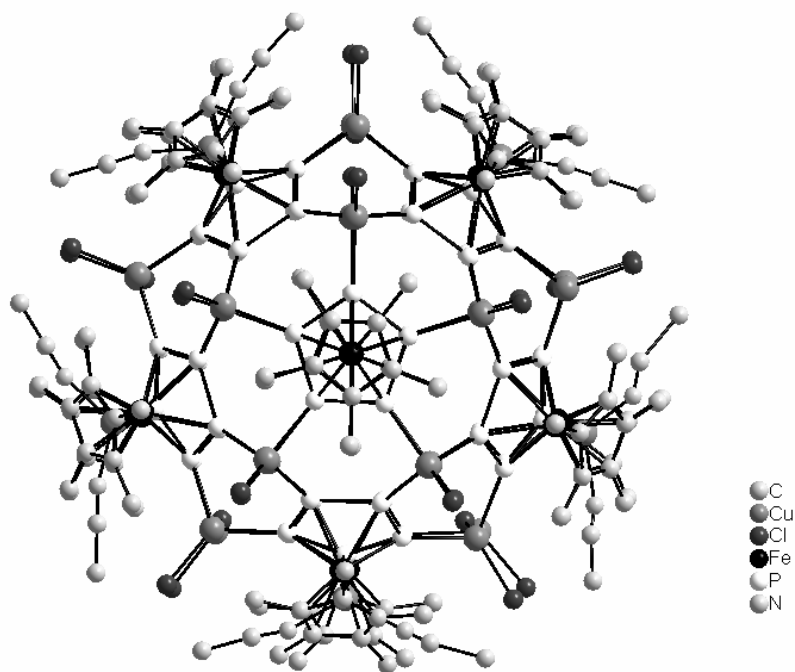


Figure 3: View of $[\{\text{Cp}^*\text{Fe}(\mu, \eta^5: \eta^1: \eta^1: \eta^1: \eta^1\text{-P}_5)\}_{12}\{\text{CuCl}\}_{10}\{\text{Cu}_2\text{Cl}_3\}_5\{\text{Cu}(\text{MeCN})_2\}_5]$ along the five-fold symmetry axis.

The formation of this novel 3D structure is based on the *cyclo*-P₅ rings in $[\text{Cp}^*\text{Fe}(\eta^5\text{-P}_5)]$ coordinating to copper in 1,2,3,4,5-mode, leading to the configuration of alternating five-membered rings (*cyclo*-P₅) and bowed six-membered rings (Cu₂P₄), a structure resembling the ring pattern of the fullerene C₆₀. This synthetic concept has recently been extended to the targeted synthesis and isolation of the spherical CuBr analogues $[\{\text{Cp}^x\text{Fe}(\mu, \eta^5: \eta^1: \eta^1: \eta^1: \eta^1\text{-P}_5)\}_{12}\{\text{CuBr}\}_{10}\{\text{Cu}_2\text{Br}_3\}_5\{\text{Cu}(\text{MeCN})_2\}_5]$ (Cp^x = $\eta^5\text{-C}_5\text{Me}_5$, $\eta^5\text{-C}_5\text{Me}_4\text{Et}$), while CuBr was previously thought to produce only 2D-polymeric structures in reactions with $[\text{Cp}^x\text{Fe}(\eta^5\text{-P}_5)]$, thus demonstrating increasing synthetic control over the exclusive preparation of oligomeric structures. [76] That such inorganic spherical molecules are synthetically feasible has led to speculations that additional 3D or fullerene-like structures are possible with further P_n-ligand complexes.

2 Research Objectives

The general aim of the following work is the use of phosphorus ligands for the synthesis of new low-coordinate compounds as well as oligomeric structures. The two metals chosen for this work, tin and tantalum, offer the possibility for investigations of phosphorus moieties bound to a main-group metal as well as a transition metal. As shown in the Introduction, tin-phosphorus chemistry has garnered recent interest due to the recognition that unusual novel bonding states are accessible through the employment of supporting fragments suitable to stabilizing low-coordinate geometries about both the tin and phosphorus atoms. Although the synthesis of $\text{RSi}\equiv\text{P}$ and $\text{RGe}\equiv\text{P}$ triple-bond compounds represent pertinent goals in main-group chemistry as the next heaviest congeners of phosphalkynes, Sn/P compounds are explored here due to the diagnostic advantage of the magnetically active ^{117}Sn and ^{119}Sn nuclei and resulting ^{31}P - $^{117/119}\text{Sn}$ coupling in NMR experiments. For tantalum, the ability to support novel low-coordinate phosphorus ligands has been demonstrated in existing complexes with tris(amido)amine and tris(siloxy) ligand sets, and it is expected that such systems with further ligands sets are within reach. The use of tantalum-phosphorus compounds for the synthesis of oligomeric or extended structures has not yet been demonstrated and is attempted in this work. The following work addresses four main themes, the results of which are organized into four separate chapters:

- (1) The use of the transition-metal fragments $\text{CpFe}(\text{CO})_2$ and $\text{W}(\text{CO})_5$ as stabilizing agents for low-coordinate tin-phosphorus compounds (section 3.1).
- (2) The use of a sterically encumbering terphenyl group (Ph^*) and other aryl groups (Ph , Trip) for the kinetic and thermal stabilization of low-coordinate tin-phosphorus compounds. The experiments in this section are directed toward synthetic approaches expected to yield Sn-P triple-bond compounds on the type $\text{Ph}^*\text{Sn}\equiv\text{P}$ (section 3.2).
- (3) The surveying of a tris(aryloxy)amine ligand set (L^*) for complexation to tantalum(V) and subsequent reactions probing the compatibility of this set with reactive phosphorus and arsenic ligands. Experiments in this section are directed toward the preparation of new transition-metal pnictinidene complexes of the type $[\text{L}^*\text{Ta}=\text{ESiMe}_3]$ ($\text{E} = \text{P}, \text{As}$) (section 3.3).
- (4) The use of the *cyclo*- P_4 tantalum complex $[\text{Cp}''\text{Ta}(\text{CO})_2(\eta^4\text{-P}_4)]$ for reactions with copper(I) halides and production of oligomeric compounds with fullerene-like geometry via coordination through the phosphorus lone pairs (section 3.4).

2 Results and Discussion

3.1 Stabilization of Sn/P compounds by transition-metal fragments

3.1.1 Background and research objective

The group of F. Mathey has thoroughly demonstrated the use of complexation of W(CO)_5 to phosphorus for the synthesis of otherwise elusive organophosphorus compounds. [77] It was determined in our group that coordination of the Lewis-acidic W(CO)_5 fragment on the otherwise highly reactive phosphane molecule, PH_3 , enables the stabilization of an array of monosubstituted phosphanyl compounds possessing mixed Group 13/15 elements. Thus, although the monomeric compounds H_2EPH_2 ($\text{E} = \text{B}, \text{Al}, \text{Ga}$) are not known to exist in the free state, reactions of the nitrogen-base stabilized chloroborane or unsubstituted trielanes ($\text{E} = \text{Al}, \text{Ga}$) with $\text{Li}[\text{PH}_2\text{W(CO)}_5]$ or $[\text{H}_3\text{PW(CO)}_5]$, respectively, resulted in the isolation and full characterization of $[(\text{Me}_3\text{N} \cdot \text{EH}_2\text{PH}_2)\text{W(CO)}_5]$ via either salt elimination or thermal H_2 elimination.

Another small molecule of interest is the unsubstituted diphosphanyl stannylene, $\text{Sn(PH}_2)_2$, which has never been isolated. It is expected that such a species, if generated, would form dimeric or oligomeric compounds or extended structures through donation of the P lone pair to further Sn centers, represented as $[\text{Sn(PH}_2)_2]_n$ ($n \geq 2$). That the value of n would be at least 2 is evidenced by the isolation of the dimeric compound of the form $[\text{Sn(PR}_2)_2]_2$, where R is a relatively bulky trimethylsilyl group and two of the PR_2 ligands are bridging, as described in the Introduction. In such phosphanyl stannylene compounds, a monomeric structure has been observed only for extremely bulky R groups. Furthermore, for the known phosphandiyl stannylenes $[\text{SnPR}]_n$, the size of the cluster seems to vary as a direct function of the size of R, with the size of R qualitatively inversely proportional to the value of n . Since PH_2 is extremely small, the dimeric compound $[\text{Sn(PH}_2)_2]_2$ or oligomeric/extended structures $[\text{Sn(PH}_2)_2]_n$ would presumably prevail in the absence of donor/acceptor stabilization.

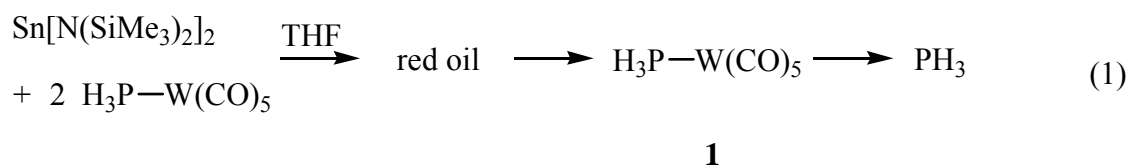
In light of the results obtained for the series of compounds $[(\text{Me}_3\text{N} \cdot \text{EH}_2\text{PH}_2)\text{W(CO)}_5]$, it was expected that through hindrance of the lone-pair $\text{P} \rightarrow \text{Sn}$ interaction with the W(CO)_5 fragment, it would be possible to stabilize the $\text{Sn(PH}_2)_2$ moiety as a monomer.

3.1.2 Reactions of SnCl_2 and $\text{Sn}[\text{N}(\text{SiMe}_3)_2]_2$ with $\text{Li}[\text{H}_2\text{PW}(\text{CO})_5]$ and $[\text{H}_3\text{PW}(\text{CO})_5]$

Reaction of SnCl_2 with two equivalents $\text{Li}[\text{H}_2\text{PW}(\text{CO})_5]$ in toluene resulted in immediate precipitation of a red oil. Investigation of the oil revealed that it was insoluble in common hydrocarbon solvents and Et_2O , but soluble in THF and CH_2Cl_2 . Since the expected salt-elimination product, LiCl , is appreciably soluble in THF, the oil could best be extracted with CH_2Cl_2 . However the oil was observed to be unstable in CH_2Cl_2 solution, as evidenced by slow darkening. In order to have a means of studying this system without production of LiCl and thus without the need for using CH_2Cl_2 , an alternate approach was deemed compulsory.

A common strategy for producing diphosphanyl stannylenes stems from the general higher acidity of P–H bonds than N–H. Thus, $\text{Sn}[\text{N}(\text{SiMe}_3)_2]_2$ serves as a common starting material for this purpose, as Sn–P bond formation can be effected through transamination with P–H-containing reactants and elimination of $\text{HN}(\text{SiMe}_3)_2$. The reaction of $\text{Sn}[\text{N}(\text{SiMe}_3)_2]_2$ with two equivalents $[\text{H}_3\text{PW}(\text{CO})_5]$ was carried out in toluene. Again, a red oil precipitated immediately, leaving a colorless solution. The colorless mother liquor was decanted and the oil examined by $^{31}\text{P}\{^1\text{H}\}$ -NMR spectroscopy in $\text{THF-}d_8$. The spectrum, measured only a few hours after the reaction, revealed a broad main signal ($\Delta\nu_{1/2} = 400$ Hz) centered at -184.7 ppm, in which no tin satellites could be differentiated from the signal noise. Tungsten satellites appeared as incompletely resolved shoulders of the main signal, giving an approximate $^1J_{\text{PW}}$ coupling constant of 210 Hz. The chemical shift and $^1J_{\text{PW}}$ coupling constant correspond somewhat with the data for $[\text{H}_3\text{PW}(\text{CO})_5]$ ($\delta = -183$ ppm, $^1J_{\text{PW}} = 216$ Hz) [78]. However, $[\text{H}_3\text{PW}(\text{CO})_5]$ as a authentic sample appears as a sharp quartet with well-resolved P–W and P–H coupling, so the presence of $[\text{H}_3\text{PW}(\text{CO})_5]$ as the main component could be ruled out. The broadness of the current signal indicates either an ionic species in rapid exchange on the NMR time-scale or possibly a transient species. When this solution was allowed to stand in a vacuum-sealed glass NMR tube and measured again after a few days, the ^{31}P -NMR spectrum revealed disproportionation of the protons and the unambiguous presence of $[\text{H}_3\text{PW}(\text{CO})_5]$ as the main P-containing product. After one month, the ^{31}P -NMR spectrum revealed free phosphane, PH_3 (quartet, $\delta = -244$ ppm, $^1J_{\text{PH}} = 187$ Hz) as the main P-containing product (ca. 90% of total signal intensity) along with traces of $[\text{H}_3\text{PW}(\text{CO})_5]$ (ca. 7%). Neither $[\text{H}_3\text{PW}(\text{CO})_5]$ nor PH_3 were observed in the reaction mixture during the first ^{31}P -NMR measurement, which essentially rules out the possibility of moisture

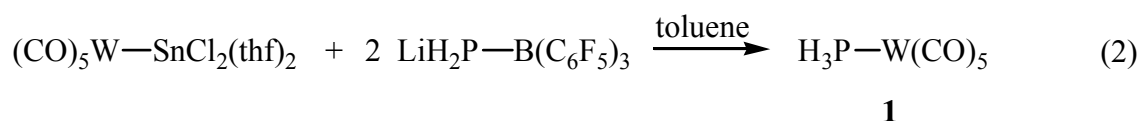
contamination as the proton source during the course of the reaction and makes disproportionation the more plausible interpretation.



Similar results were obtained by the reaction of $[(\text{CO})_5\text{WSnCl}_2(\text{thf})_2]$ with two equivalents $\text{Li}[\text{H}_2\text{PW}(\text{CO})_5]$, according to ^{31}P -NMR spectroscopy. The only difference from the above result is that the spectrum of this reaction mixture was not as clean, revealing several unidentifiable phosphorus signals in addition to the signals mentioned above. Similar salt-elimination routes to tungsten pentacarbonyl-stabilized phosphanyl stannylenes were also carried out under milder conditions, in which the Sn(II) chlorides SnCl_2 , $[\text{tmeda}\cdot\text{SnCl}_2]$, or $[\text{bpy}\cdot\text{SnCl}_2]$ were treated with two equivalents of $[\text{H}_3\text{PW}(\text{CO})_5]$ in THF in the presence of NEt_3 or DBU. While each of these reactions produced a red solution as above, attempts to separate the produced nitrogen-base salts failed. The reaction involving $[\text{bpy}\cdot\text{SnCl}_2]$ was particularly sluggish, requiring long reaction times (> 2 days) and resulting in isolation of yellow crystals of unreacted $[\text{bpy}\cdot\text{SnCl}_2]$, as determined by an X-ray diffraction experiment. [79]

3.1.3 Reaction of $[(\text{CO})_5\text{WSnCl}_2(\text{thf})_2]$ with $\text{Li}[\text{H}_2\text{PBAR}^{\text{F}}_3]$

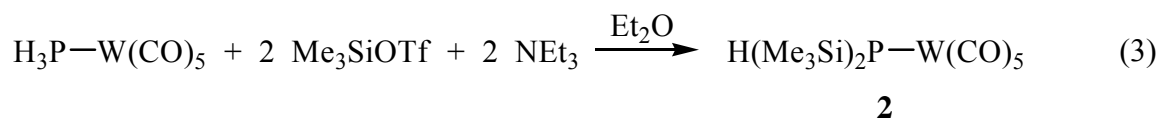
In order to gain further insight into the Lewis-acid stabilized PH_2 system with Sn(II) compounds, a similar reaction was carried out with a different Lewis acid, the perfluorinated triaryl borane $\text{B}(\text{C}_6\text{F}_5)_3$ (BAR^{F}_3). Thus, $[(\text{CO})_5\text{WSnCl}_2(\text{thf})_2]$ was treated with two equivalents of $\text{Li}[\text{PH}_2\text{BAR}^{\text{F}}_3]$ in toluene. The ^{31}P -NMR spectrum was recorded in $\text{THF}-d_8$ and revealed the clean formation of $[\text{H}_3\text{PW}(\text{CO})_5]$ ($> 90\%$ of total intensity of phosphorus-containing compounds). This result shows both the pattern of proton disproportionation as well as exchange of the Lewis-acid moieties between phosphorus and tin.



The migration of a $M(\text{CO})_5$ ($M = \text{Cr}, \text{Mo}, \text{W}$) moiety from $\text{Sn}(\text{II})$ to phosphorus is not a common phenomenon. Reactions of $[(\text{CO})_5\text{WSnCl}_2(\text{thf})]$ with $t\text{Bu}_2\text{PSiMe}_3$ resulted in a polymeric species with formation of P-Sn σ -bonds through trimethylchlorosilane elimination and formation of intermolecular $\text{P} \rightarrow \text{Sn}$ dative bonds, while no migration of the $\text{W}(\text{CO})_5$ fragment from Sn to P was observed. [80] Notably, interactions of $[(\text{CO})_5\text{WSnCl}_2(\text{thf})]$ with triorganophosphanes R_3P ($\text{R} = \text{Et}, n\text{Bu}, t\text{Bu}, \text{Ph}$) gave the Lewis acid/base adducts $[(\text{CO})_5\text{WSnCl}_2 \cdot \text{PR}_3]$ in essentially quantitative yield and did not lead to $\text{W}(\text{CO})_5$ migration. [81] Presumably, the small size of the PH_2 or PH_3 unit in the current work contributes to better access to the tungsten center and enhances the occurrence of metal-carbonyl migration.

3.1.4 Synthesis of $[\text{H}(\text{Me}_3\text{Si})_2\text{PW}(\text{CO})_5]$ (**2**)

In order to hinder the proton disproportionation pathways detailed above while protecting the phosphorus atom with bulky silyl ligands, the starting complex $[\text{H}(\text{Me}_3\text{Si})_2\text{PW}(\text{CO})_5]$ was prepared. In this regard, it would be expected that $[\text{Sn}\{\text{P}(\text{SiMe}_3)_2\text{W}(\text{CO})_5\}_2]$, the Lewis-acid stabilized monomeric analogue of the known phosphanyl-bridging dimer $[\text{Sn}\{\text{P}(\text{SiMe}_3)_2\}_2]$, would be accessible. A modern procedure is not known for preparative isolation of $[\text{H}(\text{Me}_3\text{Si})_2\text{PW}(\text{CO})_5]$, and its preparation was adapted from a convenient method for synthesizing $\text{P}(\text{SiMe}_3)_3$ from PH_3 . [82] Thus, $[\text{H}_3\text{PW}(\text{CO})_5]$ was treated with two equivalents each of Me_3SiOTf and NEt_3 in Et_2O , resulting in elimination of $\text{NEt}_3 \cdot \text{HOTf}$ and formation of the P-Si bonds. The ^{31}P -NMR spectrum of the crude reaction mixture revealed the presence of $[\text{H}(\text{Me}_3\text{Si})_2\text{PW}(\text{CO})_5]$ as the main product (>92%), along with traces of $[(\text{Me}_3\text{Si})_3\text{PW}(\text{CO})_5]$ (2%) and $[\text{H}_2(\text{Me}_3\text{Si})\text{PW}(\text{CO})_5]$ (4%), thus indicating the selective formation of the doubly silylated complex. The high selectivity is likely the result of steric crowding about the P atom, as addition of a third Me_3Si group would have a much slower rate than formation of the first two P-Si bonds. Work-up of the reaction mixture afforded $[\text{H}(\text{Me}_3\text{Si})_2\text{PW}(\text{CO})_5]$ as colorless crystals in 45% yield.

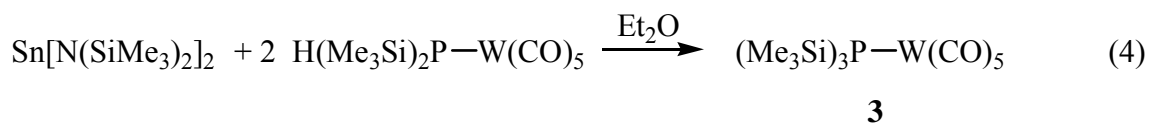


The ^{31}P -NMR spectrum of **2** reveals a doublet at $\delta -215.7$ ppm, about 30 ppm upfield of $[\text{H}_3\text{PW}(\text{CO})_5]$. The $^1J_{\text{PH}}$ and $^1J_{\text{PW}}$ coupling constants of 282 Hz and 160 Hz, respectively, are only slightly smaller than those of $[\text{H}_3\text{PW}(\text{CO})_5]$, but lie in the normal range for $\text{W}(\text{CO})_5$ -

bound protonated phosphanes. The EI-MS spectrum of **2** reveals the molecular ion peak and fragments for successive CO loss as well as a peak for Me₃Si addition. The latter peak indicates either traces of [(Me₃Si)₃PW(CO)₅] in the sample or disproportionation under the conditions of the mass spectrometer. The ¹H-NMR spectrum shows a signal at 0.19 ppm for the trimethylsilyl groups with observable coupling to the phosphorus nucleus (³J_{HP} = 5.0 Hz); however, a signal for the P-bound proton could not be detected.

3.1.5 Reactions of SnCl₂ and Sn[N(SiMe₃)₂]₂ with Li[(Me₃Si)₂PW(CO)₅] and [H(Me₃Si)₂PW(CO)₅]

The reactivity of [H(Me₃Si)₂PW(CO)₅] with Sn(II) compounds was investigated by two means. The first involved *in situ* generation of Li[(Me₃Si)₂PW(CO)₅], which has been previously reported in the literature either by selective cleavage of one P–Si bond of [(Me₃Si)₃PW(CO)₅] by reaction with *n*BuLi in DME [83] or by reaction of [H₃PW(CO)₅] with three equivalents *n*BuLi and two equivalents Me₃SiCl [78]. In the current case, deprotonation of [H(Me₃Si)₂PW(CO)₅] with one equivalent *n*BuLi in THF generated a clean solution of Li[(Me₃Si)₂PW(CO)₅], according to ³¹P-NMR in THF-*d*₈ (singlet, δ = –325 ppm). Reaction of Li[(Me₃Si)₂PW(CO)₅] with SnCl₂ in THF and examination by ³¹P-NMR revealed a singlet at –251 ppm flanked by tungsten satellites (¹J_{PW} = 150 Hz) but no tin satellites, as the main product, along with several unknown P-containing by-products. Investigation by the second method, direct reaction of [H(Me₃Si)₂PW(CO)₅] with Sn[N(SiMe₃)₂]₂ in Et₂O, revealed a similar ³¹P-NMR spectrum in C₆D₆. Work-up of the latter reaction mixture led to isolation of colorless crystals of [(Me₃Si)₃PW(CO)₅] (**3**).



Compound **3** has been previously prepared by adduct formation through irradiation of P(SiMe₃)₃ with [W(CO)₅(thf)] [84] or by the silylation of [H₃PW(CO)₅] with three equivalents each of *n*BuLi and Me₃SiCl. [78] That **3** could form as a result of the disproportionation of silyl groups via reactions of the doubly silylated complexes Li[(Me₃Si)₂PW(CO)₅] or [H(Me₃Si)₂PW(CO)₅] with Sn(II) centers is without precedent. This transformation resembles the proton disproportionation reactions detailed above and corroborates their interpretation as disproportionations rather than protonation reactions

through moisture contamination. Notably, thermal decomposition of $[\text{Sn}\{\text{P}(\text{SiMe}_3)_2\}_2]_2$ was shown to produce $\text{P}(\text{SiMe}_3)_3$ as the major phosphorus-containing product, [16] which provides a precedent for the preferential formation of the trisilylated phosphane in silylphosphanyl stannylene chemistry.

Structure of $[(\text{Me}_3\text{Si})_3\text{PW}(\text{CO})_5]$ (**3**)

Single crystals of **3** were grown from dilute Et_2O solutions at -25°C , and an X-ray diffraction analysis was carried out. **3** crystallizes in the trigonal space group $P3_1$. The molecular structure is shown in Figure 4, and selected bond lengths and angles are listed in Table 1.

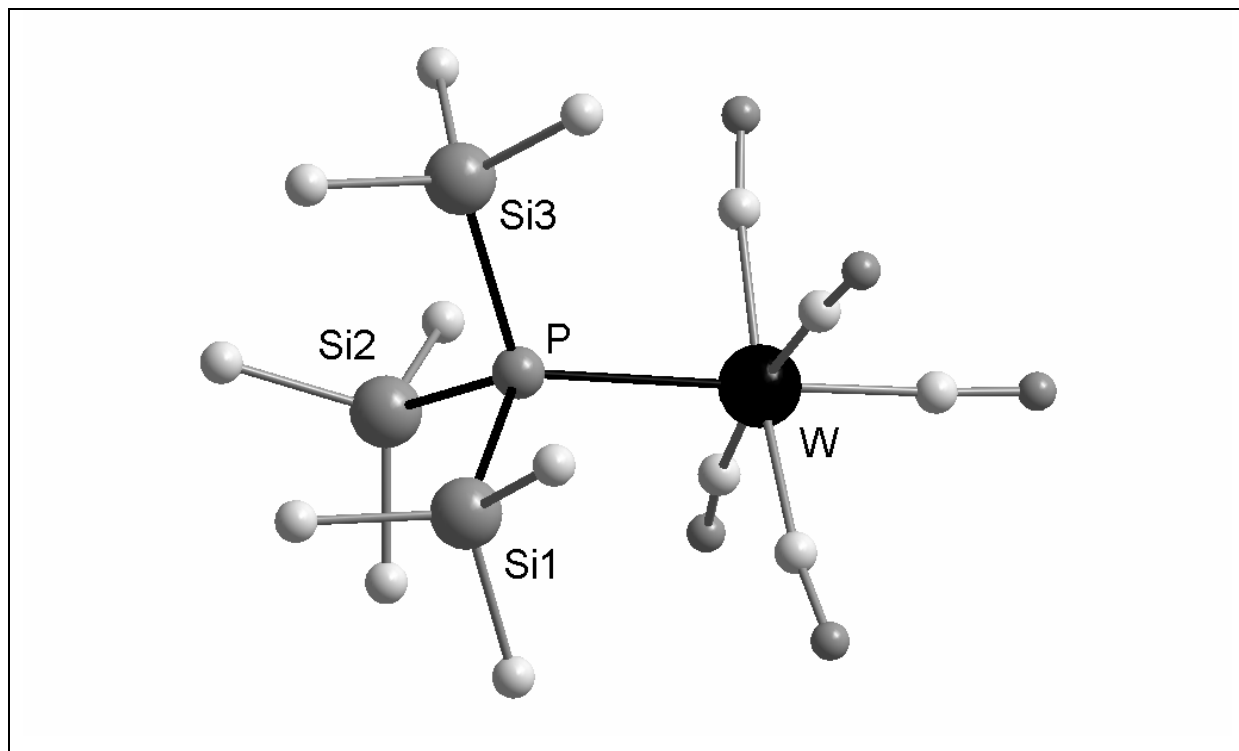


Figure 4: Molecular structure of $[(\text{Me}_3\text{Si})_3\text{PW}(\text{CO})_5]$ (**3**) in the crystal. H atoms have been omitted for clarity.

Table 1: Selected bond lengths [Å] and angles [°] in **3**.

W-P	2.653(3)	W-C _{trans}	2.025(11)
W-C _{cis}	2.064(13) ^a	P-Si(1)	2.286(4)
P-Si(2)	2.299(4)	P-Si(3)	2.300(4)
W-P-Si(1)	112.05(13)	Si(1)-P-Si(2)	105.59(16)
W-P-Si(2)	113.68(15)	Si(1)-P-Si(3)	106.46(17)
W-P-Si(3)	113.30(13)	Si(2)-P-Si(3)	105.10(16)
P-W-C _{cis}	88.3(4) – 96.8(4)	C _{cis} -W-C _{trans}	86.3(5) – 88.8(6)
W-C _{cis} -O	172.4(12) – 174.0(12)		

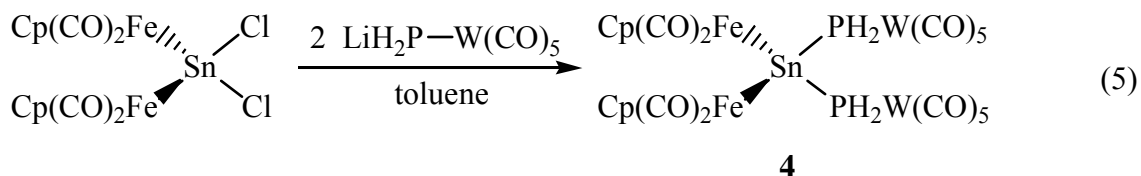
^a Mean value is given

In the molecular structure of **3** the phosphorus atom is in distorted tetrahedral geometry with the Si-P-Si angles (105.10(16)° – 106.46(17)°) significantly less obtuse than the Si-P-W angles (112.05(13)° – 113.68(15)°), revealing a slight closing up of the pyramid about phosphorus formed by the Me₃Si groups and tungsten pentacarbonyl fragment. This effect is less pronounced than in the related complex [Ph₃PW(CO)₅], which bears sterically less encumbering phenyl groups at phosphorus (C_{aryl}-P-C_{aryl}: 102.0(2)° – 103.6(2)°; C_{aryl}-P-W: 111.6(1)° – 118.4(1)°). [85] The tungsten atom in **3** exhibits nearly octahedral geometry, with the P-W-C_{cis} bond angles (88.3(4)° – 96.8(4)°) slightly larger, on average, than the C_{cis}-W-C_{trans} angles (86.3(5)° – 88.8(6)°). The W-C_{cis}-O bonds all deviate from linearity (172.4(12)° – 174.0(12)°), likely as a result of repulsion from the bulky Me₃Si groups; such repulsion is less evident from the smaller phenyl groups in [Ph₃PW(CO)₅] (W-C_{cis}-O: 176.9(5)° – 178.3(6)°). The P-W bond length in **3** (2.653(3) Å) is longer than the P-W bond lengths in both [H₃PW(CO)₅] (2.491(2) Å) [86] and [Ph₃PW(CO)₅] (2.545(1) Å). In general, from the examples presented here, the P-W bond lengths in such complexes increase with increasing steric bulk of the P-bound groups.

3.1.6 Reaction of [Fp₂SnX₂] (X = Cl, Br) with Li[H₂PW(CO)₅]

Since unsubstituted or Lewis-acid or Lewis-base stabilized Sn(II) centers were found to induce fragmentation at phosphorus and Lewis-acid exchange reactions with W(CO)₅-supported phosphane ligands, the starting materials [Fp₂SnX₂] (Fp = CpFe(CO)₂, X = Cl, Br) were investigated as a more stable alternative. While many organotin phosphanides of the form R₂Sn(PR₂)₂ are known, [87] transition-metal supported analogues have not been previously reported.

Reaction of $[\text{Fp}_2\text{SnCl}_2]$ with two equivalents of *in situ* generated $\text{Li}[\text{H}_2\text{PW}(\text{CO})_5]$ in toluene at low temperature resulted in slow darkening from light red to dark red. Overnight stirring and recrystallization from toluene led to isolation of red crystals of $[\text{Fp}_2\text{Sn}\{\text{PH}_2\text{W}(\text{CO})_5\}_2]$ (**4**) in moderate yield. Use of the alternate starting material $[\text{Fp}_2\text{SnBr}_2]$ resulted in the same product.



Complex **4** represents the first known transition-metal complex bearing the diphosphanyl stannane moiety, $\text{Sn}(\text{PH}_2)_2$, without organic substituents. While attempts in this work to stabilize $\text{Sn}(\text{PH}_2)_2$ with a divalent tin center failed, the $\text{Sn}(\text{PH}_2)_2$ ligand is stabilized in **4** as a formal tin(IV) compound. The corresponding parent compound, $\text{Sn}(\text{PH}_2)_2$, has never been isolated in the free state, while theoretical calculations have been carried out on the free compound with regard to its stability and tautomerization into the Sn-P multiply bonded species $(\text{H}_2\text{P})(\text{H})\text{Sn}=\text{PH}$. [18] Contrary to speculation that such a transformation could be thermally induced, $[\text{Fp}_2\text{Sn}\{\text{PH}_2\text{W}(\text{CO})_5\}_2]$ displays considerable thermal stability. Heating **4** to reflux in benzene for three hours showed virtually no changes in the ^{31}P -NMR spectrum. This result stands in contrast to the reported thermal elimination of PH_3 from $t\text{Bu}_2\text{Sn}(\text{PH}_2)_2$, [88,89] thus making a case for the stabilizing effect of the $\text{CpFe}(\text{CO})_2$ and $\text{W}(\text{CO})_5$ groups in **4**.

The proton-decoupled ^{31}P -NMR spectrum of **4** in toluene- d_8 reveals a singlet at -177.2 ppm with both tungsten and fully-resolved $^{117/119}\text{Sn}$ satellites. The chemical shift is slightly downfield from that of $[\text{H}_3\text{PW}(\text{CO})_5]$ ($\delta = -186$ ppm) and $[(\text{Me}_3\text{N}\cdot\text{BH}_2\text{PH}_2)\text{W}(\text{CO})_5]$ ($\delta = -184.2$ ppm). The tungsten and tin satellite intensities in the ^{31}P -NMR spectrum of **4** (^{183}W : 13%; ^{119}Sn : 7.3%; ^{117}Sn : 6.7%)¹ are on the order of the natural abundances for the respective isotopes. [90] The $^1J_{\text{PW}}$ coupling constant of 174 Hz is slightly smaller than that of $[\text{H}_3\text{PW}(\text{CO})_5]$ (214 Hz) and correlates well with the related phosphanyltrielane compounds $[(\text{Me}_3\text{N}\cdot\text{EH}_2\text{PH}_2)\text{W}(\text{CO})_5]$ (E = B: 177 Hz; E = Ga: 165 Hz). The $^1J_{\text{P}^{117}\text{Sn}}$ and $^1J_{\text{P}^{119}\text{Sn}}$ coupling constants of 893 Hz and 934 Hz, respectively, for **4** are slightly higher than those for

¹ Experimental tin satellite intensities in this work often deviate slightly from the expected intensity of 16.3% for one-to-one tin/phosphorous compounds, as attributable likely to the error inherent in the small signal-to-noise ratio for the satellites.

known organotin phosphanides with a Sn-P single bond ($\text{Me}_3\text{SnPtBu}_2$: $^1J_{\text{P}117\text{Sn}} = 760.0$ Hz, $^1J_{\text{P}119\text{Sn}} = 795.4$ Hz; Me_3SnPH_2 : $^1J_{\text{P}117\text{Sn}} = 443$ Hz, $^1J_{\text{P}119\text{Sn}} = 463$ Hz). [91] The $^1J_{\text{P}117\text{Sn}}$ and $^1J_{\text{P}119\text{Sn}}$ coupling constants for **4** are, however, considerably higher than for the related tungsten pentacarbonyl complexes [$\{\text{Trip}_2(\text{X})\text{Sn}\}\text{P}(\text{H})(\text{Mes})\text{W}(\text{CO})_5$] (X = F: $^1J_{\text{P}117\text{Sn}} = 200.1$ Hz, $^1J_{\text{P}119\text{Sn}} = 209.6$ Hz; X = Cl: $^1J_{\text{P}117\text{Sn}} = 253.6$ Hz, $^1J_{\text{P}119\text{Sn}} = 259.0$ Hz; X = Br: $^1J_{\text{P}117\text{Sn}} = 291.1$ Hz, $^1J_{\text{P}119\text{Sn}} = 302.8$ Hz) [92] and [$\text{Me}_3\text{Sn}t\text{Bu}_2\text{PW}(\text{CO})_5$] ($^1J_{\text{P}117\text{Sn}} = 76.5$ Hz, $^1J_{\text{P}119\text{Sn}} = 80.0$ Hz). [91]

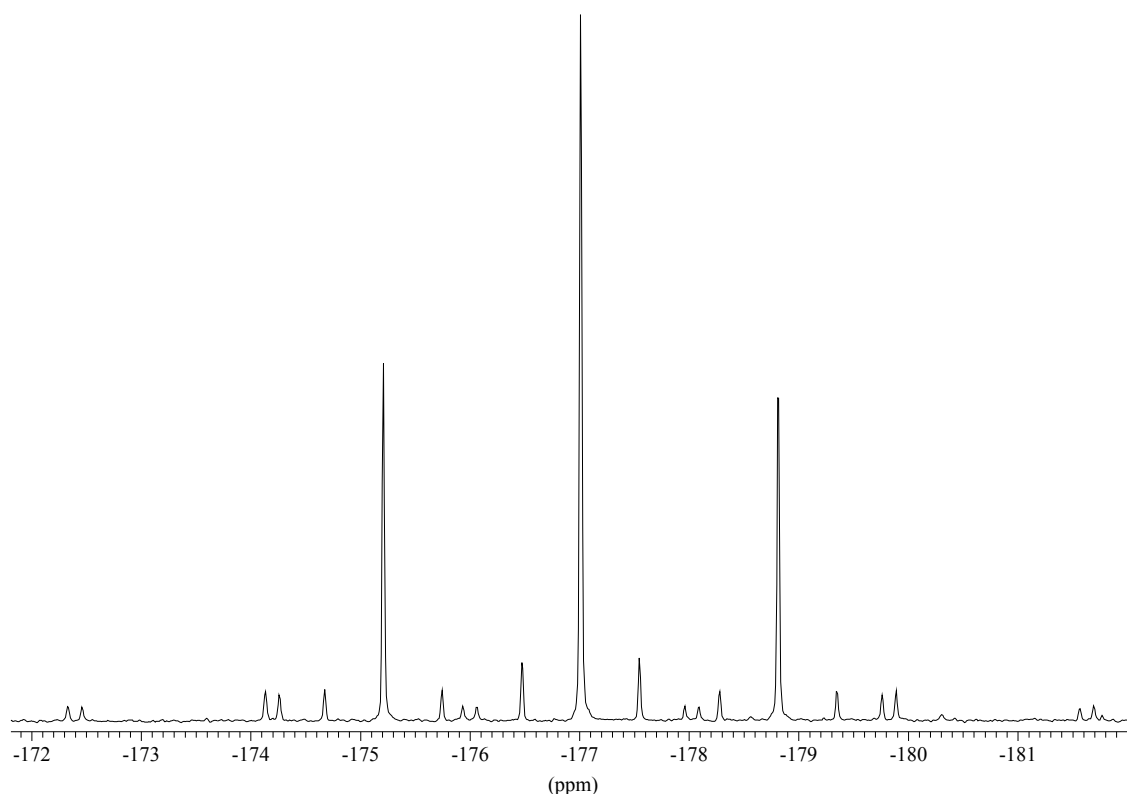


Figure 5: Proton-coupled ^{31}P -NMR signal for **4**.

In the proton-coupled ^{31}P -NMR spectrum (Figure 5), the signal is split into a characteristic triplet ($^1J_{\text{PH}} = 292$ Hz), indicating the presence of two protons on each phosphorus atom. Each signal of the triplet retains both the ^{183}W and resolved $^{117/119}\text{Sn}$ satellites upon proton coupling. The $^1J_{\text{PH}}$ coupling constant of 292 Hz is only slightly smaller than the $^1J_{\text{PH}}$ coupling constants in [$\{\text{Trip}_2(\text{X})\text{Sn}\}\text{P}(\text{H})(\text{Mes})\text{W}(\text{CO})_5$] (X = F: $^1J_{\text{PH}} = 304.3$ Hz; X = Cl: $^1J_{\text{PH}} = 304.3$ Hz; X = Br: $^1J_{\text{PH}} = 302.2$ Hz). The expected triplet for **4** could not be found in the $^{119}\text{Sn}\{^1\text{H}\}$ -NMR spectrum over a measurement range from -1500 to $+1500$ ppm.

In the ^1H -NMR spectrum, one signal is found for the cyclopentadienyl ligands at 4.24 ppm, and the P-H protons appear as a slightly broadened doublet at 3.79 ppm with a $^1J_{\text{HP}}$ coupling constant of 292 Hz. While the $^1J_{\text{HP}}$ coupling constant agrees well with those of the related phosphanyltrielane complexes $[(\text{Me}_3\text{N}\cdot\text{EH}_2\text{PH}_2)\text{W}(\text{CO})_5]$ (E = B: $\delta = 2.48$ ppm, $^1J_{\text{HP}} = 297$ Hz; E = Al: $\delta = 1.93$ ppm, $^1J_{\text{HP}} = 283$ Hz; E = Ga: $\delta = 1.84$ ppm, $^1J_{\text{HP}} = 293$ Hz), [7] the chemical shift of **4** lies much farther downfield. The ^{13}C -NMR spectrum reveals a signal for the cyclopentadienyl ligands at 84.3 ppm. Downfield signals for the CO ligands were observed for tungsten-bound *cis*- and *trans*- CO ligands as well as for the Fe-carbonyl groups. The combination of ^1H - and ^{13}C -NMR spectra of **4** indicate a lack of preferential geometric conformation of the Fp fragments or of the $\text{H}_2\text{PW}(\text{CO})_5$ groups on the NMR time scale, pointing to free rotation about the Sn–Fe and Sn–P bonds. Only the slight broadening of the P-H protons may be a result of some degree of hindered rotation about the Sn–P bonds, which would make the protons diastereotopic.

In the IR spectrum (KBr pellet), a grouping of six peaks was found at CO stretching frequencies, representing both the iron-bound and tungsten-bound CO ligands. The medium absorption at 2320 cm^{-1} is tentatively assigned to the P-H groups. The EI mass spectrum of **4** was measured at various temperatures ranging from 90°C to 280°C . In each measurement the molecular ion peak could not be observed. Rather, only peaks corresponding to $\text{H}_2\text{PW}(\text{CO})_5$ and $\text{PSnH}_2\text{PW}(\text{CO})_5$ units were observed as well as fragmentation of $\text{H}_2\text{PW}(\text{CO})_5$.

Structure of $[\text{Fp}_2\text{Sn}\{\text{PH}_2\text{W}(\text{CO})_5\}_2]$ (**4**)

Single crystals of **4** were grown from dilute toluene solutions at -25°C , and an X-ray diffraction analysis was carried out. **4** crystallizes with one molecule toluene per formula unit in the monoclinic space group $P2/c$. The molecular structure is shown in Figure 6, and selected bond lengths and angles are listed in Table 2.

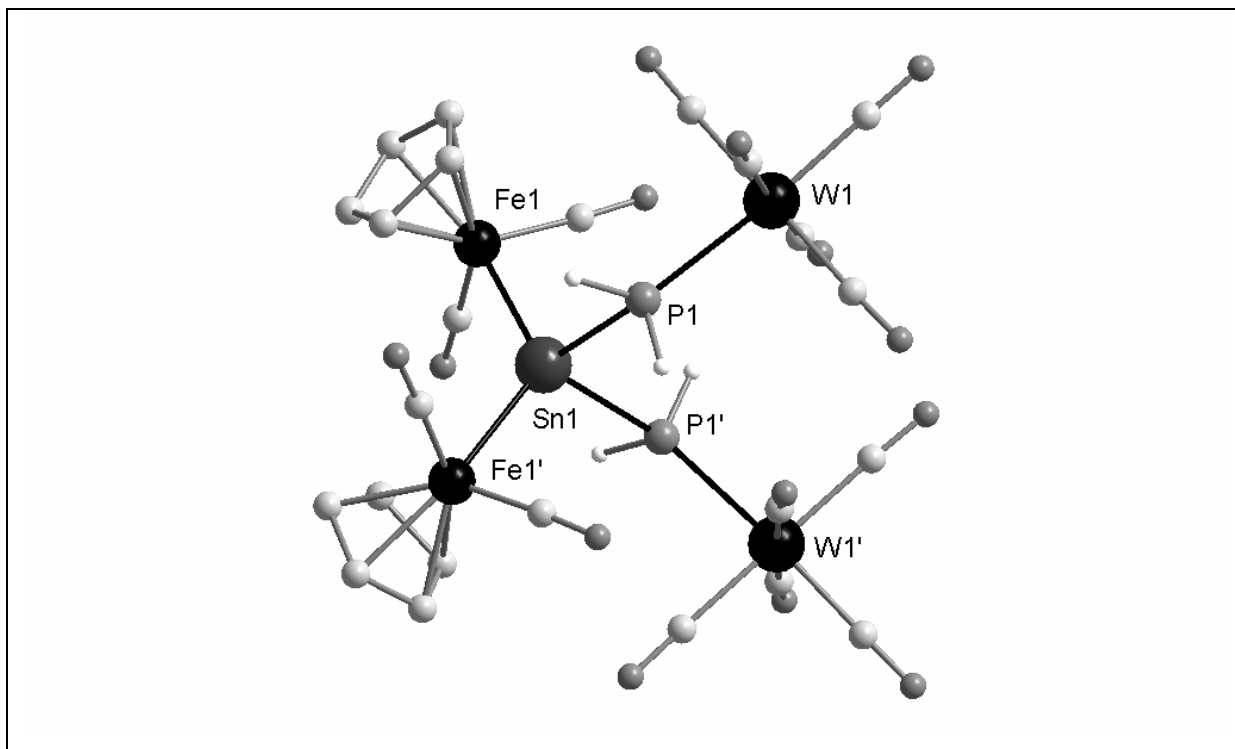


Figure 6: Molecular structure of $[\text{Fp}_2\text{Sn}\{\text{PH}_2\text{W}(\text{CO})_5\}_2]$ (**4**) in the crystal. Carbon-bound H atoms have been omitted for clarity.

Table 2: Selected bond lengths [\AA] and angles [$^\circ$] in **4**.

Sn-P	2.568(2)	Sn-Fe	2.550(1)
W-P	2.548(2)	Fe-C _{Cp}	2.084(9) ^a
W-C _{cis}	2.046(8) ^a	W-C _{trans}	1.994(8)
Fe-C(3)	1.759(8)	Fe-C(4)	1.762(8)
P-Sn-P	95.97(8)	Fe-Sn-Fe	121.62(5)
Fe-Sn-P	108.38(5)	W-P-Sn	130.98(6)
Fe-Sn-P'	109.73(4)		

^a Mean value is given

The principal feature of the molecular structure of **4** is the central $\text{Sn}(\text{PH}_2)_2$ ligand, which is σ -bonded through tin to two organometallic $\text{Cp}(\text{CO})_2\text{Fe}$ fragments and coordinated through the phosphorus lone pairs to two $\text{W}(\text{CO})_5$ fragments. The $\text{H}_2\text{PW}(\text{CO})_5$ groups are rotated relative to one another about the molecular C_2 axis, giving the complex an overall C_2 symmetry in the crystal structure. In the unit cell two molecules of **4** are found, and there exist two distinct orientations which are related to each other through a crystallographic inversion center located between the molecules. As a result, compound **4** is found in the crystal as an enantiomeric pair, as required by the crystallographic symmetry for the C_2 symmetric

conformation centered on a crystallographic C_2 axis. Each tin atom in **4** is centered directly on a crystallographic C_2 axis. The two orientations are shown in Figure 7, in which two molecules of **4** are viewed along two distinct crystallographic C_2 axes. The positions of the molecules in Figure 7 are not shown as they appear in the crystal; rather, the positions of the molecules have been manually adjusted so that the two orientations can be seen relative to one another. As a result, a mirror plane can be envisioned between the two molecules, such that one orientation is not superimposable on the other orientation. While compound **4** exists as an enantiomeric pair in the crystal with the conformations related by a crystallographic inversion point, the NMR data above shows no preferential orientation in solution. It can then be reasonably concluded that the $H_2PW(CO)_5$ groups in compound **4** shift rapidly in solution between the two extreme orientations shown in Figure 7.

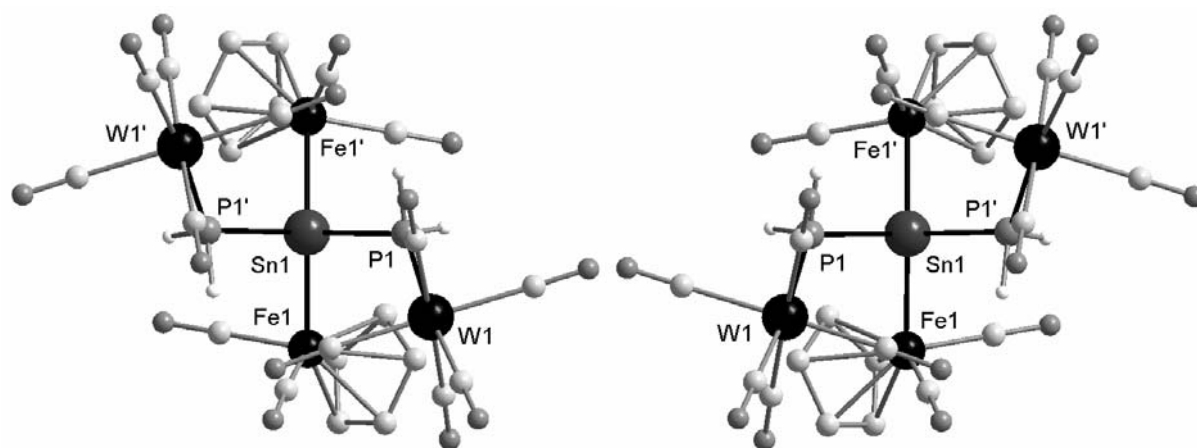


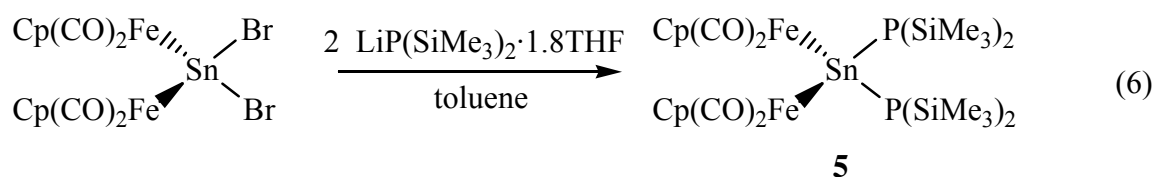
Figure 7: Views of $[Fp_2Sn\{PH_2W(CO)_5\}_2]$ (**4**) in the crystal along two distinct crystallographic C_2 axes. Carbon-bound H-atoms have been removed for clarity.

The central tin atom in **4** is found in distorted tetrahedral geometry, whereby the phosphanyl moieties are pinched together with a P-Sn-P angle of $95.97(8)^\circ$, while the Fe-Sn-Fe angle of $121.62(5)^\circ$ is considerably larger. This strong deviation from tetrahedral geometry about tin is also observed in other compounds with a central Fp_2Sn unit, as in e.g. $[Fp_2Sn(N_3)_2]$ (N-Sn-N: $92.8(4)^\circ$; Fe-Sn-Fe: $127.2(1)^\circ$). [93] The Sn-Fe bond length ($2.550(1)$ Å) is slightly elongated in comparison to that in the starting material $[Fp_2SnCl_2]$ ($2.492(8)$ Å). [94] The W-P bond in **4** ($2.548(2)$ Å) is slightly elongated compared to that in $[H_3PW(CO)_5]$ ($2.491(2)$ Å) [86] and more comparable to those in the related phosphanyltriellane complexes $[(Me_3N\cdot EH_2PH_2)W(CO)_5]$ (E = B: $2.537(2)$ Å; E = Al: $2.5491(9)$ Å; E = Ga: $2.537(2)$ Å). [7]. However, the angle about P in **4** is significantly less

acute (W-P-Sn: 130.98(6)°) than the E-P-W angles in [(Me₃N·EH₂PH₂)W(CO)₅] (E = B: 116.4(1)°; E = Al: 118.44(4)°; E = Ga: 114.72(7)°). Comparable crystallographically characterized compounds possessing a Sn–P bond supported by tungsten pentacarbonyl coordination through the phosphorus lone pair are exceedingly rare. [95] Compound **4** represents the first known W(CO)₅-supported phosphanyl stannane with only protons at the phosphorus atom, and searches for related transition-metal supported Sn phosphanyl compounds with tin–transition-metal bonds resulted in no hits.

3.1.7 Reaction of [Fp₂SnBr₂] with LiP(SiMe₃)₂·1.8THF

While bis(trimethylsilyl)phosphanide ligands have been incorporated in a wealth of transition-metal complexes, especially those of the Group 4 members Ti and Zr, such ligands have found only limited use in tin(IV) compounds. Parallels have been noted between the phosphanide chemistry of tin and that of Group 4 transition metals. [26] In order to probe the chemistry of silylated phosphanides with a transition-metal supported tin center and to examine similarities or differences to that of related organotin compounds, the reaction of the transition-metal supported stannane [Fp₂SnBr₂] with two equivalents of LiP(SiMe₃)₂·1.8THF was carried out at low temperature in toluene. Immediately upon mixing the reactants, a gradual darkening of the original orange-red solution to dark red was observed. After overnight stirring, work-up and recrystallization from *n*-hexane produced dark red platelets of [Fp₂Sn{P(SiMe₃)₂}]₂ (**5**) in good yield.



The formation of [Fp₂Sn{P(SiMe₃)₂}]₂ parallels the synthesis of *t*Bu₂Sn{P(SiMe₃)₂}]₂ from *t*Bu₂SnCl₂ and two equivalents LiP(SiMe₃)₂·1.8THF. [88] **5** is soluble in common hydrocarbon solvents and is stable in refluxing benzene for 3 hours without decomposition, as shown by ³¹P-NMR. This observation stands in contrast to the behavior of *t*Bu₂Sn{P(SiMe₃)₂}]₂, which is stable only at temperatures below –50°C, but mirrors the thermal stability exhibited by compound **4**.

In the ³¹P-NMR spectrum of **5**, a singlet is found at –182.9 ppm with a set of tin satellites. The chemical shift lies about 70 ppm downfield of the signal observed for *t*Bu₂Sn{P(SiMe₃)₂}]₂ (δ = –252.7 ppm) and about 90 ppm downfield of the shift observed in

$\text{Me}_3\text{SnP}(\text{SiMe}_3)_2$ ($\delta = -270.7$ ppm). [96] The combined tin satellite intensity in **5** (16%) is in accordance with the total isotope abundance for the ^{117}Sn and ^{119}Sn nuclei (total abundance = 16.3%), and the $^1J_{\text{P}^{117}\text{Sn}}$ and $^1J_{\text{P}^{119}\text{Sn}}$ coupling constants are 1186 Hz and 1240 Hz, respectively, which are higher than those for $t\text{Bu}_2\text{Sn}\{\text{P}(\text{SiMe}_3)_2\}_2$ (984.7, 1030.4 Hz). The larger coupling constants likely come as a result of stronger donation of the phosphorus lone pair to the more highly acidic Fe-bound tin center. In support of this argument, the $^1J_{\text{P}^{117}\text{Sn}}$ and $^1J_{\text{P}^{119}\text{Sn}}$ coupling constants for **4** (893, 934 Hz), in which the phosphorus lone pairs are bound by $\text{W}(\text{CO})_5$ fragments, are significantly smaller.

The $^{119}\text{Sn}\{^1\text{H}\}$ -NMR spectrum of **5** exhibits a signal at -392.1 ppm which is split into a triplet, as expected for a tin center bound to two phosphorous atoms. The $^1J_{\text{SnP}}$ coupling constant is 1240 Hz, which correlates with the $^1J_{\text{P}^{119}\text{Sn}}$ value (1240 Hz) observed in the ^{31}P -NMR spectrum.

In the IR spectrum of **5**, two vibrational signals are found in the range of terminal CO ligands, as attributed to the $[\text{CpFe}(\text{CO})_2]$ fragments. In the ^1H - and ^{13}C -NMR spectra, the expected singlets are found for the cyclopentadienyl and CO ligands. However, for the $\text{P}(\text{SiMe}_3)_2$ ligands, two sets of overlapping doublets are found in both the ^1H - and ^{13}C -NMR spectra. This indicates either hindered rotation about the Sn–P bonds, presumably as a result of the steric effects of the large SiMe_3 groups, or a bonding situation in which the silyl phosphanide ligands are not magnetically equivalent on the NMR time scale. As reasoned for the disubstituted bis(trimethylsilyl)phosphanide- [97] and the analogous disubstituted bis(trimethylsilyl)arsenide- [98] complexes of zirconium(IV), resonance structures can be envisioned where one phosphanide or arsenide ligand is doubly bonded to the metal center and the other singly bonded. In cases where the ^1H - and ^{13}C -NMR signals of the silylphosphanide/silylarsenide ligands are equivalent, such resonance forms can be ruled out. In **5**, donation of a phosphorus lone pair to the tin center can potentially contribute to a higher Sn–P bond order; in that case, such donation would lead to a geometry about phosphorus closer to planarity than the trigonal pyramidal geometry characteristic of phosphanide single bonding. This point is addressed in the structural characterization below.

Structure of $[\text{Fp}_2\text{Sn}\{\text{P}(\text{SiMe}_3)_2\}_2]$ (**5**)

An X-ray structural analysis was carried out on red single crystals of **5**, which were grown from *n*-hexane solutions at -25°C . **5** crystallizes in the orthorhombic space group $P2_1ab$. The molecular structure is shown in Figure 8, and selected bond lengths and angles are listed in Table 3.

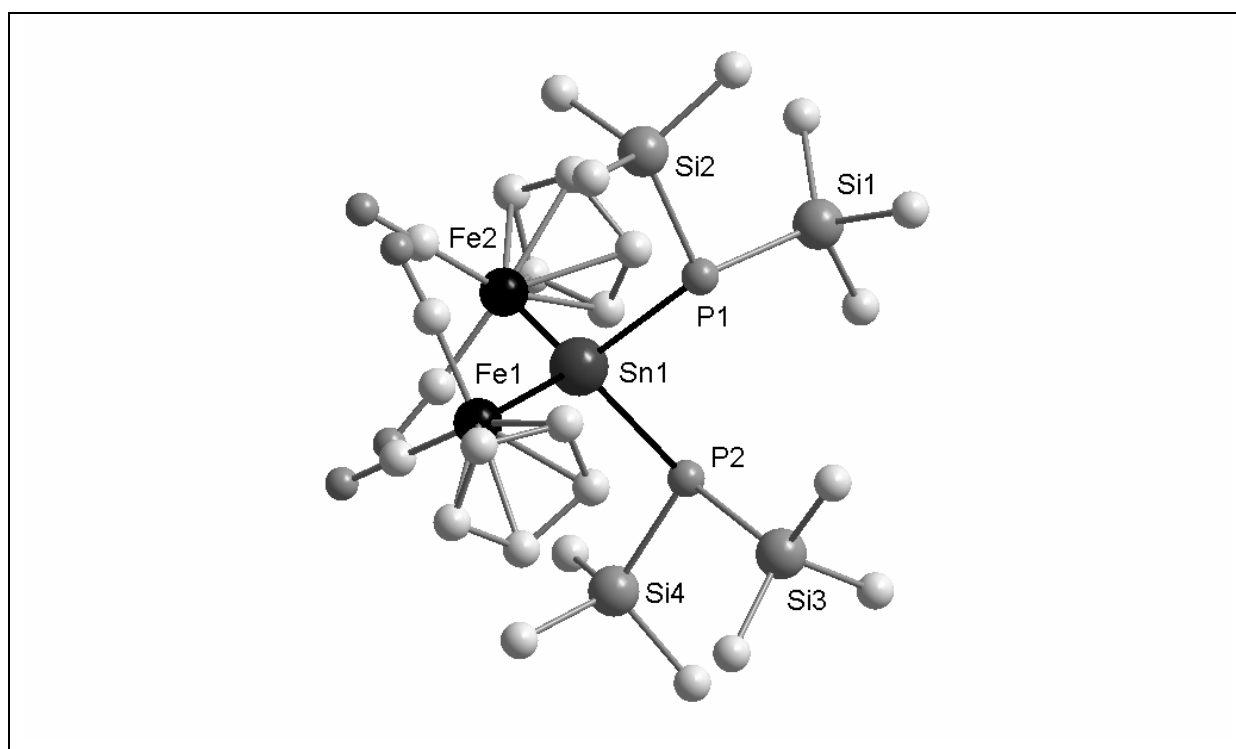


Figure 8: Molecular structure of $[\text{Fp}_2\text{Sn}\{\text{P}(\text{SiMe}_3)_2\}_2]$ (**5**) in the crystal. H atoms have been omitted for clarity.

Table 3: Selected bond lengths [Å] and angles [°] in **5**.

Sn-Fe(1)	2.638(1)	Sn-Fe(2)	2.649(1)
Sn-P(1)	2.612(1)	Sn-P(2)	2.590(1)
Fe(1)-C _{Co}	1.756(5) ^a	Fe(2)-C _{Co}	1.762(5) ^a
Fe(1)-C _{Cp}	2.101(5) ^a	Fe(2)-C _{Cp}	2.113(5) ^a
P(1)-Si	2.271(1) ^a	P(2)-Si	2.274(1) ^a
P-Sn-P	96.26(3)	Fe-Sn-Fe	119.32(2)
Fe(1)-Sn-P(1)	101.89(3)	Fe(1)-Sn-P(2)	118.18(2)
Fe(2)-Sn-P(1)	117.93(3)	Fe(2)-Sn-P(2)	101.66(2)
Sn-P(1)-Si(1)	118.29(5)	Sn-P(2)-Si(3)	117.77(4)
Sn-P(1)-Si(2)	111.06(4)	Sn-P(2)-Si(4)	112.52(4)
Si(1)-P(1)-Si(2)	102.45(6)	Si(3)-P(2)-Si(4)	101.83(6)

^a Mean value is given

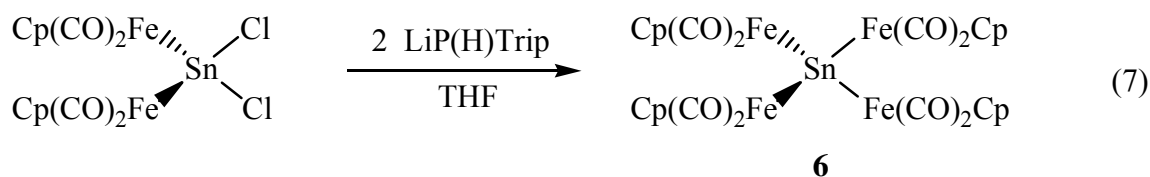
As with compound **4**, the central tin atom in **5** is surrounded by two iron atoms and two phosphorus atoms in distorted tetrahedral geometry. With a P-Sn-P bond angle of 96.26(3)° and an Fe-Sn-Fe bond angle of 119.32(2)°, the tetrahedral geometry about Sn in **5** is

slightly less distorted than that in **4** (P-Sn-P: $95.97(8)^\circ$; Fe-Sn-Fe: $121.62(5)^\circ$). The $\text{P}(\text{SiMe}_3)_2$ ligands are arranged with the silyl groups facing away from one another, thus alleviating steric crowding. Though the $\text{P}(\text{SiMe}_3)_2$ ligands were shown to be magnetically equivalent on the NMR time scale by means of ^{31}P -NMR, there exists no mirror symmetry plane or C_2 axis of symmetry in the crystal structure of **5**, thus making the two P atoms, the two Fe atoms, and the four Si atoms each symmetrically unique. This feature correlates well with the observations in the ^1H - and ^{13}C -NMR spectra of **5**, in which the silyl group protons and carbon atoms were reasoned to be magnetically inequivalent at room temperature on the NMR time scale. The Sn-P bond distances in **5** ($2.612(1)$ Å, $2.590(1)$ Å) differ slightly from one another, which is likely a result of crystal packing effects or repulsion of the bulky silyl groups rather than direct electronic effects. Both Sn-P bond distances in **5** are longer than those found in **4** ($2.568(2)$ Å) and therefore can be best described as having only single-bond character. The Sn-Fe bond lengths in **5** ($2.638(1)$ Å, $2.649(1)$ Å) are significantly longer than the Sn-Fe bond in **4** ($2.550(1)$ Å). The P atoms in **5** are found in trigonal pyramidal geometry, as observed in the angles about phosphorus (Sn-P(1)-Si(1): $118.29(5)^\circ$; Sn-P(1)-Si(2): $111.06(4)^\circ$; Si(1)-P(1)-Si(2): $102.45(6)^\circ$; Sn-P(2)-Si(3): $117.77(4)^\circ$; Sn-P(2)-Si(4): $112.52(4)^\circ$; Si(3)-P(2)-Si(4): $101.83(6)^\circ$), such that the silyl ligands on each respective P atom are slightly pinched together relative to the Sn-P-Si angles. This considerable deviation from planarity supports the description of the Sn-P bonds as having single-bond character. This interpretation is in accordance with the ^{31}P -NMR spectrum of **5**, in which the phosphorus signal ($\delta = -182.9$; $^1J_{\text{P117Sn}} = 1186$ Hz, $^1J_{\text{P119Sn}} = 1240$ Hz) appears in the singly bonded range, whereas compounds with Sn=P double bonds appear in the downfield region (δ ca. +200 ppm). Furthermore, the $^1J_{\text{P117Sn}}$ and $^1J_{\text{P119Sn}}$ coupling constants in **5** correspond to Sn-P single bonds, while compounds with Sn=P double bonds generally exhibit considerably larger $^1J_{\text{P117Sn}}$ and $^1J_{\text{P119Sn}}$ coupling constants (ca. 2000 Hz).

3.1.8 Reaction of $[\text{Fp}_2\text{SnCl}_2]$ with $\text{LiP}(\text{H})\text{Trip}$

The reaction behavior of alkali-metal primary phosphanides with both transition-metal centers and main-group metals has been widely investigated (see Introduction). Some novel transformations have been observed, such as P-P bond formation and M-P multiple bond formation. Thus, the reaction of $[\text{Fp}_2\text{SnCl}_2]$ with two equivalents of $\text{LiP}(\text{H})\text{Trip}$ (Trip = 2,4,6-*i*Pr₃C₆H₂) was carried out at low temperature in THF. It was expected that the Trip group would provide sufficient steric protection to stabilize any low-coordinate species formed following the potential elimination of the primary phosphane TripPH_2 . However, work-up of

the reaction mixture and recrystallization from toluene resulted in the isolation of the disproportionation product $[\text{Fp}_4\text{Sn}]$ (**6**).



Although cleavage of the Fe–Sn bond in complexes bearing the central Fp_2Sn core is rare in halide-substitution reactions of $[\text{Fp}_2\text{SnCl}_2]$, the Merzweiler group observed the formation of $[\{\text{CpFe(CO)}_2\}_2\{\text{CpFe(CO)}\}\text{Sn}_3\text{S}_4]$, which bears only one iron fragment per tin atom and exhibits formation of an iron–sulfur bond, in reactions of $[\text{Fp}_2\text{SnCl}_2]$ with $\text{S}(\text{SiMe}_3)_2$, a relatively mild source of sulfide ligands. [99] The formation of **6** apparently stems from a similar fragmentation and subsequent Fe–Sn bond formation.

Complex **6** is extremely air sensitive, with solutions turning from violet to pale yellow within seconds upon exposure to oxygen. The ^1H -NMR spectrum of **6** gives a single signal for the Cp groups. In the ^{13}C -NMR spectrum, a grouping of three peaks is found for the Cp groups, and a grouping of three signals is found for the carbonyl groups. This likely indicates some hindrance in rotation about the Sn–Fe bonds, thus making the carbon atoms magnetically inequivalent on the NMR time scale. However, the protons are far enough removed from the rotational hindrance, and no splitting of the ^1H signals is observed.

The IR spectrum reveals two strong absorptions in the terminal CO region. In the FD mass spectrum, the molecular ion peak was not observed, and repeated measurement was precluded by the extreme air sensitivity of solutions of **6**. A single signal grouping was found in the FD mass spectrum and was identified as $[\text{Fp}_3\text{Sn}]^+$, corresponding to loss of one Fp group.

Structure of $[\text{Fp}_4\text{Sn}]$ (**6**)

An X-ray structural analysis was carried out on violet-red rhomboidal plates of **6**, which were grown from toluene solutions at -25°C . **6** crystallizes in the monoclinic space group $P2_1/c$ with one molecule of toluene per formula unit in the crystal lattice. The molecular structure is shown in Figure 9, and selected bond lengths and angles are listed in Table 4.

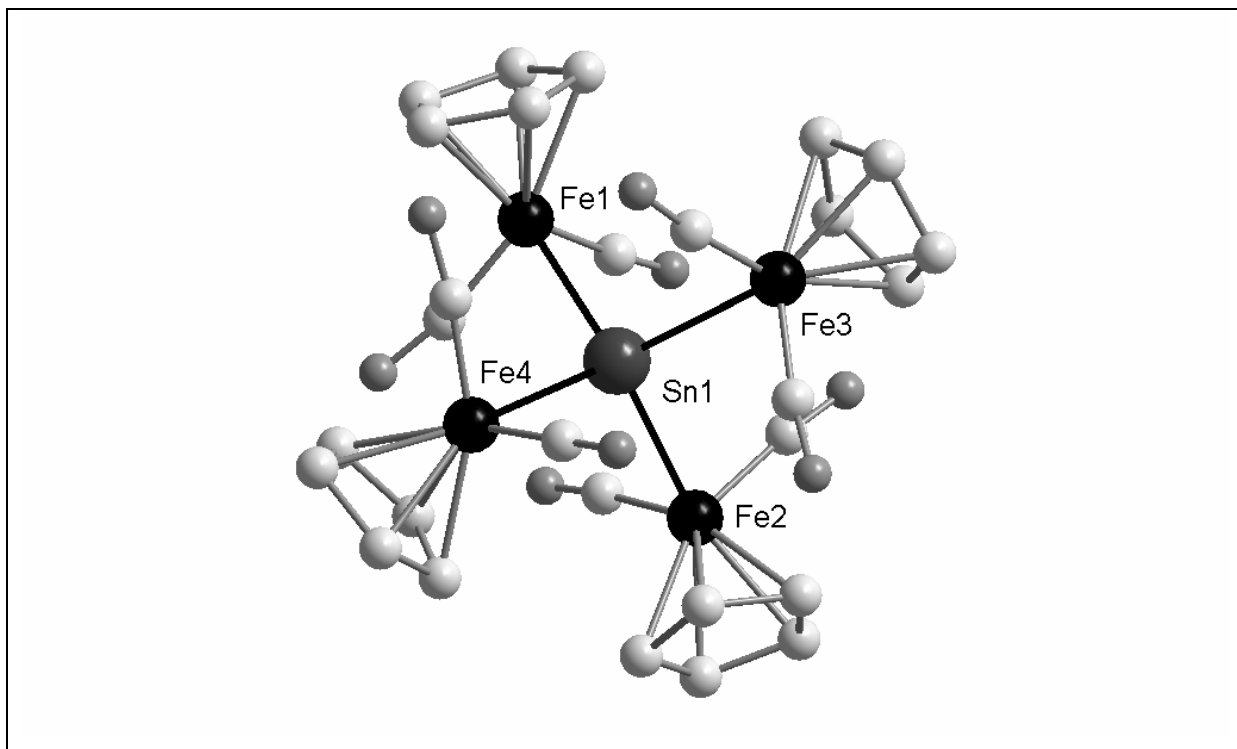


Figure 9: Molecular structure of $[\text{P}_4\text{Sn}]$ (**6**) in the crystal. H atoms have been omitted for clarity.

Table 4: Selected bond lengths [\AA] and angles [$^\circ$] in **6**.

Sn(1)-Fe(1)	2.726(3)	Sn(1)-Fe(2)	2.750(3)
Sn(1)-Fe(3)	2.718(3)	Sn(1)-Fe(4)	2.722(3)
Fe(1)-C _{Co}	1.75(3) ^a	Fe(1)-C _{Cp}	2.111(17) ^a
Fe(1)-Sn-Fe(2)	111.42(10)	Fe(1)-Sn-Fe(3)	110.73(11)
Fe(1)-Sn-Fe(4)	105.78(10)	Fe(2)-Sn-Fe(3)	105.47(10)
Fe(2)-Sn-Fe(4)	112.14(11)	Fe(3)-Sn-Fe(4)	111.42(10)

^a Mean value is given

In the crystal structure of **6**, the central tin atom is surrounded by four $\text{CpFe}(\text{CO})_2$ fragments, whereby the tin–iron bonds are arranged in distorted tetrahedral geometry. The Fe–Sn–Fe bond angles range from $105.47(10)^\circ$ to $112.14(11)^\circ$, with two of the six angles significantly less obtuse (Fe(1)–Sn–Fe(4): $105.78(10)^\circ$; Fe(2)–Sn–Fe(3): $105.47(10)^\circ$) than the remaining four. The Sn–Fe bond lengths vary significantly, ranging from 2.718(3) \AA to 2.750(3) \AA , and all four are inequivalent in the crystal, giving complex **6** an overall low symmetry (C_1) in the solid state. The average Sn–Fe bond distance of 2.729 \AA is considerably longer than the Sn–Fe bond distances of **4** (2.550(11) \AA) and **5** (2.6377(6) \AA , 2.6487(7) \AA), indicating possible electrostatic repulsion between the electropositive tin and iron centers. The

Sn-Fe bond distances in **6** are also significantly longer than those in the tetranuclear complex $[\text{ClSnFp}_2\text{Co}(\text{CO})_4]$ (2.568(3) Å, 2.575(2) Å), [100] which in contrast to complex **6**, contains one Sn-halide bond.

Several tin(IV) compounds supported by three transition-metal fragments are known, [101] generally containing at least one Sn-halide bond or Sn-carbon bond. However, pentanuclear complex **6** represents the first known homoleptic tin compound surrounded by four iron centers. The triironstannylene complex $[(\text{CO})_4\text{FeSnFp}_2]$ was generated *in situ* by the reaction of $[\text{Fp}_2\text{SnCl}_2]$ and trapped with pyridine to form the Lewis acid-base adduct $[(\text{CO})_4\text{Fe}\{\text{SnFp}_2(\text{py})\}]$, [102] with the intermediate and final product containing a tin(II) center with the Sn lone pair coordinated to the $\text{Fe}(\text{CO})_4$ fragment. However, no species involving four tin-iron bonds has been previously described, while the only other known pentanuclear tin complexes are the tetracobaltstannanes $[\text{Sn}\{\text{Co}(\text{CO})_4\}_4]$ [103] and $[\text{Sn}\{\text{Co}(\text{CO})_3\text{PR}_2\text{R}'\}_4]$ ($\text{R} = \text{R}' = n\text{Bu}$ [104], Ph [105], OMe, OPh, 2- SO_3^- - C_6H_4 · Na^+ [106]; $\text{R} = \text{Ph}$, $\text{R}' = 2\text{-SO}_3^-$ - C_6H_4 · Na^+ [106]), each featuring four Sn-Co bonds.

3.2 Investigations into tin-phosphorus compounds supported by bulky aryl groups

3.2.1 Background and research objective

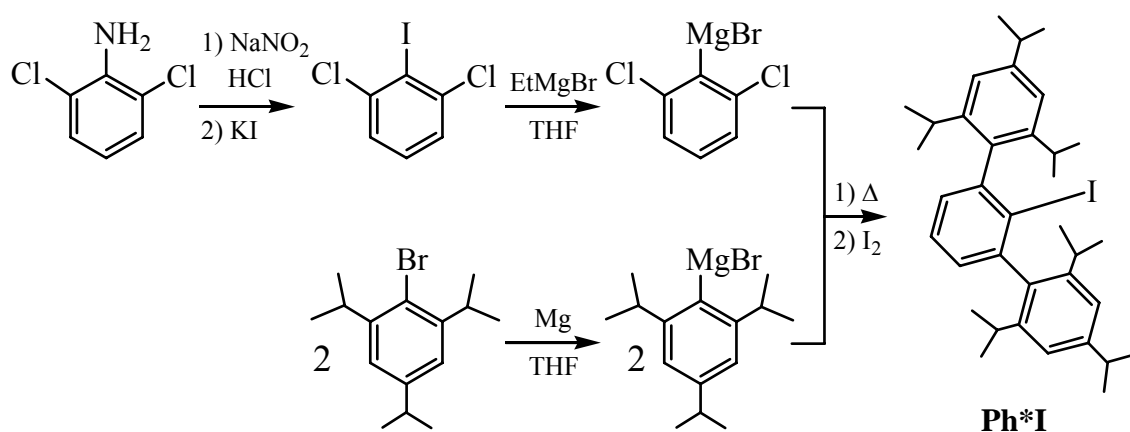
Tin-phosphorus compounds with low coordination at either tin ($CN \leq 3$) or phosphorus ($CN \leq 2$) are quite rare and can exhibit interesting bonding properties, usually in the form of Sn-P multiple bonding. Compounds leading to novel Sn-P multiple bonding have to date only been prepared from Sn(IV) starting materials. To this end, compounds of the form $R_2Sn(X)P(H)R$ have been deprotonated with a strong base, and salt elimination leads to the Sn=P double-bond species, whereby the oxidation state of tin does not formally change throughout the transformation. There are no examples in the literature that successfully make use of Sn(II) starting materials to accomplish Sn-P multiple bonding. While such oxidation approaches are more common for germanium, [107] precedent for such an approach to Sn-P multiple bonding is found in known oxidative reactions of Sn(II) compounds, e.g. $Sn[N(SiMe_3)_2]_2$, with organoazides RN_3 to give stannaimines of the type $\{(Me_3Si)_2N\}_2Sn=NR$. [108]

Investigations into the chemistry of tin(II)-phosphorus compounds have generally comprised only homoleptic Sn(II) phosphanides. This is clearly the result of the scarcity of monomeric Sn(II) starting materials with heteroleptic ligand sets, whereby one ligand is labile and the other stable against substitution. The frequent use of terphenyl-element starting materials has recently opened pathways to novel low-coordinate compounds (see Introduction). Specifically, Ph^*SnCl ($Ph^* = 2,6-Trip_2-C_6H_3$) was isolated and shown to be capable of adopting a monomeric form both in the solid state and in solutions at room temperature. [109]

The achievement of low-coordination in tin chemistry has unlocked new and unusual bonding situations. [110] The use of the Ph^* ligand on tin provides a unique heteroleptic template for preparing tin-phosphorus compounds with low-coordination geometries. With the relatively stable Sn-C_{aryl} bond anchoring the tin atom at one site, reactivity with phosphorus compounds can be probed at the remaining coordination sites. As a result, a heteroleptic terphenyl-tin phosphanide would represent an optimal precursor for the synthesis of Sn=P triple-bond compounds of the type $Ph^*Sn=P$, and experiments in the following chapter are directed toward this goal.

3.2.2 Preparation of Ph*SnCl

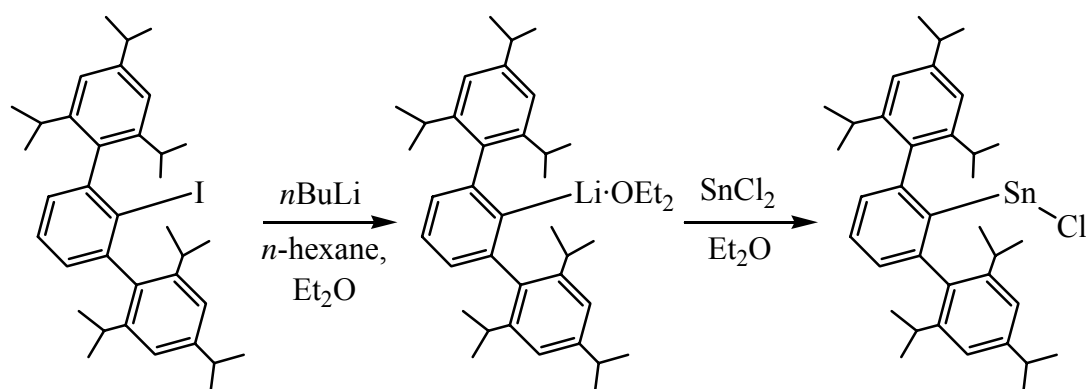
The preparation of Ph*I was reported by Power *et al.* by the route shown in Scheme 4. [111] Although there are various reports of commercial, while highly expensive, 2,6-dichloro-1-iodobenzene in the literature, none of the modern reports contains a detailed synthetic preparation. A complete procedure is given in the Experimental Section of this work and was devised using the literature preparation for the related 2,6-dibromo-1-iodobenzene as a guideline. [112] Thus, treatment of 2,6-dichloroaniline with NaNO₂ in concentrated HCl at low temperature generated the corresponding diazonium salt, which was quenched with excess KI and crystallized from toluene/EtOH to give 2,6-dichloro-1-iodobenzene in 70% yield. The melting point agreed well with the reported value, [113] and ¹H- and ¹³C-NMR data confirmed the high purity of the crystallized product.



Scheme 4: Preparation of Ph*I.

Starting from 2,6-dichloro-1-iodobenzene and commercial TripBr, the terphenyl iodide could be prepared on an approximate 25-gram scale following the literature procedure with slight modification (see Experimental Section). From Ph*I, lithiation with *n*BuLi in a mixture of *n*-hexane and Et₂O provides Ph*Li·OEt₂, from which Ph*SnCl is accessible via reaction with anhydrous SnCl₂. Although Ph*SnCl crystallizes in both the monomeric and Cl-bridged dimeric forms, it was possible to isolate the orange, monomeric compound by slow evaporation of the solvent from a clean solution of Ph*SnCl at low temperature (ca. -30°C) followed by slow warming of the highly concentrated solution to room temperature. While both dimeric and monomeric forms exist in equilibrium in solution, the dimeric form predominates at low temperature, but is highly soluble and stays in solution even at high

concentrations. As the temperature of a cold, concentrated solution approaches room temperature, the concentration of the less soluble monomeric form increases to form a supersaturated solution, from which Ph^*SnCl crystallizes immediately as large, orange blocks. The isolation of Ph^*SnCl in the monomeric form yields no synthetic advantage in subsequent steps, but mixtures of monomer and dimer do not crystallize in high yield; as a result, the advantage of isolating monomeric form lies only in the higher yield and greater ease of isolation.

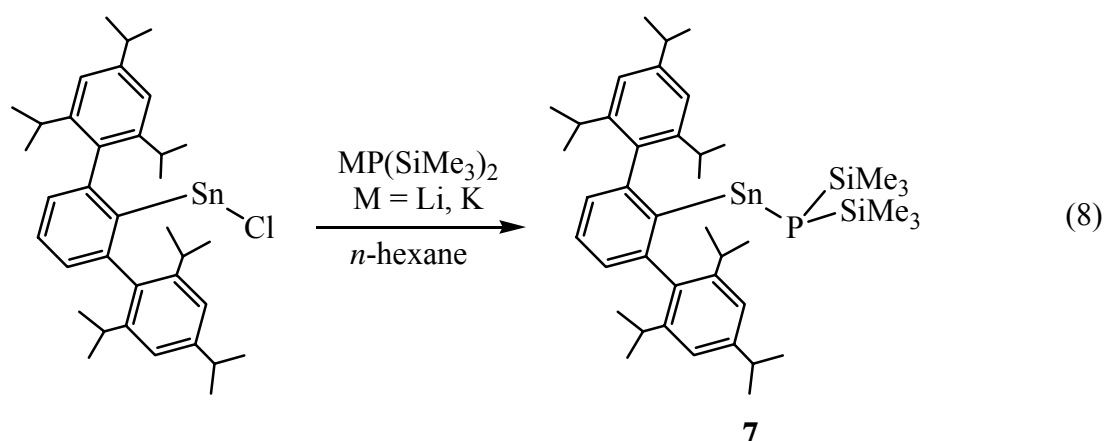


Scheme 5: Preparation of Ph^*SnCl

3.2.3 Reactions of Ph^*SnCl with alkali-metal phosphanides

3.2.3.1 Synthesis of $\text{Ph}^*\text{SnP}(\text{SiMe}_3)_2$ (7)

Treatment of orange Ph^*SnCl with either $\text{LiP}(\text{SiMe}_3)_2 \cdot 1.8\text{THF}$ or $\text{KP}(\text{SiMe}_3)_2$ in *n*-hexane at low temperature resulted in a rapid color change to intense violet. Allowing the solution to stir overnight at room temperature and recording a ^{31}P -NMR spectrum of the crude reaction mixture in C_6D_6 revealed formation of a major phosphorus-containing product resonating at a chemical shift of $\delta = -123.1$ ppm with poorly resolved tin satellites ($^1J_{\text{P117Sn}} = 1396$ Hz, $^1J_{\text{P119Sn}} = 1453$ Hz), as shown in Figure 10, along with traces of the hydrolysis product $\text{HP}(\text{SiMe}_3)_2$ ($\delta = -236.3$, $^1J_{\text{PH}} = 183$ Hz).



The total intensity of the tin satellites of the main product is 12%, which is slightly less than the total natural abundance for the ^{117}Sn and ^{119}Sn isotopes (16.3%), thus indicating formation of a monomeric species. It was previously shown in the products $[\text{Sn}\{\text{P}(\text{SiMe}_3)_2\}_2]_2$, which possesses two terminal and two bridging $\text{P}(\text{SiMe}_3)_2$ ligands, and $\text{Sn}[\text{P}(\text{SiPh}_3)_2]_2$, which possesses exclusively terminal $\text{P}(\text{SiPh}_3)_2$ ligands, that the respective ^{31}P -NMR signals for terminal and bridging phosphonate ligands bear tin satellites with intensities in the ranges of 14-16% and 26-27%, respectively. [16,17] Thus, it can be reasonably concluded that the new product exists in the monomeric conformation, formulated as $\text{Ph}^*\text{SnP}(\text{SiMe}_3)_2$ (**7**), which was isolated upon work-up as violet crystals in moderate yield.

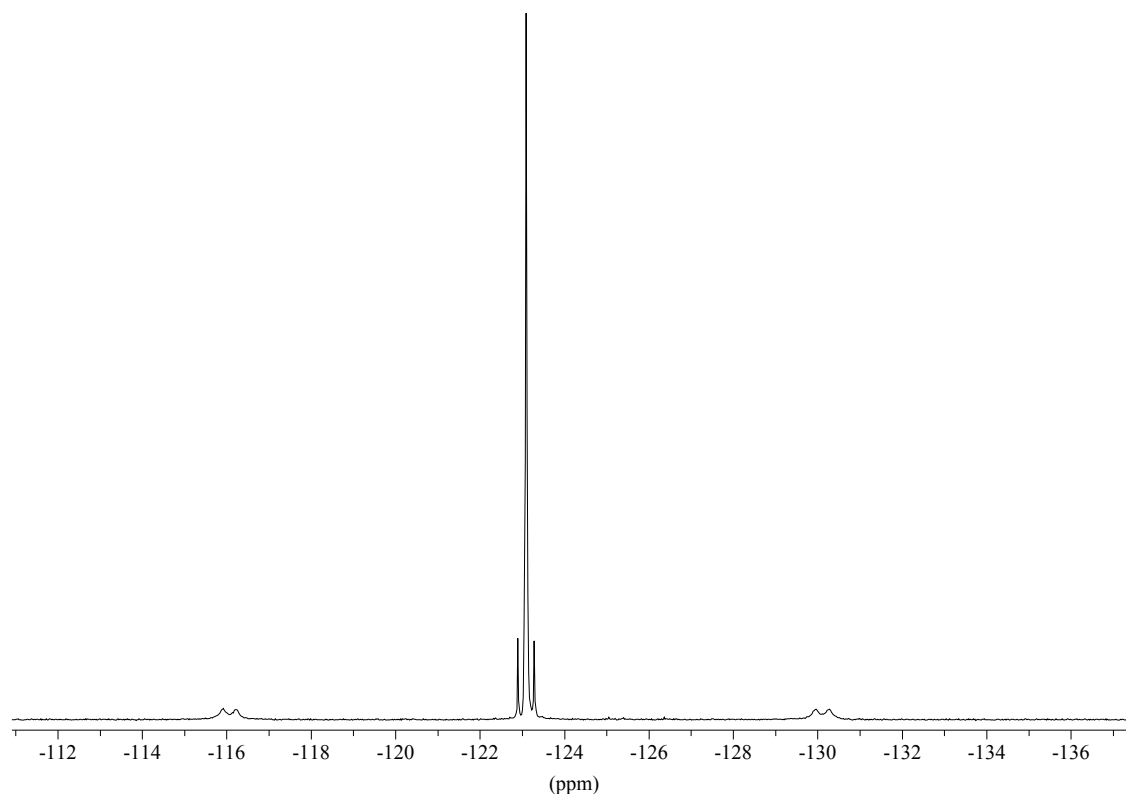


Figure 10: ^{31}P -NMR signal from $\text{Ph}^*\text{SnP}(\text{SiMe}_3)_2$ (**7**) in C_6D_6 .

In the ^{31}P -NMR spectrum of **7**, the observed ^{117}Sn and ^{119}Sn satellites are accompanied by an additional set of satellites of significantly lower coupling. These satellites were attributed to coupling to the silyl ^{29}Si nuclei ($^1J_{\text{PSi}} = 37.8$ Hz), and this assignment was verified by a ^{29}Si -NMR spectrum of **7**, in which a doublet was observed at $\delta = 4.08$ ppm with a coupling constant of $^1J_{\text{SiP}} = 38.5$ Hz. The ^{119}Sn -NMR spectrum of **7** reveals a doublet at $\delta = 1919$ ppm ($^1J_{\text{SnP}} = 1453$ Hz). The appearance of the signal as a doublet indicates the presence of only one phosphorus atom bound to the tin atom and confirms the formulation of **7** as a monomer. The chemical shift lies in the extreme downfield region and is consistent with the low coordination number of tin. [114] The value of 1919 ppm is significantly downfield of the amide analogue $\text{Ph}^*\text{SnN}(\text{SiMe}_3)_2$ ($\delta = 1140$ ppm) [115] and represents one of the lowest-field ^{119}Sn -NMR signals known for aryltin compounds. Related arylstannylene compounds that have recently been shown to possess extraordinarily low-field ^{119}Sn signals include $\text{Ph}^*\text{Sn}t\text{Bu}$ ($\delta = 1904$ ppm) [116], $[\text{CpCr}(\text{CO})_3\text{SnPh}^*]$ ($\delta = 2298$ ppm) [117], and $(\text{Ph}^*\text{Ph}_2\text{Sn})\text{Sn}$ (3752 ppm for the central tin atom) [118]. The latter approaches the shift found for $[\{(\text{CO})_5\text{Cr}\}_3\text{Sn}]^{2-}$ ($\delta = 3924$ ppm) [119], which corresponds to the current record for low-field ^{119}Sn shifts.

$\text{Ph}^*\text{SnP}(\text{SiMe}_3)_2$ represents the first aryltin(II) phosphanide as well as the first heteroleptic tin(II) phosphanide to be isolated as a monomer. **7** is soluble in common hydrocarbon solvents and decomposes to unknown products in the presence of halogenated solvents. In *n*-hexane solution, **7** is thermally stable, exhibiting no change according to ^{31}P -NMR after 3 hours at 68°C . Solutions of **7** decompose upon exposure to minor traces of oxygen to such an extent that handling under an argon atmosphere is recommendable in place of dinitrogen. **7** is stable in the presence of THF and pyridine, indicating a lack of access to the tin center by donor ligands as a result of steric constraints; in contrast, treatment of the sterically more accessible Ph^*SnCl with pyridine results in immediate discoloration due to formation of the adduct $\text{py}\cdot\text{Sn}(\text{Cl})\text{Ph}^*$. [109]

The ^1H - and ^{13}C -NMR spectra of **7** strongly resemble those for the related amide $\text{Ph}^*\text{SnN}(\text{SiMe}_3)_2$. Hindered rotation about the $\text{C}_{\text{aryl}}\text{-C}_{\text{aryl}}$ bonds is indicated by the inequivalence of the *ortho*-*i*Pr groups of the terphenyl ligand. The ^{13}C chemical shift of the *ipso*- C_6H_3 carbon is found in the downfield region ($\delta = 181.31$ ppm), a property characteristic of known aryl stannylenes. For the protons and carbon atoms of the silyl groups, coupling to phosphorus was observed ($^3J_{\text{HP}} = 4.0$ Hz, $^2J_{\text{CP}} = 9.5$ Hz), but no tin coupling could be detected.

The EI mass spectrum of **7** revealed the molecular ion peak along with a fragmentation pattern indicating first loss of the silyl groups and successive loss of phosphorus and tin and ultimately fragmentation of the terphenyl ligand.

Structure of $\text{Ph}^*\text{SnP}(\text{SiMe}_3)_2$ (**7**)

Violet crystals of **7** were grown from concentrated solutions of *n*-hexane at -25°C , and an X-ray diffraction analysis was carried out. **7** crystallizes in the triclinic space group $P\bar{1}$. The molecular structure is shown in Figure 11, and selected bond lengths and angles are given in Table 5.

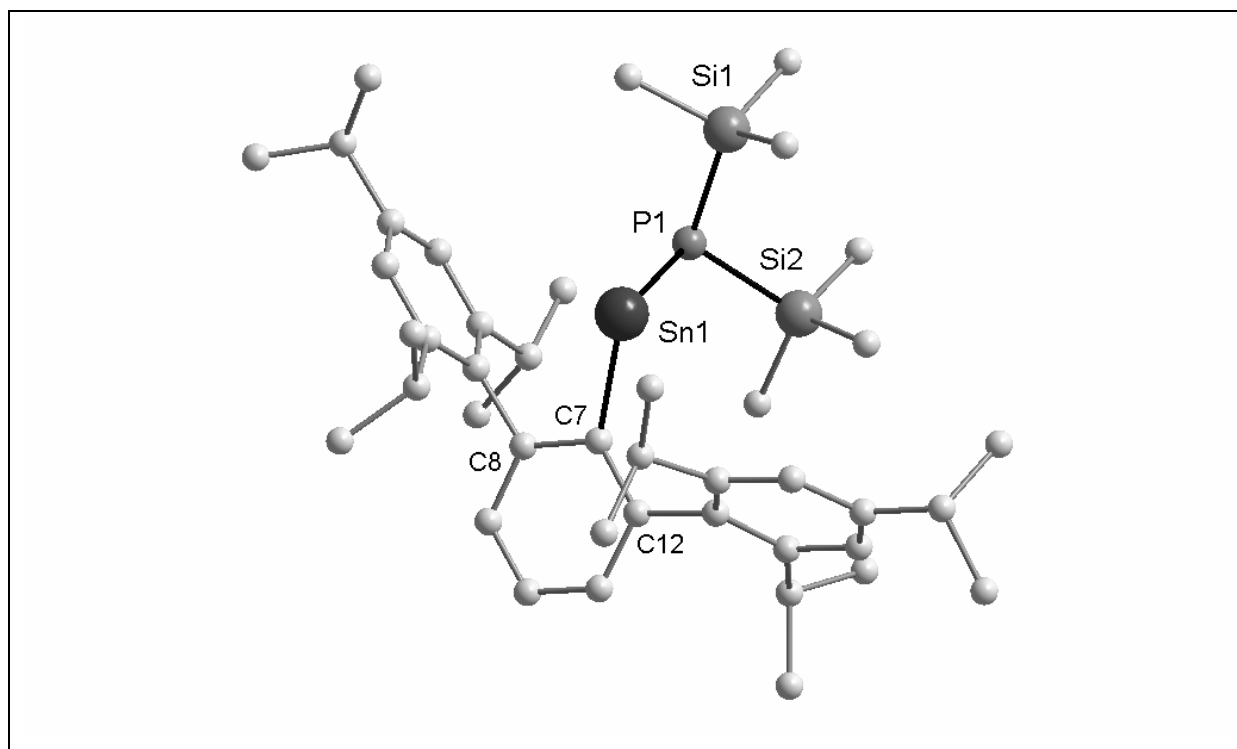


Figure 11: Molecular structure of $\text{Ph}^*\text{SnP}(\text{SiMe}_3)_2$ (**7**) in the crystal. H atoms have been omitted for clarity.

Table 5: Selected bond lengths [\AA] and angles [$^\circ$] in **7**.

Sn-P	2.528(1)	Sn-C _{ipso}	2.226(4)
P-Si(1)	2.245(2)	P-Si(2)	2.241(2)
C _{ipso} -C(8)	1.402(5)	C _{ipso} -C(12)	1.410(4)
C _{ipso} -Sn-P	105.56(9)	Si(1)-P-Si(2)	110.72(7)
Si(1)-P-Sn	97.34(5)	Si(2)-P-Sn	110.05(5)
C(8)-C _{ipso} -Sn	110.6(2)	C(12)-C _{ipso} -Sn	128.1(3)
C(8)-C _{ipso} -C(12)	118.9(3)		

In the crystal structure of **7**, the tin atom possesses a coordination number of 2 and lies in a bent geometry ($\text{C}_{\text{ipso}}\text{-Sn-P}$: $105.56(9)^\circ$), which is a characteristic feature for structurally characterized stannylene compounds. The angle about tin is more obtuse than that in Ph^*SnCl ($\text{C}_{\text{ipso}}\text{-Sn-Cl}$: 99.67°), [109] attributable in part to the larger steric bulk of the silylphosphanyl ligand compared to chloride. The phosphorus atom is located in a distorted trigonal pyramidal geometry between the tin atom and two silicon atoms. Since the P atom does not approach planarity, it can be concluded that the phosphorus lone pair does not participate significantly in donation to the Sn center. This correlates well with the tin-phosphorus coupling constants ($^1J_{\text{P117Sn}} = 1396 \text{ Hz}$, $^1J_{\text{P119Sn}} = 1453 \text{ Hz}$), which are well below the range for compounds

known to exhibit tin-phosphorus double bonding ($^1J_{\text{PSn}} \approx 2000$ Hz). The Sn-P bond length in **7** (2.528(1) Å) is slightly shorter than the Sn-P bond lengths found in **4** (2.568(2) Å) and **5** (2.590(1) Å, 2.612(1) Å). Structurally characterized tin compounds with *terminal* phosphanide ligands are exceedingly rare, offering very little basis for comparison. Even the compounds possessing Sn=P double bonds (see Introduction) are not accompanied by crystallographic data. A relevant terminal *t*Bu₂P ligand is bound to tin in the anionic complex Li(thf)[Sn(P*t*Bu₂)₃] [10] and displays a considerably longer Sn-P bond length (2.702(3) Å) than that in **7**. A question concerning the Sn-P bond order in **7** arises in light of the literature description of analogous carbene compounds RCPR₂ as having three resonance forms: RC-PR₂ ↔ RC⁻=P⁺R₂ ↔ RC≡PR₂. [120] These carbene resonance forms range from having a C-P single bond to the zwitterionic form with a C=P double bond to the C≡P triple-bond description. Similar resonance forms could be considered for the stannylene analogue **7**. The Sn-P bond distance has been calculated for the compounds Ar''Sn≡P and Sn=PAr'' (Ar'' = 2,6-{2,4,6-[(H₃Si)₃C]₃-C₆H₂]₂-C₆H₃) at the ONIOM(B3LYP/LANL2DZ:PM3) level and revealed a distance of 2.481 Å for Ar''Sn≡P and 2.527 Å for Sn=PAr''. [55] The Sn-P bond distance for compound **7** lies close to that calculated for the hypothetical double-bond compound Sn=PAr''; however, the geometry about P and the spectroscopic data are more in line with single-bond character for **7**.

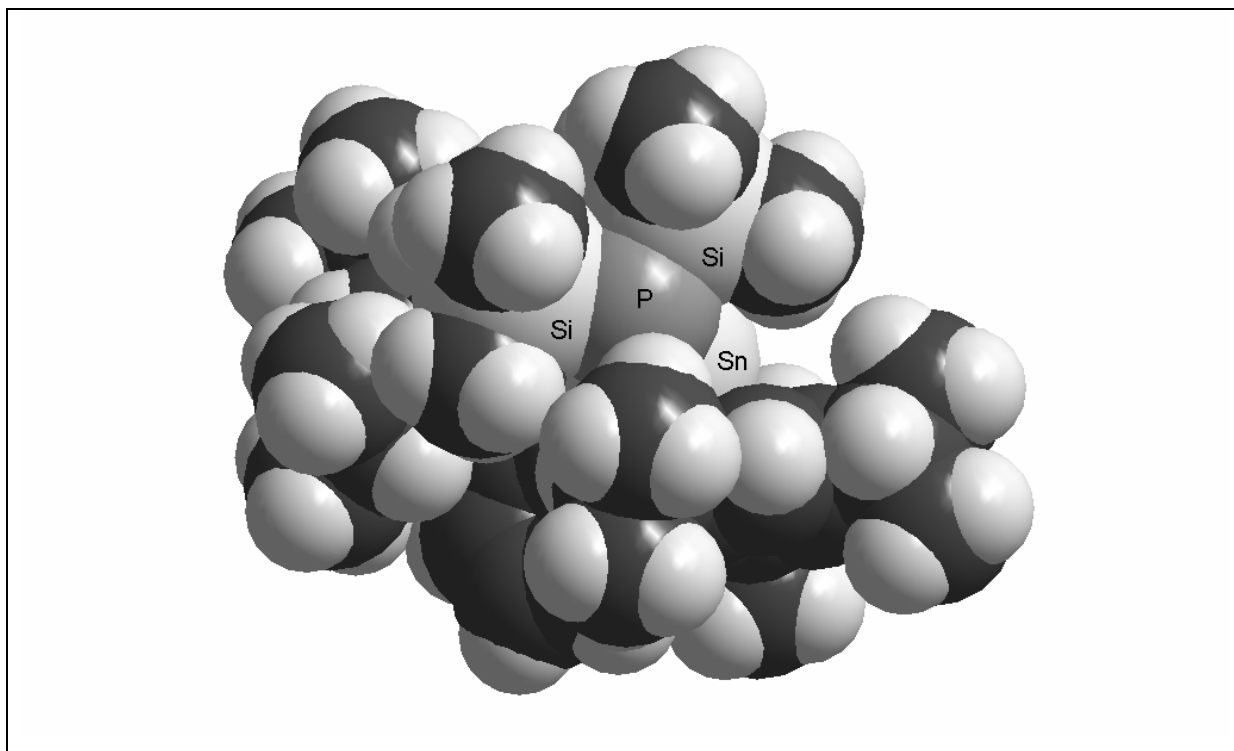
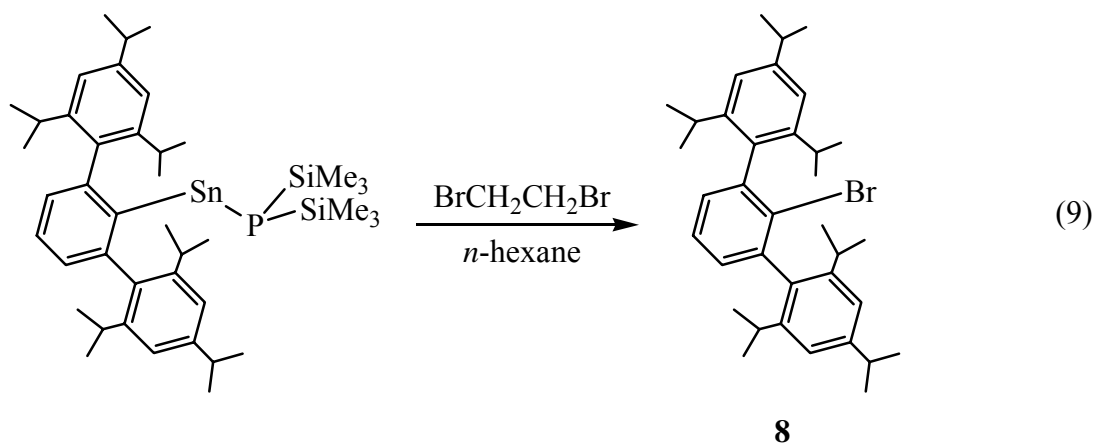


Figure 12: Space-filling model of the molecular structure of Ph*SnP(SiMe₃)₂ (**7**).

The bulky nature of the Ph* ligand allows the isolation of the terminal stannylene phosphanide **7**. The space-filling model in Figure 12 shows the tin atom to be nearly completely protected by the terphenyl ligand, while the phosphorus atom, though protected by the bulky silyl groups, is relatively exposed. As such, the reactivity of Ph*SnP(SiMe₃)₂ would be expected to take place predominantly at the Sn–P and P–Si bonds, while the C_{aryl}–Sn bond would be expected to remain relatively inert.

3.2.3.2 Reactivity of Ph*SnP(SiMe₃)₂ (**7**)

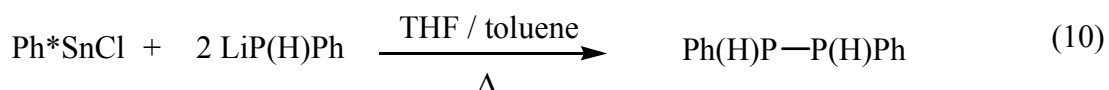
Given the wealth of oxidative reactions of bivalent tin amides with organic halides, transition-metal halides, [121] acid chlorides/anhydrides [122], and chalcogens [123], among others, to give well-defined Sn(IV) addition products, it was expected that chemical oxidation of Ph*SnP(SiMe₃)₂ would be feasible. A host of reagents bearing halides or pseudohalides were selected such that either spontaneous or thermal silane elimination would be viable upon oxidation, and formation of Ph*Sn=P or Ph*Sn=P→ML_n would be conceivable. However, low-temperature reactions of Ph*SnP(SiMe₃)₂ with C₂Cl₆, Cp₂Ti(OTf)₂, Hg(OTf)₂, Tl(OOCCF₃)₃, benzoyl chloride, Me₃NO, and tropylium tetrafluoroborate each resulted in cleavage of the Sn–P bond and generation of an intractable mixture of products, according to ³¹P-NMR spectra of the respective crude reaction mixtures. Reaction of Ph*SnP(SiMe₃)₂ with BrCH₂CH₂Br at low temperature resulted in gradual discoloration of the violet solution to a clear beige. The ³¹P-NMR spectrum revealed a main phosphorus-containing product (> 65%) at δ –167.2 ppm with tin satellites (¹J_{P117Sn} = 1719 Hz, ¹J_{P119Sn} = 1799 Hz). Work-up of the solution and crystallization from *n*-hexane afforded colorless crystals of Ph*Br, [124] as identified by an X-ray diffraction experiment.



The P-containing compound corresponding to the main ^{31}P resonance could not be isolated from the other minor products upon repeated attempts at recrystallization, as compound **8** crystallized out preferentially from each attempt. The formation of Ph^*Br attests to the instability of the $\text{C}_{\text{aryl}}\text{--Sn}$ bond toward strong oxidizing reagents.

3.2.3.3 Reactions of Ph^*SnCl with LiP(H)Ph , LiP(H)Trip , and Li_2PTrip

While the preliminary reactivity studies on $\text{Ph}^*\text{SnP(SiMe}_3)_2$ revealed a lack of robustness in preserving the tin and phosphorus groups about the protective terphenyl ligand, alternative systems involving comparatively inert $\text{P--C}_{\text{aryl}}$ bonds were considered. Thus, reaction of Ph^*SnCl with the primary phenyl phosphanide, LiP(H)Ph , was anticipated to afford the monomeric arylstannylene phosphanide, $\text{Ph}^*\text{SnP(H)Ph}$, with a phenyl group and reactive proton at the phosphorus atom. Stable stannylene phosphanides with P--H bonds have thus far not been reported in the literature. In light of experiments by Schrock and co-workers, in which treatment of sterically protected tris(amido)amine tungsten(IV) and molybdenum(IV) complexes with LiP(H)Ph at elevated temperatures led serendipitously to triply bonded phosphido ligands [125,126], the reaction of Ph^*SnCl with LiP(H)Ph was initially carried out under the same conditions reported for those transformations.

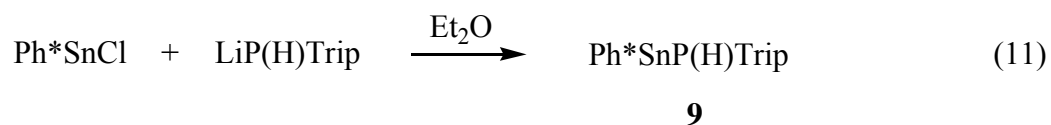


Reaction of Ph^*SnCl with two equivalents of LiP(H)Ph in a mixture of toluene/THF (3:1) at 80°C revealed the formation of the 1,2-diphenyldiphosphane, Ph(H)P--P(H)Ph , as the main product as indicated by ^{31}P -NMR ($\delta = -65.87$ ppm, -69.33 ppm). [127] The formation of Ph(H)P--P(H)Ph represents a formal oxidation of the LiP(H)Ph reagent, or it could also be explained as a metal-halogen exchange between the Sn and P reagents. P–P bond-forming reactions induced by main-group elements have been intensively explored by the Wright group, and it has been observed that the remarkable strength of the P–P bond is a driving force in these reactions. [24] Similar P–P bond-forming transformations have also been observed in reactions of cyclopentadienyl-substituted phosphanides with Zr(IV) salts. [128]

Attempts were made to treat Ph^*SnCl with LiP(H)Ph at low temperature in order to stabilize any formed tin-phosphorus products before formation of Ph(H)P--P(H)Ph . Thus, reaction of Ph^*SnCl with only one equivalent LiP(H)Ph in *n*-hexane starting at -78°C was

carried out. The ^{31}P -NMR spectrum of the crude reaction mixture revealed minimal amounts of $\text{Ph}(\text{H})\text{P}-\text{P}(\text{H})\text{Ph}$, showing that high temperatures are not required for P–P bond formation, along with a signal tentatively attributable to $\text{Ph}^*\text{SnP}(\text{H})\text{Ph}$ ($^{31}\text{P}\{^1\text{H}\}$ -NMR: $\delta = -120.9$ ppm; $^1J_{\text{P}117\text{Sn}} = 946$ Hz, $^1J_{\text{P}119\text{Sn}} = 1014$ Hz; tin satellite intensity = 19%) due to the proximity of its shift and poor resolution of its tin satellites similar to those of $\text{Ph}^*\text{SnP}(\text{SiMe}_3)_2$. Upon proton coupling, a higher-order spin system is observed, in which the signal is split into a doublet with less intense peaks in between, which may signify a phosphanide-bridged structure. The P–H coupling is here calculated based on the more intense doublet peaks ($^1J_{\text{PH}} = 296$ Hz). As the main product of the reaction, a signal of unknown identity was observed with two sets of tin satellites ($^{31}\text{P}\{^1\text{H}\}$ -NMR: $\delta = -100.9$ ppm; $^1J_{\text{P}117\text{Sn}(1)} = 1198$ Hz, $^1J_{\text{P}119\text{Sn}(1)} = 1252$ Hz; $^1J_{\text{P}117\text{Sn}(2)} = 1546$ Hz, $^1J_{\text{P}119\text{Sn}(2)} = 1617$ Hz, total tin satellite intensity = 18%), which showed a higher-order system similar to that of the previous signal upon proton coupling ($^1J_{\text{PH}} = 382$ Hz). The isolation of the compound corresponding to this latter signal was not possible through repeated attempts at recrystallization.

Since the reaction of Ph^*SnCl with $\text{LiP}(\text{H})\text{Ph}$ showed a lack of selectivity even at low temperatures, a larger aryl group at phosphorus was chosen to bolster the selectivity. Thus, reaction of Ph^*SnCl with $\text{LiP}(\text{H})\text{Trip}$ was carried out in Et_2O at low temperature. The crude $^{31}\text{P}\{^1\text{H}\}$ -NMR spectrum revealed a relatively clean reaction mixture with a slightly broadened main signal (ca. 70%, $\Delta\nu_{1/2} = 150$ Hz) attributable to $\text{Ph}^*\text{SnP}(\text{H})\text{Trip}$ (**9**) ($\delta = -70.9$ ppm, $^1J_{\text{P}117/119\text{Sn}} = 934$ Hz), which was split into a doublet upon proton coupling ($^1J_{\text{PH}} = 186$ Hz), along with traces of $\text{Trip}(\text{H})\text{P}-\text{P}(\text{H})\text{Trip}$ ($\delta = -113.9$ ppm) and TripPH_2 ($\delta = -158.3$ ppm) as the only other phosphorus-containing products.



The generation of $\text{Trip}(\text{H})\text{P}-\text{P}(\text{H})\text{Trip}$ mirrors the formation of $\text{Ph}(\text{H})\text{P}-\text{P}(\text{H})\text{Ph}$ above and has been previously described so far only in P–P coupling transformations at Mo(V) centers. [129] The color of the proposed product **9** is intense violet, the same color as for the analogous bis(trimethylsilyl)phosphanide, $\text{Ph}^*\text{SnP}(\text{SiMe}_3)_2$ (**7**).

The $^{31}\text{P}\{^1\text{H}\}$ -NMR signal from **9** is a singlet with unresolved $^{117/119}\text{Sn}$ satellites. The proton-coupled ^{31}P -NMR signal (Figure 13) is a doublet with two sets of unresolved $^{117/119}\text{Sn}$ satellites. The observation of unresolved $^{117/119}\text{Sn}$ satellites is reminiscent of the poorly resolved satellites observed in the ^{31}P signal for **7**. The total tin satellite intensity for the signal

from **9** is 12%, which is in the lower range of the total abundance of ^{117}Sn and ^{119}Sn and therefore indicates a monomeric species in which the TripP(H) ligands are not bridging the tin centers through the phosphorus lone pairs. Attempts to isolate compound **9** through fractional crystallization were unsuccessful even from highly concentrated solutions at extremely low temperature (-78°C), perhaps due to the exceptional solubility of the compound.

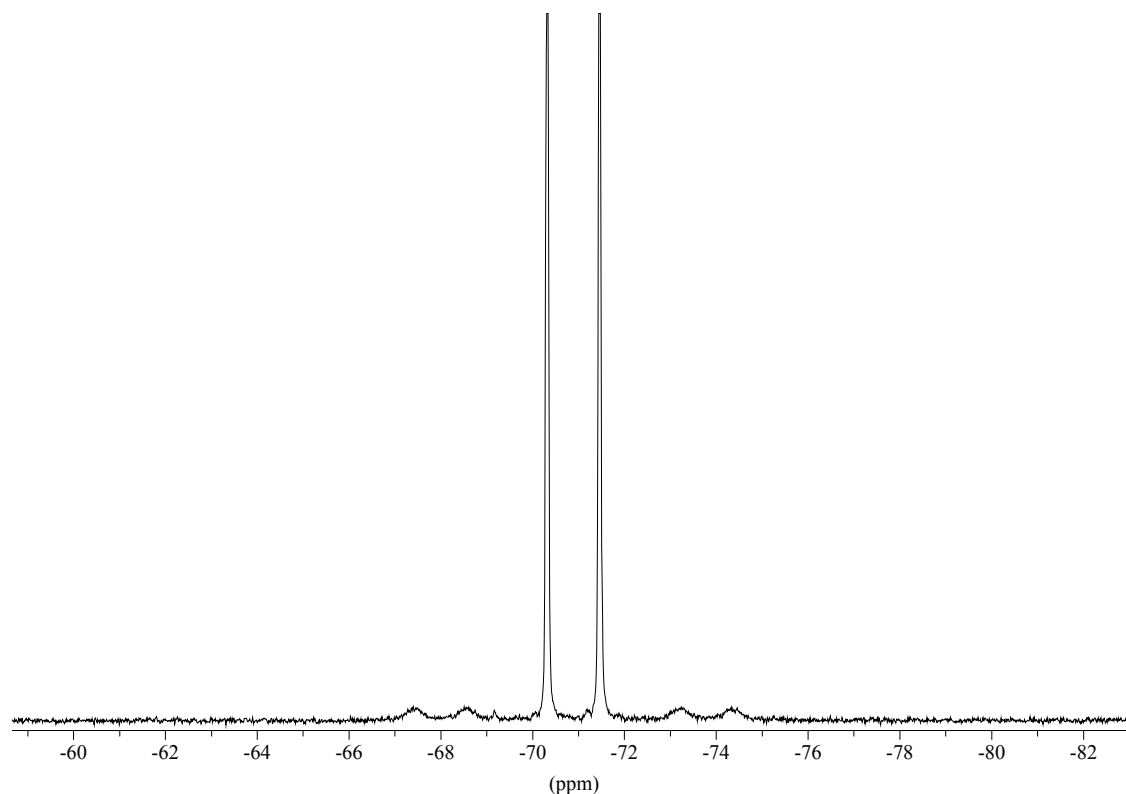


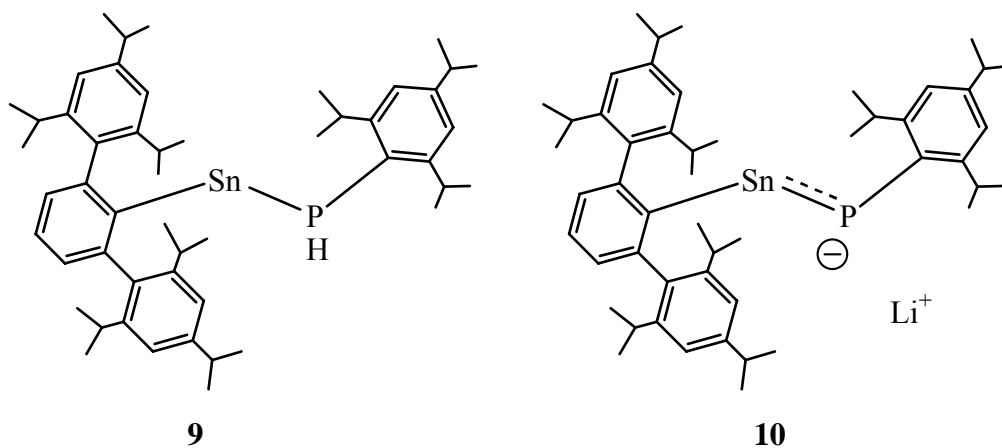
Figure 13: ^{31}P -NMR signal attributed to $\text{Ph}^*\text{SnP(H)Trip}$ (**9**) in C_6D_6 .

Experiments aimed at deprotonating *in situ* generated $\text{Ph}^*\text{SnP(H)Trip}$ with *n*BuLi produced a mixture of unidentified products according to ^{31}P -NMR. In recognition of the possibility of nucleophilic attack of *n*BuLi on the tin center, a route was chosen to circumvent the direct use of *n*BuLi with the stannylene. Thus, TripPH_2 was twice deprotonated by *n*BuLi, and the resulting doubly lithiated phosphanide Li_2PTrip was added to Ph^*SnCl . According to ^{31}P -NMR, a mixture of products was generated, from which Trip(H)P-P(H)Trip could be identified (ca. 20%). The main product (ca. 40%) was observed as a broad downfield signal proposed tentatively here to be $\text{Li}^+[\text{Ph}^*\text{SnPTrip}]^-$ (**10**) ($\delta = 229.7$ ppm, $\Delta\nu_{1/2} = 280$ Hz, $^1J_{\text{P}^{117}\text{Sn}} = 1735$ Hz, $^1J_{\text{P}^{119}\text{Sn}} = 2004$ Hz). The broadness of the observed signal is a characteristic

indicator for lithium-coordinated anions, where the lithium shifts rapidly between ion-contact and ion-separated forms. No P-H coupling was observed in the proton-coupled spectrum.

The attempts to produce $\text{Li}^+[\text{Ph}^*\text{SnPTrip}]^-$ (**10**) by lithiation of $\text{Ph}^*\text{SnP(H)Trip}$ (**9**) with $n\text{BuLi}$ did not result in observation of the downfield signal observed in the reaction of Ph^*SnCl with Li_2PTrip . Instead, Trip(H)P-P(H)Trip was formed in ca. 30%, TripPH_2 was observed in ca. 20%, and an unidentified signal with resolved tin satellites ($\delta = -182.8$ ppm, $^1J_{\text{P117Sn}} = 717$ Hz, $^1J_{\text{P119Sn}} = 741$ Hz), which split into a doublet upon proton coupling ($^1J_{\text{PH}} = 206$ Hz) was observed in ca. 35% intensity.

The low-field ^{31}P -NMR shift of proposed compound **10** and the large $^1J_{\text{P117/119Sn}}$ coupling constants signify a situation of multiple bonding between tin and phosphorus. The bonding about tin and phosphorus in the anionic moiety $[\text{Ph}^*\text{SnPTrip}]^-$ is isoelectronic to the neutral compound $\text{Ph}^*\text{Sb=PMes}$ with a known double bond. [53] $[\text{Ph}^*\text{SnPTrip}]^-$ can also be thought of as isolobal to the doubly reduced acetylene analogue $[\text{Ph}^*\text{Sn}=\text{SnPh}^*]^{2-}$, which has been suggested as having a $\text{Sn}=\text{Sn}$ double bond, [51h] as well as isolobal to the general family of dipnictenes $\text{RE}=\text{ER}$ ($\text{E} = \text{P}, \text{As}, \text{Sb}$), each with undisputed double-bond character. [130] The bonding between Sn and P is tentatively represented in Scheme 6 with a bond order greater than one, with the possibility that double bonding is the more accurate description for anionic compounds of the form $[\text{ArSnPAr}]^-$.



Scheme 6: Proposed structures for $\text{Ph}^*\text{SnP(H)Trip}$ (**9**, left) and $\text{Li}^+[\text{Ph}^*\text{SnPTrip}]^-$ (**10**, right).

Theoretical Considerations for $\text{Li}^+[\text{Ph}^*\text{SnPTrip}]^-$ (**10**)

In light of the proposed composition of compound **10**, an interesting question arises about the bonding situation in such a structure. A Sn(II) compound in which both the tin and phosphorus atoms are two-coordinate is so far unprecedented, as all known doubly bonded

Sn=P species are three-coordinate at the tin atom. As noted above, the Sn-P bonding in anionic compound **10** is expected to be isolobal to dianionic $[\text{ArSnSnAr}]^{2-}$ or neutral $[\text{ArPPAr}]$. Three interesting considerations for **10** are the energetically lowest molecular geometry about tin and phosphorus, the appearance of the frontier molecular orbitals, and the charge distribution within the anionic compound. Calculations were carried out² on the model compound $[\text{PhSnPPh}]^-$ using the Gaussian 03 program [131] at the DFT-B3LYP/RB level with the SDD effective core potential for the Sn atom. In the current study, the lithium counterion was not considered in order to rule out influence of contacts between the lithium cation and anionic portions of $[\text{PhSnPPh}]^-$.

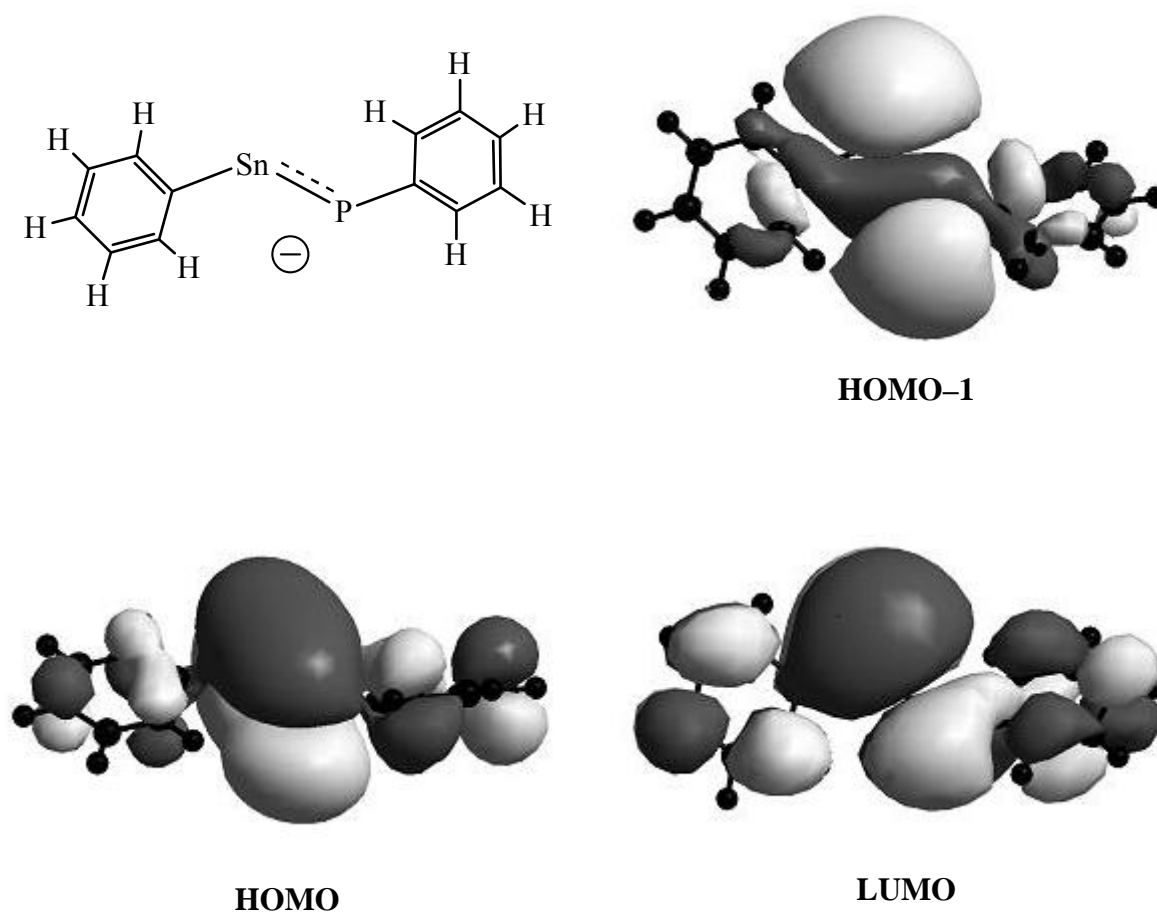


Figure 14: Molecular orbitals for model compound $[\text{PhSnPPh}]^-$. Upper left: graphical representation of anion considered; upper right: HOMO-1; lower left: HOMO; lower right: LUMO.

² Calculations were carried out by Fabian Dielmann in the Scheer group, University of Regensburg.

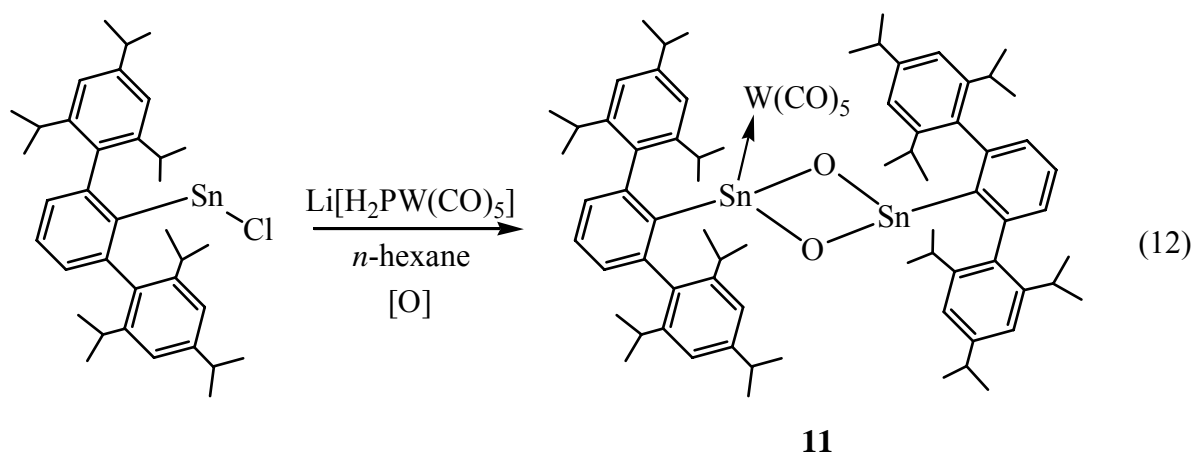
The calculated structure of $[\text{PhSnPPh}]^-$ resulted in a *trans*-bent orientation of the phenyl ligands, which are slightly rotated relative to one another. The $\text{C}_{\text{aryl}}\text{-Sn-P}$ and $\text{Sn-P-C}_{\text{aryl}}$ angles in the optimized structure are 94.3° and 103.2° , respectively. The angle about tin is considerably less obtuse than that in compound **7** ($105.56(9)^\circ$), which could be attributed partially to the lower degree of steric bulk of Ph in comparison to Ph^* . In Figure 14, the orbital iso-surfaces for the frontier molecular orbitals are represented. The HOMO–1 (upper right) and HOMO (lower left) are of the bonding σ - and π -types, respectively, while the LUMO (lower right) is of the antibonding π^* -type. This situation is in agreement with the view of $[\text{PhSnPPh}]^-$ having an $\text{Sn}=\text{P}$ double bond, though a concrete bond order cannot be assigned from these data. Furthermore, the molecular orbital representations reveal participation of the phenyl groups in the Sn-P bonding, particularly in the π -type and π^* -type orbitals, which is an indication of the stabilization aryl groups offer to such multiply bonded systems. The Mulliken atomic charges in $[\text{PhSnPPh}]^-$ were calculated to be +0.12 for Sn and –0.25 for P, while the remainder of the overall negative charge is distributed throughout the phenyl groups (avg. charge on C: –0.23; avg. charge on H: +0.20). The negative charge is weighted slightly more heavily toward the phosphorus-bound phenyl group (total = –0.45) than the tin-bound phenyl group (total = –0.42). The distribution of charge throughout the phenyl groups also demonstrates an aspect of the stabilization of aryl groups in multiply bonded anionic main-group moieties.

3.2.3.4 Reaction of Ph^*SnCl with $\text{Li}[\text{H}_2\text{PW}(\text{CO})_5]$

In order to probe the possibility of preparing a monomeric aryl stannylene with reactive P-H bonds and without organic substituents at phosphorus, Ph^*SnCl was treated with $\text{Li}[\text{H}_2\text{PW}(\text{CO})_5]$ in *n*-hexane at -78°C . The orange solution gradually became light red, and overnight stirring produced a beige-red solution. The $^{31}\text{P}\{^1\text{H}\}$ - and ^{31}P -NMR spectra for the crude reaction mixture were recorded in C_6D_6 and revealed an array of 6 main phosphorus-containing products in approximately equal proportions. One signal at –187 ppm bears tungsten satellites ($^1J_{\text{PW}} = 213$ Hz) and is split into a quartet in the proton-coupled spectrum ($^1J_{\text{PH}} = 342$ Hz) and is assigned as $[\text{H}_3\text{PW}(\text{CO})_5]$. Formation of $[\text{H}_3\text{PW}(\text{CO})_5]$ mimics the previously observed behavior of $\text{Li}[\text{H}_2\text{PW}(\text{CO})_5]$ in the presence of SnCl_2 or $[\text{H}_3\text{PW}(\text{CO})_5]$ in the presence of $\text{Sn}[\text{N}(\text{SiMe}_3)_2]_2$ (cf. Section 3.1.2). Each of the remaining five signals is split into triplets in the proton-coupled ^{31}P -NMR spectra, indicating preservation of the intact PH_2 unit. One signal at –226 ppm bears one set of ^{183}W satellites ($J_{\text{PW}} = 157$ Hz) and no tin satellites. Another signal at –206 ppm bears two sets of ^{183}W satellites ($J_{\text{PW}} = 195, 391$ Hz)

and no tin satellites. Two further signals at -251 ppm and -269 ppm bear tin satellites ($J_{\text{P117/119Sn}} = 760$ Hz and $J_{\text{P117/119Sn}} = 621$ Hz, respectively) and no tungsten satellites; the phosphorus-tin coupling for these latter signals lies in the normal range of known Sn(IV) phosphanides, whereas such coupling for Sn(II) phosphanides normally falls within the range of 800 to 1500 Hz. The final signal at -164 ppm bears no observable tungsten or tin satellites.

From the ^{31}P -NMR data, it would seem clear that a large extent of ligand exchange is occurring, specifically in the cases where tin satellites are observed but no tungsten satellites. Repeated crystallization of the filtered reaction mixture yielded colorless crystals of $[\text{H}_3\text{PW}(\text{CO})_5]$, as evidenced by mass spectrometry and ^{31}P -NMR. Decanting the mother liquor away from $[\text{H}_3\text{PW}(\text{CO})_5]$ and storage of the highly concentrated solution at -25°C for several weeks resulted in deposition of a few orange crystals, from which one was selected for an X-ray diffraction experiment. The identity of this crystal was determined to be the oxygen-bridged ditin complex $[\text{Ph}^*\text{Sn}\{\text{W}(\text{CO})_5\}(\mu\text{-O})_2\text{SnPh}^*]$ (**11**), in which one of the tin atoms is coordinated to a tungsten pentacarbonyl fragment.



The formation of **11** comes apparently as a result of contamination with moisture or oxygen, likely due to the excess handling and long crystallization period. The most notable feature of **11** is the coordination of tin to the $\text{W}(\text{CO})_5$ fragment, which was introduced into the reaction mixture as a phosphorus-coordinated adduct. Isolation of **11** is reminiscent of the $\text{W}(\text{CO})_5$ migration from tin to phosphorus, as had been observed only spectroscopically in the reaction of $[(\text{CO})_5\text{WSnCl}_2(\text{thf})_2]$ with $\text{LiH}_2\text{PBar}^{\text{F}}_3$ (cf. Section 3.1.3). An EI mass spectrum was recorded on **11**, and peaks corresponding to the $\text{Sn}_2\text{O}_2\{\text{W}(\text{CO})_5\}$ core could be observed with sequential loss of CO ligands. Fragments from the Ph^* ligand were not observed, possibly due to the extremely high temperature required for the measurement (380°C), aside of one peak corresponding to *i*Pr.

Structure of $[\text{Ph}^*\text{Sn}\{\text{W}(\text{CO})_5\}(\mu\text{-O})_2\text{SnPh}^*]$ (11**)**

A few orange crystals of **11** were grown, alongside co-crystallized $[\text{H}_3\text{PW}(\text{CO})_5]$, from concentrated solutions of *n*-hexane at -25°C , and an X-ray diffraction analysis was carried out on a selected orange crystal. **11** crystallizes in the orthorhombic space group *Pnma*. The molecular structure is shown in Figure 15, and selected bond lengths and angles are given in Table 6.

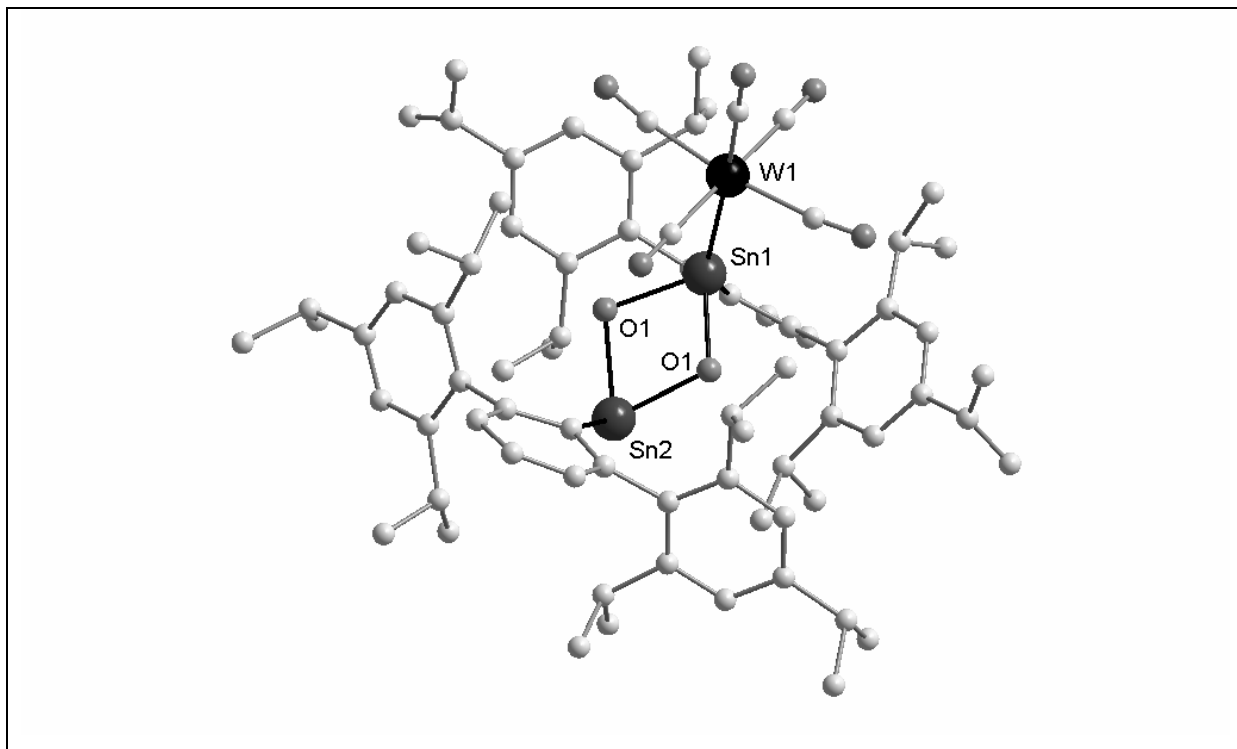


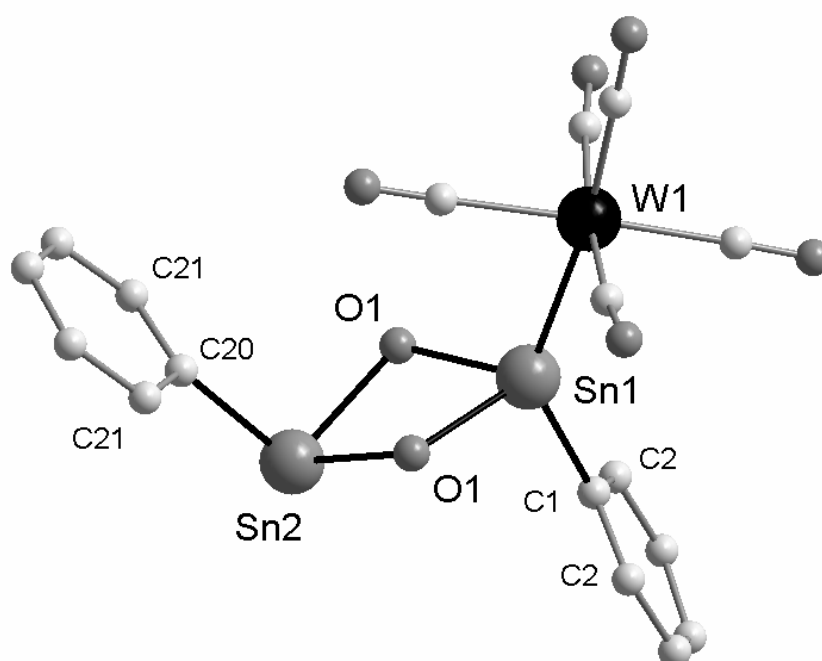
Figure 15: Molecular structure of $[\text{Ph}^*\text{Sn}\{\text{W}(\text{CO})_5\}(\mu\text{-O})_2\text{SnPh}^*]$ (**11**) in the crystal. H atoms have been omitted for clarity.

Table 6: Selected bond lengths [Å] and angles [°] in **11**.

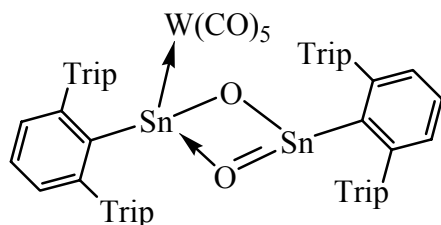
W-Sn(1)	2.743(2)	Sn(1)-C(1)	2.183(9)
Sn(1)-O	2.140(5)	Sn(2)-C(20)	2.217(9)
Sn(2)-O	2.224(5)	C(1)-C(2)	1.413(9)
W-C _{trans}	1.978(15)	C(20)-C(21)	1.412(8)
W-C _{cis}	2.058(14) ^a		
O-Sn(1)-O	73.0(3)	O-Sn(2)-O	69.9(3)
O-Sn(1)-W	111.57(14)	Sn(1)-O-Sn(2)	105.6(2)
C(1)-Sn(1)-W	137.9(3)	C(2)-C(1)-Sn(1)	120.6(4)
C(1)-Sn(1)-O	101.9(3)	C(21)-C(20)-Sn(2)	120.5(4)
C(20)-Sn(2)-O	99.2(3)		

^a Mean value is given

In the crystal structure of **11**, $[\text{Ph}^*\text{Sn}\{\text{W}(\text{CO})_5\}(\mu\text{-O})_2\text{SnPh}^*]$ lies on a crystallographic mirror plane bisecting the Sn_2O_2 four-membered ring through the Sn atoms and bisecting the $\text{W}(\text{CO})_5$ unit and Ph^* groups. The bridging oxygen atoms are slightly bowed in the same direction and the Ph^* groups lie in *trans*-bent arrangement. A view of the inner region is represented in Figure 16, in which the Trip groups have been cut away for visible access to the trinuclear core.

**Figure 16:** View of the inner $\text{Sn}_2\{\text{W}(\text{CO})_5\}(\mu\text{-O})_2$ unit of **11**. The *o*-Trip groups and H atoms have been omitted for clarity.

The large $C_{aryl}\text{-Sn-W}$ angle ($137.9(3)^\circ$) illustrates the steric crowding about Sn(1) in **11** as does the pronounced pinching of the oxygen atoms about the tin atoms (O-Sn(1)-O: $73.0(3)^\circ$; O-Sn(2)-O: $69.9(3)^\circ$). The Sn-W bond length ($2.743(2)$ Å) falls within the range of other known tungstenpentacarbonyl-coordinated stannylene complexes (compare: [(salen)Sn=W(CO)₅] (salen = 2,2'-*N,N'*-bis(salicylidene)ethylenediamine) ($2.712(1)$ Å) [132]; [(CO)₅WSn(Cl)Fe(CO)₄]₂²⁻ ($2.799(1)$ Å) [133]; [Mes*(R)Sn=W(CO)₅] (R = CH₂-CMe₂-3,5-*t*Bu₂C₆H₃) ($2.751(1)$ Å) [134]). A most conspicuous feature of the structure of **11** is the 3-coordinate tin atom, Sn(2). While the donation to W(CO)₅ designates Sn(1) as a divalent center, the logical description of Sn(2) as tetravalent does not agree well with Sn(2) being only 3-coordinate, unless multiple Sn-O bonding is involved.



Scheme 7: Proposed bonding scheme in $\text{Sn}_2\text{O}_2\{\text{W}(\text{CO})_5\}$ core of **11**.

The Sn-O bond lengths (Sn(1)-O: $2.140(5)$ Å, Sn(2)-O: $2.224(5)$ Å) differ slightly from one another, but are considerably longer than the Sn-O bonds in *cyclo*-[Trip₂SnO]₃ ($1.956(2)$ Å, $1.970(2)$ Å), which contains exclusively Sn-O single bonds. [135] The elongated Sn-O bonds in **11** can be attributed to the steric crowding about the tin centers caused by the bulky terphenyl ligands. Thus, the most logical

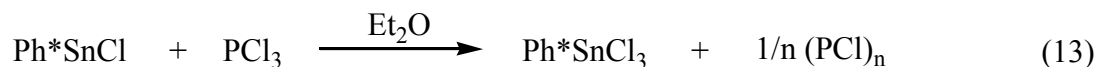
bonding scheme which fits the existence of the 3-coordinate tin center is one in which the Sn(2)-O bond is represented by a double bond, and this oxygen ligand further donates to the stannylene center, Sn(1). One resonance form for this description is depicted in Scheme 7. The structure proposal in Scheme 7 is not consistent with the Sn-O bond lengths, since the Sn(2)-O bond should be a multiple bond by this description but is longer than the Sn(1)-O bond. An explanation for this discrepancy may be the constrained geometry of the core in **11** caused by steric repulsion from the W(CO)₅ group. If steric repulsion indeed plays a role, the bond lengths within the core would no longer be a reliable measure of bond order. To elucidate the proposal of compound **11** possessing a Sn(II)/Sn(IV) combination, Mößbauer spectroscopy would be required; however, this was not possible in the current work, as the experimental yield, only a few crystals among a mixture of compounds, did not suffice for measurement.

3.2.4 Reactions of Ph*SnCl with PCl₃ and Cp*PCl₂

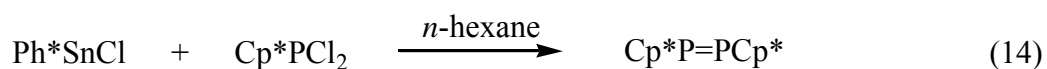
It has been shown that sterically hindered, heavier Group 14 carbene analogues (E = Ge, Sn, Pb) undergo insertions into the P-Cl bonds of phosphorus trichloride, PCl₃. [136] For

stannylene and plumbylene compounds, only chlorination of the Group 14 element was observed, and no compound was isolated with an E–P bond. However, by using organodichlorophosphanes RPCl_2 ($\text{R} = \text{Ph}, \text{Mes}$), compounds were isolated possessing E–P bonds. [137] In the case of the corresponding germylene, a product could be isolated in which a rare $\text{E}(\text{Cl})\text{-P}(\text{Cl})$ unit was present. It was expected in this work, then, that the Ph^* group would provide enough steric protection to stabilize products of the type $\text{Ph}^*\text{Sn}(\text{Cl})\text{-PCl}_2$ or $\text{Ph}^*\text{Sn}(\text{Cl})\text{-P}(\text{Cl})\text{R}$ in reactions of Ph^*SnCl with PCl_3 or RPCl_2 .

Treatment of Ph^*SnCl with PCl_3 in *n*-hexane at low temperature resulted in immediate discoloration of the orange solution. Upon overnight stirring at room temperature, a colorless solution with a yellow precipitate was observed. After work-up of the colorless solution, the crude, colorless product was identified as Ph^*SnCl_3 by ^1H -NMR (for complete NMR data, cf. Section 3.2.6). Upon recrystallization, Ph^*SnCl_3 could be isolated as colorless crystals in 68% yield. The yellow precipitate formed during the reaction was not investigated spectroscopically; however, based on its lack of solubility in common organic solvents, the precipitate is presumably the polymeric phosphorus chloride $(\text{PCl})_n$, which was identified as an insoluble yellow precipitate in published reactions of $\text{Me}_2\text{Si}(t\text{BuN})_2\text{Sn}$ with PCl_3 . [136]



The reaction of Ph^*SnCl with Cp^*PCl_2 was carried out in *n*-hexane at low temperature. Immediate discoloration of the orange Ph^*SnCl solution was observed, resulting in a yellow solution. This solution was characterized by ^{31}P -NMR in C_6D_6 , which revealed three main phosphorus-containing products, including $\text{Cp}^*\text{P}=\text{PCp}^*$ ($\delta = 504.9$ ppm; literature value: $\delta = 504$ ppm in C_6D_6 [138]) and unreacted Cp^*PCl_2 ($\delta = 128.1$ ppm). Tin–phosphorus bond formation was indicated in the proton-decoupled spectrum by a peak centered at -89 ppm with tin satellites ($J_{\text{P}117\text{Sn}} = 1413$ Hz, $J_{\text{P}119\text{Sn}} = 1478$ Hz), which split into a doublet of quartets in the proton-coupled experiment. This signal accounted for only ca. 15% of the total signal intensity of the complete spectrum and could not be assigned unambiguously. The presumable presence of the oxidation product Ph^*SnCl_3 in the reaction mixture was not verified.

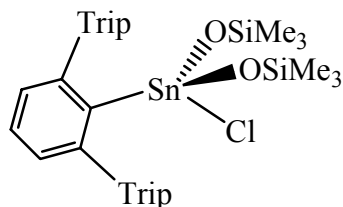
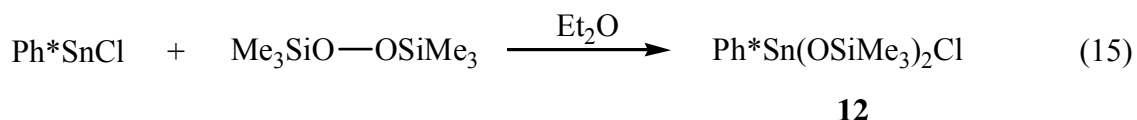


The observed formation of $\text{Cp}^*\text{P}=\text{PCp}^*$ mirrors the known reaction of Mes^*PCl_2 with $\text{Me}_2\text{Si}(t\text{BuN})_2\text{Sn}$ and isolation of $\text{Mes}^*\text{P}=\text{PMes}^*$ in good yield. [139] The current results indicate that, even with the $\text{Sn}(\text{II})$ center supported by the bulky Ph^* ligand and the P atom supported by the relatively bulky Cp^* ligand, bimolecular rearrangement and P–P formation could not be hindered.

3.2.5 Oxidation of Ph^*SnCl with $\text{Me}_3\text{SiOOSiMe}_3$ and Me_3NO

3.2.5.1 Synthesis of $\text{Ph}^*\text{Sn}(\text{OSiMe}_3)_2\text{Cl}$ (**12**)

Treatment of Ph^*SnCl with trimethylsilylperoxide, $\text{Me}_3\text{SiOOSiMe}_3$ [140], at 0°C in Et_2O resulted in immediate discoloration of the orange solution. After stirring for one hour at room temperature and filtration, $\text{Ph}^*\text{Sn}(\text{OSiMe}_3)_2\text{Cl}$ (**12**) could be isolated as colorless crystals from Et_2O in moderate yield.



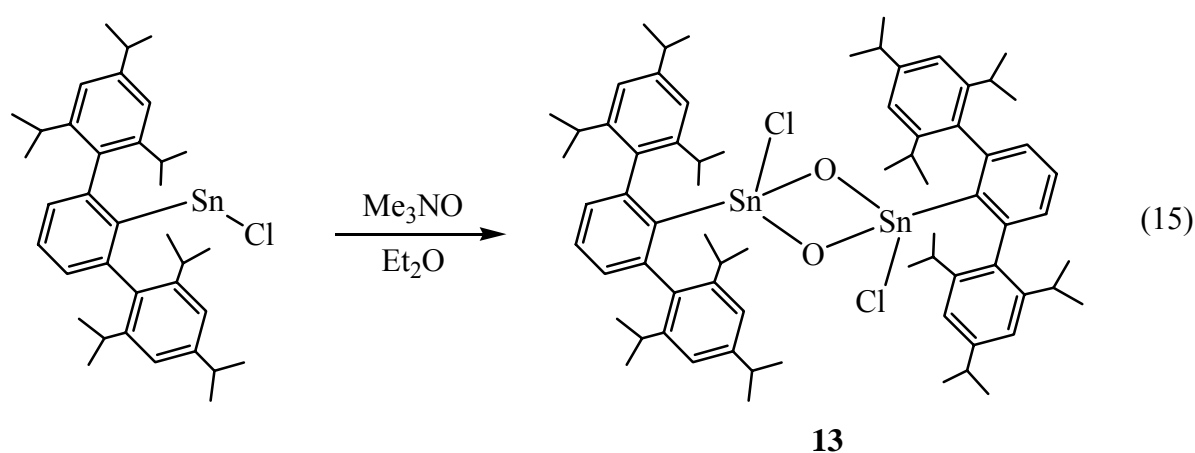
Scheme 8: Proposed structure of **12**.

Compound **12** was isolated as a sticky solid and is highly soluble in common hydrocarbons. The ^1H -NMR spectrum of **12** revealed a sharp signal at 0.13 ppm for the trimethylsiloxy groups along with a few neighboring peaks likely resulting from impurity or unreacted trimethylsilylperoxide. The *i*Pr protons on the tertiary carbons overlap and give a broad multiplet. In the EI mass spectrum, the molecular ion peak was not found, but a peak corresponding to the molecular ion minus one methyl group was found, along with further peaks signalling successive loss of the silyloxy ligands and fragmentation of the Ph^* ligand. No higher peaks indicating a dimeric structure with bridging silyloxy ligands were found. Thus, the structure is proposed to be monomeric, as shown in Scheme 8.

3.2.5.2 Synthesis of $[\text{Ph}^*\text{Sn}(\mu\text{-O})\text{Cl}]_2$ (**13**)

In an attempt to prepare the kinetically stabilized heavier Group 14 acid halide analogue $\text{Ph}^*\text{Sn}(\text{O})\text{Cl}$, Ph^*SnCl was treated with solid trimethylamine *N*-oxide, Me_3NO , at

0°C in Et₂O. Immediately upon mixing the orange solution underwent rapid discoloration. After stirring at room temperature for two hours, colorless crystals of [Ph*Sn(μ -O)Cl]₂ (**13**) could be isolated by crystallization from the filtered reaction mixture. **13** formally represents a dimerization of the targeted acid halide analogue, Ph*Sn(O)Cl, a compound class that has yet to be described experimentally for tin. The clean addition of oxygen to Sn(II) to form [Ph*Sn(μ -O)Cl]₂ stands in contrast to attempts to prepare a ketone analogue for tin by Power *et al.*, in which the reaction of Ar₂Sn (Ar = 2,6-Mes₂C₆H₃) with Me₃NO resulted in formal addition of H₂O to the expected product Ar₂Sn=O and led instead to the dihydroxy compound Ar₂Sn(OH)₂. [141]



The ¹H-NMR and ¹³C-NMR spectra of **13** show no remarkable features and, like the ¹H-NMR spectrum of **12**, reveal overlapping multiplets for the protons bound to the tertiary *i*Pr carbons. The signals in the aryl region of the ¹H-NMR spectrum of **13** are unresolved, as is often observed in Ph* compounds. The FD-MS spectrum in toluene revealed the molecular ion as the base peak, thus showing the existence of **13** in the dimeric form in solution as well as in the solid state. No signal for the hypothetical monomeric form, Ph*Sn(O)Cl was observed in the FD-MS spectrum.

Structure of [Ph*Sn(μ -O)Cl]₂ (**13**)

An X-ray diffraction experiment was carried out for **13** on colorless prisms grown from concentrated solutions of Et₂O. **13** crystallizes in the triclinic space group *P* $\bar{1}$. The molecular structure is shown in Figure 17, and selected bond lengths and angles are given in Table 7.

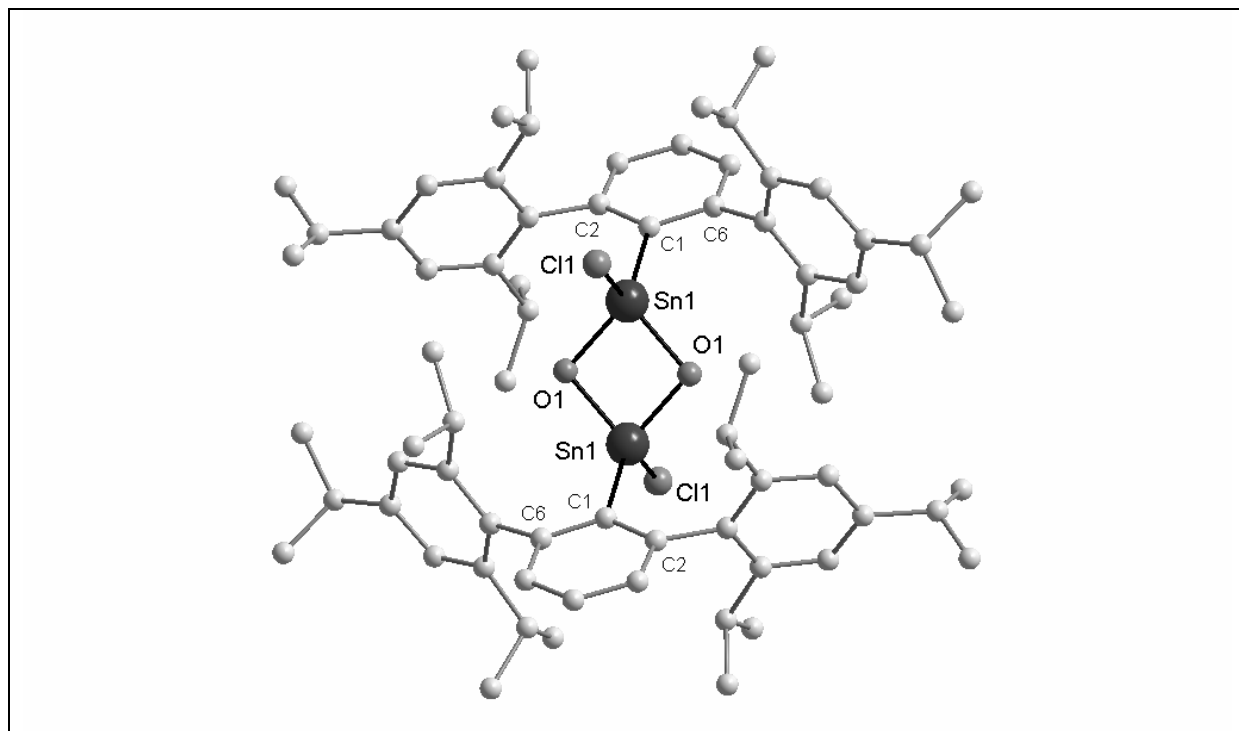


Figure 17: Molecular structure of $[\text{Ph}^*\text{Sn}(\mu\text{-O})\text{Cl}]_2$ (**13**) in the crystal. H atoms have been omitted for clarity.

Table 7: Selected bond lengths [\AA] and angles [$^\circ$] in **13**.

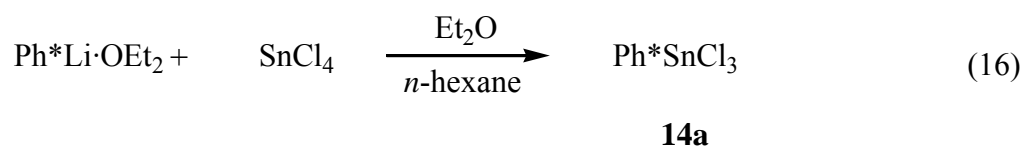
Sn-O	1.994(2)	Sn-Cl	2.343(1)
Sn-C _{ipso}	2.137(3)	C _{ipso} -C(2)	1.415(4)
C _{ipso} -C(6)	1.396(4)		
Sn-O-Sn	95.38(9)	O-Sn-O	84.62(9)
Cl-Sn-O	108.47(6)	Cl-Sn-O'	106.36(7)
C _{ipso} -Sn-O	117.28(10)	C _{ipso} -Sn-O'	119.98(9)
Sn-C _{ipso} -C(2)	118.8(2)	Sn-C _{ipso} -C(6)	118.3(2)
Cl-Sn-C _{ipso}	115.76(8)		

The molecular structure of **13** is located on an inversion center, such that the central Sn_2O_2 unit is a planar rhombus and only one unique Sn-O bond length results. The planarity of the Sn_2O_2 core mirrors that of $[\text{R}_2\text{Sn}(\mu\text{-O})]_2$ ($\text{R} = \text{CH}(\text{SiMe}_3)_2$) [142] and analogues possessing heavier chalcogenide ligands, as in $[\text{tBu}_2\text{Sn}(\mu\text{-E})]_2$ ($\text{E} = \text{S}, \text{Se}, \text{Te}$) [143] or $[(\text{Trip}_2\text{Sn})_2(\mu\text{-O})(\mu\text{-S})]$ [144]. However, while all Sn-O bonds in **13** have the same length, the Sn-O bonds in $[\{(\text{Me}_3\text{Si})_2\text{CH}\}_2\text{Sn}(\mu\text{-O})]_2$ are of varying lengths, such that a non-rhomboidal parallelogram form of the Sn_2O_2 core results. The Sn atoms are in distorted tetrahedral geometry with the C_{ipso}-Sn-O angles ($117.28(10)^\circ$, $119.98(9)^\circ$) significantly larger than the

Cl-Sn-O angles ($106.36(7)^\circ$, $108.47(6)^\circ$), likely a result of steric repulsion from the Ph* ligands. The O-Sn-O angles ($84.62(9)^\circ$) are considerably more acute than the Sn-O-Sn angles ($95.38(9)^\circ$) in **13**. The Sn-O bond distance ($1.994(2)$ Å) is significantly shorter than those in compound **11** ($2.140(5)$ Å, $2.224(5)$ Å) and compares well with the Sn-O bond lengths in *cyclo*-[(Me₃Si)₃CSn(OH)O]₃ (Sn-O_{ring}: 1.965 Å; Sn-O_{OH}: 1.968 Å), [145] but is longer than those of [$\{(Me_3Si)_2CH\}_2Sn(\mu-O)]_2$ ($1.94(2)$ Å, $1.98(1)$ Å). The Sn-C_{ipso} bond length ($2.137(3)$ Å) is considerably shorter than the Sn-C_{ipso} bond length ($2.226(4)$ Å) in **7**, reflecting the difference in a tetravalent aryl stannane and a divalent aryl stannylene.

3.2.6 Synthesis of Ph*SnCl₃ (**14a**)

The most direct preparation of Ph*SnCl₃ (**14a**) was achieved by reaction of Ph*Li·OEt₂ with SnCl₄ in mixtures of *n*-hexane and Et₂O. Colorless microcrystals could be obtained from work-up and recrystallization from *n*-hexane in a relatively low yield of 37%. The procedure by which Ph*SnCl is oxidized by PCl₃ proved to give a higher yield of 68% (cf. Section 3.2.4). However, the current transmetalation method saves the step of preparing Ph*SnCl and allows the synthesis of Ph*SnCl₃ to be carried out on a significantly larger scale. The synthesis of Ph*SnBr₃ (**14b**) was achieved analogously by the reaction of Ph*Li·OEt₂ with SnBr₄. Details concerning synthesis and characterization of **14b** are included only in the Experimental Section and are nearly completely analogous to those of Ph*SnCl₃.



Ph*SnCl₃ and Ph*SnBr₃ have not been previously described, nor are the germanium congeners, Ph*GeCl₃ and Ph*GeBr₃, known, while the related Si(IV) compounds Ph*SiF₃ [146] and Ph*SiCl₃ [147] have been reported. Ph*SiBr₃ has not been described.

The ¹H-NMR spectrum of **14a** (Figure 18) exhibits three well-resolved doublets for the primary *i*Pr protons, indicating inequivalence of the *ortho*-*i*Pr groups on each respective *meta*-Trip ring. The signals representing protons of the tertiary *i*Pr carbons are observed as overlapping multiplets. For Ph*Sn compounds in this work and in the literature, it seems to be a common trend that the protons of the tertiary *i*Pr carbons generally overlap for Sn(IV) compounds but appear as distinct signals for Sn(II) compounds as well as in Ph*I. The aryl

region of the ^1H -NMR spectrum of **14a** is mostly resolved, with the exception that the *meta*-protons of the central ring appear as a broad signal rather than the expected resolved doublet.

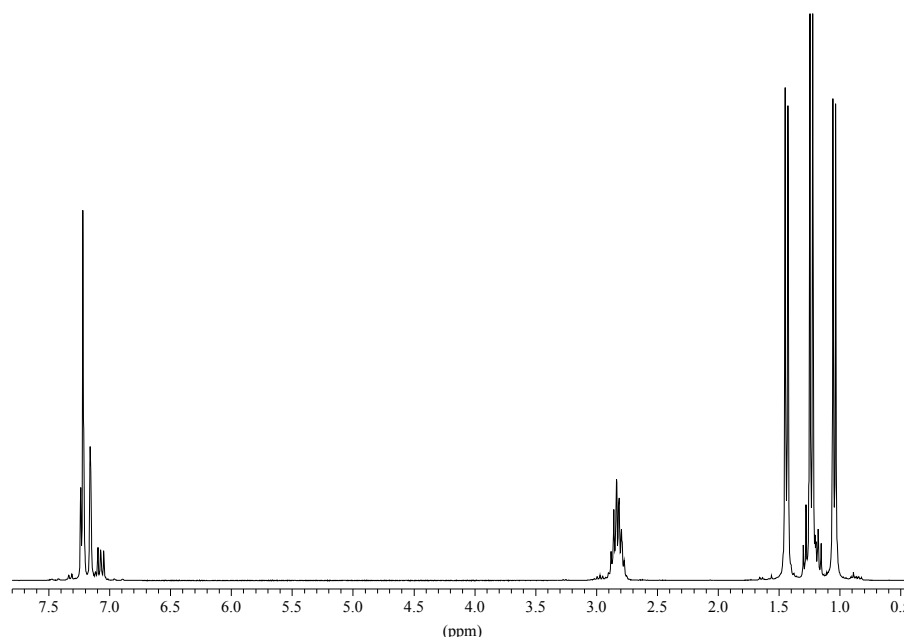


Figure 18: ^1H -NMR spectrum of **14a** in C_6D_6 .

The ^{13}C -NMR of **14a** reveals five signals in the aliphatic region. Although symmetry would dictate that four signals should be found (or six signals in cases where the *ortho*-*i*Pr groups are not equivalent), five aliphatic signals are commonly reported in the literature for Ph^* compounds. This likely indicates equivalence of the tertiary *i*Pr carbons, which are positionally fixed within the plane of the Trip rings, and inequivalence of the primary *i*Pr carbons, which lie both above and below the plane defined by the Trip rings. The EI mass spectrum of **14a** reveals the molecular ion peak along with peaks indicating successive loss of Cl and SnCl_3 and fragmentation of Me and *i*Pr groups from the Ph^* ligand.

The $^{119}\text{Sn}\{^1\text{H}\}$ -NMR spectra of **14a** and **14b** reveal singlets centered at -113.8 ppm and -332.6 ppm, respectively. These values are in the range of ^{119}Sn signals for known aryltin trihalides (PhSnCl_3 : $\delta = -60.6$ ppm [148], $\delta = -65$ ppm [149]; MesSnCl_3 : $\delta = -85.5$ ppm [150]; PhSnBr_3 : $\delta = -225$ ppm [149])

Structure of Ph^*SnCl_3 (**14a**)

An X-ray diffraction experiment was carried out on colorless crystals of **14a** grown from concentrated solutions of *n*-hexane. **14a** crystallizes in the triclinic space group $P\bar{1}$. The molecular structure is shown in Figure 19, and selected bond lengths and angles are given in Table 8.

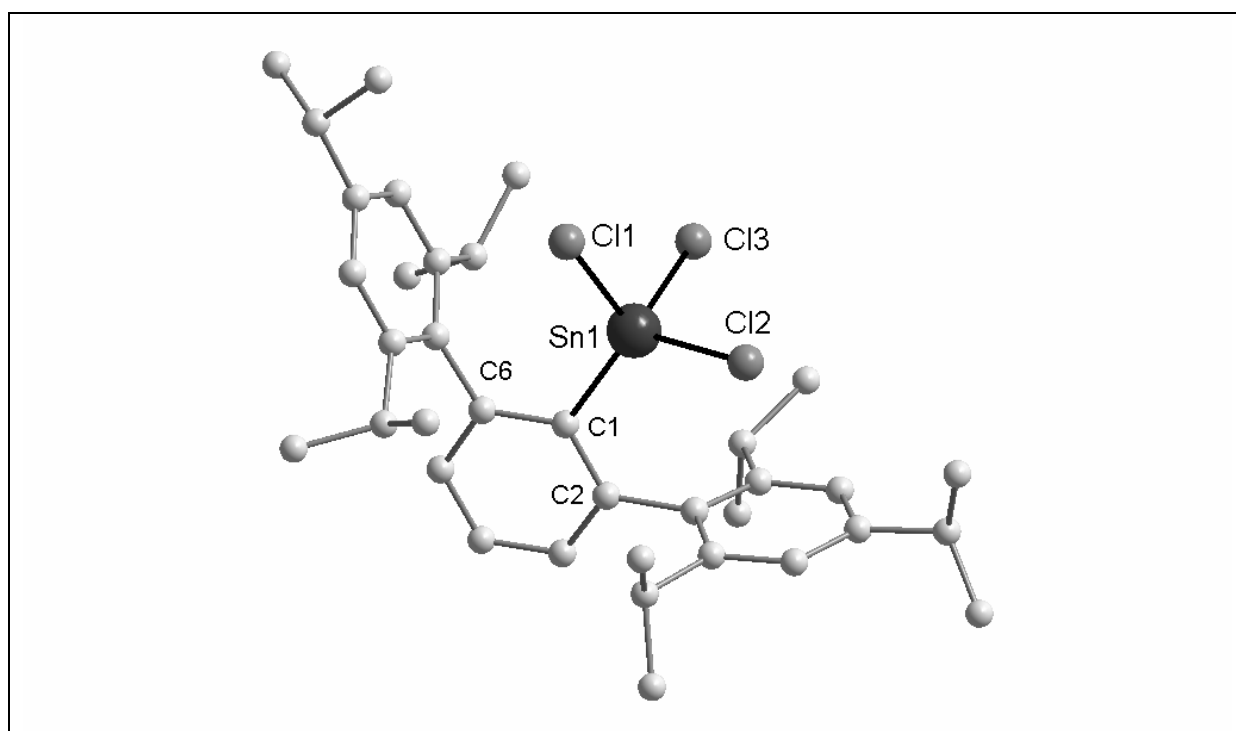


Figure 19: Molecular structure of Ph*SnCl₃ (**14a**) in the crystal. H atoms have been omitted for clarity.

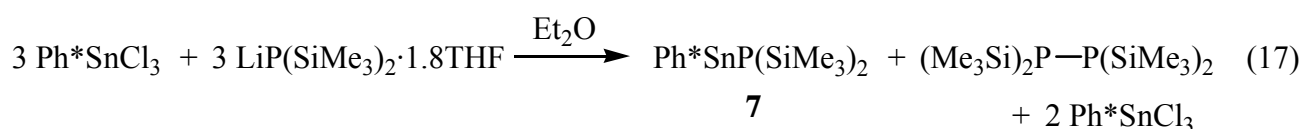
Table 8: Selected bond lengths [Å] and angles [°] in **14a**.

Sn-Cl(1)	2.322(2)	Sn-Cl(2)	2.321(2)
Sn-Cl(3)	2.328(2)	Sn-C _{ipso}	2.155(5)
C _{ipso} -C(2)	1.406(6)	C _{ipso} -C(6)	1.405(7)
Cl(1)-Sn-Cl(2)	98.12(6)	Cl(1)-Sn-Cl(3)	102.96(8)
Cl(2)-Sn-Cl(3)	101.67(8)	C _{ipso} -Sn-Cl(1)	119.88(13)
C _{ipso} -Sn-Cl(2)	122.05(13)	C _{ipso} -Sn-Cl(3)	109.26(14)
Sn-C _{ipso} -C(2)	119.0(3)	Sn-C _{ipso} -C(6)	119.5(3)

The molecular structure of **14a** shows the Trip rings rotated approximately perpendicular about the central phenyl ring and otherwise exhibits no unusual features concerning the Ph* ligand. The geometry about tin is distorted tetrahedral with the chloride ligands pinched toward each other (Cl-Sn-Cl: 98.12(6)°, 102.96(8)°, 101.67(8)°) and away from the Ph* ligand (C_{ipso}-Sn-Cl: 119.88(13)°, 122.05(13)°, 109.26(14)°), presumably a result of the bulkiness of the Ph* ligand.

3.2.7 Reactions of Ph*SnCl₃ (**14a**), Ph*Sn(OSiMe₃)₂Cl (**12**), and [Ph*Sn(μ -O)Cl]₂ (**13**) with [P(SiMe₃)₂]⁻

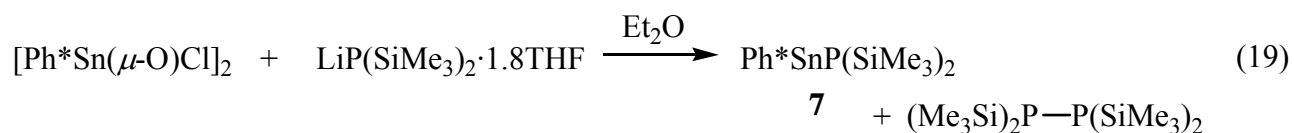
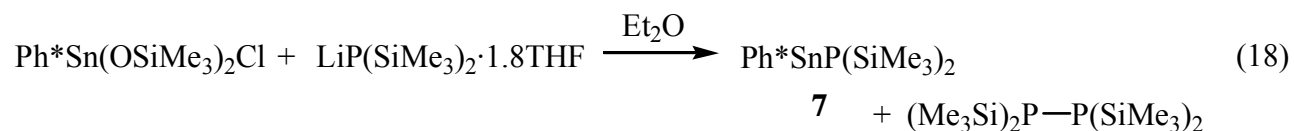
An interesting aspect of the synthesized reagents Ph*SnCl₃ (**14a**), Ph*Sn(OSiMe₃)₂Cl (**12**), and [Ph*Sn(μ -O)Cl]₂ (**13**) is their potential use as Sn(IV) entry points to Sn-P ligands. In the synthesis of phosphalkynes, an acyl halide is treated with LiP(SiMe₃)₂ and successively treated with NaOH to induce silane elimination and formation of the low-coordinate carbon-phosphorus triple-bond compounds RC \equiv P. [151] Thus, the three synthesized Sn(IV) compounds were probed to investigate whether these show potential for similar chemistry. Compounds **14a**, **12**, and **13** were each treated with LiP(SiMe₃)₂·1.8THF in Et₂O at low temperature. In each case, the colorless solution darkened and formed an intense violet solution after overnight stirring at room temperature. For the reaction starting from Ph*SnCl₃, the ³¹P-NMR spectrum of the crude reaction mixture revealed the formation of Ph*SnP(SiMe₃)₂ (**7**) and trimethylsilyldiphosphane, (Me₃Si)₂PP(SiMe₃)₂ (δ = -216 ppm [152]) in approximate 1:1 ratio as the main phosphorus-containing products. Work-up of the violet reaction mixture led to deposition of colorless crystals, identified as unreacted Ph*SnCl₃ by ¹H-NMR. Thus, a complete, balanced reaction equation can be written starting from three equivalents each of Ph*SnCl₃ and LiP(SiMe₃)₂·1.8THF, whereby two equivalents Ph*SnCl₃ still remain in the crude product.



The reduction of Ph*SnCl₃ by LiP(SiMe₃)₂ and P–P bond formation were unexpected in light of the recent report detailing the reaction of Ph*SiF₃ with LiP(SiMe₃)₂ to give the silane-elimination product Ph*Si(F)₂P{Li(thf)₃}SiMe₃. [45] Clearly, the relative stability of divalent stannylenes over silylenes plays a chief role in the differing redox behavior of Ph*SnCl₃ in reaction with the lithium phosphanide. In order to ascertain whether a heavier alkali-metal phosphanide could induce preferential salt elimination over reduction, the analogous reaction was carried out with Ph*SnCl₃ and KP(SiMe₃)₂. The ³¹P-NMR spectrum of the crude reaction mixture revealed the same phosphorus-containing products as that with LiP(SiMe₃)₂·1.8THF.

The reactions of Ph*Sn(OSiMe₃)₂Cl (**12**) and [Ph*Sn(μ -O)Cl]₂ (**13**) with LiP(SiMe₃)₂·1.8THF revealed an analogous coloration to intense violet and similar reactivity

patterns. The ^{31}P -NMR spectra of the crude reaction mixtures were not as clean as the spectrum involving Ph^*SnCl_3 , but $\text{Ph}^*\text{SnP}(\text{SiMe}_3)_2$ and $(\text{Me}_3\text{Si})_2\text{PP}(\text{SiMe}_3)_2$ could be identified as the main phosphorus-containing products.



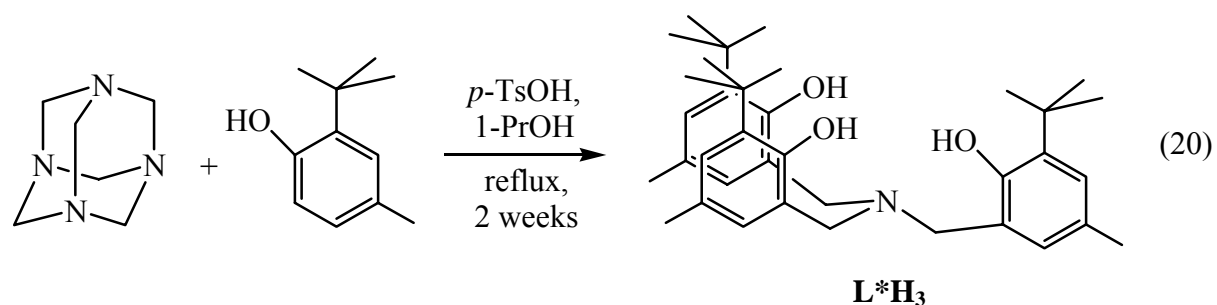
The above reactivity of the tin(IV) precursors reveals a preferential reduction pathway over salt elimination in reactions with alkali-metal phosphanides, regardless of the nature of the halide or pseudohalide substituents on tin.

3.3 Tris(aryloxy)amine tantalum complex for probing reactivity with phosphanide reagents

3.3.1 Background and research objective

The use of bulky tris(amido)amine ligands has opened the way for the stabilization of a host of novel Group 5 and Group 6 transition-metal complexes with low-coordinate phosphorus ligands. Complexes such as $[(N_3N)Ta=PR]$ and $[(N_3N)W\equiv P]$ have proven the utility of the N_3N ligand in kinetically stabilizing multiply bonded phosphorus. Similarly, bulky monodentate silyloxy ligands were used to prepare the tantalum phosphinidine $[(\text{silox})_3Ta=PPh]$ (see Introduction), while monodentate alkyloxy and aryloxy ligands were employed in the syntheses of tungsten phosphido complexes $[(tBuO)_3W\equiv P \rightarrow W(CO)_5]$ and $[thf(Ph'O)_3W\equiv P \rightarrow W(CO)_5]$ ($Ph' = 3,5\text{-Me}_2C_6H_3$). [153,154]

In the following work, the recently published chelating tris(aryloxy)amine, tris(2-hydroxy-3-*tert*-butyl-5-methylbenzyl)amine (L^*H_3), [155] is investigated for its applicability to tantalum complexes useful for reactions with reactive phosphorus sources. Such a tris(aryloxy)amine ligand combines aspects of the monodentate siloxy, alkyloxy, and aryloxy ligands mentioned above with the principle of a trianionic set anchored by an axial amine, as in the N_3N ligand. L^*H_3 is prepared in a one-pot synthesis by thermolysis of hexamethylenetetramine with 2-*tert*-butyl-4-methylphenol in the presence of *p*-toluenesulfonic acid hydrate.



In transition-metal complexes, the ancillary L^* ligand would be expected to provide a protective pocket about the metal and a degree of stabilization through the axial amine donor, as in N_3N , while providing a rigid aryl skeleton. The steric bulk of the L^* ligand would presumably be considerable, given the literature report of formation of the disubstitution complex $[(2,6\text{-}tBu_2C_6H_3O)_2TaCl_3]$ from treatment of $TaCl_5$ with an excess of the related

aryloxide $\text{LiOC}_6\text{H}_3t\text{Bu}_{2,6}$, [156] whereby further substitution is disallowed by the *ortho*-*t*Bu groups. The *ortho*-*t*Bu groups in a complexed L^* ligand would be expected to orient along the axial vector, thus creating steric bulk about the remaining coordination sites.

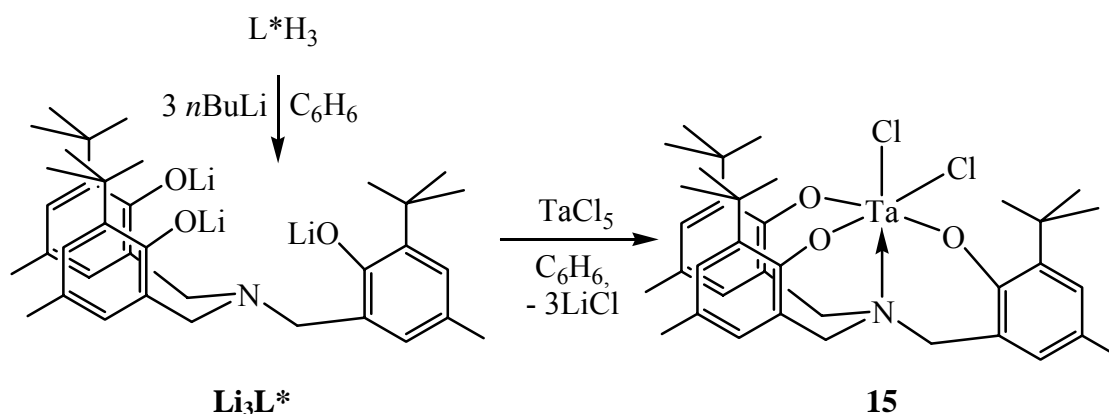
The reactive $\text{LiE}(\text{SiMe}_3)_2$ ($\text{E} = \text{P}, \text{As}, \text{Sb}, \text{Bi}$) reagents [157] have been widely employed in our group in reactions with tungsten complexes of the type $[\{(\text{RNCH}_2\text{CH}_2)_3\text{N}\}\text{WCl}]$ ($\text{R} = \text{SiMe}_3, i\text{Pr}, \text{Np}$) to produce novel tungsten-bound E_1 ligands. [158] With tantalum, an analogous approach has been successfully used by Arnold *et al.* in the reaction of $[(\text{N}_3\text{N})\text{TaCl}_2]$ with LiESiMe_3 ($\text{E} = \text{Se}, \text{Te}$) to prepare the terminal transition-metal chalcogenides $[(\text{N}_3\text{N})\text{Ta}=\text{E}]$. [159] In the current work, the reactivity of $\text{LiE}(\text{SiMe}_3)_2$ is probed in reaction with a Ta(V) complex supported by the tris(aryloxy)amine ligand L^* . The reactions in this chapter are directed toward synthesis of the phosphinidene complex $[\text{L}^*\text{Ta}=\text{PSiMe}_3]$, which would be expected to serve as an interesting precursor for further Ta-P chemistry via reactions targeting cleavage of the P-Si bond.

3.3.2 Synthesis of $[\text{L}^*\text{TaCl}_2]$ (15)

3.3.2.1 Route via lithiation of L^*H_3

Following a literature procedure for lithiation of related tris(aryloxy) reagents, [160] the tris(aryloxy)amine, tris(2-hydroxy-3-*tert*-butyl-5-methylbenzyl)amine (L^*H_3) was triply lithiated in benzene with three equivalents of *n*BuLi at room temperature. Allowing the solution to stir at room temperature resulted in precipitation of Li_3L^* as a white powder. After stirring overnight, the product could be isolated by filtration and washing with *n*-hexane.

Li_3L^* is insoluble in hydrocarbons and dissolves well in THF and CH_2Cl_2 , but decomposes in CH_2Cl_2 after a few hours. Li_3L^* is extremely sensitive to oxygen, with solutions immediately turning blue-violet upon exposure to air. The ^1H - and ^{13}C -NMR spectra of Li_3L^* reveal threefold symmetry in solution, and the signals in the ^1H -NMR spectrum are broadened.

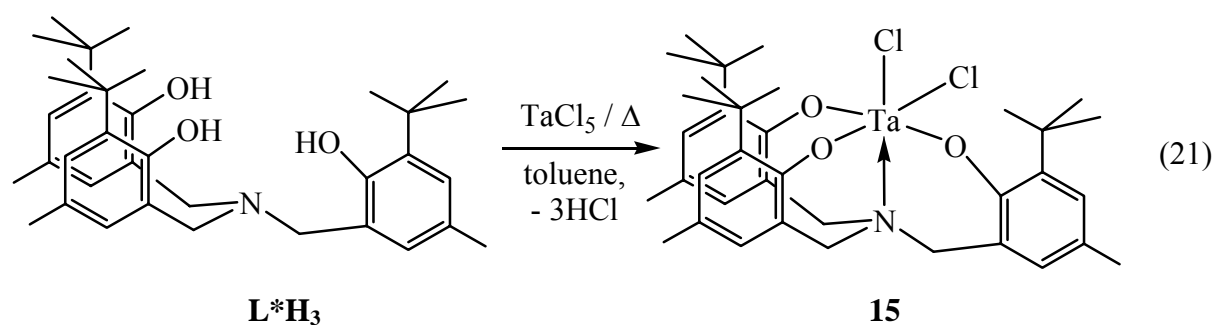


Scheme 9: Synthesis of $[\text{L}^*\text{TaCl}_2]$ (**15**) via salt-elimination route.

The reaction of Li_3L^* with TaCl_5 was carried out in benzene at room temperature. After stirring overnight and work-up, the crude product could be isolated as a yellow powder. Recrystallization from Et_2O provided spectroscopically pure yellow crystals of $[\text{L}^*\text{TaCl}_2]$ (**15**) in moderate yield.

3.3.2.2 Direct thermolysis of L^*H_3 with TaCl_5

A second method for preparing $[\text{L}^*\text{TaCl}_2]$ directly from L^*H_3 and TaCl_5 was investigated. Alcohols have been shown to react directly with Ta–Cl bonds under thermal conditions with elimination of HCl, producing tantalum(V) alkoxides within a few hours. [161] Thus, L^*H_3 and TaCl_5 were mixed in toluene and heated to reflux. In a trial run, the evolution of HCl was evidenced by purging the reaction vessel with N_2 and testing the outlet gas with litmus paper. For preparation of $[\text{L}^*\text{TaCl}_2]$ on a 1 g scale, the reaction was monitored by litmus paper, and a reaction time of 4 hours was determined. Evaporation of the cooled reaction mixture led to isolation of crude $[\text{L}^*\text{TaCl}_2]$ (**15**) as a yellow powder. Recrystallization from Et_2O afforded pure **15**. That **15** can be prepared by the lithiation and direct thermolysis routes is somewhat surprising in light of the results reported for $[\text{L}'\text{TaCl}_2]$ ($\text{L}' = \text{tris}(2\text{-oxy-3,5-dimethylbenzyl})\text{amine}$), which could only be synthesized via the bis(amido) intermediate $[\text{L}'\text{Ta}(\text{NMe}_2)_2]$. [162]



In the ^1H -NMR of **15** (Figure 20), the protons of the tris(aryloxy)amine ligand appear as two sets of signals in 2:1 ratio, thus indicating a structure with octahedral geometry and C_s symmetry, whereby the σ -plane bisects the complex through the tantalum center, two chloride ligands, amine donor, and ‘middle’ phenolate group. The protons of the amine-bound methylene group corresponding to the middle phenolate are observed as a singlet, while the protons of the ‘lateral’ methylene groups appear as a pair of doublets representing diastereotopic protons. The protons of the aryl-*t*Bu and aryl-Me groups appear as sets of two signals, respectively, in 2:1 ratio. Likewise, the ^{13}C -NMR spectrum reveals 8 aliphatic and 12 aryl resonances, whereby the *t*Bu and some of the aryl signals appear clearly as sets in approximate 2:1 ratio. Since the aryl signals partially overlap with the solvent signals for the spectra taken in C_6D_6 , additional ^1H - and ^{13}C -NMR spectra were obtained in CD_2Cl_2 (see Experimental Section). The ^1H -NMR spectrum shown in Figure 20 shows the presence of some impurity (denoted with *) as well as traces of Et_2O , which was used as the crystallization solvent.

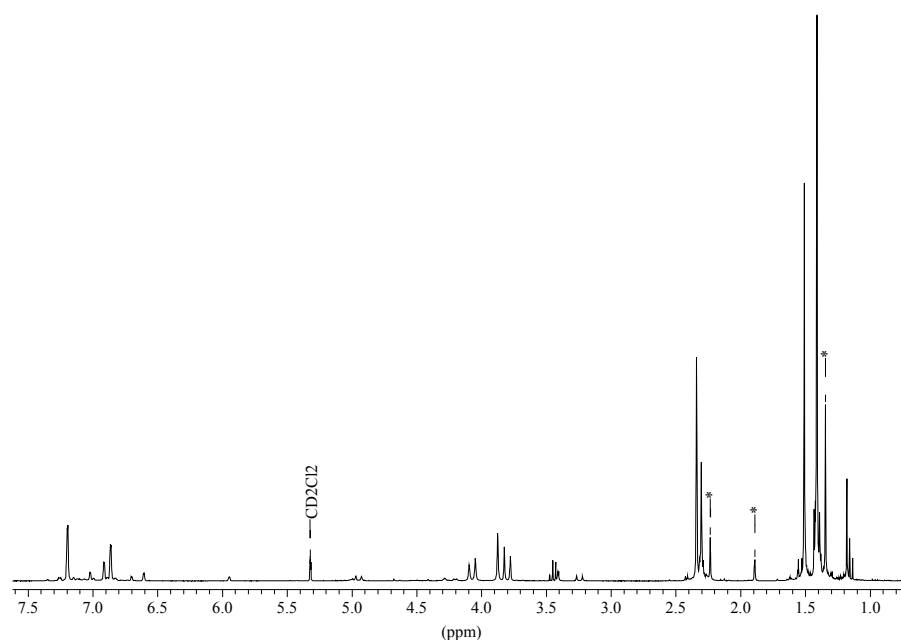


Figure 20: ^1H -NMR spectrum of $[\text{L}^*\text{TaCl}_2]$ (**15**) (C_s symmetry) in CD_2Cl_2 . Impurity is designated with (*).

The C_s symmetry of $[\text{L}^*\text{TaCl}_2]$ stands in contrast to the C_{3v} -symmetric tris(amido)amine ligand in $[(\text{N}_3\text{N})\text{TaCl}_2]$. For other tris(aryloxy)amine tantalum complexes octahedral, C_s -symmetric geometry is observed for $[\text{L}'\text{TaX}_2]$ ($\text{X} = \text{Cl}, \text{OMe}, \text{OEt}, \text{NMe}_2$), [162,163] while C_{3v} symmetry is observed for $[\text{L}'\text{TaBz}_2]$ ($\text{Bz} = \text{benzyl}$). [164] Apparently, for tris(aryloxy)amine ligand sets, C_s symmetry is more favorable with halides and pseudohalides occupying the remaining two coordination sites of $\text{L}'\text{Ta}$, while C_{3v} symmetry is more favored for benzyl groups. This relation cannot yet be generalized for alkyl groups, as $[\text{L}'\text{TaBz}_2]$ represents the only known tris(aryloxy)amino tantalum dialkyl complex.

In the EI mass spectrum the parent peak corresponds to the molecular ion. Subsequent fragmentation is observed involving loss of the chloride ligands and cleavage of the phenolate groups.

Structure of $[\text{L}^*\text{TaCl}_2]$ (**15**)

An X-ray diffraction experiment was carried out on yellow prisms of **15** grown from concentrated solutions of Et_2O . **15** crystallizes in the monoclinic space group $P2_1/c$. The molecular structure is shown in Figure 21, and selected bond lengths and angles are given in Table 9.

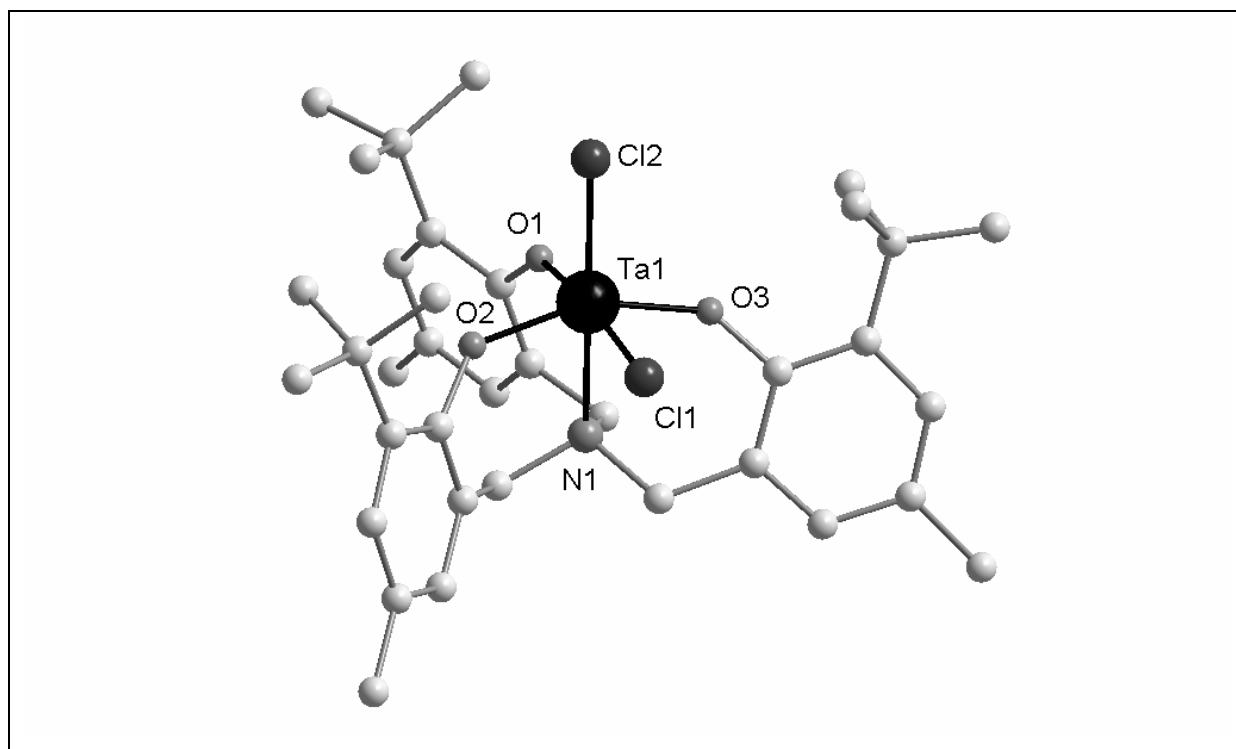


Figure 21: Molecular structure of $[L^*TaCl_2]$ (**15**) in the crystal. H atoms have been omitted for clarity.

Table 9: Selected bond lengths [\AA] and angles [$^\circ$] in **15**.

Ta-Cl _{eq}	2.406(3)	Ta-Cl _{ax}	2.334(2)
Ta-O(1)	1.914(6)	Ta-O(2)	1.929(7)
Ta-O(3)	1.911(7)	Ta-N	2.327(7)
N-Ta-Cl _{eq}	92.3(2)	N-Ta-Cl _{ax}	172.7(2)
O(1)-Ta-N	80.0(3)	O(2)-Ta-N	81.7(3)
O(3)-Ta-N	77.8(3)	O(1)-Ta-O(2)	91.8(3)
O(3)-Ta-O(2)	156.2(3)	O(3)-Ta-O(1)	96.5(3)
O(1)-Ta-Cl _{eq}	172.0(2)	O(2)-Ta-Cl _{eq}	84.9(2)
O(3)-Ta-Cl _{eq}	83.9(2)	O(1)-Ta-Cl _{ax}	93.2(2)
O(2)-Ta-Cl _{ax}	101.4(2)	O(3)-Ta-Cl _{ax}	100.4(2)
Cl _{eq} -Ta-Cl _{ax}	94.59(10)		

The molecular structure of **15** reveals the complex arranged in approximate C_s symmetry, in agreement with solution ^1H - and ^{13}C -NMR spectroscopic results. This mode of coordination contrasts that of related tris(thiolate)amine iron(II) and iron(III) complexes [165] or other tris(aryloxy)amine complexes of iron(III) [166] and titanium(IV), [167] which each exhibit trigonal bipyramidal geometry about the metal and overall C_{3v} symmetry. Whereas the

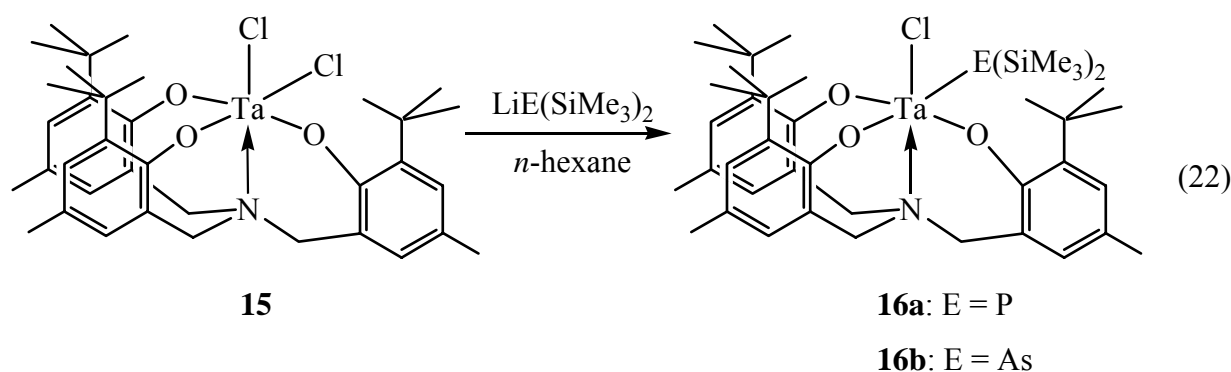
phenolate ligands adopt a *trans-mer*-arrangement in [(2,6-*i*Pr₂C₆H₃O)₃TaCl₂(PMe₂Ph)], the phenolate ligands in **15** are forced into a *fac* arrangement by the amine backbone. [161] The geometry about tantalum in **15** is distorted octahedral, such that the N-Ta-Cl_{ax} axis deviates slightly from linearity (172.7(2)°) and the phenolate ligands are pulled away from the axial chloride ligand by the rigid tris(aryloxy)amine framework. As a result, the O-Ta-N angles (80.0(3)°, 81.7(3)°, 77.8(3)°) are all significantly less than 90°, and the O-Ta-Cl_{ax} angles (93.2(2)°, 101.4(2)°, 100.4(2)°) are all significantly greater than 90°. The equatorial Ta-Cl bond length is slightly longer than the axial Ta-Cl bond length. The Ta-O bond lengths in **15** (1.914(6) Å, 1.929(7) Å, 1.911(7) Å) are slightly longer than those of *trans-mer*-[(2,6-*i*Pr₂C₆H₃O)₃TaCl₂(PMe₂Ph)] (1.863(2) Å, 1.913(2) Å, 1.897 Å). The Ta-O bond opposite the equatorial chloride ligand is the longest in **15**, and a similar *trans*-effect is observed in *trans-mer*-[(2,6-*i*Pr₂C₆H₃O)₃TaCl₂(PMe₂Ph)], in which the longest Ta-O bond is that opposite the phosphane ligand. The Ta-N_{ax} bond length in **15** is slightly shorter than the Ta-N_{ax} bond in the related TREN-type complex [(N₃N^{Et})Ta=CHCH₂]₂ (N₃N^{Et} = (Et₃SiNCH₂CH₂)₃N) (Ta-N: 2.375(10) Å) [168] and considerably shorter than the Ta-N_{ax} bond in [(N₃N)Ta(Me)OTf] (Ta-N: 2.536 Å) [169]. In **15** the rigidity of the tri(aryloxy)amine ligand likely plays a key role in the short Ta-N_{ax} bond length.

3.3.3 Synthesis of [L*Ta(Cl)E(SiMe₃)₂] (E = P (**16a**), As(**16b**))

The reaction of [L*TaCl₂] was carried out with LiE(SiMe₃)₂·1.8THF in *n*-hexane starting at -78°C. By allowing the yellow reaction mixture to warm slowly, no color change was observed until the solution had reached -15°C, at which point the solution abruptly turned red (E = P) or violet-red (E = As). For the phosphorus analogue, the ³¹P-NMR spectrum of the crude reaction mixture in C₆D₆ revealed a signal at 26.1 ppm, along with signals for HP(SiMe₃)₂, P(SiMe₃)₃, and several unidentified decomposition products. After measurement, the solution changed to pale yellow upon standing at room temperature for 24 hours. Upon second measurement of the sample a few days later, the signal at 26.1 ppm had disappeared, and a new far downfield signal at 389.3 ppm had appeared only as a minor product, while all other signals remained the same (the major product before and after decomposition is HP(SiMe₃)₂). The new signal lies in the region associated with terminal phosphinidene complexes and represents < 5% of the total signal intensity, but such a product could not be isolated from these reactions.

Rapid work-up of the red (E = P) and violet-red (E = As) solutions at low temperature and recrystallization from Et₂O afforded a few crystals of [L*Ta(Cl)E(SiMe₃)₂] (E = P (**16a**),

As (**16b**) suitable for characterization by X-ray diffraction and mass spectrometry. Complexes **16a** and **16b** are unstable in solution, decomposing slowly even during storage at -25°C and decomposing rapidly at room temperature. As a result no clean ^1H or ^{13}C -NMR spectra could be obtained. The isolation of **16a** and **16b** was reproducible and largely independent of the stoichiometry used; reaction of $[\text{L}^*\text{TaCl}_2]$ with two equivalents $\text{LiE}(\text{SiMe}_3)_2 \cdot 1.8\text{THF}$ yielded the same results as with one equivalent. The isolation of **16a** and **16b** represents an important step in tantalum chemistry, as no bis(trimethylsilyl)phosphanide or bis(trimethylsilyl)arsenide complexes of tantalum have so far been reported. Primary phosphide tantalum complexes have been obtained in the Hey-Hawkins group, whereby reactions of $[\text{Cp}^*\text{TaCl}_4]$ with two equivalents of $\text{LiP}(\text{H})\text{R}$ ($\text{R} = t\text{Bu}$, Cy , Ph , Mes) result in tantalum–tantalum bond formation and isolation of bridging tantalum(IV) phosphinidene complexes. [170]



In the EI mass spectrum of **16a** the molecular ion peak was not found, though peaks corresponding to loss of SiMe_3 and Me groups were detected. The parent peak at 831.4 corresponds to loss of one SiMe_3 group and two Me groups. The EI mass spectrum of **16b** displayed a similar fragmentation pattern, with the parent peak at 757.2 corresponding to $[\text{L}^*\text{TaCl}]^+$.

The reactivity of $[\text{L}^*\text{Ta}(\text{Cl})\text{P}(\text{SiMe}_3)_2]$ was investigated with the chloride-abstraction reagents $\text{KO}t\text{Bu}$ and AgOTf in THF and Et_2O , respectively, in attempts to prepare $[\text{L}^*\text{Ta}=\text{PSiMe}_3]$. Due to observed decomposition at room temperature, it was necessary to generate $[\text{L}^*\text{Ta}(\text{Cl})\text{P}(\text{SiMe}_3)_2]$ *in situ* at low temperature, and either $\text{KO}t\text{Bu}$ or AgOTf was added as a solid at 0°C . After warming to room temperature, a pale yellow solution resulted, and in the ^{31}P -NMR spectra only signals previously observed for decomposition of $[\text{L}^*\text{Ta}(\text{Cl})\text{P}(\text{SiMe}_3)_2]$ were revealed, signifying that the final chloride could not be abstracted by this method before decomposition of **16a**. The reluctance of the tris(aryloxy)amine

tantalum platform to support the hypothesized Ta=P double-bond complex $[L^*Ta=PSiMe_3]$ can be attributed both to the preferential C_s symmetry of the auxiliary ligand and the stronger donation properties of the phenolate ligands compared to amide ligands, as in $[(N_3N)Ta=PCy]$, in that too much electron density at tantalum disfavors multiple-bond formation.

Structure of $[L^*Ta(Cl)P(SiMe_3)_2]$ (**16a**)

An X-ray diffraction experiment was carried out on red prisms of **16a** grown from concentrated solutions of Et_2O . **16a** crystallizes in the monoclinic space group $P2_1/n$. The molecular structure is shown in Figure 22, and selected bond lengths and angles are given in Table 10.

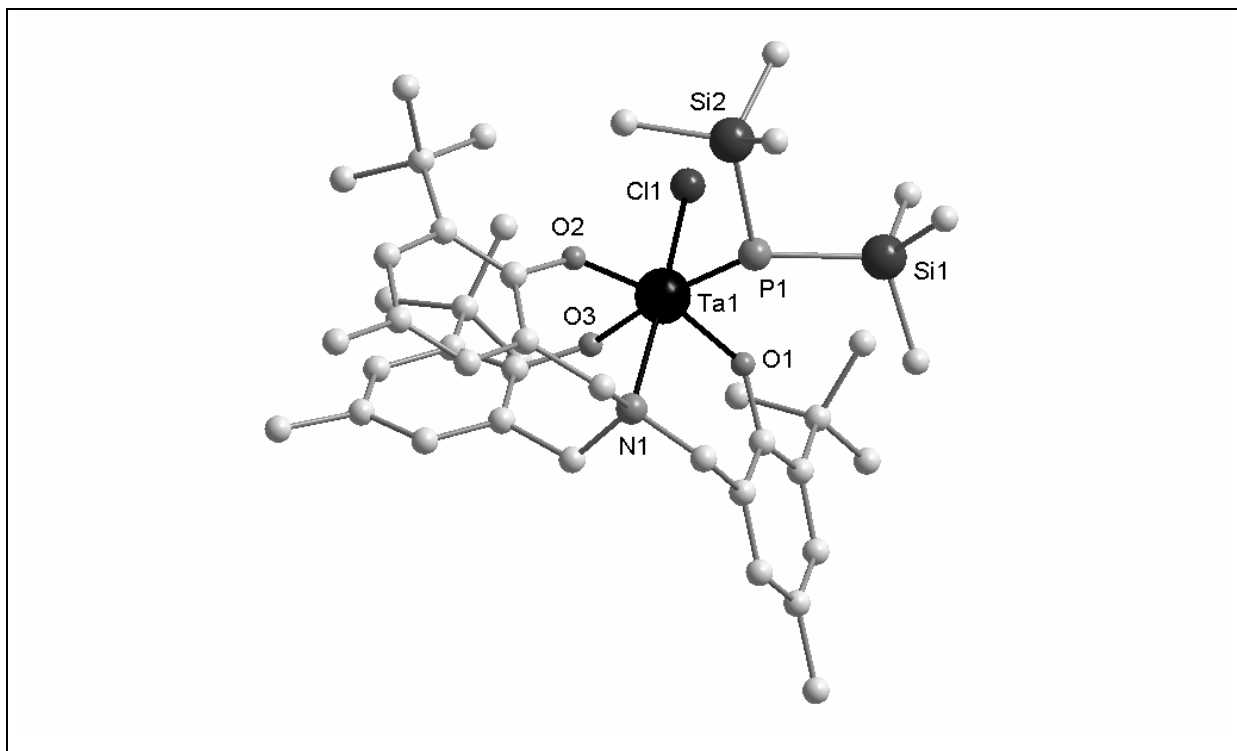


Figure 22: Molecular Structure of $[L^*Ta(Cl)P(SiMe_3)_2]$ (**16a**) in the crystal. H atoms have been omitted for clarity.

Table 10: Selected bond lengths [Å] and angles [°] in **16a**.

Ta-P	2.540(1)	Ta-Cl	2.362(1)
Ta-O(1)	1.904(3)	Ta-O(2)	1.904(3)
Ta-O(3)	2.005(3)	Ta-N	2.347(4)
N-Ta-P	88.11(9)	N-Ta-Cl	176.06(9)
O(1)-Ta-N	81.79(12)	O(2)-Ta-N	79.82(13)
O(3)-Ta-N	83.97(13)	O(1)-Ta-P	89.52(9)
O(2)-Ta-P	90.91(9)	O(3)-Ta-P	171.75(10)
O(1)-Ta-Cl	98.30(10)	O(2)-Ta-Cl	99.98(10)
O(3)-Ta-Cl	92.11(10)	O(1)-Ta-O(2)	161.58(13)
O(1)-Ta-O(3)	87.06(12)	O(2)-Ta-O(3)	89.97(12)
Si(1)-P-Ta	115.44(6)	Si(2)-P-Ta	119.38(7)
Cl-Ta-P	95.82(5)		

As was observed in the structure of **15**, the ligand set in compound **16a** is found in C_s symmetry, such that the tantalum center is in distorted octahedral geometry. The bis(trimethylsilyl)phosphanide ligand occupies an equatorial position, which correlates with a reactivity patten in accordance with the longer equitorial Ta-Cl bond length compared to the axial Ta-Cl bond length in **15** and correlates with the observed substitution behavior of related tris(aryloxy)amine tantalum diethoxides, in which the equatorial ethoxide ligand is generally more reactive to substitution. [162] The N-Ta-Cl axis in **16a** deviates only slightly from linearity (176.06(9)°). As with complex **15**, the Ta–O bonds are bent slightly away from the axial chloride ligand. The phosphorus atom possesses trigonal pyramidal geometry; however, the Ta-P-Si bond angles (115.44(6)°, 119.38(7)°) are somewhat more obtuse than ideal trigonal pyramidal geometry, signifying a slight flattening of the phosphanide ligand.

The Structure of [L*Ta(Cl)As(SiMe₃)₂] (**16b**)

An X-ray diffraction experiment was carried out on violet-red prisms of **16b** grown from concentrated solutions of Et₂O. **16b** crystallizes in the monoclinic space group $P2_1/n$. The molecular structure is shown in Figure 23, and selected bond lengths and angles are given in Table 11.

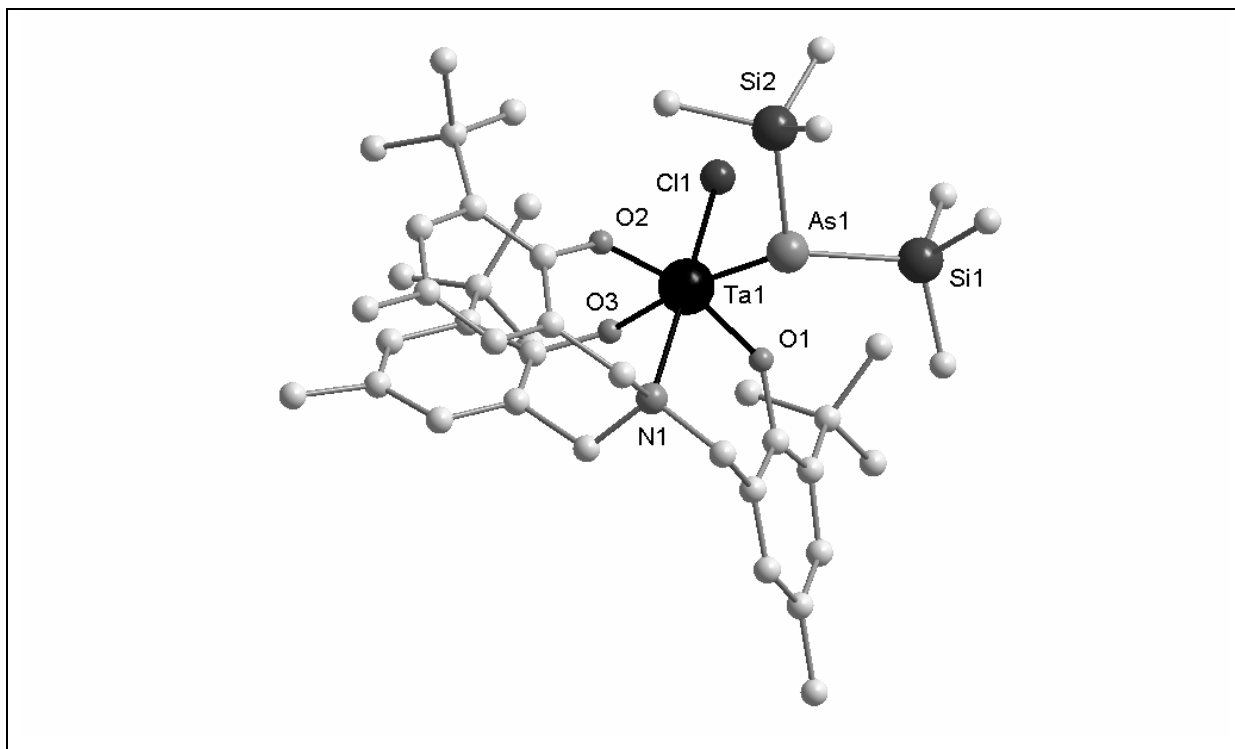


Figure 23: Molecular structure of $[L^*Ta(Cl)As(SiMe_3)_2]$ (**16b**) in the crystal. H atoms have been omitted for clarity.

Table 11: Selected bond lengths [Å] and angles [°] in **16b**.

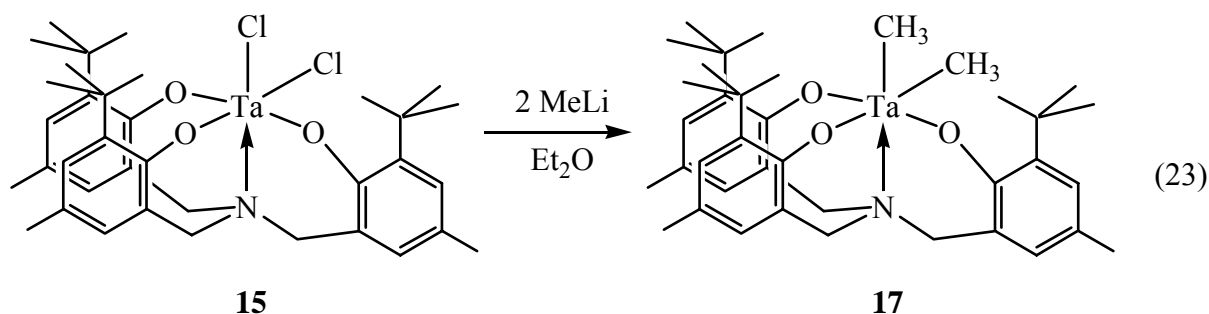
Ta-As	2.637(2)	Ta-Cl	2.351(8)
Ta-O(1)	1.894(13)	Ta-O(2)	1.889(15)
Ta-O(3)	1.947(11)	Ta-N	2.325(18)
N-Ta-As	87.0(4)	N-Ta-Cl	176.7(4)
O(1)-Ta-N	81.0(7)	O(2)-Ta-N	81.4(7)
O(3)-Ta-N	82.5(6)	O(1)-Ta-As	89.2(4)
O(2)-Ta-As	91.5(4)	O(3)-Ta-As	169.3(5)
O(1)-Ta-Cl	98.1(6)	O(2)-Ta-Cl	99.4(5)
O(3)-Ta-Cl	94.4(5)	O(1)-Ta-O(2)	162.3(7)
O(1)-Ta-O(3)	87.2(5)	O(2)-Ta-O(3)	88.9(6)
Si(1)-As-Ta	113.4(2)	Si(2)-As-Ta	117.2(2)
Cl-Ta-As	96.10(16)		

The molecular structure of **16b** is nearly isomorphous to that of **16a**. The bis(trimethylsilyl)arsenide ligand occupies the equatorial position, and the tris(aryloxy)amine ligand is bent slightly away from the axial chloride. The arsenic atom is found in trigonal pyramidal geometry, with the Ta-As-Si bond angles (113.4(2)°, 117.2(2)°) slightly more

obtuse than ideal trigonal pyramidal geometry. The Ta-O bond *trans* to the arsenide ligand in **16b** (1.947(11) Å) is shorter than the corresponding Ta-O bond in **16a** (2.005(3) Å), likely as a result of a less pronounced *trans* effect from the poorer donating arsenide ligand than the corresponding phosphanide ligand.

3.3.4 Synthesis of [L*TaMe₂] (**17**)

Because the axial chloride in [L*TaCl₂] proved resistant to substitution in the above reactions with the lithium phosphanide and arsenide, reaction of [L*TaCl₂] with two equivalents MeLi was carried out to gauge the substitution potential of [L*TaCl₂] toward dialkylation. It was expected that the more strongly nucleophilic methyl anion would lead to disubstitution. Treatment of [L*TaCl₂] with a solution of MeLi in Et₂O at low temperature resulted in a pale yellow solution and precipitation of LiCl. Work-up and crystallization from the reaction mixture afforded pale yellow needles of [L*TaMe₂].



The ¹H- and ¹³C-NMR spectra of **17** reveal C_{3v} symmetry of the molecule in solution. This observation is unexpected given the C_s symmetry observed in complexes **15** and **16a,b**. The ¹H-NMR spectrum is shown in Figure 24. The aryl-Me and aryl-*t*Bu groups appear each as a single signal, and the aryl-protons appear as doublets. The protons representing the N-bound methylene group are obstructed by a quartet from residual Et₂O present in the sample. Et₂O could not be completely removed from samples of **17** even despite thorough drying in high vacuum.

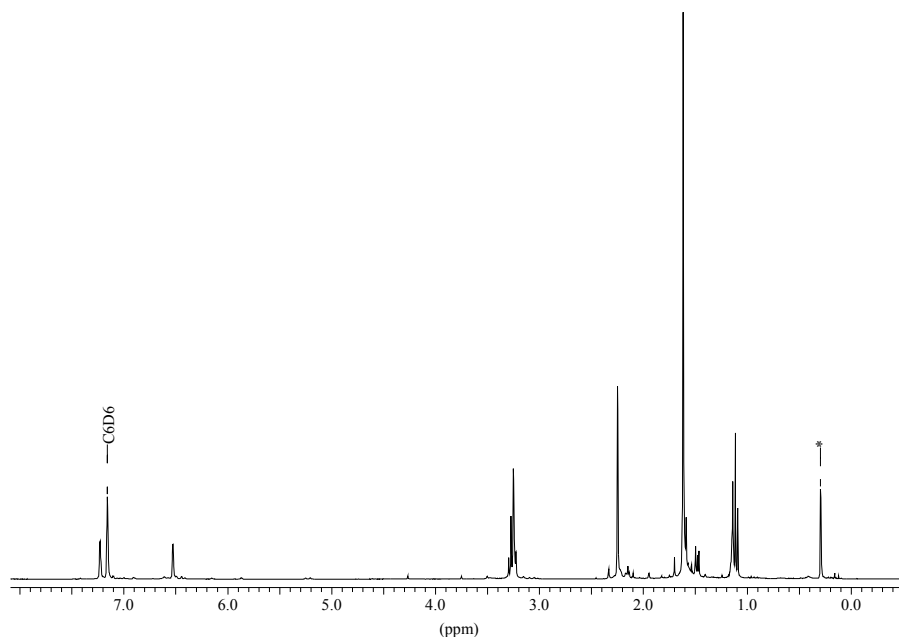


Figure 24: ^1H -NMR spectrum of $[\text{L}^*\text{TaMe}_2]$ (**17**) (C_{3v} symmetry) in C_6D_6 . Impurity is designated with (*).

In both the ^1H - and ^{13}C -NMR spectra, signals representing the Ta-bound methyl groups could not be assigned. The ^1H -NMR signal for Ta- CH_3 would be expected in the high-field region and is found at -0.21 ppm in $[(2,6\text{-Ph}_2\text{C}_6\text{H}_3\text{O})_3\text{TaMe}_2]$. [171] The ^{13}C -NMR signal for Ta- CH_3 in $[(2,6\text{-Ph}_2\text{C}_6\text{H}_3\text{O})_3\text{TaMe}_2]$ is found at 64.8 ppm, approximately the same shift as found for a selection of Ta-bound methyl groups reported in the literature. However, aside of the peak representing the N-bound methylene group ($\delta = 58.90$ ppm) and a trace of Et_2O ($\delta = 64.49$ ppm), no signal was observed within 20 ppm of 65 ppm for **17**.

In the EI mass spectrum of **17**, the molecular ion peak is observed, and the parent peak corresponds to $[\text{L}^*\text{Ta}]^+$. No peak corresponding to the partially alkylated compound $[\text{L}^*\text{Ta}(\text{Me})\text{Cl}]$ is observed, indicating complete alkylation in the isolated product. This observation stands in contrast to the results reported above for reactions of $[\text{L}^*\text{TaCl}_2]$ with $\text{LiE}(\text{SiMe}_3)_2$, in which the axial chloride remained unsubstituted even in the presence of excess $\text{LiE}(\text{SiMe}_3)_2$.

Structure of $[\text{L}^*\text{TaMe}_2]$ (**17**)

An X-ray diffraction experiment was carried out on pale yellow prisms of **17** grown from concentrated solutions of Et_2O . **17** crystallizes in the monoclinic space group $P2_1/c$. The molecular structure is shown in Figure 25, and selected bond lengths and angles are given in Table 12.

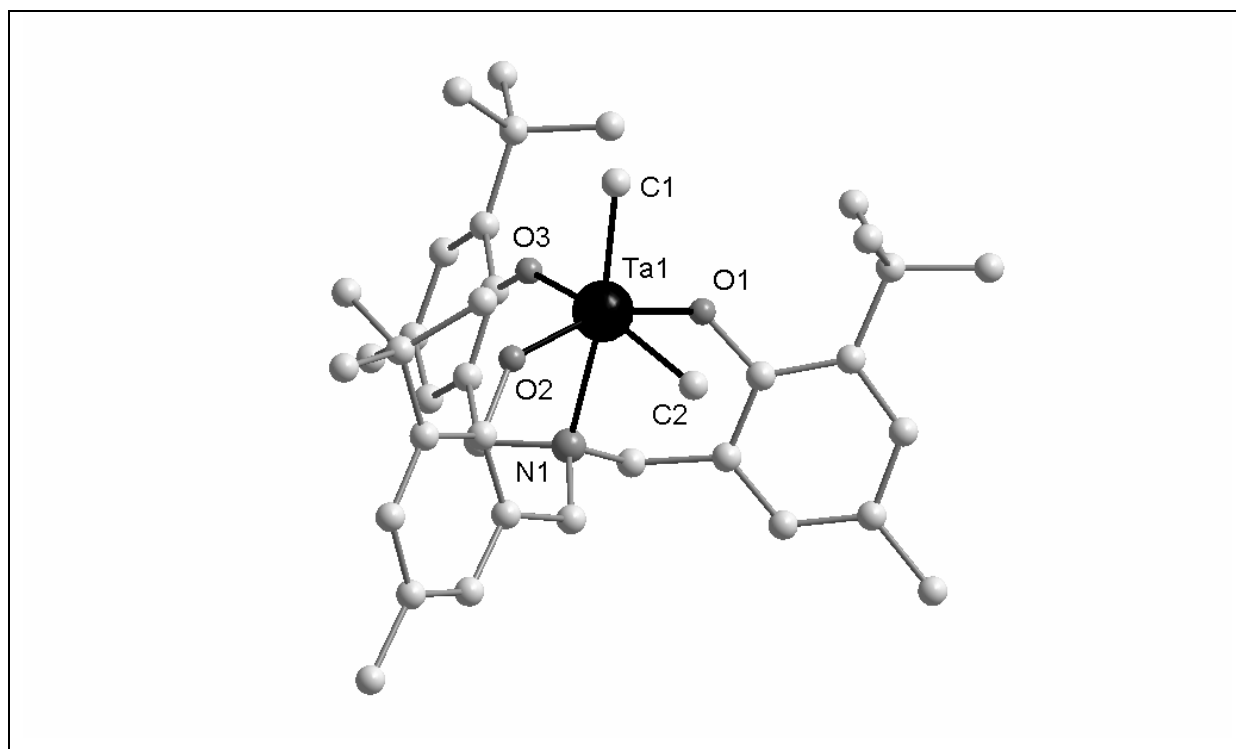


Figure 25: Molecular structure of $[L^*TaMe_2]$ (**17**) in the crystal. H atoms have been omitted for clarity.

Table 12: Selected bond lengths [\AA] and angles [$^\circ$] in **17**.

Ta-C _{eq}	2.311(4)	Ta-C _{ax}	2.200(5)
Ta-O(1)	1.942(5)	Ta-O(2)	1.906(5)
Ta-O(3)	1.938(4)	Ta-N	2.434(5)
N-Ta-C _{eq}	90.65(17)	N-Ta-C _{ax}	171.8(2)
O(1)-Ta-N	82.62(18)	O(2)-Ta-N	77.55(19)
O(3)-Ta-N	77.83(18)	O(1)-Ta-O(2)	157.28(19)
O(3)-Ta-O(2)	96.14(19)	O(3)-Ta-O(1)	90.38(19)
O(1)-Ta-C _{eq}	84.87(18)	O(2)-Ta-C _{eq}	84.37(18)
O(3)-Ta-C _{eq}	168.04(18)	O(1)-Ta-C _{ax}	101.2(2)
O(2)-Ta-C _{ax}	99.9(2)	O(3)-Ta-C _{ax}	94.8(2)
C _{eq} -Ta-C _{ax}	96.9(2)		

The molecular structure of **17** is nearly isomorphous to that of **15**, except that both chloride ligands are replaced by methyl ligands. Compound **17** exhibits approximate C_s symmetry in the crystal, although the ^1H - and ^{13}C -NMR spectra indicated C_{3v} symmetry. A similar situation is represented by $[L^*TaBz_2]$, which exhibits C_s symmetry in the crystal and C_{3v} symmetry in solution. [164] The tantalum atom is located in distorted octahedral geometry,

and analogously to complex **15**, the Ta-O bonds are bent slightly away from the methyl ligands. The N-Ta-C_{ax} axis deviates from linearity (171.8(2)°) more strongly than in complexes **15** and **16a,b**. The axial Ta-C bond length is longer than the equatorial Ta-C bond, indicating a larger *trans* effect of the phenolate ligand than the amine donor. The Ta-C bond lengths (2.311(4) Å, 2.200(5) Å) are within the range of known Ta-CH₃ distances, as in [(PhC₆H₃(C₆H₄)O)(2,6-Ph₂C₆H₃)₂TaMe] (Ta-C_{Me}: 2.215(7) Å). [172]

3.4 *cyclo*-P₄ tantalum complex for formation of supramolecular assemblies

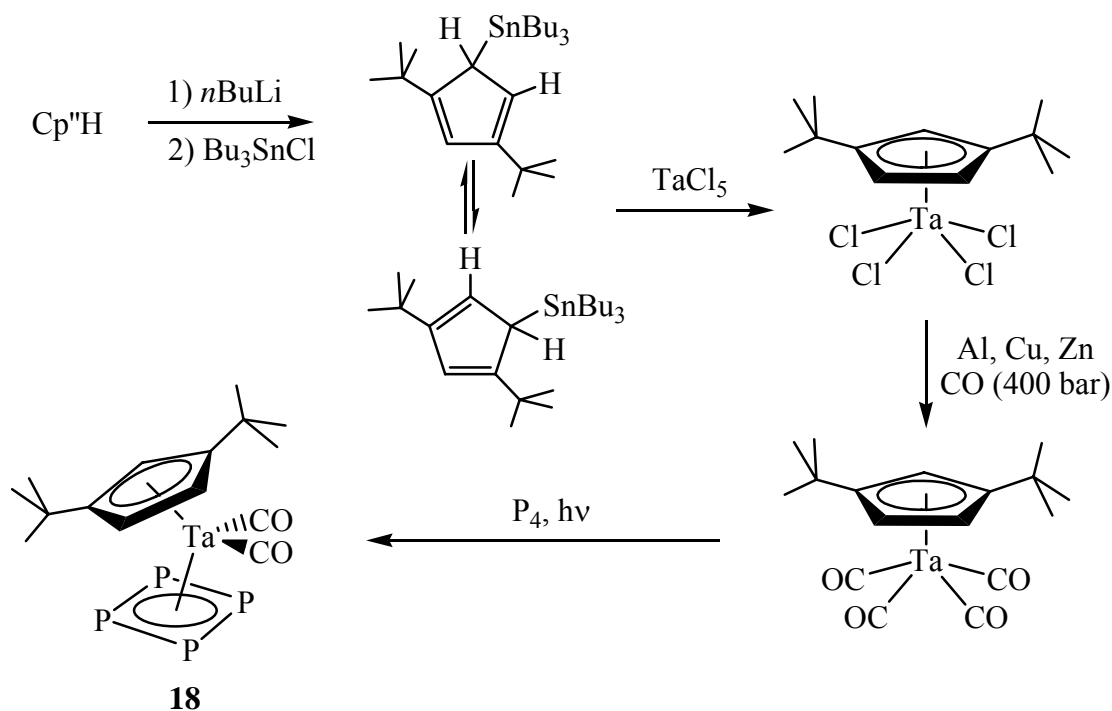
3.4.1 Background and research objective

While the coordination chemistry for various μ, η^2 -P₂ and *cyclo*-P_n (n = 3,5) ligand complexes has been investigated with late transition-metal salts (see Introduction), the coordination chemistry of *cyclo*-P₄ ligand complexes has remained largely untouched. Two obvious candidates exist for the exploration of the coordination chemistry of metal-bound *cyclo*-P₄ ligands. The *cyclo*-P₄ complex [Cp*Nb(CO)₂(η^4 -P₄)] [173] was reported by Scherer *et al.*, but extensive details about its reactivity have not been reported, perhaps due to the low yield in its preparation. The related tantalum complex [Cp''Ta(CO)₂(η^4 -P₄)] [174,175] could be synthesized in considerably higher yield and was chosen for this reason for the current study in forming supramolecular assemblies with late transition-metal salts. Unlike the pentaphosphaferrocene starting material [Cp*Fe(η^5 -P₅)], [Cp''Ta(CO)₂(η^4 -P₄)] possesses a sterically encumbering Cp'' group, which is tilted non-parallel relative to the *cyclo*-P₄ ring (Cp''(centroid)-Ta-P₄(centroid) = 144.2°). As a result, in addition to the four-membered phosphorus ring, the bulky nature of the Cp'' ring and tilted position of the Cp'' ring relative to the *cyclo*-P₄ ligand would be expected to play a role in the types of assemblies formed by [Cp''Ta(CO)₂(η^4 -P₄)] with copper(I) halides. Additionally, the *t*Bu groups would be expected to enhance solubility of potential oligomeric products.

Previous studies have demonstrated the ability of [Cp''Ta(CO)₂(η^4 -P₄)] to participate in insertion reactions with organometallic niobium and cobalt centers as well as in donor-acceptor interactions with further Lewis-acidic tantalum fragments. [174] Reactions with copper(I) halides would be expected to yield oligomeric compounds related to the fullerene-like molecule [$\{\text{Cp}^*\text{Fe}(\mu, \eta^5: \eta^1: \eta^1: \eta^1: \eta^1: \eta^1\text{-P}_5)\}_{12} \{\text{CuCl}\}_{10} \{\text{Cu}_2\text{Cl}_3\}_5 \{\text{Cu}(\text{MeCN})_2\}_5$], which possesses alternating five- and six-membered rings. [75] In the current case, the *cyclo*-P₄ ring in [Cp''Ta(CO)₂(η^4 -P₄)] offers the possibility of preparing a fullerene-like structure with four-membered rings. While four-membered carbon rings are not found in stable fullerene cages, [Cp''Ta(CO)₂(η^4 -P₄)] provides transition-metal stabilized four-membered phosphorus rings for exploring the synthesis of geometries not currently experimentally approachable in carbon-only chemistry.

3.4.2 Preparation of $[\text{Cp}''\text{Ta}(\text{CO})_2(\eta^4\text{-P}_4)]$ (**18**)

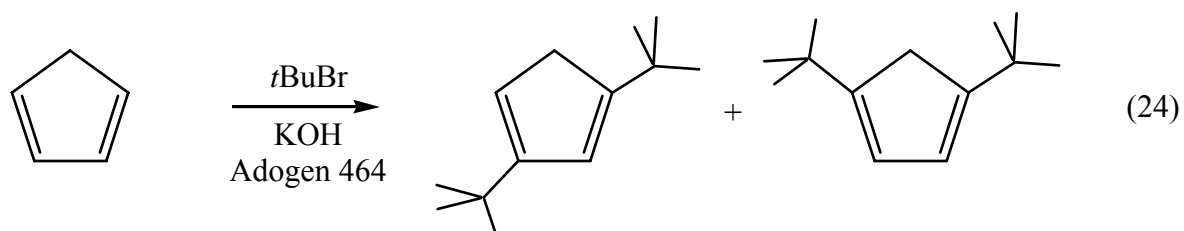
Starting from $\text{Cp}''\text{H}$, the four-step synthetic procedure for the preparation of $[\text{Cp}''\text{Ta}(\text{CO})_2(\eta^4\text{-P}_4)]$ (**18**) is shown in Scheme 10.



Scheme 10: Synthetic route to the *cyclo*- P_4 complex $[\text{Cp}''\text{Ta}(\text{CO})_2(\eta^4\text{-P}_4)]$ (**18**).

Several preparations for $\text{Cp}''\text{H}$ have been reported in the literature. Historically $\text{Cp}''\text{H}$ has been produced by the alkylation of anionic Cp systems, such as cyclopentadienyl Grignards or alkali-metal cyclopentadienide, which necessitate use of a stringent inert atmosphere and normally successive synthetic steps for each alkylation. [176,177] Since routes going through $\text{Cp}'\text{H}$ require two synthetic steps from commercially available or freshly cracked cyclopentadiene, it was expedient to incorporate a method that produces $\text{Cp}''\text{H}$ in high yield under mild conditions in only one step. A phase-transfer procedure starting from CpH was published in which CpH was doubly alkylated using $t\text{BuBr}$, an excess of KOH as base, and the phase-transfer agent Adogen 464. [178] The choice of KOH is critical to producing dialkylated $\text{Cp}''\text{H}$ as the main product, since use of the stronger base NaH or KH with $t\text{BuBr}$ results principally in trialkylation and generation of $\text{Cp}'''\text{H}$. [179] Though the procedure with Adogen 464 was reported to yield $\text{Cp}''\text{H}$ in 90% yield, subsequently reported experiments revealed problems of irreproducibility with this procedure and an experimental yield of 44% using Aliquat 336 as an alternative catalyst. [180] Initial attempts with the phase-transfer method using Adogen 464 in this work gave satisfying results with yields of

approximately 40%. Though the yield is considerably lower than that published, isolation on a relatively large scale (> 25 g) sufficed for all further steps. In the isolated product, two substitution patterns were observed, the 1,3- and 1,4-*t*Bu₂-cyclopentadiene isomers, in approximate 2:1 ratio as determined by ¹H-NMR spectroscopy. The third potential isomer, 2,5- *t*Bu₂-cyclopentadiene, was not observed in the final product.



Stannylation of Cp''H by successive treatment with *n*BuLi and *n*Bu₃SnCl afforded Cp''Sn(*n*Bu)₃ in high yield. [181] During distillation of the product, it is advisable not to let the distillation column or bridge cool at any point; use of a powerful heat gun for this purpose is recommendable. Reaction of Cp''Sn(*n*Bu)₃ with TaCl₅ provided the tetrachloride complex [Cp''TaCl₄], which was obtained in pure form by recrystallization from toluene at -25°C. For the reduction/carbonylation step, [Cp''TaCl₄] was dissolved in THF and transferred under nitrogen into an autoclave with powders of Al, Cu, and Zn. Although a stirring autoclave was recommended for highest yields, [182] only an autoclave rotating at an approximate 45° angle was available. Using this type of autoclave with a CO pressure of 400 bar at a temperature of 100°C for 5 days, [Cp''Ta(CO)₄] could be obtained in crystalline form in 65% yield. For the photolysis of [Cp''Ta(CO)₄] with P₄ to prepare complex **18**, it was ascertained that the yield depended heavily on the reaction conditions. For best results, the reaction time was not allowed to exceed 20 minutes, nitrogen was purged through the solution during reaction, and the solution was stirred vigorously and uniformly. A yield of 26% was obtained in this work for the synthesis of complex **18**, while yields approaching 58% had been previously reported. [174]

3.4.3 Synthesis of [{Cp''Ta(CO)₂(μ,η⁴:η¹:η¹:η¹:η¹-P₄)}₆{CuCl}]₈ (19a)

Layering a solution of CuCl in MeCN/CH₂Cl₂ (1:1) onto a solution of [Cp''Ta(CO)₂(η⁴-P₄)] in CH₂Cl₂ in 1:1 stoichiometry resulted in immediate precipitation of an orange, microcrystalline powder. A powder diffraction experiment was carried out on the

isolated powder. The spectrum is provided in Figure 26, showing the indexed peaks which were selected for analysis. Analysis of these data indicated a compound crystallizing in the trigonal space group $R\bar{3}$ with refined cell parameters $a = 22.863(8)$ Å and $c = 22.716(10)$ Å and a cell volume of $10282.6(77)$ Å³.

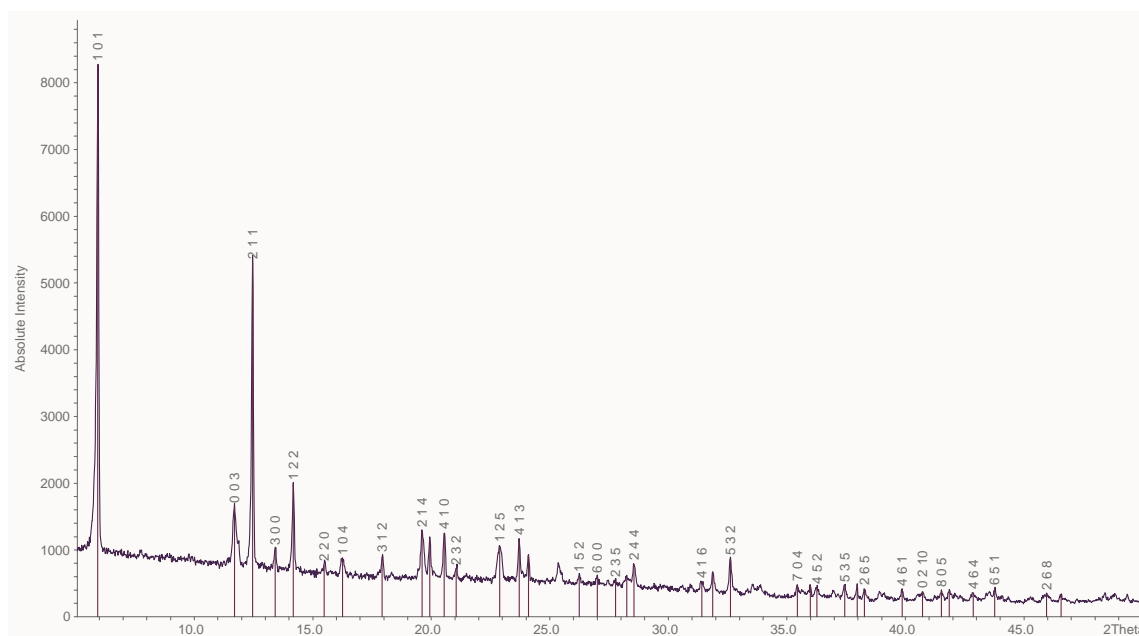
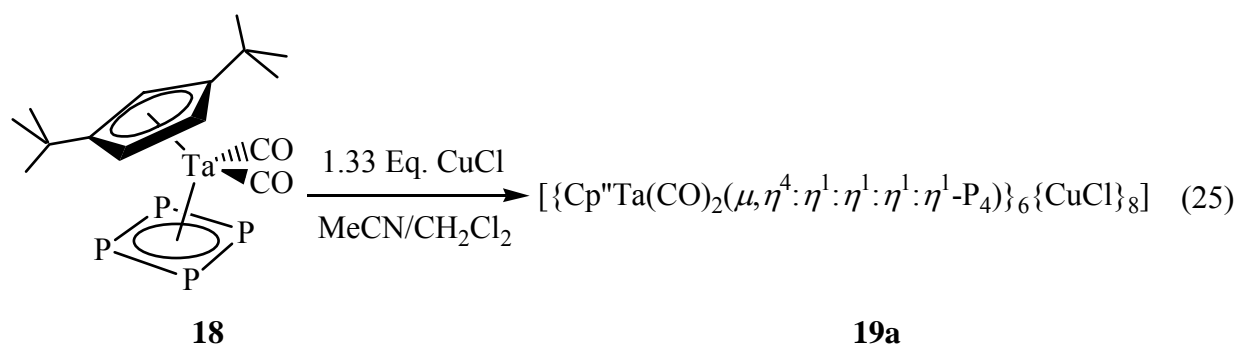


Figure 26: Indexed powder diffraction spectrum of **19a**.

Within the microcrystalline powder a few larger, cube-shaped crystals were found, which could additionally be measured by a single-crystal X-ray diffraction experiment and identified as the oligomeric spherical molecule $[\{\text{Cp}''\text{Ta}(\text{CO})_2(\mu, \eta^4: \eta^1: \eta^1: \eta^1\text{-P}_4)\}_6\{\text{CuCl}\}_8]$ (**19a**). The formation of **19a** seems largely independent of the stoichiometry used. While **19a** possesses a $[\text{Cp}''\text{Ta}(\text{CO})_2(\eta^4\text{-P}_4)]/\text{CuCl}$ ratio of 3:4, **19a** is formed in approximately 50% yield from the reaction in 1:1 stoichiometry. Reaction of $[\text{Cp}''\text{Ta}(\text{CO})_2(\eta^4\text{-P}_4)]$ with a large excess of CuCl (ca. 1:5 **18**:CuCl) also resulted in formation of **19a** in low yield. For optimized results, the 3:4 stoichiometry was used, and **19a** could be isolated in yields as high as 66%.



For the reproducible preparation of single crystals of **19a** in high yield, a double-layering system was developed, such that the reactants could come into contact as slowly as possible. When a solution of CuCl was layered directly onto a solution of $[\text{Cp}^*\text{Ta}(\text{CO})_2(\eta^4\text{-P}_4)]$, the immediate precipitation of crystals of **19a** was observable at the phase interface. In order to allow the reactants to diffuse more slowly, a middle layer was used. In this system (see Experimental Section), the total volume was held to the same volume used in the two-component system, while the proportion of MeCN was systematically increased from the bottom layer to the top. Thus, onto a solution of $[\text{Cp}^*\text{Ta}(\text{CO})_2(\eta^4\text{-P}_4)]$ in CH_2Cl_2 was layered MeCN/ CH_2Cl_2 (1:2), followed by a solution of CuCl in MeCN/ CH_2Cl_2 (1:1). As such, the reactants were forced to diffuse into the empty middle layer first, before coming into contact with one another, ensuring slow reaction and crystal growth.

19a is insoluble in all common organic solvents, even in the more polar solvents such as MeOH, H_2O , ethyl acetate, THF, DME, 1,2-dichlorobenzene, MeCN, and acetone. In DMF, **19a** appears to dissolve only by dissociation, whereby the $\text{P} \rightarrow \text{Cu}$ dative bonds are ruptured by the highly polar donor solvent. ^1H - and ^{31}P -NMR spectra were measured of a colorless solution of DMF- d_7 decanted immediately from a freshly prepared suspension of **19a** and revealed only traces of free $[\text{Cp}^*\text{Ta}(\text{CO})_2(\eta^4\text{-P}_4)]$. Allowing such a suspension to stand for one week or sonicating overnight resulted in darkening of the solution to light brown, and ^1H - and ^{31}P -NMR spectra showed increased concentrations of clean $[\text{Cp}^*\text{Ta}(\text{CO})_2(\eta^4\text{-P}_4)]$. Similarly, the ^{31}P -NMR spectrum (in CD_2Cl_2) of the decanted mother liquor from synthesis of **19a** showed only the presence of $[\text{Cp}^*\text{Ta}(\text{CO})_2(\eta^4\text{-P}_4)]$. Throughout all NMR experiments with **19a**, no compounds other than $[\text{Cp}^*\text{Ta}(\text{CO})_2(\eta^4\text{-P}_4)]$ could be detected.

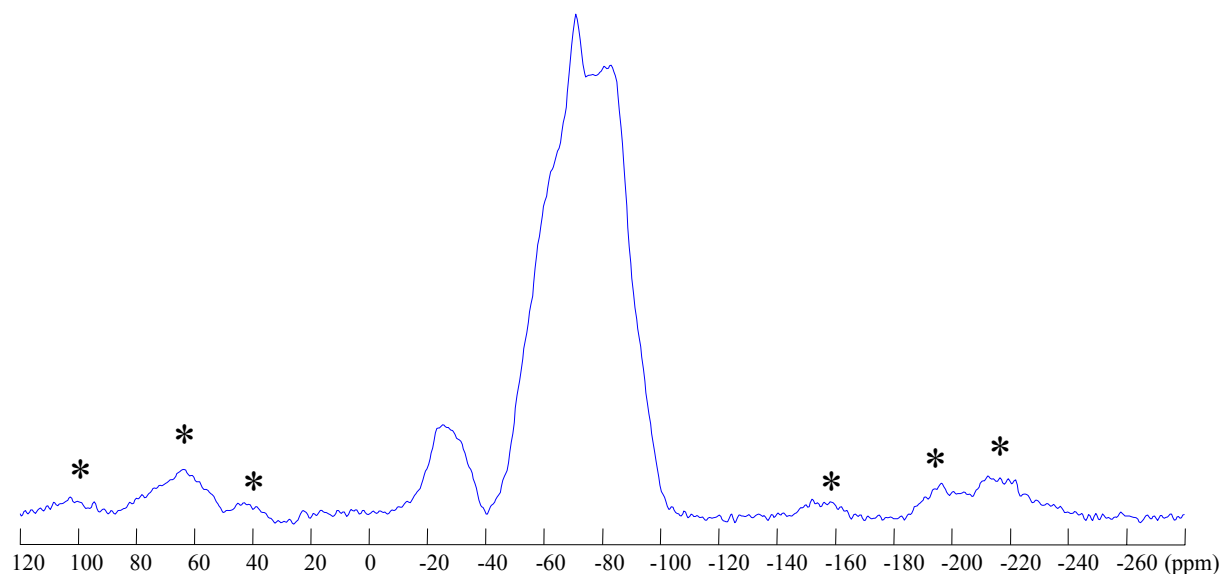


Figure 27: ^{31}P -MAS-NMR spectrum of **19a** at room temperature. Extraneous peaks are marked with asterisks (*).

The solid-state ^{31}P -MAS-NMR spectrum of **19a** was measured at room temperature and revealed two poorly resolved peaks as shown in Figure 27. The more intense signal appears centered at about -70 ppm, about 80 ppm high-field of the solution-NMR signal for complex **18** in CD_2Cl_2 . [175] The lack of resolution in the ^{31}P -MAS-NMR spectrum of **19a** was attributed to dipolar interactions of the phosphorus nuclei with the quadrupole tantalum and copper centers.

An ESI mass spectrum was recorded on a DMF solution freshly decanted from a suspension of **19a** and revealed peaks corresponding to $[\{\text{Cp}''\text{Ta}(\text{CO})_2\text{P}_4\}_2\text{Cu}_2\text{Cl}]^+$ and $[\{\text{Cp}''\text{Ta}(\text{CO})_2\text{P}_4\}_2\text{Cu}]^+$, indicating the presence of Cu-coordinated $[\text{Cp}''\text{Ta}(\text{CO})_2(\eta^4\text{-P}_4)]$ fragments in solution, though no such coordination could be detected in the solution NMR spectra. A further peak was observed corresponding to the disproportionation fragment $[\{\text{Cp}''\text{Ta}(\text{CO})_2\text{P}_4\}_4\text{Cu}]^+$. The IR spectrum of **19a** revealed two CO stretches at 2040 and 1974 cm^{-1} , which are shifted to higher wave numbers from the free $[\text{Cp}''\text{Ta}(\text{CO})_2(\eta^4\text{-P}_4)]$ complex ($1983, 1952\text{ cm}^{-1}$). Correct C,H elemental analysis was obtained on a sample of **19a**.

Structure of $[\{\text{Cp}''\text{Ta}(\text{CO})_2(\mu, \eta^4: \eta^1: \eta^1: \eta^1\text{-P}_4)\}_6\{\text{CuCl}\}_8]$ (**19a**)

An X-ray diffraction experiment was carried out on orange blocks of **19a** obtained directly from the reaction mixture in $\text{MeCN}/\text{CH}_2\text{Cl}_2$. **19a** crystallizes with one molecule CH_2Cl_2 in the trigonal space group $R\bar{3}$.

The cell constants obtained from the single-crystal X-ray diffraction experiment match well with the cell constants obtained from the powder-diffraction experiment, with only small variations. These data are summarized in Table 13.

Table 13: Cell constants from powder and single-crystal X-ray diffraction on **19a**.

	Powder	Single-crystal
a [Å]	22.863(8)	22.845(3)
c [Å]	22.716(10)	22.658(5)
Volume [Å ³]	10282.6(77)	10241(3)

The molecular structure of **19a** is shown in Figure 28, and selected bond lengths and angles are given in Table 14.

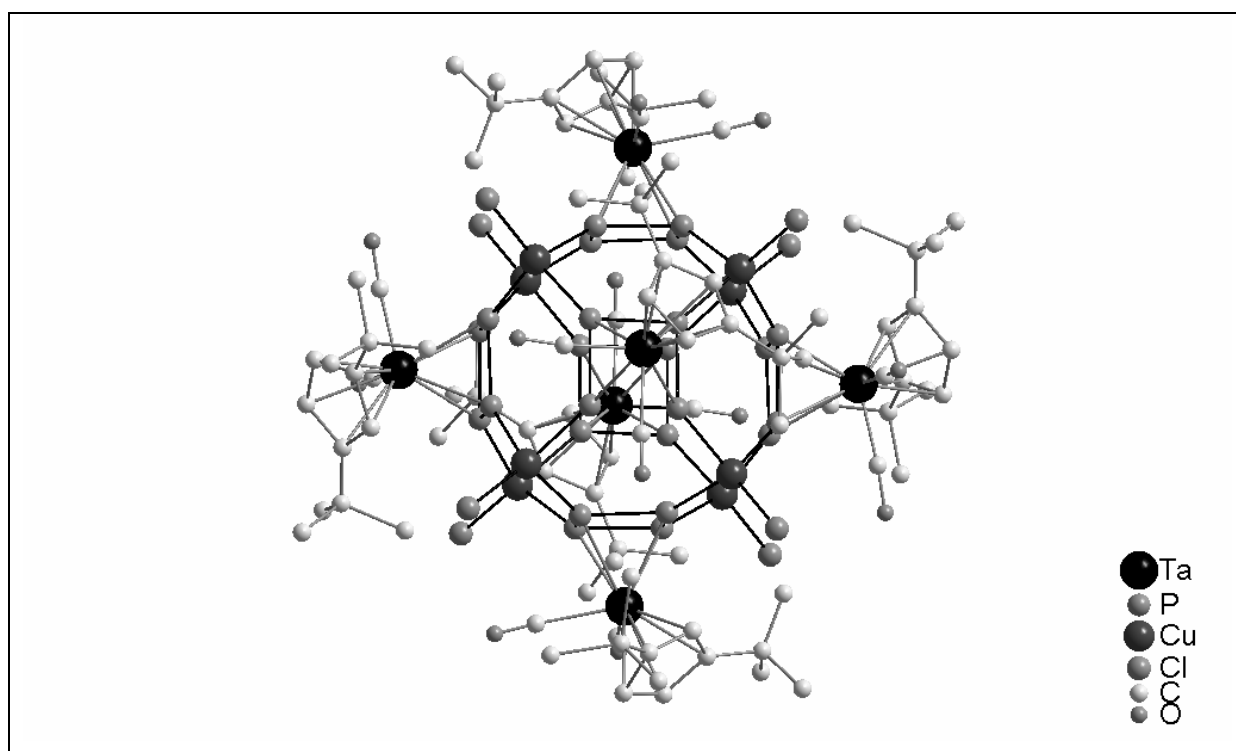


Figure 28: Molecular structure of $[\{\text{Cp}''\text{Ta}(\text{CO})_2(\mu, \eta^4: \eta^1: \eta^1: \eta^1: \eta^1\text{-P}_4)\}_6\{\text{CuCl}\}_8]$ (**19a**). H atoms have been omitted for clarity.

Table 14: Selected bond lengths [Å] and angles [°] in **19a**.

P(1)-P(4)	2.161(3)	P(1)-P(2)	2.189(3)
P(2)-P(3)	2.187(3)	P(3)-P(4)	2.157(3)
Cu(1)-P(1)	2.295(2)	Cu(2)-P(4)	2.331(2)
Cu(2)-P(2)'	2.342(2)	Cu(2)-P(3)'	2.317(2)
Ta(1)-C _{Co} (14)	2.121(8)	Ta(1)-C _{Co} (15)	2.127(8)
Ta-C _{Cp} ''	2.415(7) ^a	Ta-P	2.640(2) ^a
Cu(1)-Cl(1)	2.238(5)	Cu(2)-Cl(2)	2.239(2)
P(4)-P(1)-P(2)	88.13(9)	P(3)-P(2)-P(1)	90.98(9)
P(4)-P(3)-P(2)	88.27(10)	P(3)-P(4)-P(1)	92.54(10)
Cl(1)-Cu(1)-P(1)	117.55(7)	Cl(2)-Cu(2)-P(4)	118.13(7)
Cl(2)-Cu(2)-P(2)'	120.17(8)	Cl(2)-Cu(2)-P(3)'	117.13(8)
P(1)-Cu(1)-P(1)'	100.32(8)	P(4)-Cu(2)-P(2)'	98.61(7)
P(4)-Cu(2)-P(3)'	97.99(7)	P(2)'-Cu(2)-P(3)'	100.76(7)

^a Mean value is given

The molecular structure of **19a** comprises a closed-cage core (shown in Figure 29) with a crystallographic three-fold axis passing through the Cu(1)-Cl(1) bonds and diagonally through the middle of the cage. The overall structure resembles an extended cube in which the six faces are represented by the *cyclo*-P₄ rings and the twelve edges replaced by six-membered Cu₂P₄ rings in boat conformation. This results in a truncated spherical framework consisting exclusively of alternating planar 4-membered rings and bowed 6-membered rings.

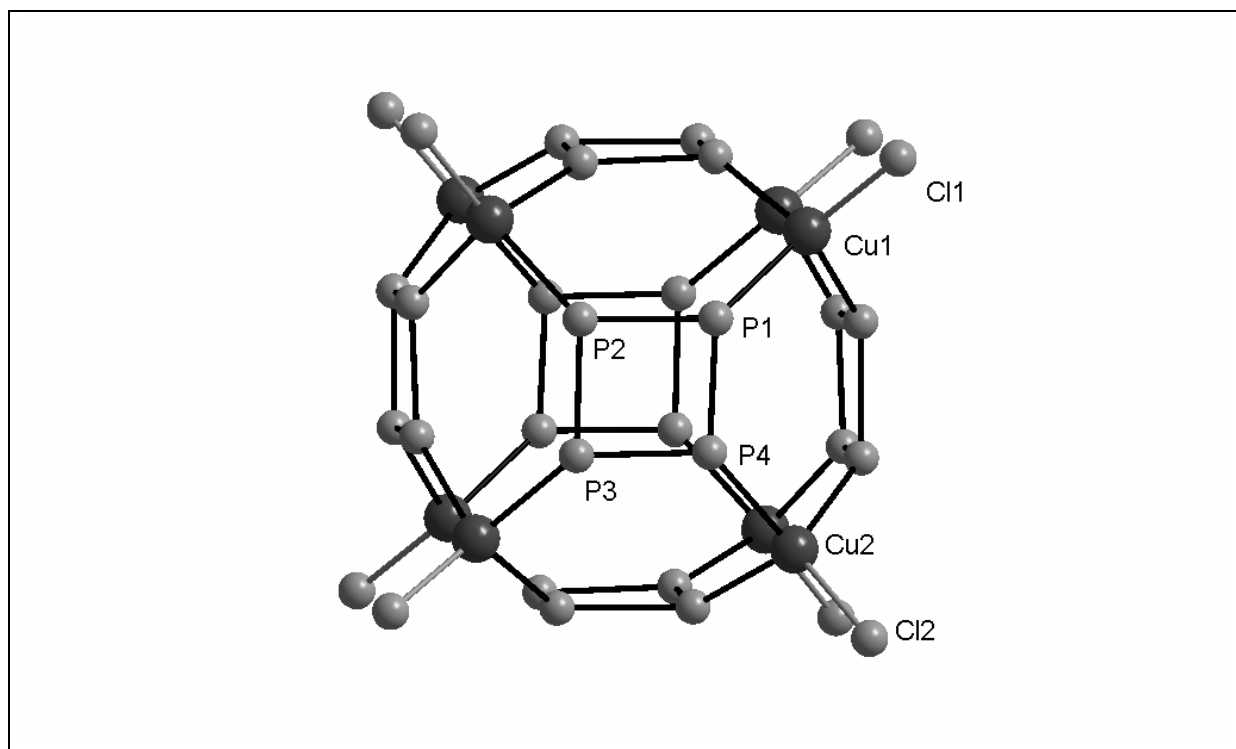


Figure 29: View of inner core of $[\{\text{Cp}''\text{Ta}(\text{CO})_2(\mu, \eta^4: \eta^1: \eta^1: \eta^1: \eta^1\text{-P}_4)\}_6\{\text{CuCl}\}_8]$ (**19a**). The $\text{Cp}''\text{Ta}(\text{CO})_2$ fragments have been omitted for clarity.

Each of the P atoms of the *cyclo*- P_4 rings is bound to Cu in 1,2,3,4-coordination mode. Each CuCl unit is bound by three $[\text{Cp}''\text{Ta}(\text{CO})_2(\eta^4\text{-P}_4)]$ units. The geometry about Cu is a puckered tetrahedron with the P-Cu-P angles ranging from $97.99(7)^\circ$ to $100.76(7)^\circ$ and the Cl-Cu-P angles ranging from $117.13(8)^\circ$ to $120.17(8)^\circ$. This puckering is also observed in the spherical molecule $[\{\text{Cp}^*\text{Fe}(\mu, \eta^5: \eta^1: \eta^1: \eta^1: \eta^1\text{-P}_5)\}_{12}\{\text{CuCl}\}_{10}\{\text{Cu}_2\text{Cl}_3\}_5\{\text{Cu}(\text{MeCN})_2\}_5]$, [75] whereas the geometry about Cu in mononuclear complexes such as $[(\text{Ph}_3\text{P})_3\text{CuCl}]$ (P-Cu-P (avg.): $109.8(7)^\circ$; Cl-Cu-P: $109.1(7)^\circ$) is a more uniform tetrahedron. [183] The Cu-Cl bond distances in **19a** (2.238(5) Å and 2.239(2) Å) are slightly shorter in comparison to $[(\text{Ph}_3\text{P})_3\text{CuCl}]$ (2.34(2) Å) and significantly shortened in comparison to the Cu-Cl bonds in the polymeric starting material $[(\text{MeCN})\text{CuCl}]_\infty$ (2.406 Å). [184]

The *cyclo*- P_4 rings in **19a** are planar and are arranged in a distorted kite conformation, such that two adjacent P-P bonds (P(1)-P(2): 2.189(3) Å; P(2)-P(3): 2.187(3) Å) are significantly longer than the other two adjacent P-P bonds (P(1)-P(4): 2.161(3) Å; P(3)-P(4): 2.157(3) Å). This kite conformation was also observed for the free $[\text{Cp}''\text{Ta}(\text{CO})_2(\eta^4\text{-P}_4)]$ complex. The average P-P bond distance in **19a** (2.174 (3) Å) is slightly elongated compared to the starting $[\text{Cp}''\text{Ta}(\text{CO})_2(\eta^4\text{-P}_4)]$ complex (P-P (avg.): 2.162(3) Å). In comparison to the *cyclo*- P_4 ring in $[\text{Cp}''\text{Ta}(\text{CO})_2(\eta^4\text{-P}_4)]$ (P-P-P (acute): $88.6(1)^\circ$, $88.5(1)^\circ$; P-P-P (obtuse):

90.9(1)°, 92.0(1)°), the *cyclo*-P₄ rings in **19a** exhibit a slightly more pronounced kite form (P-P-P(acute): 88.13(9)°, 88.27(10)°; P-P-P(obtuse): 90.98(9)°, 92.52(10)°).

The overall structural motif of the P₂₄Cu₈ core in **19a** is distorted *O_h*-symmetric, with the deviations from *O_h* symmetry arising from the variations in P-P bond length within each [Cp''Ta(CO)₂(η^4 -P₄)] subunit. However, despite the variations in P-P bond length, only one unique [Cp''Ta(CO)₂(η^4 -P₄)] unit is present in the molecule, and the *C*₃ symmetry element is preserved. Two views of **19a** along the crystallographic *C*₃ axis are shown in Figure 30.

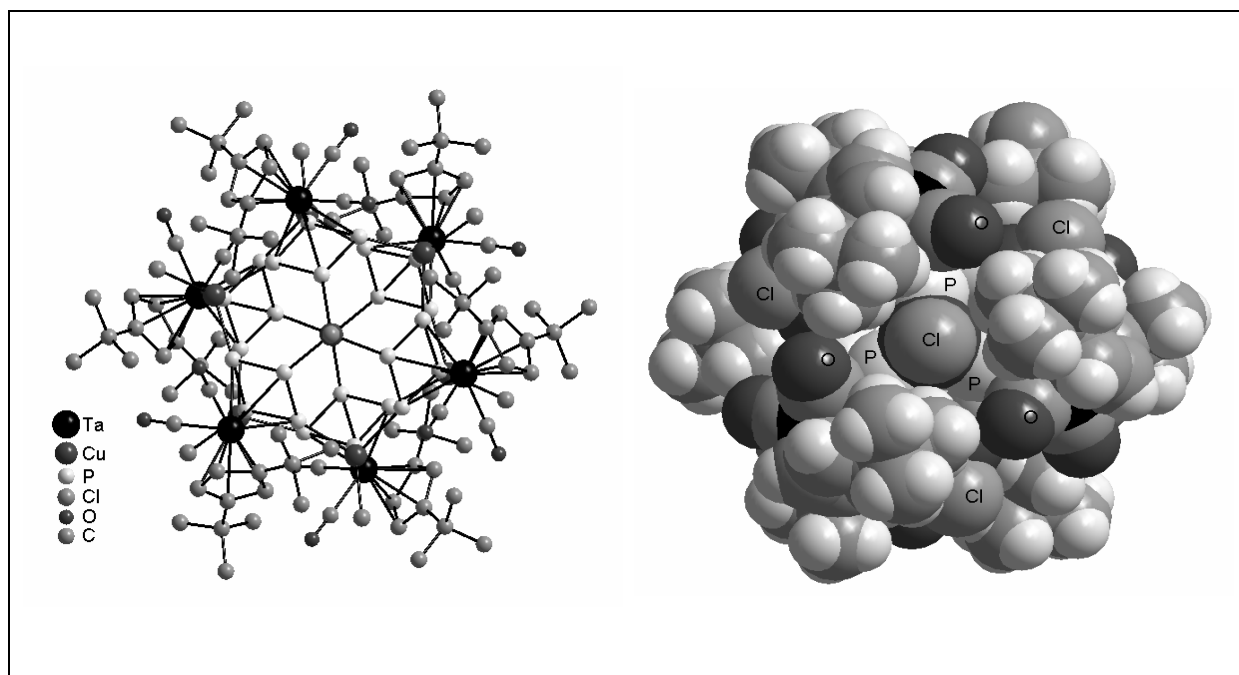


Figure 30: Ball-and-stick (left) and space-filling (right) models of the molecular structure of [$\{\text{Cp}''\text{Ta}(\text{CO})_2(\mu, \eta^4: \eta^1: \eta^1: \eta^1\text{-P}_4)\}_6\{\text{CuCl}\}_8$] (**19a**) viewed along the crystallographic *C*₃ axis. H atoms have been omitted for clarity only in the ball-and-stick model.

The core of **19a** possesses 32 inorganic atoms and can be described as fullerene-like in geometry, due to the motif of alternating four-membered and six-membered rings. However, no fullerene possessing the above 32-atom motif has been experimentally described. A fullerene possessing 32 atoms was predicted by Kroto as having exceptional stability compared to other small fullerenes. [185] However, a geometry possessing four-membered rings seems unfavorable since high strain energy renders four-membered carbon rings less stable than corresponding five- and six-membered rings, and only low-symmetry can be envisioned for molecules containing few or no four-membered rings for *C*₃₂. [186] For the most highly symmetric version of *C*₃₂ with *O_h* symmetry, eight four-membered rings are required. [187] As a result, it is clear that use of the *cyclo*-P₄ complex [Cp''Ta(CO)₂(η^4 -P₄)] in the formation of **19a** provides a source of transition-metal stabilized P₄ units and has

allowed the synthesis of a geometrical motif not yet imaginable in preparative carbon chemistry. A similar motif as that of **19a** has been considered in theoretical calculations on the T_d -symmetric Group 13/15 oligomers $[\text{HMEH}]_{16}$ ($M = \text{B, Al, Ga, In}$; $E = \text{N, P, As}$), [188-190] in which Group 13 and Group 15 atoms alternate throughout a 32-atom core composed of four- and six-membered rings. However, no such motif has yet been observed in an isolated compound.

The inner cavity of **19a** possesses an approximate cube shape, with the eight Cu atoms representing the corners and the six *cyclo*- P_4 ligands representing the faces. An inner diameter of such a cube-like cavity can be regarded as the diameter of the largest spherical shape spatially allowed inside the cavity by the given atoms. For this purpose, inner diameters here are calculated as geometrically opposing atomic distances minus the following van der Waals radii: P, 0.18 nm; Cu, 0.14 nm. Thus, a diameter of 0.60 nm measured to the corners (Cu to Cu) and a diameter of 0.44 nm measured to the faces (P to P) are calculated for the inner cavity of **19a**. The outer diameter (i.e. the diameter of the smallest spherical shape that can encompass the entire molecule) is calculated as twice the largest distance from the theoretical center of the molecule to the *tert*-butyl H atoms, plus twice the van der Waals radius of 0.06 nm for H. The outer diameter calculated for **19a** is 2.19 nm. For comparison, the fullerene cage C_{60} carries outer dimensions of 0.7 nm, while the spherical molecule $[\{\text{Cp}^*\text{Fe}(\mu, \eta^5: \eta^1: \eta^1: \eta^1: \eta^1: \eta^1\text{-P}_5)\}_{12}\{\text{CuCl}\}_{10}\{\text{Cu}_2\text{Cl}_3\}_5\{\text{Cu}(\text{MeCN})_2\}_5]$ has an inner diameter of the cavity of 1.25 nm and an outer diameter of 2.13 nm.

A measure of purity of the isolated crystals of **19a** is indicated in the powder-diffraction data. In Figure 31 is shown a comparison of the experimental powder-diffraction data (upper) and a powder-diffraction spectrum (lower) simulated from the cell constants obtained from the single-crystal X-ray diffraction experiment. As seen in Figure 31, the experimental powder-diffraction data nearly perfectly mirrors the simulated spectrum, which indicates there are no impurities in the powdered sample. The high purity of samples of **19a** was confirmed by correct C,H analysis.

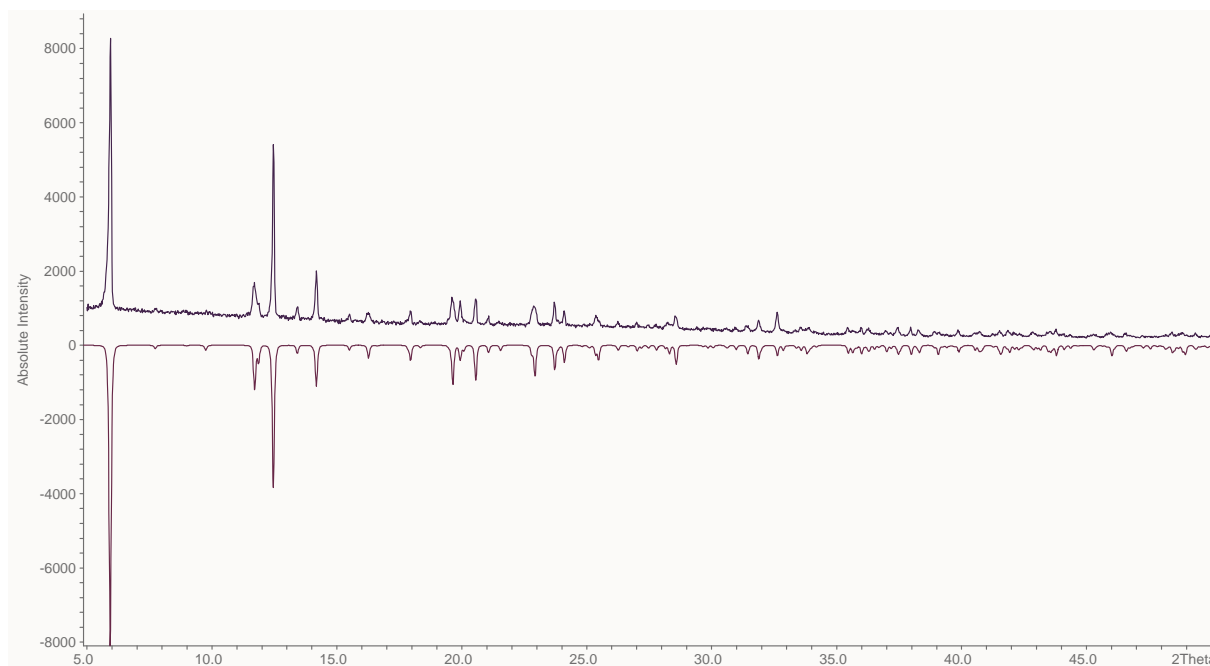
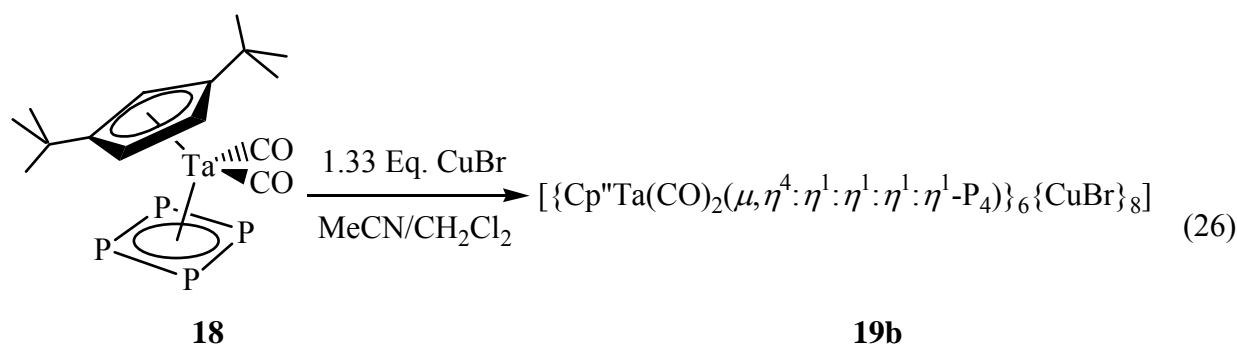


Figure 31: "Negative-over" arrangement of powder-diffraction spectrum of **19a** (upper) and simulated diffraction scheme (lower) generated from experimental unit-cell data from the single-crystal X-ray diffraction study.

3.4.4 Synthesis of $[\{\text{Cp}''\text{Ta}(\text{CO})_2(\mu, \eta^4: \eta^1: \eta^1: \eta^1: \eta^1\text{-P}_4)\}_6\{\text{CuBr}\}_8]$ (**19b**)

In light of the synthesis of **19a** from $[\text{Cp}''\text{Ta}(\text{CO})_2(\eta^4\text{-P}_4)]$ and CuCl, the potential for synthesizing analogous assemblies with CuBr was addressed. In a first trial, a solution of $[\text{Cp}''\text{Ta}(\text{CO})_2(\eta^4\text{-P}_4)]$ in DMF- d_7 , which had been used for NMR studies, was diluted with CH_2Cl_2 and layered with a mixture of MeCN/ CH_2Cl_2 , followed by a solution of CuBr in MeCN. This resulted in precipitation of orange-red microcrystals, from which a few larger crystals were selected and were identified by an X-ray diffraction experiment as the spherical molecule $[\{\text{Cp}''\text{Ta}(\text{CO})_2(\mu, \eta^4: \eta^1: \eta^1: \eta^1: \eta^1\text{-P}_4)\}_6\{\text{CuBr}\}_8]$ (**19b**). In order to optimize the reaction conditions, the reaction was repeated using identical conditions as those used for the synthesis of **19a** – only MeCN/ CH_2Cl_2 as solvents (without DMF- d_7), a 3:4 stoichiometry of $[\text{Cp}''\text{Ta}(\text{CO})_2(\eta^4\text{-P}_4)]/\text{CuBr}$, the same total volume as that used for **19a** (see Experimental Section) – and an improved yield of 64% was obtained. A second X-ray diffraction experiment was carried out and revealed the spherical structure of **19b**, with only minor deviations from the first measurement. Crystallographic details are reported below from the first measurement (crystals grown in the presence of DMF- d_7), and the differences from the second measurement (DMF- d_7 free) are pointed out where appropriate.



The IR spectrum of **19b** reveals vibrational frequencies for terminal CO ligands at 2042 and 1972 cm^{-1} , which agrees well with the IR signals observed in **19a**. Correct C,H elemental analysis of **19b** was obtained, with only minor deviations from the calculated values.

Structure of $[\{\text{Cp}''\text{Ta}(\text{CO})_2(\mu, \eta^4: \eta^1: \eta^1: \eta^1\text{-P}_4)\}_6\{\text{CuBr}\}_8]$ (**19b**)

An X-ray diffraction experiment was carried out on orange blocks of **19b** obtained directly from the reaction mixture in MeCN/CH₂Cl₂/DMF-*d*₇. **19b** crystallizes with approximately one molecule CH₂Cl₂ per formula unit in the trigonal space group $R\bar{3}$. The molecular structure of **19b** is shown in Figure 32, and selected bond lengths and angles are given in Table 15.

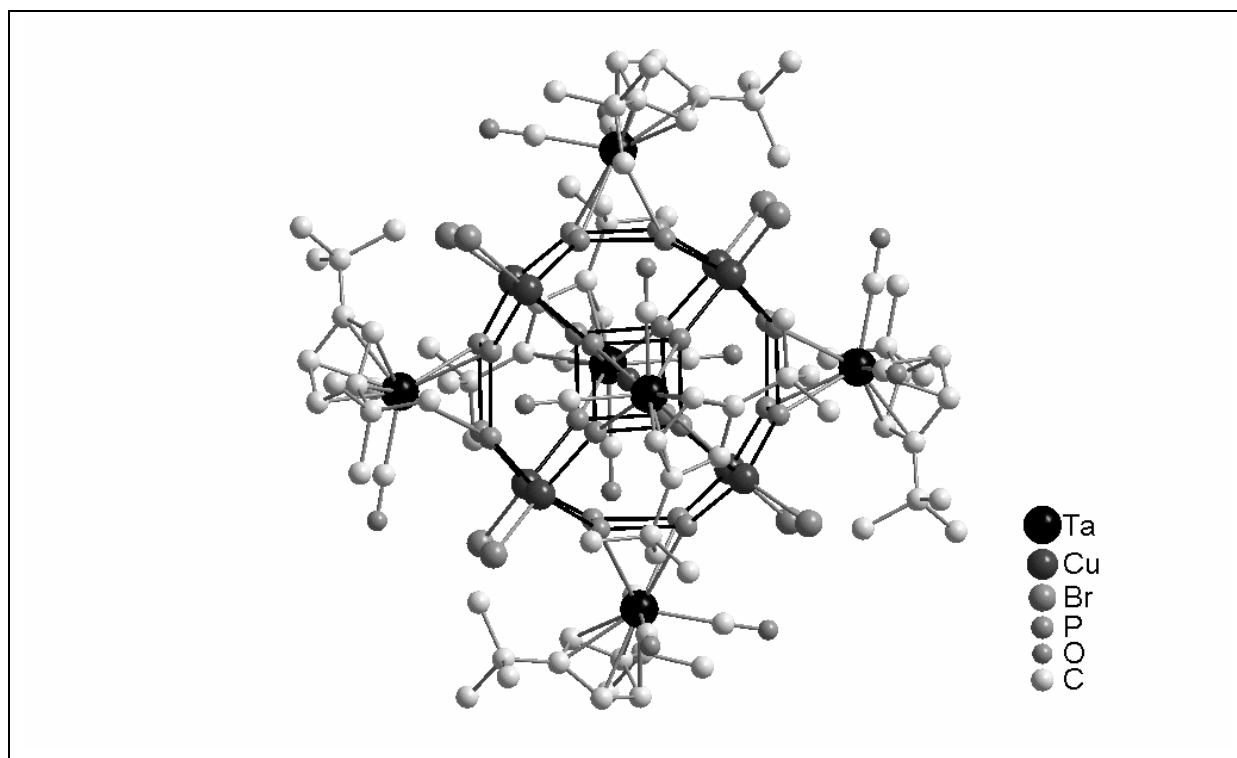


Figure 32: Molecular structure of $[\{\text{Cp}''\text{Ta}(\text{CO})_2(\mu, \eta^4: \eta^1: \eta^1: \eta^1: \eta^1\text{-P}_4)\}_6\{\text{CuBr}\}_8]$ (**19b**). H atoms have been omitted for clarity.

Table 15: Selected bond lengths [Å] and angles [°] in **19b**.³

P(1)-P(4)	2.140(3)	P(1)-P(2)	2.143(3)
P(2)-P(3)	2.173(3)	P(3)-P(4)	2.171(3)
Cu(1)-P(1)	2.302(2)	Cu(2)-P(2)	2.295(2)
Cu(1)-P(3)'	2.313(2)	Cu(1)-P(4)'	2.298(2)
Ta(1)-C _{Co} (14)	2.119(8)	Ta(1)-C _{Co} (15)	2.104(8)
Ta-C _{Cp''}	2.392(8) ^a	Ta-P	2.621(2) ^a
Cu(1)-Br(1)	2.3470(12)	Cu(2)-Br(2)	2.319(3)
P(4)-P(1)-P(2)	92.56(11)	P(3)-P(2)-P(1)	88.17(10)
P(4)-P(3)-P(2)	90.91(10)	P(3)-P(4)-P(1)	88.29(10)
Br(1)-Cu(1)-P(1)	118.11(7)	Br(2)-Cu(2)-P(2)	117.96(7)
Br(1)-Cu(1)-P(3)'	121.28(7)	Br(1)-Cu(1)-P(4)'	114.65(7)
P(1)-Cu(1)-P(3)'	98.95(8)	P(1)-Cu(1)-P(4)'	98.90(8)
P(3)'-Cu(1)-P(4)'	101.22(8)	P(2)-Cu(2)-P(2)'	99.81(8)

^a Mean value is given

³ Bond lengths and angles are reported here from the measurement of crystals grown in the presence of DMF-*d*₇. For the corresponding data from the measurement of crystals grown in the absence of DMF-*d*₇, see the crystal data for **19b** in the Crystallographic Data section.

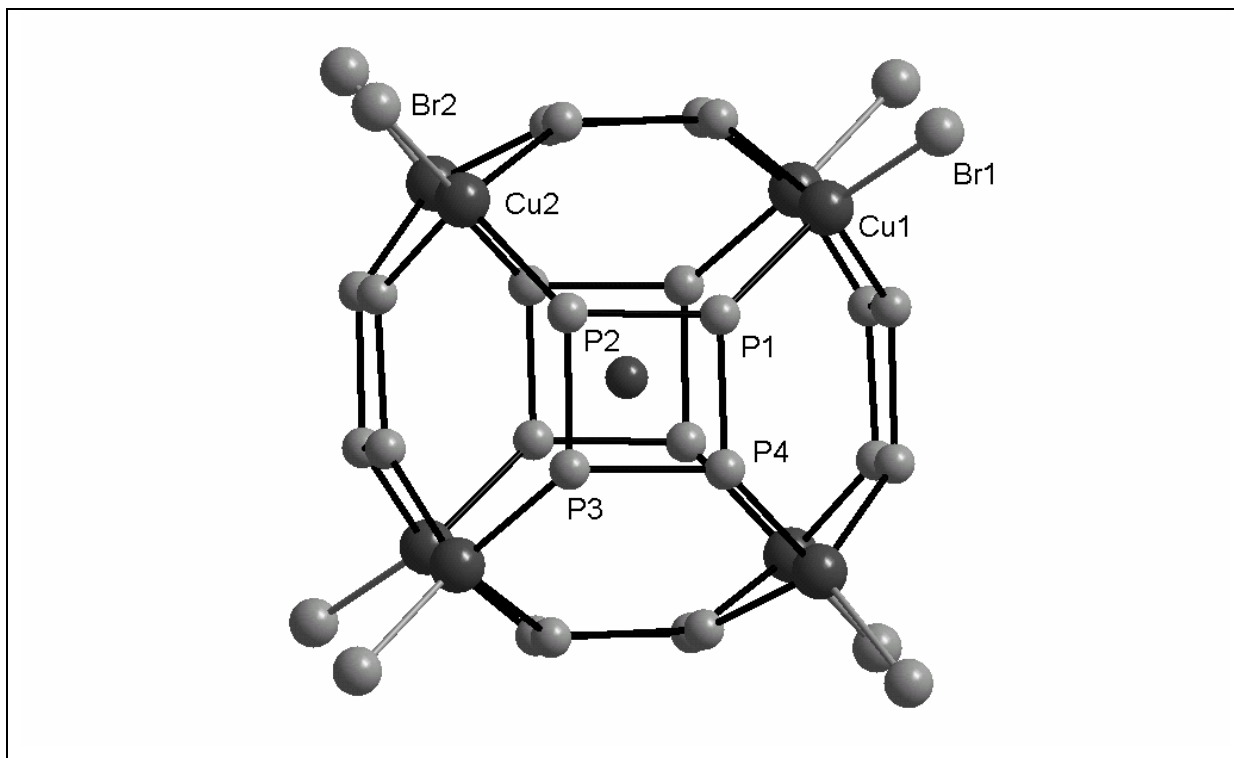


Figure 33: View of inner core of $[\{\text{Cp}''\text{Ta}(\text{CO})_2(\mu, \eta^4: \eta^1: \eta^1: \eta^1: \eta^1\text{-P}_4)\}_6\{\text{CuBr}\}_8]$ (**19b**). The $\text{Cp}''\text{Ta}(\text{CO})_2$ fragments have been omitted for clarity.

The structure of **19b** is essentially isomorphous to that of **19a**, with the exception that the chloride ligands have been replaced by bromide ligands, and exhibits the same spherical shape and alternating pattern of four- and six-membered rings of the core. The *cyclo*-P₄ rings maintain the same distorted kite formation as in **19a**, but the P-P bond distances in **19b** are slightly shorter (P(1)-P(4): 2.140(3) Å; P(1)-P(2): 2.143(3) Å; P(2)-P(3): 2.173(3) Å; P(3)-P(4): 2.171(3) Å). The P-P-P angles in **19b** (P-P-P(acute): 88.17(10)°, 88.29(10)°; P-P-P(obtuse): 92.56(11)°, 90.91(10)°) are, however, nearly identical to those in **19a**. The P-Cu bond lengths are nearly the same as those in **19a**. The method employed above for calculating inner diameters of the cavity and overall outer diameter was also used for **19b**. In **19b** the inner cavity has diameters of 0.42 nm (P to P) and 0.61 (Cu to Cu). The phosphorus-phosphorus diameter is shortened compared to that of **19a** (0.44 nm), in accordance with the smaller P-P bond lengths in **19b**, while the copper-copper diameter is larger compared to that of **19a** (0.60 nm), which is a reflection of the longer P-Cu bonds in **19b**. The outer diameter of **19b** is 2.17 nm, which is slightly smaller than that of **19a** (2.19 nm) and seems to be a result of the shorter average P-Ta distances in **19b** (2.621(2) Å) than in **19a** (2.640(2) Å).

Particularly conspicuous in the structure of **19b** is the presence of non-negligible electron density at the exact center of the core. The presence of one or more atoms at the core of such a spherical assembly is not unprecedented, as the presence of a $[\text{Cp}^*\text{Fe}(\eta^5\text{-P}_5)]$ unit

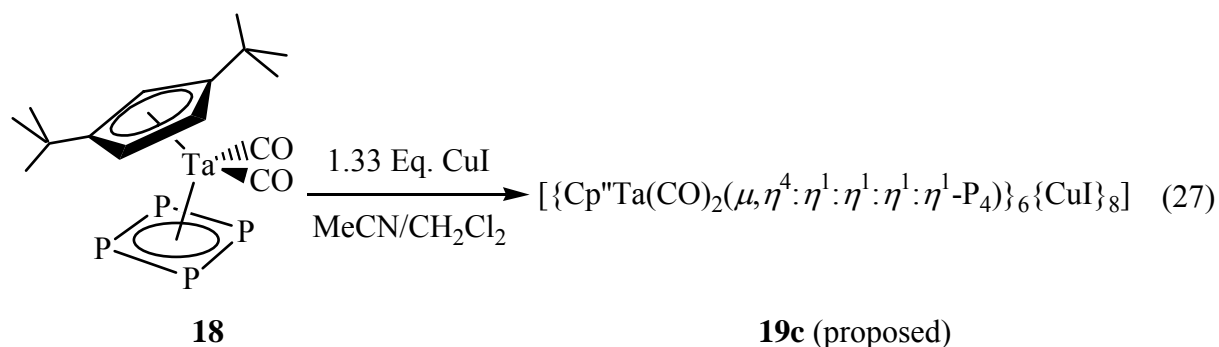
was detected in $[\{\text{Cp}^*\text{Fe}(\mu, \eta^5: \eta^1: \eta^1: \eta^1: \eta^1\text{-P}_5)\}_{12}\{\text{CuX}\}_{10}\{\text{Cu}_2\text{X}_3\}_5\{\text{Cu}(\text{MeCN})_2\}_5]$ ($\text{X} = \text{Cl}, \text{Br}$). [75,76] In the current case, the electron density at the center of **19b** seems to originate from only one atom, and its refinement fits best with nitrogen from the data set on a crystal grown from $\text{CH}_2\text{Cl}_2/\text{MeCN}/\text{DMF-}d_7$. To test the hypothesis that ammonia, NH_3 , would possibly be encapsulated in the core of **19b**, the IR spectrum was re-examined; however, no peaks conclusively associated with ammonia were found. If ammonia would be present, its most likely source would be traces from decomposed $\text{DMF-}d_7$. As mentioned above, a second measurement of the structure of **19b** was carried out on crystals grown from solutions free of $\text{DMF-}d_7$. In this measurement, electron density corresponding to one heavy (non-H) atom was again found in the center. However, the data for this measurement gave the best refinement values when the central atom was refined as oxygen, indicating the possibility of encapsulated water. As with the physical measurement carried out in search of ammonia, the IR spectra did not show conclusive presence of water. The IR spectrum of **19b** was carefully compared to that of **19a**, the structure of which showed no encapsulated species, and no differences associated with small molecules such as ammonia or water were observed. Elemental analysis was performed on crystals grown in the absence of $\text{DMF-}d_7$ but also proved inconclusive, as one molecule of ammonia or water within a molecule of the very large **19b** does not weigh enough to give a contribution significantly over the standard deviation from the calculated values without ammonia or water in the core.⁴ As a result, it cannot be stated at this point without doubt that ammonia or water is present inside of **19b**. The possibility that the residual electron density results from ‘artifact’ has been acknowledged and cannot be ruled out at this point.

3.4.5 Reaction of $[\text{Cp}''\text{Ta}(\text{CO})_2(\eta^4\text{-P}_4)]$ (**18**) with CuI

In attempted extension of the series of assemblies of type **19a,b** to all copper(I) halides, a solution of $[\text{Cp}''\text{Ta}(\text{CO})_2(\eta^4\text{-P}_4)]$ was layered with CuI in the same fashion as for compounds **19a,b** (3:4 stoichiometry of $[\text{Cp}''\text{Ta}(\text{CO})_2(\eta^4\text{-P}_4)]/\text{CuI}$). As with the previous

⁴ Elemental analyses of compounds **19** typically showed a value of ~0.2% nitrogen, even for **19a**, where no nitrogen was detected crystallographically in the core. For **19b**, elemental analysis for N is found to be 0.12%. The calculated contribution of ammonia to the nitrogen percentage in the overall molecule **19b** is approximately 0.3%. Thus, though nitrogen is found in the sample by elemental analysis, it does not calculate to an entire atom N per molecule **19b**, and does not reveal more nitrogen than in samples of **19a**, where no nitrogen is suspected in the core. Therefore, the elemental analysis data here is not conclusive for proving existence of nitrogen in the core of **19b**. Analysis for oxygen has not yet been carried out on samples of **19b**; however, the C and H values deviate from the calculated C,H values to an appreciable extent (see Experimental Section), a problem complicated by the presence of fractional equivalents of CH_2Cl_2 within the lattice. As a result, it is expected that elemental analysis is not the appropriate physical measurement to prove the existence of one molecule of water in the core.

reactions, an orange, microcrystalline solid precipitated out within 24 hours. Multiple attempts to carry out an X-ray diffraction study failed, as the crystals did not diffract. An IR spectrum revealed vibrational frequencies for terminal CO ligands at the exact wave numbers as observed for **19b** (2042, 1972 cm^{-1}). Elemental analysis was performed on the orange crystals, and C and H values are in line with those calculated for the composition $[\{\text{Cp}''\text{Ta}(\text{CO})_2(\eta^4\text{-P}_4)\}_6\{\text{CuI}\}_8]$.



The IR and elemental analysis data, together with the orange color and lack of solubility in organic solvents, indicate that this compound is the copper(I) iodide analogue $[\{\text{Cp}''\text{Ta}(\text{CO})_2(\mu, \eta^4:\eta^1:\eta^1:\eta^1:\eta^1\text{-P}_4)\}_6\{\text{CuI}\}_8]$ (**19c**), which is thus proposed here as the first spherical P_n -complex assembly incorporating CuI. Traces of nitrogen (0.36%) were found in samples through elemental analysis, which corresponds to slightly more than one atom nitrogen per molecule **19c**, assuming the proposed composition $[\{\text{Cp}''\text{Ta}(\text{CO})_2(\mu, \eta^4:\eta^1:\eta^1:\eta^1:\eta^1\text{-P}_4)\}_6\{\text{CuI}\}_8]$. However, it cannot be speculated yet whether this nitrogen comes from traces of MeCN or from a possibly encapsulated molecule of ammonia until structural data is available.

4 Experimental Section

4.1 General remarks

4.1.1 Methods

All manipulations, except where otherwise noted, were conducted under argon in a Braun Labmaster 130 glovebox or on a vacuum line ($\leq 10^{-3}$ mbar) using standard Schlenk techniques under prepurified nitrogen or argon. All experiments involving aryl-Sn(II) compounds were carried out exclusively under argon. Solvents were degassed under vacuum and saturated with nitrogen prior to distillation. *n*-Pentane, *n*-hexane, and petroleum ether were distilled from LiAlH₄; diethyl ether and tetrahydrofuran from sodium/benzophenone; toluene from sodium; and methylene chloride, acetonitrile, and dimethylformamide from CaH₂. Deuterated benzene was degassed under reduced pressure, saturated with argon, distilled from sodium/benzophenone, and stored over activated 4Å molecular sieves. DMF-*d*₇ was used without further purification from an ampule commercially packaged under nitrogen. All other deuterated solvents were degassed by three freeze-pump-thaw cycles, vacuum transferred from an appropriate drying agent, and stored over activated 4Å molecular sieves. Kieselgur was routinely stored at 110°C prior to use, then dried under vacuum and freed from traces of moisture with the aid of a heat gun. Photolysis reactions were carried out with a Hanau mercury vapor lamp (TQ 150).

4.1.2 Spectroscopy and analysis

NMR spectra were recorded on a Bruker AC250, Bruker AMX 300, Bruker Avance 300, or Bruker Avance 400. Chemical shifts are given in parts per million (ppm) and are referenced to tetramethylsilane (¹H-, ¹³C-, ²⁹Si-NMR), 85% phosphoric acid (³¹P-NMR), or tetramethylstannane (¹¹⁹Sn-NMR) as external standards. Chemical shifts in low field relative to the standard are designated by positive signs. All coupling constants *J* are given as absolute values in Hertz (Hz). In cases where the ¹¹⁷Sn and ¹¹⁹Sn satellites could not be resolved in ³¹P-NMR spectra, phosphorus-tin coupling is given as *J*_{P117/119Sn}.

Mass spectrometry was conducted with the mass spectrometer ThermoQuest Finnigan TSQ 7000 for ESI-MS and on a Varian MAT 711, MAT 8200, MAT 8230, or Finnigan MAT 95 for FD-MS and EI-MS.

Infrared spectra were recorded on a Bruker IFS280 FT-IR spectrometer or Varian FTS 800 spectrometer.

Powder diffraction analysis was carried out on a STOE Powder Diffraction System administered by the Pfitzner group, University of Regensburg.

Elemental analyses were carried out at the microanalytical laboratories of the University of Karlsruhe or the University of Regensburg.

4.2 Starting materials

The reagents used throughout this work were either synthesized or obtained from commercial suppliers and used without further purification unless explicitly stated otherwise. Me_3SiCl and SnCl_4 were freshly distilled prior to use. CpH was cracked and freshly distilled prior to use. $t\text{BuBr}$ was stirred over KOH overnight, then freshly distilled prior to use. TripBr was degassed under reduced pressure prior to use. Trimethylamine *N*-oxide was sublimed and stored under argon. P_4 was sublimed and stored under argon in the dark. CuX was purified by washing with a dilute solution of the corresponding HX , then washed with EtOH followed by Et_2O , and dried under vacuum. 1,2-dibromoethane was degassed under reduced pressure, stored for one week over activated 4 Å molecular sieves, and distilled under argon at ambient pressure. DBU was stored for one week over activated 4 Å molecular sieves, vacuum distilled, and saturated with argon. Triethylamine was degassed under reduced pressure and stored over activated 4 Å molecular sieves.

The following substances were synthesized according to literature methods: $\text{P}(\text{SiMe}_3)_3$ [191], $\text{LiP}(\text{SiMe}_3)_2 \cdot 1.8\text{THF}$ [192], $\text{KP}(\text{SiMe}_3)_2$ [193], $\text{LiAs}(\text{SiMe}_3)_2 \cdot 1.8\text{THF}$ [194], $[\text{H}_3\text{PW}(\text{CO})_5]$ [86], $\text{Li}[\text{H}_2\text{PW}(\text{CO})_5]$ [83], $\text{Li}[\text{H}_2\text{PBAr}^{\text{F}}_3]$ [195], $\text{Sn}[\text{N}(\text{SiMe}_3)_2]_2$ [196], $[(\text{CO})_5\text{WSnCl}_2(\text{thf})_2]$ [197], $[\text{tmeda} \cdot \text{SnCl}_2]$ [198], $[\text{bpy} \cdot \text{SnCl}_2]$ [199], $[(\eta^5\text{-C}_5\text{H}_5)\text{Fe}(\text{CO})_2]_2$ [200], $[\text{Fp}_2\text{SnCl}_2]$ [201], $[\text{Fp}_2\text{SnBr}_2]$ [202], TripPCl_2 [203], TripPH_2 [203], $\text{LiP}(\text{H})\text{Trip}$ [203], Li_2PTrip [204], PhPH_2 [205], $\text{LiP}(\text{H})\text{Ph}$ [206], Cp^*H [207], Cp^*Li [208], Cp^*PCl_2 [209], tris(2-hydroxy-3-*tert*-butyl-5-methylbenzyl)amine (L^*H_3) [155]. The preparations of Ph^*I [111], $\text{Ph}^*\text{Li} \cdot \text{OEt}_2$ [111], and Ph^*SnCl [109] were slightly modified from the literature procedures, as detailed below.

4.2.1 Synthesis of $[\text{H}(\text{Me}_3\text{Si})_2\text{PW}(\text{CO})_5]$ (2)

$[\text{H}_3\text{PW}(\text{CO})_5]$ (783 mg, 2.19 mmol) was dissolved in 12 mL Et_2O and cooled to -20°C . NEt_3 (0.61 mL, 442 mg, 4.38 mmol) was added by pipette. Me_3SiOTf (0.85 mL, 973 mg, 4.38

mmol) was added by pipette immediately thereafter, and a white precipitate formed. The mixture was allowed to warm to room temperature, whereby the precipitated $\text{NEt}_3 \cdot \text{HOTf}$ melted to a yellow oil. Stirring was continued at room temperature for 30 minutes, after which the mixture was allowed to stand for 10 minutes. The mixture was cooled to -20°C to freeze the $\text{NEt}_3 \cdot \text{HOTf}$, and the mother liquor was decanted and filtered cold. The volume of the pale yellow solution was reduced *in vacuo* to about 5 mL, and colorless crystals of **2** formed after storage for a few days at -25°C . Yield: 495 mg, 45%.

Analytical data for **2**:

MS (EI, 70 eV, 100°C)	m/z (%) = 574 (100) [$\text{M}^+ + \text{SiMe}_3 - \text{H}$], 546 (58) [$\text{M}^+ + \text{SiMe}_3 - \text{CO} - \text{H}$], 518 (53) [$\text{M}^+ + \text{SiMe}_3 - 2\text{CO} - \text{H}$], 502 (26) [M^+], 473.9 (15) [$\text{M}^+ - \text{CO}$], 429.9 (11) [$\text{M}^+ - 2\text{CO}$], 401.9 (4.7) [$\text{M}^+ - 3\text{CO}$], 357.9 (8.8) [$\text{H}_3\text{PW}(\text{CO})_5$] $^+$, 295.9 (0.1) [$\text{W}(\text{CO})_4$] $^+$, 267.9 (0.1) [$\text{W}(\text{CO})_3$] $^+$, 250.1 (7.8) [$\text{P}(\text{SiMe}_3)_3$] $^+$
^1H-NMR (300.13 MHz, C_6D_6)	δ [ppm] = 0.19 (d, 18H, $\text{Si}(\text{CH}_3)_3$, $^3J_{\text{HP}} = 5.0$ Hz)
^{13}C-NMR (75.47 MHz, C_6D_6)	δ [ppm] = 2.00 (d, $\text{Si}(\text{CH}_3)_3$, $^2J_{\text{CP}} = 8.1$ Hz), 195.91 (s, $\text{W-CO}_{\text{trans}}$), 197.08 (s, W-CO_{cis})
^{31}P-NMR (101.26 MHz, C_6D_6)	δ [ppm] = -215.7 (d, $^1J_{\text{PH}} = 282$ Hz, $^1J_{\text{PW}} = 160$ Hz)

4.2.2 Synthesis of 2,6-dichloro-1-iodobenzene

The following procedure was carried out with exposure to air, with a stream of N_2 only over the reaction mixture. In a 1-L flask, finely ground 2,6-dichloroaniline (40.5 g, 0.25 mol) was suspended in 250 mL concentrated HCl and cooled to 0°C . A solution of NaNO_2 (17.25 g, 0.25 mol) in 100 mL water was added dropwise with vigorous stirring over a span of 30 minutes. The yellow-orange mixture was allowed to stir at 0°C for 45 minutes further. The resulting diazonium solution was quickly filtered cold through glass wool directly into a vigorously stirred solution of KI (415 g, 2.5 mol) in 500 mL water at room temperature. A red solution resulted with floating yellow-brown solids and was stirred for 1 hour. A solution of Na_2SO_3 (10.5 g in 80 mL water) was poured portionwise into the mixture, resulting in a yellow-orange suspension. CH_2Cl_2 (400 mL) was added, and the aqueous phase was separated and washed twice with CH_2Cl_2 (100 mL each). The organic phases were combined and washed with a NaOH solution (10 g in 100 mL water). The organic phase was separated and

dried over MgSO_4 and filtered, and the solvent was removed on a rotary evaporator at 40°C . The crystalline orange-red residue was recrystallized from EtOH/toluene at -25°C . The colorless to pale-yellow needles were collected on a frit, washed with a small amount of cold petroleum ether, and dried under vacuum. Yield: 47.8 g, 70%.

Analytical data for 2,6-dichloro-1-iodobenzene:

M.p. 66-67°C

^1H -NMR (300 MHz, δ [ppm] = 6.33 (t, 1H, *p*-H, $^3J_{\text{HH}} = 8.1$ Hz), 6.72 (d, 2H, *m*-H, $^3J_{\text{HH}} = 8.1$ Hz), C_6D_6)

^{13}C -NMR (75.5 MHz, δ [ppm] = 104.14 (s, *p*-CH), 126.96 (s, *m*-CH), 129.84 (s, *o*-CCl), C_6D_6) 140.82 (s, *ipso*-Cl)

4.2.3 Synthesis of Ph*I

In a three-neck 2-L round-bottom flask, magnesium turnings were stirred under vacuum at 60°C overnight. To the cooled flask was added 140 mL THF, and a solution of TripBr (36.8 g, 0.13 mol) in THF (20 mL) was added slowly. In most cases, heating was required to initiate formation of the Grignard. Upon initiation of the Grignard reaction, the mixture was heated to reflux for two hours. During the Grignard reaction, a solution of 2,6-dichloro-1-iodobenzene (13.3 g, 0.049 mol) in THF (120 mL) in a separate 500-mL flask was treated with a solution of EtMgBr (49 mL, 1.0 M in THF, 0.049 mol) dropwise at 0°C and stirred at room temperature for one hour. This solution was then added dropwise to the cooled Grignard mixture at room temperature over a span of about 20 minutes. The resulting mixture was heated to reflux and allowed to stir overnight. The solution was decanted with a thick Teflon cannula directly into a vigorously stirred solution of iodine (49.4 g, 195 mmol) in THF (120 mL) at 0°C . This solution was allowed to stir at room temperature for 10 hours. A solution of Na_2SO_3 (40 g) in water (200 mL) was added slowly (NOTE: the amount of Na_2SO_3 used here differs from the literature procedure, as the literature amount did not suffice to quench the excess iodine), and a discoloration was observed to produce a two-layer yellow mixture. Et_2O was added, and the organic layer was separated and extracted three times with Et_2O (100 mL each). The organic layers were collected, and the solvent was removed to produce a pulpy yellow-gray solid. The residue was transferred into a 250 mL flask and attached to a distillation bridge. The substance was heated to 100°C under vacuum to distill away volatile by-products. The heat was increased to 140°C , and a heat gun was used until all oily products (often violet in color) had distilled over. The remaining pale brown-gray residue

was allowed to cool, and 150 mL EtOH was added, and the mixture was heated to reflux and stirred overnight. The resulting pale brown mixture was stored overnight (or longer) at -25°C , then quickly filtered on a glass-sintered frit. The solid was washed with MeOH (50 mL portions) until the solid was completely white and the filtrate ran colorless (about 4 times), then dried under vacuum. The resulting white powder was normally of sufficient purity for further work (the ^1H -NMR spectrum is shown below). Yield: 22.2 g, 74%. In cases where purity was not sufficient, the powder was recrystallized from $\text{Et}_2\text{O}/n$ -hexane.

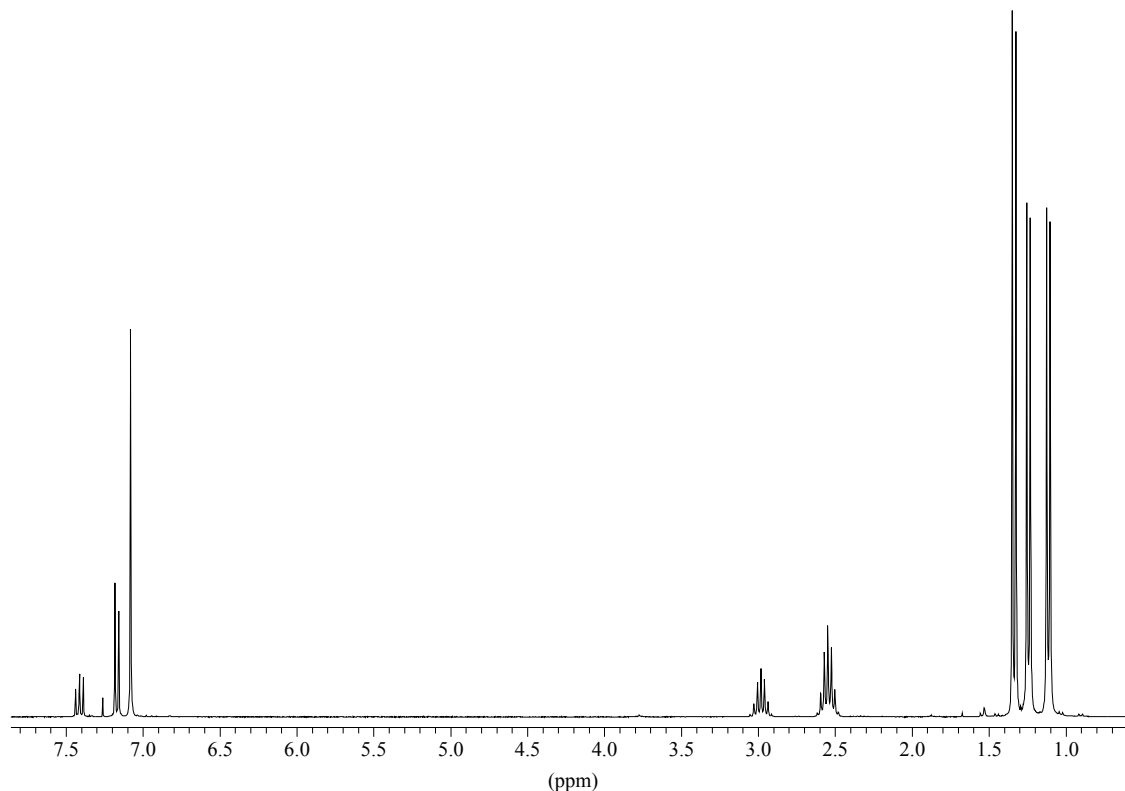


Figure 34: ^1H -NMR spectrum of Ph*I in CDCl_3 .

4.2.4 Synthesis of $\text{Ph}^*\text{Li}\cdot\text{OEt}_2$

Ph*I (3.57 g, 5.9 mmol) was dissolved in a mixture of n -hexane (50 mL) and Et_2O (50 mL) in a Schlenk tube and cooled to -78°C . A solution of $n\text{BuLi}$ (3.8 mL, 1.6 M in n -hexane, 6.1 mmol) was added by pipette with vigorous stirring. Additional dry ice was added to the bath until the Schlenk tube was covered with as much dry ice as possible. The reaction mixture was allowed to stir overnight, whereby the additional dry ice assured a long delay in warming to room temperature (NOTE: allowing the solution to warm too rapidly to room temperature induces reaction of eliminated $n\text{BuI}$ with $n\text{BuLi}$ and therefore consumption of the $n\text{BuLi}$ reagent, resulting in a poor yield). On the next day, the reaction mixture is filtered and reduced to about 20 mL in volume under reduced pressure. Storage at -25°C for a week

resulted in deposition of large, colorless crystals, which were isolated by decantation and dried under vacuum. Yield: 2.1 g, 63 %.

4.2.5 Synthesis of Ph*SnCl

Anhydrous SnCl₂ (523 mg, 2.76 mmol) was suspended in Et₂O (20 mL) and cooled to 0°C. A solution of Ph*Li·OEt₂ (1.55 g, 2.76 mmol) in Et₂O (50 mL) was added dropwise, resulting in a yellow-orange solution. (NOTE: uniform stirring is important here. If the mixture is not stirred well during addition of the Ph*Li·OEt₂ solution, the mixture turns green. If this happens, normal work-up still provides orange crystals of Ph*SnCl, albeit in somewhat lower yield. The constitution of the green color was not investigated in this work). The solution was allowed to stir overnight at room temperature, after which an orange solution with white precipitate resulted. The solvent was removed under reduced pressure, and *n*-hexane (70 mL) was added to the residue. The mixture was stirred at least 4 hours, or until all orange solids had fully dissolved. In many cases, solids stuck to the wall of the glass had to be freed manually with a spatula. The orange solution was filtered through Kieselgur. For the highest yield and largest crystals, the following crystallization procedure was implemented. The Schlenk tube containing the orange filtrate was tilted to an angle of 45°. With the Schlenk tube pressurized with argon, the stopcock was closed, and full vacuum was applied from outside, through a liquid-nitrogen cooled cold trap, up to the closed stopcock. The stopcock was slowly opened until a minimal pressure difference was observed on the vacuum line pressure gauge, and the Schlenk tube was allowed to stand under these conditions. By this method, the solution was concentrated as slowly as possible and was left untouched until the volume reached approximately 10 mL. By this time, the solution should be extremely cold (ice on the outside of the Schlenk tube) and yellow. Without disturbing the Schlenk tube, argon was allowed in, and the tube was allowed to stand undisturbed for 45 minutes, during which time the solution became orange, and large orange crystals deposited. The mixture was stored at 4°C for about three days, and the orange crystals were isolated by decantation and dried under vacuum. Yield: 1.26 g, 72 %. The mother liquor can also be dried completely under reduced pressure, resulting in a yellow-orange powder, and the recovered impure Ph*SnCl can be used for test reactions before using the ‘good’ orange crystals for scale-up.

4.3 Reactions starting from SnCl_2 and $\text{Sn}[\text{N}(\text{SiMe}_3)_2]_2$

4.3.1 Reaction of $\text{Sn}[\text{N}(\text{SiMe}_3)_2]_2$ with $[\text{H}(\text{Me}_3\text{Si})_2\text{PW}(\text{CO})_5]$, isolation of $[(\text{Me}_3\text{Si})_3\text{PW}(\text{CO})_5]$ (3)

To a colorless solution of $[\text{H}(\text{Me}_3\text{Si})_2\text{PW}(\text{CO})_5]$ (285 mg, 0.57 mmol) in Et_2O (8 mL) was added an orange solution of $\text{Sn}[\text{N}(\text{SiMe}_3)_2]_2$ (125 mg, 0.28 mmol) in Et_2O (10 mL) with vigorous stirring at -78°C . The color changed to light brown within 20 minutes. The mixture was allowed to warm to room temperature and stirred overnight. The solution was filtered through a plug of Kieselgur and reduced to *ca.* 5 mL in volume under reduced pressure. Storage at -25°C for one week afforded colorless crystals of $[(\text{Me}_3\text{Si})_3\text{PW}(\text{CO})_5]$. Yield: 72 mg, 22% based on $[\text{H}(\text{Me}_3\text{Si})_2\text{PW}(\text{CO})_5]$.

4.3.2 Reaction of SnCl_2 with $\text{Li}[(\text{Me}_3\text{Si})_2\text{PW}(\text{CO})_5]$, isolation of $[(\text{Me}_3\text{Si})_3\text{PW}(\text{CO})_5]$ (3)

$\text{Li}[(\text{Me}_3\text{Si})_2\text{PW}(\text{CO})_5]$ was generated *in situ* by the addition of *n*BuLi (0.12 mL, 1.6 M in *n*-hexane, 0.20 mmol) to a solution of $[\text{H}(\text{Me}_3\text{Si})_2\text{PW}(\text{CO})_5]$ (102 mg, 0.20 mmol) in THF (5 mL) at 0°C . The resulting yellow solution was added dropwise to a solution of SnCl_2 (19 mg, 0.10 mmol) at 0°C . The solution turned pale brown. The solution was allowed to warm to room temperature and stirred for 16 hours. The THF was removed under vacuum, and the resulting brown residue was extracted with 10 mL *n*-hexane and filtered through a plug of Kieselgur. Reduction of the volume to *ca.* 3 mL under reduced pressure and storage at -25°C resulted in a few colorless crystals, which were identified as $[(\text{Me}_3\text{Si})_3\text{PW}(\text{CO})_5]$ based on ^{31}P -NMR. Yield: 12 mg, 10% based on $[\text{H}(\text{Me}_3\text{Si})_2\text{PW}(\text{CO})_5]$.

4.4 Reactions starting from $[\text{Fp}_2\text{SnX}_2]$ ($\text{X} = \text{Cl}, \text{Br}$)

4.4.1 Synthesis of $[\text{Fp}_2\text{Sn}\{\text{PH}_2\text{W}(\text{CO})_5\}_2]$ (4)

A solution of *n*BuLi (1.43 mL, 1.6 M in *n*-hexane, 2.29 mmol) was added to a solution of $[\text{H}_3\text{PW}(\text{CO})_5]$ (819 mg, 2.29 mmol) in toluene (20 mL) at 0°C . The resulting brown suspension of $\text{Li}[\text{H}_2\text{PW}(\text{CO})_5]$ was allowed to warm to room temperature and stirred for two hours. The suspension was cooled to 0°C , and a solution of $[\text{Fp}_2\text{SnX}_2]$ ($\text{X} = \text{Cl}$: 619 mg, 1.14 mmol; $\text{X} = \text{Br}$: 724 mg, 1.14 mmol) in toluene (40 mL) was added dropwise (note: gentle warming with a heat gun was sometimes necessary to fully dissolve $[\text{Fp}_2\text{SnX}_2]$ before addition). A dark red solution formed and was allowed to warm to room temperature and

stirred overnight. The solution was filtered through Kieselgur, and the filtrate was concentrated under reduced pressure until the onset of crystallization (about 20 mL). Storage at -25°C for one week afforded red crystals of **4**. Yield: 514 mg, 38%.

Analytical data for **4**:

IR (KBr pellet)	$\tilde{\nu}$ [cm^{-1}] = 3120 (w), 3086 (w), 2320 (m, PH), 2075 (vs, CO), 2030 (s, CO), 1998 (vs, CO), 1960 (s, CO), 1953 (vs, CO), 1930 (sh, CO), 1410 (w), 1360 (w), 1062 (m), 1001 (m), 939 (m), 848 (s), 710 (vs), 630 (vs), 599 (s)
MS (EI, 70 eV, 200°C)	m/z (%) = 504.9 (9) [$\text{SnP}_2\text{H}_2\text{W}(\text{CO})_5^+$], 476.9 (17) [$\text{SnP}_2\text{H}_2\text{W}(\text{CO})_4^+$], 420.9 (13) [$\text{SnP}_2\text{H}_2\text{W}(\text{CO})_2^+$], 324.1 (30) [$\text{W}(\text{CO})_5^+$], 296.1 (33) [$\text{W}(\text{CO})_4^+$], 268.1 (100) [$\text{W}(\text{CO})_3^+$], 28.1 (13) [CO^+]
^1H-NMR (250.13 MHz, toluene- d_8)	δ [ppm] = 3.79 (d br, 4H, PH_2 , $^1J_{\text{HP}} = 292$ Hz), 4.24 (s, 5H, C_5H_5)
^{13}C-NMR (62.90 MHz, toluene- d_8)	δ [ppm] = 84.28 (s, C_5H_5), 191.45 (s, W- CO_{cis}), 197.72 (s, W- CO_{trans}), 213.50 (Fe-CO)
$^{31}\text{P}\{^1\text{H}\}$-NMR (101.26 MHz, toluene- d_8)	δ [ppm] = -177.2 (s, $^1J_{\text{PW}} = 174$ Hz, $^1J_{\text{P}117\text{Sn}} = 893$ Hz, $^1J_{\text{P}119\text{Sn}} = 934$ Hz, total Sn satellite intensity = 14%)
^{31}P-NMR (101.26 MHz, toluene- d_8)	δ [ppm] = -177.2 (t, $^1J_{\text{PH}} = 292$ Hz)

4.4.2 Synthesis of $[\text{Fp}_2\text{Sn}\{\text{P}(\text{SiMe}_3)_2\}_2]$ (**5**)

$\text{LiP}(\text{SiMe}_3)_2 \cdot 1.8\text{THF}$ (616 mg, 1.96 mmol) was added as a solid to a solution of $[\text{Fp}_2\text{SnBr}_2]$ (594 mg, 0.94 mmol) in toluene (15 mL) at -78°C . The orange-red solution gradually turned to deep red within 40 minutes. The mixture was allowed to warm to room temperature and stirred for 16 hours. The solution was filtered through a bed of Kieselgur, and the solvent was removed in vacuum. The resulting deep red residue was extracted with 10 mL *n*-hexane and filtered. The solution was concentrated to ca. 5 mL under reduced pressure and stored at -25°C . After four days compound **5** crystallized as dark red platelets. The crystals were separated from the mother liquor by decantation and dried in vacuum. Yield: 575 mg, 64%.

Analytical data for **5**:

IR (KBr pellet)	$\tilde{\nu}$ [cm ⁻¹] = 3123 (w), 2953 (m), 2890 (m), 2154 (m, br), 2012 (s, CO), 1959 (s, CO), 1414 (m), 1359 (m), 1245 (s), 1001 (m), 848 (vs), 682 (s), 633 (s), 577 (s)
¹H-NMR (300.13 MHz, C ₆ D ₆)	δ [ppm] = 0.58 (d, 18H, Si(CH ₃) ₃ , ³ J _{HP} = 2.6 Hz), 0.59 (d, 18H, Si(CH ₃) ₃ , ³ J _{HP} = 2.6 Hz), 4.52 (s, 5H, C ₅ H ₅)
¹³C-NMR (75.48 MHz, C ₆ D ₆)	δ [ppm] = 6.56 (d, Si(CH ₃) ₃ , ² J _{CP} = 7.2 Hz), 6.65 (d, Si(CH ₃) ₃ , ² J _{CP} = 7.2 Hz), 85.03 (s, C ₅ H ₅), 215.85 (s, CO)
³¹P-NMR (162.96 MHz, C ₆ D ₆)	δ [ppm] = -182.9 (¹ J _{P117Sn} = 1186 Hz, ¹ J _{P119Sn} = 1240 Hz, total Sn satellite intensity = 16%)
¹¹⁹Sn{¹H}-NMR (149.21 MHz, C ₆ D ₆)	δ [ppm] = 392.1 (t, ¹ J _{SnP} = 1240 Hz)

4.4.3 Reaction of [Fp₂SnCl₂] with LiP(H)Trip in THF, synthesis of Fp₄Sn (6)

A solution of *n*BuLi (0.48 mL, 1.6 M in *n*-hexane, 0.77 mmol) was added slowly to a solution of TripPH₂ (183 mg, 0.77 mmol) in 10 mL THF at 0°C. The yellow solution was allowed to warm to room temperature and stirred for one hour. This solution was added dropwise to a solution of [Fp₂SnCl₂] (211 mg, 0.39 mmol) in 10 mL THF at -78°C. The pale red solution turned immediately to dark red, almost black. The solution was slowly allowed to warm to room temperature and stirred overnight. The solvent was removed under vacuum, and the red-black residue was extracted with toluene (ca. 10 mL) and filtered through Kieselgur. The filtrate was reduced in volume under reduced pressure and stored at -25°C. Brownish-black plates of **6** formed after a few days, and the crystals were isolated by decantation. Yield: 16 mg, 5% based on [Fp₂SnCl₂].

Analytical data for **6**:

IR (KBr pellet)	$\tilde{\nu}$ [cm ⁻¹] = 3118 (w), 2960 (w), 2926 (w), 2361 (w), 1978 (vs, CO), 1934 (vs, CO), 1411 (m), 1065 (m), 1002 (m), 828 (s), 640 (s), 575 (s), 514 (s)
MS (FD, toluene solution)	m/z (%) = 650.90 (100) [Fp ₃ Sn ⁺]

¹H-NMR (300.13 MHz, C ₆ D ₆)	δ [ppm] = 4.54 (s, 5H, C ₅ H ₅)
¹³C-NMR (75.48 MHz, C ₆ D ₆)	δ [ppm] = 83.67 (C ₅ H ₅), 83.96 (C ₅ H ₅), 84.50 (C ₅ H ₅), 266.90 (CO), 267.33 (CO), 267.91 (CO)

4.5 Reactions starting from Ph*SnCl

4.5.1 Synthesis of Ph*SnP(SiMe₃)₂ (7)

Ph*SnCl (1.356 g, 2.1 mmol) was dissolved in 20 mL *n*-hexane and cooled to -78°C . KP(SiMe₃)₂ (465 mg, 2.1 mmol) was added as a solid. Upon warming to room temperature, the color changed from orange to deep violet. The solution was stirred overnight and filtered through Kieselgur. The filtrate was concentrated *in vacuo* to about 5 mL and stored at -25°C , whereby violet crystals of **7** deposited after one week. Yield: 799 mg, 49%. **7** can also be synthesized from Ph*SnCl and LiP(SiMe₃)₂·1.8THF by an analogous procedure in approximately the same yield.

Analytical data for **7**:

MS (EI, 70 eV, 120°C)	m/z (%) = 778.2 (2.2) [M ⁺], 763.2 (0.3) [M ⁺ – CH ₃], 705.1 (0.3) [M ⁺ – SiMe ₃], 690.2 (1.5) [M ⁺ – SiMe ₃ – CH ₃], 675.3 (1.6) [M ⁺ – SiMe ₃ – 2CH ₃], 601.1 (70) [M ⁺ – P(SiMe ₃) ₂], 482.4 (100) [M ⁺ – SnP(SiMe ₃) ₂], 467.3 (47) [M ⁺ – SnP(SiMe ₃) ₂ – CH ₃], 439.3 (14) [M ⁺ – SnP(SiMe ₃) ₂ – C ₃ H ₇], 73 (4) [SiMe ₃ ⁺], 43.1 (3) [C ₃ H ₇ ⁺]
¹H-NMR (250.13 MHz, C ₆ D ₆)	δ [ppm] = 0.16 (d, 18H, Si(CH ₃) ₃ , ³ J _{HP} = 4.0 Hz), 1.13 (d, 12H, <i>o</i> -CH(CH ₃) ₂ , ³ J _{HH} = 6.7 Hz), 1.23 (d, 12H, <i>o</i> -CH(CH ₃) ₂ , ³ J _{HH} = 6.9 Hz), 1.46 (d, 12H, <i>p</i> -CH(CH ₃) ₂ , ³ J _{HH} = 6.7 Hz), 2.79 (sept, 2H, <i>p</i> -CH(CH ₃) ₂ , ³ J _{HH} = 6.9 Hz), 3.28 (sept, 4H, <i>o</i> -CH(CH ₃) ₂ , ³ J _{HH} = 6.8 Hz), 7.14 (s, 4H, <i>m</i> -Trip)
¹³C-NMR (62.90 MHz, C ₆ D ₆)	δ [ppm] = 6.50 (d, ² J _{CP} = 9.5 Hz), 24.25 (s, CH(CH ₃) ₂), 25.09 (s, CH(CH ₃) ₂), 27.95 (s, CH(CH ₃) ₂), 32.01 (s, CH(CH ₃) ₂), 35.54 (s, CH(CH ₃) ₂), 122.81 (s), 127.73 (s), 131.90 (s), 136.10 (s), 146.28 (s), 147.69 (s), 150.10 (s), 181.31 (s, <i>ipso</i> -C ₆ H ₃)
²⁹Si{¹H}-NMR (49.69 MHz, C ₆ D ₆)	δ [ppm] = 4.08 (d, ¹ J _{SiP} = 38.5 Hz)

²⁹ Si-NMR (49.69 MHz, C ₆ D ₆)	δ [ppm] = 4.08 (dm, ¹ J _{SiP} = 38.5 Hz, ² J _{SiH} = 6.6 Hz)
³¹ P-NMR (101.36 MHz, C ₆ D ₆)	δ [ppm] = -123.1 (s, ¹ J _{P117Sn} = 1396 Hz, ¹ J _{P119Sn} = 1453 Hz, total Sn satellite intensity = 12%)
¹¹⁹ Sn-NMR (112.02 MHz, C ₆ D ₆)	δ [ppm] = 1919 (d, ¹ J _{SnP} = 1453 Hz)

4.5.2 Reaction of Ph* SnP(SiMe₃)₂ with BrCH₂CH₂Br, formation of Ph*Br (8)

Ph*SnP(SiMe₃)₂ was generated *in situ* by mixing Ph*SnCl (407 mg, 0.64 mmol) and KP(SiMe₃)₂ (140 mg, 0.64 mmol) in 15 mL *n*-hexane at -78°C and stirring at room temperature for two hours. The violet solution was cooled to -78°C, and a solution of BrCH₂CH₂Br in *n*-hexane (1.0 mL, 0.64 M, 0.64 mmol) was added. The solution was allowed to warm slowly to room temperature, whereby the color gradually changed to pale brown, and was stirred overnight. The solution was filtered through Kieselgur, and the filtrate was concentrated under reduced pressure to 4 mL. Storage at -25°C for three days afforded colorless crystals of Ph*Br. Yield: 126 mg, 35%.

4.5.3 Reaction of Ph*SnCl with LiP(H)Ph (2 equivalents)

Ph*SnCl (192 mg, 0.30 mmol) was dissolved in toluene (9 mL) and THF (3 mL). LiP(H)Ph (70 mg, 0.60 mmol) was added as a solid, and the mixture was heated to 80°C for four hours. The reaction mixture was allowed to cool to room temperature and filtered through Kieselgur, and the filtrate was concentrated to dryness and analyzed by ³¹P-NMR. Data were consistent with the formation of both *meso*-Ph(H)P-P(H)Ph and (±)-Ph(H)P-P(H)Ph in approximate 1:1 ratio as the main products. [127]

4.5.4 Reaction of Ph*SnCl with LiP(H)Ph (1 equivalent)

Ph*SnCl (187 mg, 0.29 mmol) and LiP(H)Ph (34 mg, 0.29 mmol) were weighed into a Schlenk tube, and *n*-hexane (10 mL) was added at -78°C. The solution was allowed to warm slowly to room temperature and stirred overnight. The red-orange solution was filtered through Kieselgur, and the filtrate was reduced to dryness under vacuum. The residue was examined by ³¹P-NMR in C₆D₆. Two main signals were observed, each corresponding respectively to ca. 60% (signal 1) and 20% (signal 2) of the total phosphorus intensity.

³¹P-NMR (162 MHz, C₆D₆) δ_1 [ppm] = -100.9 ppm (d, $^1J_{\text{PH}} = 382$ Hz, $^1J_{\text{P}^{117}\text{Sn}(1)} = 1198$ Hz, $^1J_{\text{P}^{119}\text{Sn}(1)} = 1252$ Hz; $^1J_{\text{P}^{117}\text{Sn}(2)} = 1546$ Hz, $^1J_{\text{P}^{119}\text{Sn}(2)} = 1617$ Hz, total tin satellite intensity = 18%)
 δ_2 [ppm] = -120.9 ppm (d, $^1J_{\text{PH}} = 296$ Hz, $^1J_{\text{P}^{117}\text{Sn}} = 946$ Hz, $^1J_{\text{P}^{119}\text{Sn}} = 1014$ Hz; total tin satellite intensity = 19%)

4.5.5 Reaction of Ph*SnCl with LiP(H)Trip, generation of Ph*SnP(H)Trip (9)

TripPH₂ (57 mg, 0.24 mmol) was dissolved in 10 mL Et₂O and cooled to -78°C. A solution of *n*BuLi (0.15 mL, 1.6 M in *n*-hexane, 0.24 mmol) was added slowly by pipette. The mixture was allowed to warm to room temperature and stirred for one hour. The resulting LiP(H)Trip solution was added dropwise to a solution of Ph*SnCl (154 mg, 0.24 mmol) in 8 mL Et₂O cooled to -78°C. The solution was allowed to warm slowly to room temperature, whereby the orange Ph*SnCl solution slowly became brown. After stirring overnight, the solution was filtered through Kieselgur and the solvent removed. The resulting brown residue was analyzed by ³¹P-NMR, which indicated formation of Trip(H)P-P(H)Trip (ca. 20%) and Ph*SnP(H)Trip (9) (ca. 70%) alongside unreacted TripPH₂ (ca. 10%).

Analytical data for 9:

³¹P-NMR (162 MHz, C₆D₆) δ [ppm] = -70.9 (br, $\Delta\nu_{1/2} = 150$ Hz, $^1J_{\text{PH}} = 186$ Hz, $^1J_{\text{P}^{117/119}\text{Sn}} = 934$ Hz; ^{117/119}Sn satellites could not be resolved, total Sn satellite intensity = 12%)

4.5.6 Reaction of Ph*SnCl with Li₂PTrip, generation of Li⁺[Ph*SnPTrip] (10, proposed)

To a solution of TripPH₂ (64 mg, 0.27 mmol) in 10 mL Et₂O was added a solution of *n*BuLi (0.34 mL, 1.6 M in *n*-hexane, 0.54 mmol) at -78°C. The resulting solution was allowed to warm to room temperature and stirred for 3 hours. The yellow solution of Li₂PTrip was added slowly to a solution of Ph*SnCl (171 mg, 0.27 mmol) in 10 mL Et₂O at -78°C. The resulting solution was allowed to warm slowly to room temperature, whereby the orange color gradually became brown. After overnight stirring, the solution was filtered through Kieselgur and the solvent removed. The resulting brown residue was analyzed by ³¹P-NMR,

whereby a mixture of signals indicated formation of Trip(H)P–P(H)Trip (ca. 20%) and $\text{Li}^+[\text{Ph}^*\text{SnPTrip}]^-$ (proposed, ca. 40%).

Analytical data for **10** (proposed):

^{31}P -NMR (162 MHz, δ [ppm] = 229.7 (br, $\Delta\nu_{1/2}$ = 280 Hz, $^1J_{\text{P117Sn}}$ = 1735 Hz, $^1J_{\text{P119Sn}}$ = 2004 Hz, total Sn satellite intensity = ca. 14%)
 C_6D_6)

4.5.7 Reaction of Ph^*SnCl with $\text{Li}[\text{H}_2\text{PW}(\text{CO})_5]$, formation of $[\text{Ph}^*\text{Sn}\{\text{W}(\text{CO})_5\}(\mu\text{-O})_2\text{SnPh}^*]$ (**11**)

A solution of Ph^*SnCl (198 mg, 0.31 mmol) in *n*-hexane (10 mL) was added dropwise to a vigorously stirred suspension of $\text{Li}[\text{H}_2\text{PW}(\text{CO})_5]$ (113 mg, 0.31 mmol) in *n*-hexane (5 mL) at -78°C . The resulting pale red-brown suspension was allowed to warm to room temperature and stirred overnight. The solution was filtered through Kieselgur, and the volume was reduced under vacuum to 1 mL. Storage at -25°C for several weeks yielded a mixture of colorless, yellow, and orange crystals, from which an orange crystal was selected for an X-ray diffraction experiment and determined crystallographically to be compound **11**. Among the mixture of crystals the presence of $[\text{H}_3\text{PW}(\text{CO})_5]$ was shown by EI mass spectrometry, but no other compounds could be identified unambiguously. The synthesis of **11** could not be reproduced, thus preventing preparative isolation and further spectroscopic characterization. The mass spectroscopy data given below were measured for the same crystal used in the X-ray experiment.

Analytical data for **11**:

MS (EI, 70 eV, m/z (%) = 594.5 (11) $[\text{Sn}_2\text{O}_2\text{W}(\text{CO})_5]^+$, 566.5 (33) $[\text{Sn}_2\text{O}_2\text{W}(\text{CO})_4]^+$, 538.5 (38) $[\text{Sn}_2\text{O}_2\text{W}(\text{CO})_3]^+$, 510.5 (16) $[\text{Sn}_2\text{O}_2\text{W}(\text{CO})_2]^+$, 43.1 (54) $[\text{C}_3\text{H}_7]^+$
 380°C)

4.5.8 Reaction of Ph^*SnCl with Cp^*PCl_2

Ph^*SnCl (179 mg, 0.26 mmol) was dissolved in *n*-hexane and cooled to -78°C . A solution of Cp^*PCl_2 (0.57 mL, 0.47 M in *n*-hexane, 0.26 mmol) was added slowly by pipette, resulting in discoloration of the orange solution to pale yellow. The solution was allowed to warm to room temperature and separated from a small amount of colorless material by decantation. The solvent was removed under reduced pressure, and the residue was examined

by ^{31}P -NMR, revealing $\text{Cp}^*\text{P}=\text{PCp}^*$ as the main phosphorus-containing product (ca. 40%), along with unreacted Cp^*PCl_2 .

4.5.9 Synthesis of $\text{Ph}^*\text{Sn}(\text{OSiMe}_3)_2\text{Cl}$ (**12**)

Excess trimethylsilylperoxide (0.2 mL, ca. 200 mg, ca. 1.1 mmol) was added by pipette to a solution of Ph^*SnCl (560 mg, 0.88 mmol) in Et_2O (10 mL) at 0°C . The color changed immediately from orange to colorless. The solution was allowed to warm to room temperature and stirred for one hour. After filtration through Kieselgur, the filtrate was concentrated under reduced pressure to 2 mL and stored at -25°C . Colorless crystals formed after one week, were separated from the mother liquor by decantation, and dried under vacuum. Yield: 172 mg, 24%.

Analytical data for **12**:

MS (EI, 70 eV, 120°C)	m/z (%) = 799.1 (1.0) $[\text{M}^+ - \text{CH}_3]$, 741.0 (1.2) $[\text{M}^+ - \text{SiMe}_3]$, 725.1 (1.6) $[\text{M}^+ - \text{OSiMe}_3]$, 652.1 (1.3) $[\text{M}^+ - \text{OSiMe}_3 - \text{SiMe}_3]$, 636.1 (0.8) $[\text{M}^+ - 2\text{OSiMe}_3]$, 601.1 (1.2) $[\text{M}^+ - 2\text{OSiMe}_3 - \text{Cl}]$, 482.2 (100) $[\text{M}^+ - \text{Sn}(\text{OSiMe}_3)_2\text{Cl}]$, 467.2 (100) $[\text{M}^+ - \text{Sn}(\text{OSiMe}_3)_2\text{Cl} - \text{CH}_3]$, 439.1 (46) $[\text{M}^+ - \text{Sn}(\text{OSiMe}_3)_2\text{Cl} - \text{C}_3\text{H}_7]$, 424.2 (20) $[\text{M}^+ - \text{Sn}(\text{OSiMe}_3)_2\text{Cl} - \text{C}_3\text{H}_7 - \text{CH}_3]$
^1H-NMR (300.13 MHz, C_6D_6)	δ [ppm] = 0.13 (s, 18H, $\text{Si}(\text{CH}_3)_3$), 1.07 (d, 12H, $\text{CH}(\text{CH}_3)_2$, $^3J_{\text{HH}} = 6.9$ Hz), 1.20 (d, 12H, $\text{CH}(\text{CH}_3)_2$, $^3J_{\text{HH}} = 6.8$ Hz), 1.30 (d, 12H, $\text{CH}(\text{CH}_3)_2$, $^3J_{\text{HH}} = 6.9$ Hz), 2.91 (mult, 6H, $\text{CH}(\text{CH}_3)_2$), 7.06 (t, 1H, <i>p</i> - C_6H_3 , $^3J_{\text{HH}} = 7.5$ Hz), 7.18 (s, 4H, <i>m</i> -Trip), 7.21 (br, 2H, <i>m</i> - C_6H_3)

4.5.10 Synthesis of $[\text{Ph}^*\text{Sn}(\mu\text{-O})\text{Cl}]_2$ (**13**)

Trimethylamine *N*-oxide (59 mg, 0.79 mmol) was added as a solid to a solution of Ph^*SnCl (500 mg, 0.79 mmol) in Et_2O (15 mL) at 0°C . The color changed within 30 minutes from orange to colorless. The solution was allowed to warm to room temperature and stirred for two hours, after which the solution had become cloudy. Et_2O was added by Teflon cannula until the solution became clear (ca. 15 mL). After filtration through Kieselgur, the filtrate was concentrated under reduced pressure until the onset of crystallization and stored at -25°C . Colorless crystals formed after four days, were separated from the mother liquor by decantation, and dried under vacuum. Yield: 216 mg, 42%.

Analytical data for **13**:

IR (KBr pellet)	$\tilde{\nu}$ [cm ⁻¹] = 3053 (m), 2860 (m), 1962 (w), 1760 (m), 1605 (s), 1564 (s), 1385 (s), 1362 (s), 1318 (s), 1251 (s), 1240 (s), 1188 (m), 1164 (vs), 1154 (m), 1100 (vs), 1080 (s), 1071 (s), 1055 (s), 916 (s), 875 (s), 805 (s), 776 (s), 750 (s), 654 (s), 497 (s)
MS (FD, toluene solution)	m/z (%) = 1304.6 (100) [M ⁺]
¹H-NMR (300.13 MHz, C ₆ D ₆)	δ [ppm] = 1.02 (d, 12H, CH(CH ₃) ₂ , ³ J _{HH} = 6.9 Hz), 1.36 (d, 12H, CH(CH ₃) ₂ , ³ J _{HH} = 6.8 Hz), 1.46 (d, 12H, CH(CH ₃) ₂ , ³ J _{HH} = 6.9 Hz), 2.86 (mult, 6H, CH(CH ₃) ₂), 7.22 (s, 4H, <i>m</i> -Trip)
¹³C-NMR (75.48 MHz, C ₆ D ₆)	δ [ppm] = 23.45 (s, CH(CH ₃) ₂), 24.20 (s, CH(CH ₃) ₂), 26.17 (s, CH(CH ₃) ₂), 31.34 (s, CH(CH ₃) ₂), 34.75 (s, CH(CH ₃) ₂), 121.64 (s), 127.71 (s), 130.17 (s), 131.08 (s), 136.59 (s), 147.22 (s), 147.90 (s), 149.88 (s)

4.6 Reactions involving Ph*Sn(IV)-halides and pseudohalides

4.6.1 Synthesis of Ph*SnCl₃ (**14a**)

Method A: SnCl₄ (0.90 mL, 2.0 g, 7.7 mmol) was dissolved in 5 mL *n*-hexane. 5 mL Et₂O was added, and the resulting white suspension was cooled to -78°C. A solution of Ph*Li·OEt₂ (4.319 g, 7.7 mmol) in 50 mL Et₂O was then added dropwise. The reaction mixture was slowly allowed to warm to room temperature and stirred overnight. The solvent was removed *in vacuo*, and the white residue extracted with 40 mL *n*-hexane. Upon filtration through Kieselgur, the filtrate was concentrated under reduced pressure to about 15 mL and stored at -25°C, whereby colorless microcrystals of **14a** precipitated overnight. The mother liquor was decanted, and the crystals were dried under vacuum. Yield: 2.01 g, 37%.

Method B: PCl₃ (45 μ L, 72 mg, 0.52 mmol) was added by pipette to a solution of Ph*SnCl (333 mg, 0.52 mmol) in *n*-hexane (20 mL) at -78°C. The solution turned immediately from orange to colorless. The solution was allowed to warm to room temperature and stirred overnight, after which a colorless solution with yellow precipitate was observed. The solution was filtered through a plug of Kieselgur, and the filtrate was concentrated to 5 mL under vacuum. Storage at -25°C for five days afforded colorless crystals. Yield: 249 mg, 68%.

Analytical data for **14a**:

Elem. Analysis	Calcd. for $C_{36}H_{49}SnCl_3$: C, 61.20%; H, 6.99%. Found: C, 62.10%; H, 6.41%
MS (EI, 70 eV, 160°C)	m/z (%) = 706.2 (13) $[M^+]$, 671.2 (4) $[M^+ - Cl]$, 481.4 (99) $[M^+ - SnCl_3]$, 466.3 (34) $[M^+ - SnCl_3 - CH_3]$, 438.4 (14) $[M^+ - SnCl_3 - C_3H_7]$
1H-NMR (300.13 MHz, C_6D_6)	δ [ppm] = 1.04 (d, 12H, o -CH(CH_3) ₂ , $^3J_{HH}$ = 6.9 Hz), 1.23 (d, 12H, 12H, o -CH(CH_3) ₂ , $^3J_{HH}$ = 6.9 Hz), 1.44 (d, 12H, p -CH(CH_3) ₂ , $^3J_{HH}$ = 6.9 Hz), 2.82 (m, CH(CH_3) ₂), 7.07 (t, 1H, p -C ₆ H ₃ , $^3J_{HH}$ = 7.7 Hz), 7.22 (s, 4H, m -Trip), 7.24 (br, 2H, m -C ₆ H ₃)
^{13}C-NMR (75.47 MHz, C_6D_6)	δ [ppm] = 23.01 (s, CH(CH_3) ₂), 24.12 (s, CH(CH_3) ₂), 26.04 (s, CH(CH_3) ₂), 31.41 (s, CH(CH_3) ₂), 34.96 (s, CH(CH_3) ₂), 122.07 (s), 131.11 (s), 131.63 (s), 134.77 (s), 141.50 (s), 147.66 (s), 147.97 (s), 151.18 (s)
$^{119}Sn\{^1H\}$-NMR (149.21 MHz, C_6D_6)	δ [ppm] = -113.8 (s)

4.6.2 Synthesis of Ph*SnBr₃ (**14b**)

Ph*SnBr₃ was prepared in the same manner as for Ph*SnCl₃ (*Method A*) starting from SnBr₄ (326 mg, 0.74 mmol) and Ph*Li·OEt₂ (418 mg, 0.74 mmol) to give colorless crystals in two crops. Yield: 248 mg, 40%.

Analytical data for **14b**:

Elem. Analysis	Calcd. for $C_{36}H_{49}SnBr_3$: C, 51.49%; H, 5.88%. Found: C, 53.11%; H, 6.11%.
MS (EI, 70 eV)	m/z (%) = 837.9 (7.0) $[M^+]$, 796.9 (3.5) $[M^+ - C_3H_7]$, 759.0 (19) $[M^+ - Br]$, 481.4 (100) $[M^+ - SnBr_3]$, 466.3 (16) $[M^+ - SnBr_3 - CH_3]$, 43.0 (41) $[C_3H_7^+]$
1H-NMR (300.13 MHz, C_6D_6)	δ [ppm] = 1.04 (d, 12H, o -CH(CH_3) ₂ , $^3J_{HH}$ = 6.6 Hz), 1.23 (d, 12H, 12H, o -CH(CH_3) ₂ , $^3J_{HH}$ = 6.6 Hz), 1.46 (d, 12H, p -CH(CH_3) ₂ , $^3J_{HH}$ = 6.8 Hz), 2.87 (m, CH(CH_3) ₂), 7.03 (t, 1H, p -C ₆ H ₃ , $^3J_{HH}$ = 7.6 Hz), 7.21 (s, 4H, m -Trip)

¹³ C-NMR (75.47 MHz, C ₆ D ₆)	δ [ppm] = 23.39 (s, CH(CH ₃) ₂), 24.16 (s, CH(CH ₃) ₂), 26.11 (s, CH(CH ₃) ₂), 31.40 (s, CH(CH ₃) ₂), 34.97 (s, CH(CH ₃) ₂), 122.15 (s), 130.65 (s), 132.10 (s), 134.35 (s), 139.37 (s), 147.30 (s), 147.82 (s), 151.02 (s)
¹¹⁹ Sn{ ¹ H}-NMR (149.21 MHz, C ₆ D ₆)	δ [ppm] = −332.6 (s)

4.6.3 Reaction of Ph*SnCl₃, Ph*Sn(OSiMe₃)₂Cl, and [Ph*Sn(μ-O)Cl]₂ with LiP(SiMe₃)₂·1.8THF

A solution of Ph*SnCl₃ (1.452 g, 2.06 mmol, 40 mL Et₂O), Ph*Sn(OSiMe₃)₂Cl (161 mg, 0.20 mmol, 10 mL Et₂O), or [Ph*Sn(μ-O)Cl]₂ (129 mg, 0.099 mmol, 10 mL Et₂O) was cooled to −78°C. LiP(SiMe₃)₂·1.8THF (1 equiv. P per Sn) was added as a solid, and the solution slowly turned violet. The solution was allowed to stir overnight at room temperature, then filtered through Kieselgur. In the cases where Ph*Sn(OSiMe₃)₂Cl and [Ph*Sn(μ-O)Cl]₂ were used as reactant, the filtrate was reduced in volume to dryness under vacuum and examined by ³¹P-NMR. In the case where Ph*SnCl₃ was used as reactant, a 5-mL aliquot of the filtrate was taken for analogous ³¹P-NMR analysis, while the rest was concentrated to ca. 5 mL under reduced pressure and stored at −25°C for one week, after which colorless crystals of Ph*SnCl₃ deposited. In all three cases, the ³¹P-NMR spectrum of the crude reaction mixture showed Ph*SnP(SiMe₃)₂ and (Me₃Si)₂PP(SiMe₃)₂ as the main phosphorus-containing products.

4.7 Reactions involving tris(aryloxy)amine (L*)

4.7.1 Synthesis of Li₃L*

Tris(2-hydroxy-3-*tert*-butyl-5-methylbenzyl)amine, L*H₃, (558 mg, 1.02 mmol) was dissolved in 20 mL benzene. A solution of *n*BuLi (2.0 mL, 1.6 M in *n*-hexane, 3.20 mmol) was added dropwise at room temperature, whereby the reaction solution became yellow, then precipitated a white powder with mild evolution of heat. The mixture was stirred overnight, and the white powder was collected by filtration and washed twice with *n*-hexane (10 mL). The powder was dried under high vacuum. Yield: 340 mg, 59%.

Analytical data for Li_3L^* :

$^1\text{H-NMR}$ (300.13 MHz, $\text{THF-}d_8$)	δ [ppm] = 1.31 (s, br, 27H, $t\text{Bu}$, $\Delta\nu_{1/2} = 27$ Hz), 2.05 (s, br, 9H, Me, $\Delta\nu_{1/2} = 24$ Hz), 3.36 (s, br, 6H, NCH_2 , $\Delta\nu_{1/2} = 21$ Hz), 6.40 (s, br, 3H, aryl- H , $\Delta\nu_{1/2} = 24$ Hz), 6.65 (s, br, 3H, aryl- H , $\Delta\nu_{1/2} = 24$ Hz)
$^{13}\text{C-NMR}$ (75.47 MHz, $\text{THF-}d_8$)	δ [ppm] = 18.24 (Me), 27.84 ($\text{C}(\text{CH}_3)_3$), 32.43 ($\text{C}(\text{CH}_3)_3$), 59.49 (NCH_2), 116.11, 123.80, 125.33, 127.34, 133.85, 162.78 (aryl)

4.7.2 Synthesis of $[\text{L}^*\text{TaCl}_2]$ (**15**)

Method A: Li_3L^* (340 mg, 0.60 mmol) was suspended in 10 mL benzene. TaCl_5 (296 mg, 0.60 mmol) was added portionwise as a solid at room temperature. The solution became yellow and was stirred overnight. The mixture was filtered through a plug of Kieselgur, which was washed twice with benzene (5 mL). The solvent was removed from the filtrate under reduced pressure to give a yellow powder. Yield: 282 mg, 59%.

Method B: TaCl_5 (632 mg, 1.76 mmol) was stirred in 15 mL toluene for 20 minutes. L^*H_3 (963 mg, 176 mmol) was added portionwise as a solid at room temperature, and the yellow suspension was heated to reflux, whereby gas evolution was observed, already starting at 95°C . The reaction flask was occasionally purged with nitrogen to facilitate elimination of HCl . After 4 hours the orange-yellow solution was allowed to cool to room temperature, and the toluene was removed under reduced pressure. The oily residue was extracted with 15 mL n -hexane and filtered through Kieselgur. The solvent was removed under reduced pressure, and the residue was crystallized from a minimum of Et_2O at 4°C . Yellow plates formed within 3 days and were isolated by decantation and dried under vacuum. Yield: 810 mg, 58%.

Analytical data for **15**:

MS (EI, 70 eV, 160°C)	m/z (%) = 793.2 (100) $[\text{M}^+]$, 757.0 (68) $[\text{M}^+ - \text{Cl}]$, 742.2 (49) $[\text{M}^+ - \text{Cl} - \text{CH}_3]$, 723.1 (1.0) $[\text{M}^+ - 2\text{Cl}]$, 665.4 (1.4) $[\text{M}^+ - 2\text{Cl} - \text{C}_4\text{H}_9]$, 545.4 (15) $[\text{M}^+ - 2\text{Cl} - \text{CH}_2\text{-2-oxy-3-}t\text{Bu-5-Me-C}_6\text{H}_2]$, 176.1 (12) $[\text{CH}_2\text{-2-oxy-3-}t\text{Bu-5-Me-C}_6\text{H}_2]^+$, 57.1 (19), $[\text{C}_4\text{H}_9]^+$
$^1\text{H-NMR}$ (300.13 MHz, C_6D_6)	δ [ppm] = 1.61 (s, 18H, $t\text{Bu}$), 1.62 (s, 9H, $t\text{Bu}$), 2.20 (s, 3H, Me), 2.25 (s, 6H, Me), 3.30 (d, 2H, NCH_2 , $J = 13.8$ Hz), 3.45 (s, 2H, NCH_2), 3.74 (d, 2H, NCH_2 , $J = 13.8$ Hz), 6.47 (d, 1H, aryl- H , $^4J_{\text{HH}} = 1.5$ Hz), 6.51 (d, 2H, aryl- H , $^4J_{\text{HH}} = 1.8$ Hz), 7.18 (d, 1H, aryl- H , $^4J_{\text{HH}} = 1.5$ Hz), 7.22 (d, 2H, aryl- H , $^4J_{\text{HH}} = 1.8$ Hz)

¹ H-NMR (300.13 MHz, CD ₂ Cl ₂)	δ [ppm] = 1.43 (s, 18H, <i>t</i> Bu), 1.52 (s, 9H, <i>t</i> Bu), 2.31 (s, 3H, Me), 2.35 (s, 6H, Me), 3.82 (d, 2H, NCH ₂ , <i>J</i> = 14.1 Hz), 3.89 (s, 2H, NCH ₂), 4.09 (d, 2H, NCH ₂ , <i>J</i> = 14.1 Hz), 6.88 (d, 2H, aryl- <i>H</i> , ⁴ <i>J</i> _{HH} = 1.8 Hz), 6.93 (d, 1H, aryl- <i>H</i> , ⁴ <i>J</i> _{HH} = 1.5 Hz), 7.21 (d, 3H, aryl- <i>H</i> , ⁴ <i>J</i> _{HH} = 1.8 Hz)
¹³ C-NMR (75.48 MHz, C ₆ D ₆)	δ [ppm] = 21.02 (Me), 29.96 (C(CH ₃) ₃), 30.49 (C(CH ₃) ₃), 31.16 (Me), 34.82 (C(CH ₃) ₃), 35.02 (C(CH ₃) ₃), 61.20 (NCH ₂), 62.38 (NCH ₂), 124.51, 125.05, 131.28, 131.64, 138.89, 139.47, 154.29, 154.71 (aryl); four additional aryl signals are obscured by overlapping C ₆ D ₆ peaks
¹³ C-NMR (75.48 MHz, CD ₂ Cl ₂)	δ [ppm] = 21.06 (Me), 29.94 (C(CH ₃) ₃), 30.32 (C(CH ₃) ₃), 30.98 (Me), 34.87 (C(CH ₃) ₃), 34.97 (C(CH ₃) ₃), 61.71 (NCH ₂), 62.59 (NCH ₂), 124.49, 125.02, 128.01, 128.41, 128.50, 128.61, 131.13, 132.68, 138.64, 139.27, 154.23, 155.14 (aryl)

4.7.3 Synthesis of [L*Ta(Cl)P(SiMe₃)₂] (**16a**) and [L*Ta(Cl)As(SiMe₃)₂] (**16b**)

Solid LiE(SiMe₃)₂·1.8THF (E = P: 264 mg, 0.84 mmol; E = As: 301 mg, 0.84 mmol) was added portionwise to a solution of [L*TaCl₂] (333 mg, 0.42 mmol) in 15 mL *n*-hexane at –78°C. The solution was allowed to warm slowly and changed color from yellow to red (E = P) or violet-red (E = As) at ca. –15°C. After 2 hours stirring at ca. 0°C, the solution was filtered quickly through a plug of Kieselgur and the solvent was removed. The red or violet-red residue was dissolved in ca. 5 mL Et₂O, reduced slightly in volume under reduced pressure, and stored at –25°C. A few red (E = P) or violet-red (E = As) crystals deposited after five days. Yield: 106 mg, 27% (**16a**); 70 mg, 17% (**16b**).

Obtainment of clean ¹H- and ¹³C-NMR spectra was precluded by decomposition of the products in solution.

Analytical data for **16a**:

MS (EI, 70 eV, 190°C) m/z (%) = 846.4 (37) [$M^+ - \text{SiMe}_3 - \text{CH}_3$], 831.5 (100) [$M^+ - \text{SiMe}_3 - 2\text{CH}_3$], 757.3 (66) [$M^+ - \text{P}(\text{SiMe}_3)_2$], 724.3 (19) [$M^+ - \text{P}(\text{SiMe}_3)_2 - \text{Cl}$], 666.4 (1.6) [$M^+ - \text{P}(\text{SiMe}_3)_2 - \text{Cl} - \text{C}_4\text{H}_9$], 545.3 (5.3) [$M^+ - \text{P}(\text{SiMe}_3)_2 - \text{Cl} - \text{CH}_2\text{-2-oxy-3-}t\text{Bu-5-Me-C}_6\text{H}_2$], 176.2 (6.9) [$\text{CH}_2\text{-2-oxy-3-}t\text{Bu-5-Me-C}_6\text{H}_2$] $^+$, 73.1 (33) [SiMe_3] $^+$, 57.1 (39) [C_4H_9] $^+$

^{31}P -NMR (162 MHz, C_6D_6) δ [ppm] = 26.1 (s)

Analytical data for **16b**:

MS (EI, 70 eV, 190°C) m/z (%) = 905.3 (2.6) [$M^+ - \text{SiMe}_3$], 890.5 (9.8) [$M^+ - \text{SiMe}_3 - \text{CH}_3$], 757.3 (100) [$M^+ - \text{As}(\text{SiMe}_3)_2$], 724.2 (22) [$M^+ - \text{As}(\text{SiMe}_3)_2 - \text{Cl}$], 545.4 (2.7) [$M^+ - \text{As}(\text{SiMe}_3)_2 - \text{Cl} - \text{CH}_2\text{-2-oxy-3-}t\text{Bu-5-Me-C}_6\text{H}_2$], 176.1 (3.4) [$\text{CH}_2\text{-2-oxy-3-}t\text{Bu-5-Me-C}_6\text{H}_2$] $^+$, 73.1 (25) [SiMe_3] $^+$, 57.1 (18) [C_4H_9] $^+$

4.7.4 Synthesis of [L^*TaMe_2] (**17**)

[L^*TaCl_2] (256 mg, 0.32 mmol) was dissolved in Et_2O and cooled to -78°C . A solution of MeLi (0.60 mL, 1.4 M in Et_2O , 0.84 mmol) was added dropwise, and the reaction mixture was allowed to warm to room temperature and stirred overnight. The pale yellow solution was filtered through a plug of Kieselgur, and the filtrate was concentrated under reduced pressure. Storage at -25°C for about one week afforded pale yellow needles, which were isolated by decantation and dried under vacuum. Yield: 36 mg, 15%.

Analytical data for **17**:

MS (EI, 70 eV, 170°C) m/z (%) = 753.3 (0.9) [M^+], 738.4 (18) [$M^+ - \text{CH}_3$], 723.4 (4.5) [$M^+ - 2\text{CH}_3$], 176.2 (34) [$\text{CH}_2\text{-2-oxy-3-}t\text{Bu-5-Me-C}_6\text{H}_2$] $^+$, 57.1 (31), [C_4H_9] $^+$

^1H -NMR (300.13 MHz, C_6D_6) δ [ppm] = 1.62 (s, 27 H, $t\text{Bu}$), 2.25 (s, 9H, Me), 3.27 (br, 6H, NCH_2), 6.52 (d, 3H, aryl- H , $^4J_{\text{HH}} = 1.8$ Hz), 7.23 (d, 3H, aryl- H , $^4J_{\text{HH}} = 1.8$ Hz)

^{13}C -NMR (75.47 MHz, C_6D_6) δ [ppm] = 19.63 (Me), 28.80 ($\text{C}(\text{CH}_3)_3$), 33.58 ($\text{C}(\text{CH}_3)_3$), 58.90 (NCH_2), 124.56, 126.40, 127.45, 128.33, 137.09, 153.37 (aryl)

4.8 Reactions involving $[\text{Cp}''\text{Ta}(\text{CO})_2(\eta^4\text{-P}_4)]$

4.8.1 Synthesis of $\text{Cp}''\text{H}$

The following procedure was carried out with exposure to air, with a stream of N_2 only over the reaction mixture. An aqueous solution of 50%-KOH (875.3 g, 15.6 mol, in 875 mL water) was prepared. In a 2-L round-bottom flask with a sturdy magnetic stirbar and efficient reflux condenser, freshly cracked CpH (30 mL, 0.39 mol), *t*BuBr (268.3 g, 1.960 mol), and half of the KOH solution were added successively. With stirring Adogen 464 (15.6 g, 1 gram per mole KOH) was added and washed into the mixture with the rest of the KOH solution. The mixture turned slowly to dark brown and was carefully heated to 60°C (Caution: heavy gas evolution and in some cases foaming!) and stirred at that temperature for 75 minutes. The mixture was then stirred for 45 minutes at 100°C. The mixture was cooled in an ice bath, and 200 mL *n*-pentane was added. After a few minutes stirring, the mixture was filtered away from precipitated KBr. The organic phase was separated, washed with 200 mL water, and dried over MgSO_4 . The solvent was removed by rotary vacuum, and the dark brown residue was fractionally distilled under vacuum over a 30 cm Vigreux column to give a yellow oil (65–75°C, $5 \cdot 10^{-2}$ mbar). Yield: 26.9 g, 40% based on CpH.

4.8.2 Preparation of $\text{Cp}''\text{Sn}(n\text{Bu})_3$

$\text{Cp}''\text{H}$ (26.6 g, 149 mmol) was dissolved in THF (1.0 L). *n*BuLi (94 mL, 1.6 M in *n*-hexane, 150 mmol) was added dropwise, regulated so that the reaction solution boiled only mildly, over a span of 35 minutes, and the solution was stirred at room temperature for 45 minutes. *n*Bu₃SnCl (43 mL, 152 mmol) was added portionwise, and the solution stirred 15 minutes. The solvent was removed under reduced pressure, and the yellow residue was extracted three times with 25 mL *n*-hexane and filtered through Kieselgur. The *n*-hexane was removed in vacuum, and the orange-yellow oil was distilled over a 15 cm Vigreux column to give $\text{Cp}''\text{Sn}(n\text{Bu})_3$ as a yellow oil (113–118°C, $2 \cdot 10^{-2}$ mbar, oil bath maintained at 180°C, and Vigreux column heated with a powerful heat gun). Yield: 63.4 g, 91%. The spectroscopic data are consistent with the published data for $\text{Cp}''\text{Sn}(n\text{Bu})_3$. [181]

4.8.3 Preparation of $[\text{Cp}''\text{TaCl}_4]$

TaCl_5 (10.3 g, 28.8 mmol) was suspended in 700 mL toluene and stirred overnight, then heated to reflux until the solid was fully dissolved. To the refluxing solution was added $\text{Cp}''\text{Sn}(n\text{Bu})_3$ (13.7 g, 14.6 mL, 29.3 mmol), and the solution was stirred under reflux for 30

minutes. The olive green solution was cooled in an ice bath, and the solvent was removed in vacuum. The brown residue was washed 6 times with 25 mL *n*-hexane to remove $n\text{Bu}_3\text{SnCl}$ and excess $\text{Cp}''\text{Sn}(n\text{Bu})_3$. The mustard-colored solid was dried under vacuum and extracted with ca. 100 mL toluene and filtered through Kieselgur. The volume of the filtrate was reduced in vacuum, until the onset of crystallization, and the solution was stored at -25°C . After a few days, yellow crystals formed and were separated from the mother liquor by decantation and dried under vacuum. Yield: 5.54 g, 36 %. Additional crops of crystals were obtained by reducing the volume of the mother liquor and storing at -25°C . The spectroscopic data are consistent with the published data for $[\text{Cp}''\text{TaCl}_4]$. [174]

4.8.4 Preparation of $[\text{Cp}''\text{Ta}(\text{CO})_4]$

$[\text{Cp}''\text{TaCl}_4]$ (2.23 g, 2.46 mmol) was dissolved in ca. 40 mL THF and filled into an autoclave with a dinitrogen purge. Protecting the solution with a stream of N_2 , the following were added as powders: Zn (1.0 g), Cu (0.4 g), Al (0.4 g). The autoclave was closed and pressurized with 400 bar CO and fixed into a rotary with a heat source and positioned at an angle of ca. 45° . The autoclave was heated to 100°C and rotated for five days. The CO pressure was carefully vented, and the deep red suspension was transferred to a Schlenk tube under N_2 and filtered. From the filtrate the solvent was removed under vacuum, and the residue was chromatographed on a short silica gel column (length: 10 cm; diameter: 2 cm), which had been covered with aluminum foil and packed with *n*-hexane. A long, orange-red fraction was eluted with *n*-hexane and collected. The solvent was removed under vacuum to give a red, crystalline solid. Yield: 1.38 g, 65%. The spectroscopic data are consistent with the published data for $[\text{Cp}''\text{Ta}(\text{CO})_4]$. [174]

4.8.5 Preparation of $[\text{Cp}''\text{Ta}(\text{CO})_2(\eta^4\text{-P}_4)]$ (18)

$[\text{Cp}''\text{Ta}(\text{CO})_4]$ (1.09 g, 2.32 mmol) and P_4 (735 mg, 5.93 mmol) were separately dissolved in ca. 10 mL and 30 mL toluene, respectively (some mild heating is required to dissolve the P_4 fully). The solutions were combined in a photolysis apparatus, and the apparatus was filled with additional toluene to the height of the lamp. With vigorous stirring the solution was irradiated for 20 minutes with a stream of N_2 purged through the solution with a Teflon cannula. The resulting dark brown solution was transferred to a Schlenk tube, and the solvent was removed under vacuum. The brown residue was chromatographed on a silica gel column (length: 45 cm; diameter: 3 cm) packed with *n*-hexane. Unreacted $[\text{Cp}''\text{Ta}(\text{CO})_4]$ was first eluted with *n*-hexane, and lemon-yellow $[\text{Cp}''\text{Ta}(\text{CO})_2(\eta^4\text{-P}_4)]$ was

eluted with *n*-hexane/toluene (15:1). The yellow fraction was collected and the solvent removed under vacuum, affording a yellow, crystalline solid. Yield: 321 mg, 26%. The spectroscopic data are consistent with the published data for $[\text{Cp}''\text{Ta}(\text{CO})_2(\eta^4\text{-P}_4)]$. [175]

Additional analytical data for **18**:

^{31}P -NMR (161.97 δ [ppm] = -7.53 (dt, $^2J_{\text{P}_{\text{A}}\text{P}_{\text{M}}} = 53$ Hz), 14.2 (t, $^1J_{\text{P}_{\text{M}}\text{P}_{\text{X}}} = 242$ Hz), 40.8 MHz, DMF- d_7) (t, $^1J_{\text{P}_{\text{M}}\text{P}_{\text{X}}} = 298$ Hz)

4.8.6 Preparation of $[\{\text{Cp}''\text{Ta}(\text{CO})_2(\mu, \eta^4: \eta^1: \eta^1: \eta^1: \eta^1\text{-P}_4)\}_6\{\text{CuX}\}_8]$ (X = Cl (**19a**), Br (**19b**), I (proposed, **19c**))

A thin Schlenk tube (diameter = 1.9 cm) was charged with a solution of $[\text{Cp}''\text{Ta}(\text{CO})_2(\eta^4\text{-P}_4)]$ (X = Cl: 70 mg, 0.13 mmol; X = Br: 52 mg, 0.095 mmol; X = I: 63 mg, 0.12 mmol) in 2 mL CH_2Cl_2 . Onto this solution was carefully layered a mixture of 4 mL CH_2Cl_2 and 2 mL MeCN, followed by a solution of CuX (X = Cl: 17 mg, 0.17 mmol; X = Br: 18 mg, 0.13 mmol; X = I: 30 mg, 0.16 mmol) in MeCN/ CH_2Cl_2 (1 mL / 1 mL). The doubly layered system was allowed to stand wrapped in aluminum foil in an undisturbed area (Note: for best results, the system may not stand near any surface where a vacuum pump is running), and orange crystals of **19** formed within 24 hours. The mixture was allowed to stand a total of 5 days to ensure thorough diffusion, and the mother liquor was decanted away. The crystals were washed once with 2 mL MeCN and twice with 2 mL CH_2Cl_2 and dried under vacuum. Yield: 59 mg, 66% (**19a**); 34 mg, 64% (**19b**).

Analytical data for **19a**· CH_2Cl_2 :

M.p. 196°C (decomposition, discoloration to black)
Elem. Analysis Calcd. for $\text{C}_{91}\text{H}_{128}\text{O}_{12}\text{Cl}_{10}\text{Cu}_8\text{P}_{24}\text{Ta}_6$: C, 26.62%; H, 3.15%.
 Found: C, 26.74%; H, 3.19%; N, ~0.2%
IR (KBr pellet) $\tilde{\nu}_{\text{CO}}$ [cm^{-1}] = 2040 (vs, br), 1974 (sh)
MS (ESI, DMF solution) m/z (%) = 2215.4 (99) $[\{\text{Cp}''\text{Ta}(\text{CO})_2\text{P}_4\}_4\text{Cu}]^+$, 1239.0 (9.0)
 $[\{\text{Cp}''\text{Ta}(\text{CO})_2\text{P}_4\}_2\text{Cu}_2\text{Cl}]^+$, 1139.1 (100) $[\{\text{Cp}''\text{Ta}(\text{CO})_2\text{P}_4\}_2\text{Cu}]^+$

Analytical data for **19b**·CH₂Cl₂:

Elem. Analysis Calcd. for C₉₁H₁₂₈O₁₂Br₈Cl₂Cu₈P₂₄Ta₆: C, 24.48%; H, 2.87%.
Found: C, 25.22%; H, 3.00%; N, 0.12%

IR (KBr pellet) $\tilde{\nu}_{\text{CO}}$ [cm⁻¹] = 2042 (vs, br), 1972 (sh)

Analytical data for **19c**·CH₂Cl₂ (proposed):

Elem. Analysis Calcd. for C₉₁H₁₂₈O₁₂Cl₂Cu₈I₈P₂₄Ta₆: C, 22.57%; H, 2.65%.
Found: C, 23.31%; H, 2.74%; N, 0.36%

IR (KBr pellet) $\tilde{\nu}_{\text{CO}}$ [cm⁻¹] = 2042 (vs, br), 1972 (sh)

5 Crystallographic Data

5.1 General remarks

In cases where suitable crystals were obtained, structural characterization was carried out on an STOE IPDS area detector diffractometer. Data sets were measured using graphite monochromated Mo-K α ($\lambda = 0.71073$) or Ag-K α ($\lambda = 0.56087$) radiation.

The unit cell parameters were determined from a collection of up to 600 reflections from various angles over the measurement range. The determination of the reflection intensities was performed through the integration of the averaged reflection profile, where high-angle reflections were omitted.

Structures were solved by direct methods with the program SHELXS-97, [210] and refined with SHELXL-97, [211] whereby the following principles apply. Reflex intensities are adjusted through the use of Lorentz- and polarization correction factors. In some cases an additional absorption correction is applied. The input for symmetrically equivalent reflections is averaged. Solution of the structure is then carried out using direct methods and successive Fourier analyses. Optimization of the atomic parameters against F_0^2 is carried out by full-matrix least squares, where the weighting factor is defined as:

$$\frac{1}{w} = \sigma^2 F_0^2 + (aP)^2 + bP \quad \text{where} \quad P = \frac{\max(F_0^2, 0) + 2F_c^2}{3}$$

The values for the parameters a and b are acquired automatically by the program SHELXL-97 and optimized. Correlation of the values is then given by:

$$R_1 = \frac{\sum \|F_0\| - \|F_c\|}{\sum \|F_0\|} \quad wR_2 = \sqrt{\frac{\sum w(F_0^2 - F_c^2)^2}{\sum w(F_0^2)^2}}$$

Atomic coordinates given in the following tables are multiplied by 10^4 , and equivalent isotropic displacement parameters are given in $\text{\AA} \cdot 10^3$. U_{eq} is defined as one third of the trace of the orthogonalized U_{ij} tensor, given as:

$$U_{eq} = \frac{1}{3} \left(\sum_{i=1}^3 \sum_{j=1}^3 U_{ij} a_i * a_j * a_i a_j \right)$$

a_i, a_j : lattice constants

The anisotropic displacement factors are given in $\text{\AA} \cdot 10^3$. Figures of molecular structures generated from crystallographic data were prepared with the programs SCHAKAL-97 [212] or DIAMOND 2.0 [213]. All such figures presented in this work were prepared in their present form with DIAMOND 2.0.

5.2 [(Me₃Si)₃PW(CO)₅] (3)

Crystallographic parameters and details of data collection and refinement for **3**:

Empirical formula	C ₁₄ H ₂₄ O ₅ PSi ₃ W
Formula weight	573.85
Temperature [K]	203(2)
Wavelength [Å]	0.56087
Crystal system	trigonal
Space group	<i>P</i> 3 ₁
Unit cell dimensions	<i>a</i> = 9.3840(13) Å <i>c</i> = 22.895(5) Å
Volume [Å ³]	1746.0(5)
<i>Z</i>	3
Calculated density [g/cm ³]	1.630
Absorption coefficient [mm ⁻¹]	2.798
<i>F</i> (000)	837
Index ranges	-10 ≤ <i>h</i> ≤ 11, -8 ≤ <i>k</i> ≤ 11, -28 ≤ <i>l</i> ≤ 24
θ range for data collection [°]	1.98 – 20.77
Reflections collected	2619
Independent reflections	2305 (<i>R</i> _{int} = 0.1152)
Completeness to θ = 20.77°	84.0%
Absorption correction	none
Refinement method	full-matrix least squares on <i>F</i> ²
Data / restraints / parameters	2305 / 1 / 220
Goodness of fit on <i>F</i> ²	1.127
<i>R</i> ₁ / <i>wR</i> ₂ (<i>I</i> > 2σ(<i>I</i>))	0.0293, 0.0601
<i>R</i> ₁ / <i>wR</i> ₂ (all data)	0.0366, 0.0701
Largest difference peak and hole [e·Å ⁻³]	0.636, -0.602

Atomic coordinates and equivalent isotropic displacement parameters for **3**:

Atom	<i>x</i>	<i>y</i>	<i>z</i>	<i>U</i> _{eq}
W(1)	-5593(1)	-6870(1)	-2112(1)	30(1)
P(1)	-4035(3)	-4362(3)	-1381(1)	27(1)
Si(1)	-1549(4)	-4023(4)	-1095(2)	35(1)
Si(2)	-3472(4)	-1875(4)	-1769(2)	35(1)
Si(3)	-5492(4)	-4639(4)	-539(1)	34(1)
C(1)	-6103(16)	-8613(16)	-1477(7)	47(3)
O(1)	-6427(14)	-9689(12)	-1178(5)	64(3)
C(2)	-7738(13)	-6842(15)	-1932(6)	37(3)
O(2)	-8966(11)	-6962(13)	-1852(5)	60(3)
C(3)	-5001(16)	-5291(16)	-2812(6)	40(3)
O(3)	-4700(13)	-4543(14)	-3234(4)	59(3)
C(4)	-3612(17)	-7192(17)	-2293(6)	44(3)
O(4)	-2666(12)	-7527(13)	-2399(5)	62(3)
C(5)	-6868(15)	-8711(17)	-2690(6)	47(3)
O(5)	-7578(14)	-9722(14)	-2992(6)	87(4)
C(6)	-2015(19)	-5900(20)	-670(8)	66(4)
C(7)	-284(16)	-2131(19)	-645(7)	61(4)
C(8)	-306(15)	-3860(18)	-1766(6)	49(3)
C(9)	-2854(16)	-259(15)	-1188(6)	45(3)
C(10)	-5378(16)	-2155(17)	-2148(7)	49(3)
C(11)	-1769(17)	-1165(18)	-2310(7)	58(4)
C(12)	-7122(17)	-4088(18)	-690(6)	50(3)
C(13)	-6496(17)	-6808(17)	-281(6)	53(4)
C(14)	-4133(17)	-3231(17)	73(6)	49(3)

Anisotropic displacement parameters for **3**:

Atom	U_{11}	U_{22}	U_{33}	U_{23}	U_{13}	U_{12}
W(1)	28(1)	31(1)	29(1)	-4(1)	0(1)	13(1)
Si(1)	28(2)	46(2)	36(2)	-2(1)	-4(1)	21(1)
Si(2)	39(2)	30(2)	38(2)	3(1)	0(1)	18(1)
Si(3)	35(2)	46(2)	29(2)	0(1)	5(1)	26(2)
C(1)	40(7)	37(7)	65(10)	-15(7)	3(6)	19(6)
O(1)	86(8)	44(6)	64(7)	21(5)	15(6)	34(6)
C(2)	27(6)	50(7)	34(7)	7(5)	6(5)	19(5)
O(2)	38(5)	79(7)	71(8)	-10(6)	9(5)	34(5)
C(3)	53(8)	49(7)	28(7)	-14(5)	-11(5)	33(6)
O(3)	74(7)	90(8)	22(5)	21(5)	8(5)	48(6)
C(4)	51(8)	55(8)	37(7)	3(6)	13(6)	34(7)
O(4)	60(6)	87(7)	68(7)	5(6)	18(5)	58(6)
C(5)	32(6)	56(8)	35(8)	-27(6)	-2(5)	8(6)
O(5)	67(7)	76(8)	75(8)	-57(7)	-12(6)	5(6)
C(6)	56(9)	71(10)	85(13)	9(9)	4(8)	42(8)
C(7)	33(7)	76(10)	67(11)	-31(8)	-15(6)	22(7)
C(8)	32(6)	75(9)	41(8)	-2(7)	10(5)	28(6)
C(9)	45(7)	44(7)	47(8)	-10(6)	-2(6)	24(6)
C(10)	49(8)	50(8)	50(9)	0(6)	-4(6)	26(6)
C(11)	44(8)	49(8)	63(10)	13(7)	13(7)	11(7)
C(12)	51(8)	73(9)	38(8)	-14(7)	4(6)	39(7)
C(13)	54(8)	62(8)	47(8)	13(7)	30(7)	33(7)
C(14)	52(8)	62(8)	37(8)	-3(6)	-2(6)	32(7)

5.3 [Fp₂Sn{PH₂W(CO)₅}₂] (4)

The P-bound protons in complex **4** were located and freely refined.

Crystallographic parameters and details of data collection and refinement for **4**·C₇H₈:

Empirical formula	C ₃₁ H ₂₂ Fe ₂ O ₁₄ P ₂ SnW ₂
Formula weight	1278.52
Crystal dimensions [mm]	0.20 x 0.15 x 0.02
Temperature [K]	203(2)
Wavelength [Å]	0.71073
Crystal system	monoclinic
Space group	<i>P2/c</i>
Unit cell dimensions	<i>a</i> = 12.092(2) Å <i>b</i> = 10.969(2) Å <i>c</i> = 15.131(3) Å <i>β</i> = 107.08(3)°
Volume [Å ³]	1918.4(7)
<i>Z</i>	2
Calculated density [g/cm ³]	2.213
Absorption coefficient [mm ⁻¹]	7.499
<i>F</i> (000)	1200
Index ranges	-10 ≤ <i>h</i> ≤ 14, -12 ≤ <i>k</i> ≤ 11, -18 ≤ <i>l</i> ≤ 18
<i>Θ</i> range for data collection [°]	2.33 – 26.00
Reflections collected	10469
Independent reflections	3537 (<i>R</i> _{int} = 0.0524)
Absorption correction	none
Completeness to <i>Θ</i> = 26.00°	93.8%
Refinement method	full-matrix least squares on <i>F</i> ²
Data / restraints / parameters	3537 / 0 / 263
Goodness of fit on <i>F</i> ²	1.066
<i>R</i> ₁ / <i>wR</i> ₂ (<i>I</i> > 2σ(<i>I</i>))	0.0449, 0.1151
<i>R</i> ₁ / <i>wR</i> ₂ (all data)	0.0500, 0.1200
Largest difference peak and hole [e·Å ⁻³]	1.759, -3.536

Atomic coordinates and equivalent isotropic displacement parameters for $4 \cdot \text{C}_7\text{H}_8$:

Atom	<i>x</i>	<i>y</i>	<i>z</i>	<i>U</i> _{eq}
W(1)	7500(1)	11334(1)	2113(1)	34(1)
Sn(1)	10000	8019(1)	2500	23(1)
P(1)	8722(1)	9586(2)	2998(1)	30(1)
Fe(1)	8756(1)	6885(1)	1085(1)	29(1)
C(3)	10039(7)	6509(7)	824(5)	39(2)
O(3)	10863(6)	6242(6)	655(4)	59(2)
C(4)	8571(6)	8272(8)	471(4)	37(2)
O(4)	8410(5)	9137(6)	41(3)	56(2)
C(11)	8504(8)	12598(8)	2966(6)	53(2)
O(11)	9031(7)	13328(8)	3424(5)	77(2)
C(12)	8437(7)	11559(8)	1206(6)	44(2)
O(12)	8913(7)	11740(8)	672(5)	68(2)
C(13)	6405(8)	12637(8)	1475(6)	52(2)
O(13)	5792(7)	13387(8)	1117(6)	75(2)
C(14)	6526(6)	11182(7)	3025(5)	41(2)
O(14)	6022(6)	11155(8)	3522(4)	66(2)
C(15)	6510(6)	10077(7)	1230(4)	40(2)
O(15)	5964(5)	9402(6)	721(4)	57(2)
C(111)	7284(10)	6618(10)	1515(9)	74(3)
C(112)	8140(11)	5697(13)	1899(6)	92(5)
C(113)	8299(9)	5079(8)	1106(9)	67(3)
C(114)	7583(10)	5578(11)	352(7)	72(3)
C(115)	6980(9)	6474(12)	583(8)	77(3)
C(1S)	5000	8097(11)	2500	48(3)
C(2S)	4632(15)	5856(17)	2044(12)	111(6)
C(3S)	4499(19)	7210(20)	1868(17)	59(6)
C(4S)	5770(30)	7850(30)	3417(16)	74(7)
C(5S)	6060(20)	6750(30)	3704(19)	86(10)
C(6S)	3730(20)	7520(50)	871(17)	128(18)

Anisotropic displacement parameters for $4 \cdot \text{C}_7\text{H}_8$:

Atom	U_{11}	U_{22}	U_{33}	U_{23}	U_{13}	U_{12}
W(1)	31(1)	31(1)	37(1)	3(1)	7(1)	3(1)
Sn(1)	27(1)	25(1)	19(1)	0	9(1)	0
P(1)	33(1)	31(1)	29(1)	1(1)	13(1)	7(1)
Fe(1)	33(1)	31(1)	24(1)	-5(1)	9(1)	-5(1)
C(3)	56(5)	34(4)	34(3)	-6(3)	23(3)	-4(3)
O(3)	60(4)	69(5)	62(4)	-3(3)	40(3)	9(3)
C(4)	35(3)	46(4)	26(3)	-2(3)	3(2)	-5(3)
O(4)	61(4)	61(4)	37(3)	16(3)	2(2)	-1(3)
C(11)	54(5)	40(5)	56(4)	8(4)	3(4)	1(4)
O(11)	81(5)	49(4)	82(5)	-5(4)	-6(4)	-16(4)
O(12)	73(4)	71(5)	74(4)	17(3)	42(4)	-4(4)
C(12)	39(4)	35(4)	56(4)	12(3)	9(3)	2(3)
C(13)	60(5)	36(5)	59(4)	6(3)	16(4)	11(4)
O(13)	64(4)	55(4)	96(5)	19(4)	8(4)	19(4)
O(14)	47(4)	107(6)	49(3)	-6(3)	21(3)	2(3)
C(14)	27(3)	46(5)	43(4)	2(3)	3(3)	10(3)
O(15)	58(3)	62(4)	44(3)	-2(3)	5(2)	-4(3)
C(15)	42(4)	44(4)	31(3)	2(3)	7(3)	0(3)
C(111)	80(7)	55(6)	115(9)	-32(6)	74(7)	-31(5)
C(112)	98(8)	115(11)	49(5)	34(6)	-1(5)	-80(8)
C(113)	67(6)	20(5)	127(9)	-4(5)	48(6)	-9(4)
C(114)	74(7)	73(8)	66(5)	-28(5)	16(5)	-37(6)
C(115)	33(5)	103(10)	83(7)	16(6)	0(5)	-15(5)
C(1S)	53(6)	32(7)	68(7)	0	29(5)	0
C(2S)	113(13)	98(12)	151(14)	1(9)	85(12)	22(9)
C(3S)	65(12)	46(13)	84(15)	25(12)	50(12)	15(10)
C(4S)	100(18)	76(19)	60(13)	5(11)	43(13)	35(15)
C(5S)	67(14)	130(30)	67(14)	58(17)	30(12)	60(17)
C(6S)	48(12)	280(50)	54(13)	60(20)	10(10)	-30(20)

5.4 [Fp₂Sn{P(SiMe₃)₂}₂] (5)

Crystallographic parameters and details of data collection and refinement for **5**:

Empirical formula	C ₂₆ H ₄₆ Fe ₂ O ₄ P ₂ Si ₄ Sn
Formula weight	827.34
Crystal dimensions [mm]	0.42 x 0.20 x 0.03
Temperature [K]	173(1)
Wavelength [Å]	0.71073
Crystal system	orthorhombic
Space group	<i>P2₁ab</i>
Unit cell dimensions	<i>a</i> = 12.1536(10) Å <i>b</i> = 17.2246(11) Å <i>c</i> = 18.0192(14) Å
Volume [Å ³]	3772.2(5)
<i>Z</i>	4
Calculated density [g/cm ³]	1.457
Absorption coefficient [mm ⁻¹]	1.655
F(000)	1688
Index ranges	-14 ≤ <i>h</i> ≤ 14, -21 ≤ <i>k</i> ≤ 20, -22 ≤ <i>l</i> ≤ 22
Θ range for data collection [°]	2.26 – 25.85
Reflections collected	25707
Independent reflections	7222 (<i>R</i> _{int} = 0.0367)
Absorption correction	numerical
Refinement method	full-matrix least squares on <i>F</i> ²
Data / restraints / parameters	7222 / 1 / 353
Goodness of fit on <i>F</i> ²	0.912
<i>R</i> ₁ / <i>wR</i> ₂ (<i>I</i> > 2σ(<i>I</i>))	0.0246, 0.0474
<i>R</i> ₁ / <i>wR</i> ₂ (all data)	0.0334, 0.0488
Largest difference peak and hole [e·Å ⁻³]	0.597, -0.250

Atomic coordinates and equivalent isotropic displacement parameters for **5**:

Atom	<i>x</i>	<i>y</i>	<i>z</i>	<i>U</i> _{eq}
Sn(1)	2791(1)	142(1)	2250(1)	22(1)
Fe(1)	896(1)	772(1)	1867(1)	29(1)
Fe(2)	4619(1)	607(1)	1585(1)	30(1)
P(1)	2707(1)	219(1)	3696(1)	26(1)
P(2)	2978(1)	-1353(1)	2171(1)	24(1)
Si(1)	4059(1)	-380(1)	4362(1)	35(1)
Si(2)	2831(1)	1462(1)	4090(1)	36(1)
Si(3)	1702(1)	-2086(1)	2772(1)	31(1)
Si(4)	2835(1)	-1802(1)	988(1)	32(1)
O(1)	1717(3)	2328(2)	2176(2)	66(1)
O(2)	1542(3)	841(2)	311(2)	57(1)
O(3)	3787(3)	268(2)	101(2)	61(1)
O(4)	3896(3)	2206(2)	1425(2)	68(2)
C(1)	149(4)	-123(3)	2470(3)	44(2)
C(2)	-277(4)	-113(3)	1743(3)	48(2)
C(3)	-788(4)	605(4)	1629(3)	55(2)
C(4)	-687(4)	1030(3)	2283(3)	55(2)
C(5)	-94(3)	579(3)	2798(2)	48(1)
C(6)	1434(3)	1692(3)	2064(2)	42(2)
C(7)	1329(3)	801(3)	935(2)	38(1)
C(8)	5410(4)	29(4)	2466(3)	48(2)
C(9)	5630(4)	-354(3)	1804(3)	44(2)
C(10)	6193(3)	150(3)	1326(3)	44(1)
C(11)	6320(4)	863(3)	1690(3)	45(2)
C(12)	5837(4)	809(3)	2401(2)	48(1)
C(13)	4068(4)	383(3)	703(2)	41(1)
C(14)	4145(4)	1567(3)	1513(2)	44(1)
C(15)	4431(4)	-1354(3)	3973(2)	41(1)
C(16)	3441(4)	-586(3)	5302(2)	55(2)
C(17)	5383(4)	173(3)	4491(3)	57(2)
C(18)	1427(4)	1926(3)	4060(3)	53(2)
C(19)	3807(4)	2084(3)	3563(3)	57(2)
C(20)	3216(4)	1508(3)	5101(3)	65(2)
C(21)	1325(4)	-1706(3)	3721(2)	41(1)
C(22)	2367(3)	-3063(2)	2929(2)	41(1)
C(23)	385(3)	-2230(2)	2245(3)	43(1)
C(24)	4163(4)	-1651(3)	470(2)	49(2)
C(25)	1689(5)	-1364(3)	429(3)	58(2)
C(26)	2648(5)	-2885(2)	980(2)	45(1)

Anisotropic displacement parameters for **5**:

Atom	U_{11}	U_{22}	U_{33}	U_{23}	U_{13}	U_{12}
Sn(1)	23(1)	21(1)	22(1)	0(1)	-1(1)	0(1)
Fe(1)	29(1)	29(1)	29(1)	4(1)	-3(1)	5(1)
Fe(2)	32(1)	27(1)	30(1)	2(1)	6(1)	-4(1)
P(1)	27(1)	29(1)	22(1)	-3(1)	-3(1)	2(1)
P(2)	27(1)	21(1)	24(1)	0(1)	0(1)	-3(1)
Si(1)	32(1)	46(1)	26(1)	-2(1)	-5(1)	6(1)
Si(2)	37(1)	36(1)	36(1)	-13(1)	-2(1)	1(1)
Si(3)	32(1)	28(1)	32(1)	5(1)	1(1)	-6(1)
Si(4)	44(1)	28(1)	25(1)	-2(1)	-3(1)	0(1)
O(1)	77(2)	28(2)	92(3)	-5(2)	-10(2)	-2(2)
O(2)	60(2)	81(3)	30(2)	13(2)	1(1)	0(2)
O(3)	76(2)	75(3)	30(2)	-3(2)	-7(2)	11(2)
O(4)	88(3)	29(2)	87(3)	13(2)	9(2)	6(2)
C(1)	31(2)	43(3)	57(3)	17(2)	2(2)	0(2)
C(2)	38(3)	52(3)	53(3)	-13(2)	5(2)	-13(2)
C(3)	24(2)	92(5)	50(3)	24(3)	-9(2)	3(3)
C(4)	41(3)	51(3)	73(3)	3(3)	17(2)	11(2)
C(5)	41(2)	68(3)	35(2)	-4(2)	3(2)	-17(2)
C(6)	41(2)	39(3)	45(3)	5(2)	-3(2)	12(2)
C(7)	33(2)	40(3)	41(2)	11(2)	-8(2)	1(2)
C(8)	28(2)	69(4)	47(3)	21(3)	3(2)	1(2)
C(9)	31(2)	32(3)	70(3)	0(2)	-9(2)	-2(2)
C(10)	34(2)	52(3)	45(2)	-4(2)	7(2)	4(2)
C(11)	31(2)	45(3)	58(3)	2(2)	8(2)	-14(2)
C(12)	40(2)	66(3)	39(2)	-16(2)	2(2)	2(2)
C(13)	44(2)	36(2)	43(3)	7(2)	11(2)	7(2)
C(14)	45(2)	44(3)	44(2)	5(2)	6(2)	-10(2)
C(15)	41(2)	48(3)	34(2)	3(2)	-6(2)	10(2)
C(16)	58(3)	79(4)	28(2)	6(2)	-4(2)	21(3)
C(17)	43(2)	71(3)	56(3)	-11(3)	-19(2)	5(2)
C(18)	49(3)	47(3)	62(3)	-23(2)	4(2)	7(2)
C(19)	57(3)	42(3)	73(3)	-22(2)	7(2)	-15(2)
C(20)	84(4)	63(3)	48(3)	-29(2)	-11(2)	8(3)
C(21)	44(2)	41(3)	39(2)	5(2)	8(2)	-7(2)
C(22)	49(2)	32(2)	43(2)	10(2)	1(2)	-4(2)
C(23)	38(2)	42(3)	50(2)	5(2)	-2(2)	-10(2)
C(24)	67(3)	44(3)	36(2)	-3(2)	8(2)	-3(2)
C(25)	81(4)	50(3)	42(3)	-1(2)	-21(2)	15(3)
C(26)	59(3)	34(2)	43(2)	-10(2)	-6(2)	-3(2)

5.5 [Fp₄Sn] (6)

Crystallographic parameters and details of data collection and refinement for **6**·C₇H₈:

Empirical formula	C ₂₈ H ₂₀ Fe ₄ O ₈ Sn, C ₇ H ₈
Formula weight	918.68
Crystal dimensions [mm]	0.30 x 0.24 x 0.05
Temperature [K]	173(1)
Wavelength [Å]	0.71073
Crystal system	monoclinic
Space group	<i>P</i> 2 ₁ /c
Unit cell dimensions	<i>a</i> = 20.6560(15) Å <i>b</i> = 9.7909(10) Å <i>c</i> = 16.4689(13) Å <i>β</i> = 94.997(9)°
Volume [Å ³]	3318.0(5)
<i>Z</i>	4
Calculated density [g/cm ³]	1.839
Absorption coefficient [mm ⁻¹]	2.502
<i>F</i> (000)	1824
Index ranges	-23 ≤ <i>h</i> ≤ 23, -11 ≤ <i>k</i> ≤ 11, -17 ≤ <i>l</i> ≤ 18
Θ range for data collection [°]	2.42 – 24.07
Reflections collected	7749
Independent reflections	3349 (<i>R</i> _{int} = 0.1137)
Absorption correction	none
Refinement method	full-matrix least squares on <i>F</i> ²
Data / restraints / parameters	3349 / 0 / 294
Goodness of fit on <i>F</i> ²	1.073
<i>R</i> ₁ / <i>wR</i> ₂ (<i>I</i> > 2σ(<i>I</i>)) ^a	0.0968, 0.2758
<i>R</i> ₁ / <i>wR</i> ₂ (all data) ^a	0.1139, 0.2841
Largest difference peak and hole [e·Å ⁻³]	1.083, -1.076

^a The poor *R*₁ / *wR*₂ values are a result of the disorder in the toluene molecule.

Atomic coordinates and equivalent isotropic displacement parameters for $\mathbf{6} \cdot \text{C}_7\text{H}_8$:

Atom	<i>x</i>	<i>y</i>	<i>z</i>	<i>U</i> _{eq}
Sn(1)	2987(1)	48(1)	3610(1)	28(1)
Fe(1)	2286(2)	-436(3)	4908(2)	36(1)
Fe(2)	3793(2)	-2109(3)	3337(2)	34(1)
Fe(3)	2189(2)	312(3)	2217(2)	37(1)
Fe(4)	3661(2)	2390(3)	3970(2)	35(1)
O(1)	2315(10)	-3280(20)	4498(14)	74(9)
O(2)	3498(10)	-472(19)	5946(10)	59(7)
O(3)	3870(9)	-2928(17)	5061(10)	50(6)
O(4)	2722(9)	-3925(17)	2880(10)	50(6)
O(5)	3319(9)	740(20)	1344(10)	58(7)
O(6)	1927(10)	3155(18)	2668(11)	59(7)
O(7)	2466(9)	3722(16)	4335(11)	54(7)
O(8)	3547(10)	3257(19)	2279(10)	63(7)
C(1)	1606(8)	1134(17)	4551(9)	42(3)
C(2)	1908(8)	1405(17)	5339(9)	42(3)
C(3)	1767(8)	306(16)	5853(9)	42(3)
C(4)	1378(8)	-644(16)	5382(9)	42(3)
C(5)	1279(8)	-133(16)	4578(9)	42(3)
C(6)	2328(12)	-2140(20)	4629(13)	40(8)
C(7)	3050(16)	-510(30)	5467(15)	51(9)
C(8)	4323(8)	-792(16)	2612(10)	45(4)
C(9)	4072(8)	-1899(16)	2139(10)	45(4)
C(10)	4335(8)	-3108(16)	2492(10)	45(4)
C(11)	4749(8)	-2749(16)	3183(9)	45(4)
C(12)	4742(8)	-1317(16)	3257(9)	45(4)
C(13)	3812(11)	-2540(20)	4386(15)	43(8)
C(14)	3103(13)	-3140(20)	3047(14)	42(8)
C(15)	1688(8)	-1493(18)	2495(9)	45(4)
C(16)	1241(8)	-409(18)	2379(9)	45(4)
C(17)	1266(8)	86(18)	1578(9)	45(4)
C(18)	1729(8)	-692(18)	1200(9)	45(4)
C(19)	1990(8)	-1668(18)	1767(9)	45(4)
C(20)	2900(14)	550(30)	1742(15)	53(9)
C(21)	2062(13)	2020(20)	2500(13)	42(8)
C(22)	4050(9)	2251(17)	5190(10)	47(4)
C(23)	4217(9)	3531(17)	4877(10)	47(4)
C(24)	4590(9)	3301(17)	4214(10)	47(4)
C(25)	4655(9)	1879(16)	4117(10)	47(4)
C(26)	4321(8)	1230(17)	4721(10)	47(4)
C(27)	2932(13)	3100(20)	4168(13)	42(8)
C(28)	3592(11)	2870(20)	2935(13)	38(8)
C(29)	168(12)	7990(20)	7875(12)	71(12)
C(30)	563(11)	8970(20)	8228(18)	81(14)
C(31)	628(12)	9100(30)	9050(18)	130(20)
C(32)	298(13)	8250(30)	9519(14)	91(17)
C(33)	-97(11)	7280(20)	9166(17)	110(20)
C(34)	-162(11)	7140(20)	8344(15)	71(12)
C(35)	90(20)	7860(50)	6950(20)	130(20)

Anisotropic displacement parameters for $6\cdot\text{C}_7\text{H}_8$:

Atom	U_{11}	U_{22}	U_{33}	U_{23}	U_{13}	U_{12}
Sn(1)	43(1)	21(1)	21(1)	0(1)	5(1)	-1(1)
Fe(1)	51(2)	31(2)	27(2)	0(1)	11(1)	-1(1)
Fe(2)	48(2)	30(2)	26(2)	1(1)	9(1)	4(1)
Fe(3)	50(2)	34(2)	26(2)	-2(1)	4(1)	2(1)
Fe(4)	49(2)	28(2)	30(2)	-2(1)	8(1)	-6(1)
O(1)	90(16)	36(12)	101(17)	6(10)	43(13)	0(10)
O(2)	89(14)	50(11)	33(10)	2(8)	-21(10)	5(10)
O(3)	77(12)	47(10)	25(9)	10(8)	5(8)	7(9)
O(4)	57(11)	38(10)	58(12)	-11(8)	17(9)	-18(9)
O(5)	60(11)	84(14)	35(10)	13(9)	25(9)	4(10)
O(6)	74(12)	43(11)	61(12)	1(9)	6(10)	8(9)
O(7)	77(13)	21(9)	66(12)	-6(8)	14(10)	3(8)
O(8)	108(16)	54(12)	27(10)	12(8)	10(9)	-10(10)
C(1)	51(6)	48(7)	28(5)	-4(4)	13(4)	1(5)
C(2)	51(6)	48(7)	28(5)	-4(4)	13(4)	1(5)
C(3)	51(6)	48(7)	28(5)	-4(4)	13(4)	1(5)
C(4)	51(6)	48(7)	28(5)	-4(4)	13(4)	1(5)
C(5)	51(6)	48(7)	28(5)	-4(4)	13(4)	1(5)
C(6)	64(15)	29(14)	31(13)	-15(9)	22(11)	-13(10)
C(7)	90(20)	37(14)	28(14)	-3(11)	18(14)	13(14)
C(8)	57(7)	40(6)	40(6)	-3(4)	10(5)	4(5)
C(9)	57(7)	40(6)	40(6)	-3(4)	10(5)	4(5)
C(10)	57(7)	40(6)	40(6)	-3(4)	10(5)	4(5)
C(11)	57(7)	40(6)	40(6)	-3(4)	10(5)	4(5)
C(12)	57(7)	40(6)	40(6)	-3(4)	10(5)	4(5)
C(13)	48(14)	38(14)	44(16)	-13(11)	17(11)	13(10)
C(14)	77(18)	15(11)	36(13)	8(9)	20(12)	20(12)
C(15)	45(6)	58(7)	32(6)	-5(5)	-1(5)	-4(5)
C(16)	45(6)	58(7)	32(6)	-5(5)	-1(5)	-4(5)
C(17)	45(6)	58(7)	32(6)	-5(5)	-1(5)	-4(5)
C(18)	45(6)	58(7)	32(6)	-5(5)	-1(5)	-4(5)
C(19)	45(6)	58(7)	32(6)	-5(5)	-1(5)	-4(5)
C(20)	71(17)	61(17)	33(14)	12(12)	32(13)	-10(14)
C(21)	75(17)	26(13)	26(12)	5(9)	5(11)	17(11)
C(22)	51(7)	52(7)	39(6)	-15(5)	2(5)	-5(5)
C(23)	51(7)	52(7)	39(6)	-15(5)	2(5)	-5(5)
C(24)	51(7)	52(7)	39(6)	-15(5)	2(5)	-5(5)
C(25)	51(7)	52(7)	39(6)	-15(5)	2(5)	-5(5)
C(26)	51(7)	52(7)	39(6)	-15(5)	2(5)	-5(5)
C(27)	79(18)	19(11)	29(12)	2(9)	11(11)	-1(11)
C(28)	52(14)	33(12)	29(13)	2(9)	10(10)	-10(10)
C(29)	90(20)	70(20)	60(20)	35(18)	40(18)	43(19)
C(30)	70(20)	70(20)	100(30)	20(20)	-6(19)	15(17)
C(31)	140(40)	100(30)	120(40)	-70(30)	-80(30)	70(30)
C(32)	90(30)	70(30)	110(30)	10(20)	-10(20)	30(20)
C(33)	80(30)	40(19)	210(50)	10(20)	60(30)	28(18)
C(34)	80(20)	60(20)	70(20)	-43(17)	-17(17)	29(16)
C(35)	110(30)	190(50)	90(30)	40(30)	30(20)	90(40)

5.6 Ph*SnP(SiMe₃)₂ (7)

Crystallographic parameters and details of data collection and refinement for **7**:

Empirical formula	C ₄₂ H ₆₇ PSi ₂ Sn
Formula weight	777.80
Crystal dimensions [mm]	0.20 x 0.20 x 0.02
Temperature [K]	200(1)
Wavelength [Å]	0.71073
Crystal system	triclinic
Space group	$P\bar{1}$
Unit cell dimensions	$a = 9.2800(19) \text{ Å}$ $b = 13.240(3) \text{ Å}$ $c = 19.576(4) \text{ Å}$ $\alpha = 83.19(3)^\circ$ $\beta = 88.44(3)^\circ$ $\gamma = 70.83(3)^\circ$
Volume [Å ³]	2255.7(8)
Z	2
Calculated density [g/cm ³]	1.145
Absorption coefficient [mm ⁻¹]	0.680
F(000)	824
Index ranges	$-5 \leq h \leq 11, -11 \leq k \leq 16, -24 \leq l \leq 24$
θ range for data collection [°]	2.81 – 26.00
Reflections collected	7625
Independent reflections	6007 ($R_{\text{int}} = 0.0483$)
Absorption correction	numerical
Refinement method	full-matrix least squares on F^2
Data / restraints / parameters	6007 / 0 / 433
Goodness of fit on F^2	1.013
R_1 / wR_2 ($I > 2\sigma(I)$)	0.0449, 0.1141
R_1 / wR_2 (all data)	0.0534, 0.1182
Largest difference peak and hole [e·Å ⁻³]	0.737, -0.597

Atomic coordinates and equivalent isotropic displacement parameters for **7**:

Atom	<i>x</i>	<i>y</i>	<i>z</i>	<i>U</i> _{eq}
Sn(1)	6815(1)	6378(1)	7339(1)	33(1)
P(1)	7753(1)	7111(1)	6227(1)	36(1)
Si(1)	5641(2)	7417(1)	5592(1)	42(1)
Si(2)	8143(2)	8661(1)	6355(1)	43(1)
C(1)	5569(8)	6037(5)	5509(2)	64(2)
C(2)	5869(8)	8079(6)	4707(2)	74(2)
C(3)	3818(7)	8224(6)	5966(2)	66(2)
C(4)	8488(11)	9322(6)	5488(2)	87(2)
C(5)	6512(8)	9620(5)	6772(2)	64(2)
C(6)	9947(7)	8266(4)	6870(2)	52(1)
C(7)	8529(4)	6289(3)	8138(1)	26(1)
C(8)	9715(4)	5300(3)	8175(2)	25(1)
C(9)	10779(5)	4973(3)	8715(2)	33(1)
C(10)	10622(5)	5615(3)	9241(2)	36(1)
C(11)	9428(5)	6561(3)	9233(2)	31(1)
C(12)	8356(4)	6926(3)	8682(1)	24(1)
C(13)	9702(4)	4543(3)	7657(2)	29(1)
C(14)	10568(5)	4502(3)	7043(2)	37(1)
C(15)	10461(6)	3820(4)	6576(2)	48(1)
C(16)	9608(7)	3164(4)	6698(2)	55(2)
C(17)	8747(7)	3185(4)	7313(2)	52(1)
C(18)	8804(5)	3866(3)	7797(2)	36(1)
C(19)	11602(6)	5175(4)	6896(2)	51(1)
C(20)	13155(8)	4589(8)	7225(3)	82(2)
C(21)	11818(7)	5497(5)	6126(2)	69(2)
C(22)	9567(10)	2393(5)	6179(3)	75(2)
C(23)	8097(16)	2620(8)	5861(6)	152(7)
C(24)	10501(9)	1274(4)	6398(2)	67(2)
C(25)	7932(5)	3827(3)	8478(2)	39(1)
C(26)	6382(7)	3706(5)	8397(3)	61(2)
C(27)	8933(7)	2919(4)	9000(2)	54(1)
C(28)	7062(4)	7969(3)	8705(1)	27(1)
C(29)	5539(5)	7950(3)	8784(2)	33(1)
C(30)	4348(5)	8931(3)	8788(2)	38(1)
C(31)	4616(5)	9916(3)	8751(2)	37(1)
C(32)	6112(5)	9907(3)	8709(2)	35(1)
C(33)	7368(5)	8954(3)	8691(1)	28(1)
C(34)	8953(5)	9049(3)	8683(2)	34(1)
C(35)	9414(6)	9216(4)	9401(2)	45(1)
C(36)	9125(6)	9981(4)	8165(2)	47(1)
C(37)	3290(6)	10955(4)	8749(2)	47(1)
C(38)	3019(10)	11579(6)	8031(3)	95(3)
C(39)	3537(7)	11656(4)	9271(2)	59(1)
C(40)	5170(6)	6906(4)	8940(2)	43(1)
C(41)	5295(10)	6580(5)	9731(3)	81(2)
C(42)	3641(9)	6933(6)	8672(4)	78(2)

Anisotropic displacement parameters for 7:

Atom	U_{11}	U_{22}	U_{33}	U_{23}	U_{13}	U_{12}
Sn(1)	30(1)	38(1)	32(1)	5(1)	-9(1)	-14(1)
P(1)	33(1)	41(1)	34(1)	0(1)	-5(1)	-16(1)
Si(1)	36(1)	58(1)	33(1)	1(1)	-6(1)	-18(1)
Si(2)	59(1)	43(1)	33(1)	0(1)	-1(1)	-25(1)
C(1)	63(4)	93(4)	56(3)	-24(2)	-6(2)	-45(4)
C(2)	68(4)	113(5)	44(2)	19(2)	-18(2)	-40(4)
C(3)	37(3)	85(4)	62(3)	3(2)	-15(2)	-4(3)
C(4)	156(8)	86(4)	44(2)	6(2)	0(3)	-80(5)
C(5)	72(4)	53(3)	59(3)	-12(2)	-19(2)	-5(3)
C(6)	46(3)	62(3)	59(2)	-19(2)	2(2)	-28(3)
C(7)	26(2)	26(2)	26(1)	-1(1)	-2(1)	-7(2)
C(8)	20(2)	22(2)	31(1)	-4(1)	-4(1)	-4(2)
C(9)	33(2)	25(2)	38(2)	-1(1)	-8(1)	-4(2)
C(10)	41(3)	34(2)	32(2)	-1(1)	-15(1)	-10(2)
C(11)	38(2)	28(2)	28(1)	-5(1)	-3(1)	-11(2)
C(12)	28(2)	18(2)	25(1)	-1(1)	0(1)	-6(2)
C(13)	25(2)	24(2)	34(2)	-6(1)	-7(1)	-1(2)
C(14)	32(2)	35(2)	36(2)	-7(1)	-4(1)	2(2)
C(15)	48(3)	48(3)	42(2)	-17(2)	-6(2)	-4(2)
C(16)	61(4)	49(3)	45(2)	-19(2)	-18(2)	-1(3)
C(17)	63(4)	39(3)	57(2)	-13(2)	-19(2)	-17(3)
C(18)	37(2)	29(2)	40(2)	-6(1)	-10(1)	-10(2)
C(19)	50(3)	55(3)	45(2)	-9(2)	13(2)	-13(2)
C(20)	54(4)	125(6)	71(3)	11(3)	-7(3)	-44(4)
C(21)	54(4)	87(4)	50(2)	-1(2)	19(2)	-5(3)
C(22)	89(6)	64(4)	74(3)	-34(3)	-30(3)	-15(4)
C(23)	147(13)	113(7)	189(9)	-88(7)	-105(9)	2(8)
C(24)	109(6)	44(3)	51(2)	-16(2)	-1(2)	-26(3)
C(25)	38(3)	34(2)	45(2)	-1(1)	-7(2)	-15(2)
C(26)	53(3)	77(4)	61(3)	19(2)	-13(2)	-42(3)
C(27)	55(3)	52(3)	51(2)	6(2)	-13(2)	-16(3)
C(28)	29(2)	23(2)	27(1)	-3(1)	-1(1)	-4(2)
C(29)	28(2)	32(2)	40(2)	-7(1)	2(1)	-10(2)
C(30)	25(2)	39(2)	51(2)	-11(2)	4(2)	-7(2)
C(31)	34(2)	31(2)	40(2)	-4(1)	-4(1)	-2(2)
C(32)	40(2)	21(2)	41(2)	-4(1)	-1(1)	-5(2)
C(33)	31(2)	26(2)	26(1)	-5(1)	-2(1)	-9(2)
C(34)	39(2)	27(2)	39(2)	-9(1)	-1(1)	-12(2)
C(35)	44(3)	47(3)	51(2)	-10(2)	-10(2)	-22(2)
C(36)	50(3)	45(3)	52(2)	-7(2)	5(2)	-25(2)
C(37)	37(3)	33(3)	65(2)	-9(2)	-8(2)	-1(2)
C(38)	96(6)	72(5)	64(3)	3(3)	-22(3)	41(4)
C(39)	55(4)	42(3)	72(3)	-23(2)	1(2)	0(3)
C(40)	41(3)	33(2)	60(2)	-17(2)	14(2)	-15(2)
C(41)	133(7)	50(3)	67(3)	-7(2)	42(4)	-44(4)
C(42)	52(5)	62(4)	138(5)	-42(3)	24(4)	-33(3)

5.7 [Ph*Sn{W(CO)₅}(μ-O)SnPh*] (11)

Crystallographic parameters and details of data collection and refinement for **11**:

Empirical formula	C ₇₇ H ₉₈ O ₇ Sn ₂ W
Formula weight	1556.78
Crystal dimensions [mm]	0.20 x 0.20 x 0.06
Temperature [K]	203(2)
Wavelength [Å]	0.71073
Crystal system	orthorhombic
Space group	<i>Pnma</i>
Unit cell dimensions	<i>a</i> = 18.983(4) Å <i>b</i> = 18.340(4) Å <i>c</i> = 23.227(5) Å
Volume [Å ³]	8086(3)
<i>Z</i>	4
Calculated density [g/cm ³]	1.279
Absorption coefficient [mm ⁻¹]	2.077
F(000)	3160
Index ranges	-23 ≤ <i>h</i> ≤ 23, -22 ≤ <i>k</i> ≤ 19, -28 ≤ <i>l</i> ≤ 15
Θ range for data collection [°]	2.06 – 25.90
Reflections collected	34381
Independent reflections	7712 (<i>R</i> _{int} = 0.0814)
Completeness to Θ = 25.90°	94.8%
Absorption correction	numerical
Refinement method	full-matrix least squares on <i>F</i> ²
Data / restraints / parameters	7712 / 0 / 424
Goodness of fit on <i>F</i> ²	1.054
<i>R</i> ₁ / <i>wR</i> ₂ (<i>I</i> > 2σ(<i>I</i>))	0.0603, 0.1533
<i>R</i> ₁ / <i>wR</i> ₂ (all data)	0.0971, 0.1792
Largest difference peak and hole [e·Å ⁻³]	1.105, -1.880

Atomic coordinates and equivalent isotropic displacement parameters for **11**:

Atom	<i>x</i>	<i>y</i>	<i>z</i>	<i>U</i> _{eq}
W(1)	2557(1)	2500	7225(1)	45(1)
Sn(1)	2420(1)	2500	4809(1)	38(1)
Sn(2)	3195(1)	2500	6165(1)	36(1)
O(1)	2655(2)	1806(3)	5570(2)	38(1)
O(2)	1120(5)	2500	6515(6)	81(3)
O(3)	1650(9)	2500	8341(7)	124(6)
O(4)	4027(7)	2500	7893(7)	106(5)
O(5)	2581(4)	783(4)	7360(4)	82(2)
C(1)	4263(5)	2500	5817(5)	33(2)
C(2)	4633(3)	1839(4)	5739(4)	38(2)
C(3)	5334(4)	1852(5)	5541(4)	48(2)
C(4)	5675(6)	2500	5434(6)	50(3)
C(5)	4298(3)	1116(4)	5858(4)	40(2)
C(6)	3950(4)	733(4)	5406(4)	46(2)
C(7)	3624(5)	87(6)	5534(5)	66(3)
C(8)	3640(5)	-221(5)	6078(5)	65(3)
C(9)	3998(5)	139(5)	6499(5)	61(2)
C(10)	4346(4)	794(4)	6407(4)	47(2)
C(11)	3966(4)	1012(5)	4786(4)	50(2)
C(12)	4621(5)	747(7)	4479(5)	70(3)
C(13)	3348(5)	778(7)	4429(5)	70(3)
C(14)	3279(9)	-942(7)	6202(7)	113(6)
C(15)	2966(13)	-1016(9)	6698(13)	227(17)
C(16)	3586(16)	-1501(9)	5950(20)	430(40)
C(17)	4787(5)	1143(6)	6874(5)	61(2)
C(18)	4554(6)	941(7)	7478(5)	74(3)
C(19)	5585(6)	901(9)	6819(6)	99(5)
C(20)	1254(4)	2500	4857(5)	37(2)
C(21)	873(3)	1841(4)	4815(4)	38(2)
C(22)	139(4)	1850(5)	4803(5)	59(3)
C(23)	-218(6)	2500	4797(8)	68(4)
C(24)	1219(4)	1112(4)	4733(4)	40(2)
C(25)	1248(4)	602(5)	5185(4)	45(2)
C(26)	1506(5)	-87(5)	5065(4)	53(2)
C(27)	1719(5)	-294(5)	4526(5)	60(2)
C(28)	1679(4)	203(5)	4091(4)	55(2)
C(29)	1434(4)	905(5)	4180(4)	43(2)
C(30)	958(4)	758(5)	5782(4)	51(2)
C(31)	283(5)	334(8)	5892(5)	84(4)
C(32)	1472(5)	596(5)	6267(4)	62(2)
C(33)	1952(7)	-1079(6)	4410(6)	87(4)
C(34)	2608(9)	-1172(11)	4178(14)	192(13)
C(35)	1421(10)	-1443(8)	3982(9)	140(7)
C(36)	1354(5)	1401(6)	3659(4)	59(2)
C(37)	1994(6)	1436(8)	3273(5)	88(4)
C(38)	733(6)	1198(8)	3305(6)	87(4)
C(39)	1626(7)	2500	6754(8)	63(4)
C(40)	1985(8)	2500	7936(8)	71(4)
C(41)	3510(9)	2500	7667(7)	66(4)
C(42)	2565(4)	1392(6)	7279(4)	54(2)

Anisotropic displacement parameters for **11**:

Atom	U_{11}	U_{22}	U_{33}	U_{23}	U_{13}	U_{12}
W(1)	57(1)	46(1)	31(1)	0	7(1)	0
Sn(1)	32(1)	50(1)	32(1)	0	2(1)	0
Sn(2)	37(1)	39(1)	31(1)	0	2(1)	0
O(1)	36(2)	43(3)	34(3)	-6(2)	-6(2)	0(2)
O(2)	62(6)	72(7)	108(10)	0	-18(6)	0
O(3)	174(13)	118(12)	79(11)	0	76(10)	0
O(4)	124(10)	84(9)	111(12)	0	-76(9)	0
O(5)	102(6)	47(5)	96(7)	1(4)	-10(4)	1(4)
C(1)	32(5)	32(5)	36(6)	0	-2(4)	0
C(2)	31(3)	40(4)	44(5)	-1(3)	-8(3)	2(3)
C(3)	40(4)	44(5)	61(6)	-7(4)	0(4)	4(3)
C(4)	36(5)	59(8)	55(8)	0	7(5)	0
C(5)	35(3)	36(4)	48(5)	-1(4)	-2(3)	5(3)
C(6)	39(4)	40(5)	59(6)	-14(4)	3(3)	2(3)
C(7)	65(6)	58(6)	73(8)	-20(6)	3(5)	-14(5)
C(8)	84(7)	47(5)	63(7)	-4(5)	9(5)	-22(5)
C(9)	80(6)	49(6)	55(6)	11(5)	9(5)	1(5)
C(10)	53(4)	35(4)	53(6)	-2(4)	2(4)	3(3)
C(11)	47(4)	48(5)	54(6)	-10(4)	-5(4)	3(4)
C(12)	64(6)	97(9)	51(7)	-15(6)	5(4)	6(5)
C(13)	66(6)	87(8)	57(7)	-31(6)	-11(5)	4(5)
C(14)	156(13)	73(9)	110(13)	-15(8)	55(10)	-60(9)
C(15)	280(30)	57(10)	340(40)	17(15)	180(30)	-47(13)
C(16)	330(30)	37(9)	940(110)	-30(30)	440(50)	-21(14)
C(17)	71(6)	56(6)	56(7)	1(5)	-15(5)	-4(4)
C(18)	91(7)	75(8)	57(7)	16(6)	-9(5)	8(6)
C(19)	72(7)	143(13)	80(10)	28(9)	-9(6)	0(7)
C(20)	23(4)	47(6)	42(7)	0	-2(4)	0
C(21)	35(3)	42(4)	37(5)	-2(3)	-4(3)	-4(3)
C(22)	39(4)	45(5)	92(9)	1(5)	-2(4)	-8(4)
C(23)	32(6)	60(9)	113(14)	0	-5(6)	0
C(24)	44(4)	32(4)	44(5)	-7(3)	-4(3)	-7(3)
C(25)	48(4)	43(5)	44(5)	-10(4)	-2(3)	-7(3)
C(26)	74(5)	37(5)	48(6)	-6(4)	-7(4)	0(4)
C(27)	65(5)	50(5)	64(7)	-13(5)	-12(5)	4(4)
C(28)	59(5)	50(5)	55(6)	-21(5)	8(4)	0(4)
C(29)	41(4)	46(5)	40(5)	-5(4)	-1(3)	-10(3)
C(30)	63(5)	44(5)	46(5)	-7(4)	1(4)	-4(4)
C(31)	73(6)	118(11)	60(8)	-21(7)	6(5)	-20(6)
C(32)	83(6)	54(6)	50(6)	8(5)	-2(5)	-10(5)
C(33)	129(10)	53(7)	79(9)	-25(6)	-3(7)	29(6)
C(34)	143(16)	101(15)	330(40)	-60(20)	-23(18)	40(12)
C(35)	214(19)	69(9)	137(19)	-35(10)	-52(14)	10(11)
C(36)	73(6)	57(6)	46(6)	-6(4)	-1(4)	-5(4)
C(37)	102(8)	125(11)	36(6)	13(7)	13(5)	-7(7)
C(38)	87(7)	107(10)	67(9)	15(7)	-25(6)	-7(7)
C(39)	64(8)	46(8)	80(11)	15(7)	2(7)	0
C(40)	81(9)	58(9)	72(12)	0	30(8)	0
C(41)	108(11)	46(8)	42(8)	0	-11(8)	0
C(42)	58(5)	65(7)	40(5)	-1(4)	-3(4)	6(4)

5.8 [Ph*Sn(μ -O)Cl]₂ (13)

Crystallographic parameters and details of data collection and refinement for **13**:

Empirical formula	C ₇₂ H ₉₈ Cl ₂ O ₂ Sn ₂
Formula weight	1303.82
Crystal dimensions [mm]	0.22 x 0.16 x 0.12
Temperature [K]	173(1)
Wavelength [Å]	0.71073
Crystal system	triclinic
Space group	$P\bar{1}$
Unit cell dimensions	$a = 9.8878(9)$ Å $b = 12.9459(11)$ Å $c = 15.8338(14)$ Å $\alpha = 66.618(10)^\circ$ $\beta = 87.098(11)^\circ$ $\gamma = 86.625(10)^\circ$
Volume [Å ³]	1856.3(3)
Z	1
Calculated density [g/cm ³]	1.166
Absorption coefficient [mm ⁻¹]	0.783
F(000)	680
Index ranges	$-12 \leq h \leq 12$, $-15 \leq k \leq 15$, $-19 \leq l \leq 18$
θ range for data collection [°]	2.46 – 25.81
Reflections collected	13161
Independent reflections	6646 ($R_{\text{int}} = 0.0228$)
Absorption correction	none
Refinement method	full-matrix least squares on F^2
Data / restraints / parameters	6646 / 0 / 371
Goodness of fit on F^2	0.886
R_1 / wR_2 ($I > 2\sigma(I)$)	0.0330, 0.0779
R_1 / wR_2 (all data)	0.0419, 0.0802
Largest difference peak and hole [e·Å ⁻³]	1.396, -0.478

Atomic coordinates and equivalent isotropic displacement parameters for **13**:

Atom	<i>x</i>	<i>y</i>	<i>z</i>	<i>U</i> _{eq}
Sn(1)	-215(1)	1034(1)	-835(1)	30(1)
Cl(1)	1615(1)	2227(1)	-1247(1)	51(1)
O(1)	507(2)	-541(2)	-522(1)	35(1)
C(1)	-1903(3)	1596(2)	-1720(2)	26(1)
C(2)	-1962(3)	1239(2)	-2454(2)	29(1)
C(3)	-3174(3)	1483(3)	-2928(2)	35(1)
C(4)	-4251(3)	2062(3)	-2701(2)	37(1)
C(5)	-4141(3)	2457(3)	-2009(2)	34(1)
C(6)	-2950(3)	2232(2)	-1507(2)	29(1)
C(7)	-768(3)	723(3)	-2791(2)	33(1)
C(8)	-644(3)	-447(3)	-2567(2)	38(1)
C(9)	387(4)	-872(3)	-2982(3)	51(1)
C(10)	1330(4)	-183(4)	-3604(2)	53(1)
C(11)	1231(4)	953(4)	-3783(2)	54(1)
C(12)	212(4)	1432(3)	-3393(2)	45(1)
C(13)	-1649(4)	-1266(3)	-1890(3)	47(1)
C(14)	-2707(5)	-1578(4)	-2417(4)	68(1)
C(15)	-936(5)	-2330(3)	-1200(3)	55(1)
C(16)	2418(5)	-668(5)	-4079(3)	79(2)
C(18)	2129(8)	-505(14)	-4959(7)	277(11)
C(19)	125(5)	2711(4)	-3668(3)	72(2)
C(20)	1493(6)	3245(4)	-3796(3)	82(2)
C(21)	-681(6)	3292(5)	-4529(5)	134(3)
C(22)	-2788(3)	2775(2)	-835(2)	29(1)
C(23)	-3216(3)	2259(2)	95(2)	30(1)
C(24)	-3133(3)	2851(3)	662(2)	33(1)
C(25)	-2635(3)	3936(3)	336(2)	35(1)
C(26)	-2177(3)	4411(2)	-580(2)	37(1)
C(27)	-2246(3)	3864(2)	-1176(2)	34(1)
C(28)	-3790(3)	1082(3)	485(2)	34(1)
C(29)	-3495(4)	400(3)	1508(2)	42(1)
C(30)	-5333(3)	1170(3)	348(2)	43(1)
C(31)	-2611(4)	4624(3)	925(2)	41(1)
C(32)	-2713(4)	3933(3)	1958(3)	56(1)
C(33)	-3729(4)	5564(3)	635(3)	57(1)
C(34)	-1830(4)	4480(3)	-2193(2)	46(1)
C(35)	-466(4)	5045(3)	-2333(3)	56(1)
C(36)	-2940(5)	5345(4)	-2705(3)	77(2)
C(37)	3787(6)	-592(12)	-3853(6)	198(7)

Anisotropic displacement parameters for **13**:

Atom	U_{11}	U_{22}	U_{33}	U_{23}	U_{13}	U_{12}
Sn(1)	28(1)	29(1)	33(1)	-12(1)	-6(1)	1(1)
Cl(1)	39(1)	49(1)	62(1)	-15(1)	-7(1)	-12(1)
O(1)	39(1)	32(1)	35(1)	-14(1)	-5(1)	7(1)
C(1)	23(1)	23(1)	30(1)	-8(1)	-2(1)	-2(1)
C(2)	32(2)	27(1)	28(1)	-9(1)	2(1)	-6(1)
C(3)	37(2)	39(2)	32(1)	-18(1)	-4(1)	-3(1)
C(4)	32(2)	41(2)	38(2)	-16(1)	-10(1)	0(1)
C(5)	30(2)	32(2)	43(2)	-17(1)	-2(1)	3(1)
C(6)	30(2)	23(1)	34(1)	-11(1)	-1(1)	-4(1)
C(7)	31(2)	40(2)	30(1)	-16(1)	-2(1)	1(1)
C(8)	36(2)	43(2)	42(2)	-24(1)	3(1)	1(2)
C(9)	47(2)	57(2)	57(2)	-33(2)	3(2)	7(2)
C(10)	38(2)	81(3)	44(2)	-31(2)	2(1)	12(2)
C(11)	41(2)	74(3)	39(2)	-15(2)	13(1)	-3(2)
C(12)	40(2)	52(2)	34(2)	-9(1)	6(1)	-3(2)
C(13)	48(2)	38(2)	63(2)	-30(2)	16(2)	-6(2)
C(14)	54(2)	60(2)	101(3)	-43(2)	4(2)	-13(2)
C(15)	69(3)	33(2)	70(2)	-28(2)	13(2)	-8(2)
C(16)	54(3)	116(4)	69(3)	-45(3)	12(2)	21(3)
C(18)	110(6)	660(30)	214(9)	-351(15)	-86(6)	168(11)
C(19)	68(3)	50(2)	72(3)	-1(2)	27(2)	-6(2)
C(20)	94(4)	69(3)	71(3)	-14(2)	27(3)	-34(3)
C(21)	81(4)	79(4)	159(6)	44(4)	-24(4)	-17(3)
C(23)	25(1)	29(1)	39(2)	-16(1)	0(1)	-1(1)
C(24)	28(2)	34(2)	42(2)	-22(1)	3(1)	0(1)
C(25)	29(2)	34(2)	50(2)	-25(1)	-3(1)	1(1)
C(26)	38(2)	27(1)	48(2)	-17(1)	-2(1)	-5(1)
C(27)	35(2)	28(1)	41(2)	-15(1)	-3(1)	0(1)
C(28)	34(2)	31(2)	42(2)	-21(1)	6(1)	-5(1)
C(29)	49(2)	36(2)	41(2)	-14(1)	9(1)	-8(2)
C(30)	36(2)	43(2)	58(2)	-28(2)	8(1)	-10(2)
C(31)	37(2)	42(2)	58(2)	-34(2)	-1(1)	-3(2)
C(32)	64(3)	60(2)	60(2)	-41(2)	-1(2)	-3(2)
C(33)	58(2)	48(2)	83(3)	-45(2)	-8(2)	7(2)
C(34)	69(2)	31(2)	40(2)	-13(1)	0(2)	-15(2)
C(35)	65(3)	43(2)	56(2)	-16(2)	13(2)	-16(2)
C(36)	86(3)	64(3)	58(2)	4(2)	-22(2)	-12(3)
C(37)	58(3)	450(19)	192(8)	-247(11)	-24(4)	72(7)

5.9 Ph*SnCl₃ (14a)

Crystallographic parameters and details of data collection and refinement for **14a**:

Empirical formula	C ₃₆ H ₄₉ Cl ₃ Sn
Formula weight	706.79
Crystal dimensions [mm]	0.12 x 0.10 x 0.03
Temperature [K]	203(2)
Wavelength [Å]	0.71073
Crystal system	triclinic
Space group	$P\bar{1}$
Unit cell dimensions	$a = 8.4790(17) \text{ Å}$ $b = 13.799(3) \text{ Å}$ $c = 16.691(3) \text{ Å}$ $\alpha = 70.59(3)^\circ$ $\beta = 85.67(3)^\circ$ $\gamma = 72.24(3)^\circ$
Volume [Å ³]	1753.4(6)
Z	2
Calculated density [g/cm ³]	1.339
Absorption coefficient [mm ⁻¹]	0.980
F(000)	732
Index ranges	$-9 \leq h \leq 9, -16 \leq k \leq 16, -20 \leq l \leq 20$
θ range for data collection [°]	2.40 – 25.94
Reflections collected	12082
Independent reflections	6320 ($R_{\text{int}} = 0.0617$)
Completeness to $\theta = 25.94^\circ$	92.2%
Absorption correction	numerical
Refinement method	full-matrix least squares on F^2
Data / restraints / parameters	6320 / 0 / 373
Goodness of fit on F^2	1.034
R_1 / wR_2 ($I > 2\sigma(I)$)	0.0532, 0.1263
R_1 / wR_2 (all data)	0.0835, 0.1442
Largest difference peak and hole [e·Å ⁻³]	0.713, -0.902

Atomic coordinates and equivalent isotropic displacement parameters for **14a**:

Atom	<i>x</i>	<i>y</i>	<i>z</i>	<i>U</i> _{eq}
Sn(1)	5631(1)	9027(1)	2105(1)	37(1)
Cl(1)	6738(2)	7683(1)	1498(1)	60(1)
Cl(2)	5443(2)	10502(1)	890(1)	62(1)
Cl(3)	7907(2)	8997(2)	2822(1)	73(1)
C(1)	3613(6)	8933(3)	2964(3)	26(1)
C(2)	2533(6)	9887(4)	3057(3)	29(1)
C(3)	1296(7)	9808(4)	3646(3)	33(1)
C(4)	1145(7)	8823(4)	4133(3)	39(1)
C(5)	2206(7)	7878(4)	4050(3)	35(1)
C(6)	3463(6)	7920(4)	3456(3)	29(1)
C(7)	2678(7)	10966(4)	2505(3)	31(1)
C(8)	1747(7)	11497(4)	1735(3)	36(1)
C(9)	2022(8)	12454(4)	1209(4)	46(2)
C(10)	3122(9)	12895(5)	1414(4)	50(2)
C(11)	3946(8)	12391(4)	2192(4)	47(1)
C(12)	3722(7)	11435(4)	2750(3)	36(1)
C(13)	509(9)	11064(5)	1481(4)	52(2)
C(14)	-1237(11)	11816(7)	1434(7)	88(3)
C(15)	941(15)	10800(10)	642(6)	107(4)
C(16)	3503(10)	13891(5)	795(4)	60(2)
C(17)	4490(11)	13611(6)	85(5)	72(2)
C(18)	2076(12)	14842(6)	535(6)	90(3)
C(19)	4564(8)	10953(5)	3629(4)	43(1)
C(20)	6204(12)	11184(7)	3684(6)	81(2)
C(21)	3355(11)	11384(6)	4261(4)	67(2)
C(22)	4541(7)	6890(4)	3332(3)	30(1)
C(23)	6085(6)	6350(4)	3768(3)	30(1)
C(24)	7089(6)	5437(4)	3592(3)	31(1)
C(25)	6584(7)	5043(4)	3021(3)	32(1)
C(26)	5031(7)	5562(4)	2641(3)	33(1)
C(27)	3999(7)	6485(4)	2777(3)	34(1)
C(28)	6598(7)	6679(4)	4474(3)	35(1)
C(29)	8439(9)	6554(6)	4511(5)	62(2)
C(30)	6003(12)	6079(6)	5308(4)	72(2)
C(31)	7714(7)	4079(4)	2796(3)	39(1)
C(32)	8742(13)	3209(6)	3513(5)	88(3)
C(33)	8749(13)	4464(6)	2062(6)	101(4)
C(34)	2274(8)	7000(5)	2345(4)	46(2)
C(35)	1274(10)	6198(7)	2589(6)	76(2)
C(36)	2338(11)	7470(8)	1387(5)	87(3)

Anisotropic displacement parameters for **14a**:

Atom	U_{11}	U_{22}	U_{33}	U_{23}	U_{13}	U_{12}
Sn(1)	34(1)	37(1)	36(1)	-12(1)	9(1)	-5(1)
Cl(1)	63(1)	51(1)	64(1)	-25(1)	22(1)	-9(1)
Cl(2)	69(1)	49(1)	53(1)	-7(1)	17(1)	-8(1)
Cl(3)	45(1)	94(1)	83(1)	-32(1)	-3(1)	-21(1)
C(1)	24(3)	24(2)	27(2)	-11(2)	0(2)	-1(2)
C(2)	25(3)	33(3)	27(2)	-11(2)	1(2)	-5(2)
C(3)	31(3)	25(2)	36(3)	-10(2)	5(2)	-1(2)
C(4)	28(3)	44(3)	42(3)	-18(2)	12(2)	-6(2)
C(5)	36(3)	32(3)	36(3)	-9(2)	3(2)	-8(2)
C(6)	28(3)	28(2)	27(2)	-9(2)	1(2)	-3(2)
C(7)	33(3)	25(2)	32(2)	-11(2)	4(2)	-2(2)
C(8)	39(3)	31(3)	31(3)	-10(2)	1(2)	-2(2)
C(9)	51(4)	36(3)	34(3)	-5(2)	4(2)	3(3)
C(10)	59(4)	34(3)	52(4)	-10(3)	16(3)	-14(3)
C(11)	50(4)	36(3)	55(4)	-15(3)	10(3)	-15(3)
C(12)	34(3)	33(3)	40(3)	-16(2)	10(2)	-9(2)
C(13)	60(5)	42(3)	46(3)	-9(3)	-15(3)	-5(3)
C(14)	54(6)	75(6)	133(8)	-29(5)	-10(5)	-17(4)
C(15)	113(9)	160(10)	81(6)	-68(7)	-10(6)	-51(7)
C(16)	76(5)	46(4)	53(4)	-5(3)	13(3)	-25(3)
C(17)	85(6)	56(4)	61(4)	-6(3)	31(4)	-23(4)
C(18)	103(7)	39(4)	106(6)	-7(4)	50(5)	-18(4)
C(19)	44(4)	39(3)	52(3)	-18(3)	-2(3)	-15(2)
C(20)	79(7)	78(5)	89(6)	-18(5)	-18(5)	-34(5)
C(21)	86(6)	71(5)	45(4)	-27(3)	2(3)	-19(4)
C(22)	35(3)	22(2)	29(2)	-8(2)	5(2)	-4(2)
C(23)	32(3)	22(2)	32(2)	-9(2)	2(2)	-3(2)
C(24)	25(3)	26(2)	37(3)	-8(2)	-3(2)	-1(2)
C(25)	34(3)	28(2)	33(3)	-12(2)	4(2)	-4(2)
C(26)	34(3)	33(3)	31(3)	-14(2)	1(2)	-7(2)
C(27)	33(3)	31(3)	32(3)	-10(2)	-1(2)	-1(2)
C(28)	36(3)	31(3)	34(3)	-10(2)	-2(2)	-5(2)
C(29)	46(4)	72(5)	76(5)	-42(4)	-12(3)	-5(3)
C(30)	125(8)	72(5)	36(3)	-25(3)	12(4)	-51(5)
C(31)	39(3)	30(3)	47(3)	-19(2)	7(2)	-3(2)
C(32)	114(7)	50(4)	75(5)	-34(4)	-25(5)	34(4)
C(33)	127(9)	52(4)	116(7)	-41(5)	83(7)	-19(5)
C(34)	35(4)	53(3)	51(3)	-28(3)	-13(3)	1(3)
C(35)	41(5)	85(6)	95(6)	-24(5)	-4(4)	-13(4)
C(36)	64(6)	109(7)	59(5)	4(4)	-27(4)	-15(5)

5.10 [L*TaCl₂] (15)

Crystallographic parameters and details of data collection and refinement for **15**:

Empirical formula	C ₃₆ H ₄₈ Cl ₂ NO ₃ Ta
Formula weight	794.60
Crystal dimensions [mm]	0.25 x 0.12 x 0.06
Temperature [K]	203(2)
Wavelength [Å]	0.56087
Crystal system	monoclinic
Space group	<i>P</i> 2 ₁ / <i>c</i>
Unit cell dimensions	<i>a</i> = 9.922(2) Å <i>b</i> = 19.546(4) Å <i>c</i> = 18.617(4) Å <i>β</i> = 90.03(3)°
Volume [Å ³]	3610.5(13)
<i>Z</i>	4
Calculated density [g/cm ³]	1.462
Absorption coefficient [mm ⁻¹]	1.733
<i>F</i> (000)	1608
Index ranges	-12 ≤ <i>h</i> ≤ 12, -24 ≤ <i>k</i> ≤ 24, -22 ≤ <i>l</i> ≤ 22
<i>θ</i> range for data collection [°]	1.62 – 21.00
Reflections collected	26369
Independent reflections	7653 (<i>R</i> _{int} = 0.1445)
Completeness to <i>θ</i> = 21.00°	96.9%
Absorption correction	numerical
Refinement method	full-matrix least squares on <i>F</i> ²
Data / restraints / parameters	7653 / 0 / 400
Goodness of fit on <i>F</i> ²	1.281
<i>R</i> ₁ / <i>wR</i> ₂ (<i>I</i> > 2σ(<i>I</i>))	0.0861, 0.1898
<i>R</i> ₁ / <i>wR</i> ₂ (all data)	0.1101, 0.2037
Largest difference peak and hole [e·Å ⁻³]	4.765, -3.210

Atomic coordinates and equivalent isotropic displacement parameters for **15**:

Atom	<i>x</i>	<i>y</i>	<i>z</i>	<i>U</i> _{eq}
Ta(1)	2608(1)	1680(1)	7043(1)	24(1)
Cl(1)	1423(3)	636(1)	7308(2)	38(1)
Cl(2)	4676(3)	1142(2)	6847(2)	42(1)
N(1)	657(7)	2332(4)	7155(4)	25(2)
O(1)	3333(6)	2575(3)	6885(4)	29(1)
O(2)	2639(7)	1803(4)	8071(4)	31(2)
O(3)	1801(6)	1579(4)	6117(4)	30(1)
C(1)	698(9)	2944(5)	6655(6)	31(2)
C(2)	1768(10)	3462(5)	6858(6)	31(2)
C(3)	3076(10)	3253(5)	6957(5)	26(2)
C(4)	4108(9)	3720(5)	7152(5)	28(2)
C(5)	3743(10)	4406(5)	7185(6)	34(2)
C(6)	2435(12)	4659(7)	7054(6)	42(3)
C(7)	1446(10)	4160(5)	6903(6)	33(2)
C(8)	2093(11)	5384(6)	7088(8)	50(3)
C(9)	5594(9)	3469(5)	7280(6)	31(2)
C(10)	6132(13)	3203(7)	6565(7)	54(3)
C(11)	5650(11)	2920(6)	7859(7)	45(3)
C(12)	6509(12)	4069(7)	7530(9)	57(4)
C(13)	407(9)	2593(5)	7911(5)	30(2)
C(14)	494(9)	2064(5)	8492(5)	29(2)
C(15)	1714(9)	1721(5)	8635(5)	26(2)
C(16)	1950(11)	1338(5)	9229(5)	34(2)
C(17)	846(12)	1268(6)	9688(6)	39(2)
C(18)	-409(12)	1568(6)	9568(6)	41(3)
C(19)	-578(9)	1980(6)	8972(6)	34(2)
C(20)	-1554(13)	1454(8)	10096(8)	58(4)
C(21)	3353(11)	1038(6)	9400(5)	38(2)
C(22)	3361(17)	699(10)	10142(8)	72(5)
C(23)	4402(15)	1602(9)	9391(9)	70(4)
C(24)	3744(17)	491(8)	8860(7)	69(5)
C(25)	-577(9)	1917(5)	6941(6)	33(2)
C(26)	-578(10)	1672(5)	6166(6)	34(2)
C(27)	594(11)	1481(5)	5785(6)	34(2)
C(28)	554(11)	1242(5)	5080(6)	36(2)
C(29)	-723(12)	1205(6)	4766(7)	43(3)
C(30)	-1888(13)	1396(7)	5109(7)	50(3)
C(31)	-1816(13)	1625(6)	5809(8)	47(3)
C(32)	-3276(16)	1366(9)	4754(10)	73(5)
C(33)	1822(14)	1008(6)	4678(6)	47(3)
C(34)	2747(14)	1637(7)	4555(7)	53(3)
C(35)	2626(14)	473(6)	5122(7)	50(3)
C(36)	1498(17)	672(9)	3951(8)	66(4)

Anisotropic displacement parameters for **15**:

Atom	U_{11}	U_{22}	U_{33}	U_{23}	U_{13}	U_{12}
Ta(1)	16(1)	29(1)	27(1)	1(1)	-3(1)	4(1)
Cl(1)	30(1)	36(1)	50(2)	5(1)	-1(1)	-3(1)
Cl(2)	26(1)	52(2)	50(2)	-1(1)	2(1)	14(1)
N(1)	7(3)	33(4)	34(4)	1(3)	0(3)	5(3)
O(1)	24(3)	29(3)	33(4)	3(3)	0(3)	-8(3)
O(2)	20(3)	42(4)	32(4)	5(3)	9(3)	5(3)
O(3)	13(3)	51(4)	27(4)	0(3)	-3(2)	2(3)
C(1)	15(4)	39(5)	39(6)	3(4)	-6(4)	3(4)
C(2)	25(5)	34(5)	32(6)	2(4)	1(4)	6(4)
C(3)	24(4)	32(5)	23(5)	1(3)	0(3)	-1(3)
C(4)	17(4)	33(5)	33(5)	5(4)	0(3)	1(3)
C(5)	31(5)	39(5)	33(6)	-6(4)	5(4)	-4(4)
C(6)	43(6)	58(7)	26(6)	2(5)	6(4)	12(5)
C(7)	25(5)	35(5)	38(6)	5(4)	3(4)	7(4)
C(8)	24(5)	39(6)	87(10)	3(6)	4(5)	12(4)
C(9)	16(4)	36(5)	42(6)	1(4)	-5(4)	1(3)
C(10)	33(6)	74(9)	54(8)	15(6)	12(5)	20(6)
C(11)	29(5)	56(7)	50(7)	15(5)	-6(5)	0(5)
C(12)	29(6)	48(7)	95(11)	9(7)	-18(6)	-12(5)
C(13)	18(4)	35(5)	37(6)	-6(4)	1(4)	4(4)
C(14)	24(5)	29(5)	34(6)	-5(4)	6(4)	-2(4)
C(15)	17(4)	39(5)	23(5)	-3(4)	-2(3)	5(4)
C(16)	48(6)	41(5)	12(5)	-14(4)	-8(4)	8(4)
C(17)	48(6)	39(6)	31(6)	3(4)	3(5)	4(5)
C(18)	35(6)	48(6)	40(7)	-3(5)	8(5)	-2(5)
C(19)	15(4)	43(6)	43(6)	-11(4)	-4(4)	2(4)
C(20)	38(7)	90(10)	47(8)	0(7)	11(6)	-15(7)
C(21)	39(6)	54(7)	21(6)	1(4)	0(4)	15(5)
C(22)	68(10)	107(13)	42(9)	13(8)	-15(7)	35(9)
C(23)	44(8)	92(12)	75(11)	14(8)	-26(7)	11(7)
C(24)	90(11)	81(10)	35(8)	-12(6)	-15(7)	53(9)
C(25)	12(4)	42(5)	44(6)	1(4)	-7(4)	-3(4)
C(26)	26(5)	30(5)	46(6)	0(4)	-10(4)	3(4)
C(27)	34(5)	30(5)	39(6)	1(4)	-7(4)	-1(4)
C(28)	41(6)	30(5)	37(6)	-2(4)	-14(4)	-5(4)
C(29)	43(6)	44(6)	42(7)	-1(5)	-22(5)	-10(5)
C(30)	38(6)	56(7)	55(8)	1(6)	-24(5)	-5(5)
C(31)	36(6)	38(6)	67(8)	2(5)	-16(5)	0(5)
C(32)	58(9)	85(11)	74(11)	-2(8)	-34(8)	5(8)
C(33)	63(8)	46(6)	32(7)	1(5)	-6(5)	-16(6)
C(34)	53(8)	69(9)	38(7)	10(6)	2(5)	-18(6)
C(35)	72(9)	38(6)	42(7)	-6(5)	2(6)	12(6)
C(36)	75(10)	86(11)	36(8)	-12(7)	-6(6)	-6(8)

5.11 [L*Ta(Cl)P(SiMe₃)₂] (16a)

Crystallographic parameters and details of data collection and refinement for **16a**:

Empirical formula	C ₄₂ H ₆₆ ClNO ₃ PSi ₂ Ta
Formula weight	936.51
Crystal dimensions [mm]	0.20 x 0.12 x 0.06
Temperature [K]	203(2)
Wavelength [Å]	0.56087
Crystal system	monoclinic
Space group	<i>P</i> 2 ₁ / <i>n</i>
Unit cell dimensions	<i>a</i> = 9.2011(18) Å <i>b</i> = 24.809(5) Å <i>c</i> = 19.706(4) Å <i>β</i> = 95.55(3)°
Volume [Å ³]	4477.2(15)
<i>Z</i>	4
Calculated density [g/cm ³]	1.389
Absorption coefficient [mm ⁻¹]	1.419
F(000)	1928
Index ranges	-11 ≤ <i>h</i> ≤ 11, -29 ≤ <i>k</i> ≤ 33, -26 ≤ <i>l</i> ≤ 26
Θ range for data collection [°]	1.53 – 22.39
Reflections collected	31936
Independent reflections	11229 (<i>R</i> _{int} = 0.0755)
Completeness to Θ = 22.39°	95.6%
Absorption correction	numerical
Refinement method	full-matrix least squares on <i>F</i> ²
Data / restraints / parameters	11229 / 0 / 478
Goodness of fit on <i>F</i> ²	1.018
<i>R</i> ₁ / <i>wR</i> ₂ (<i>I</i> > 2σ(<i>I</i>))	0.0427, 0.0861
<i>R</i> ₁ / <i>wR</i> ₂ (all data)	0.0721, 0.0954
Largest difference peak and hole [e·Å ⁻³]	1.149, -1.437

Atomic coordinates and equivalent isotropic displacement parameters for **16a**:

Atom	<i>x</i>	<i>y</i>	<i>z</i>	<i>U</i> _{eq}
Ta(1)	19(1)	2399(1)	8003(1)	22(1)
Cl(1)	2568(1)	2259(1)	8167(1)	43(1)
P(1)	12(2)	2831(1)	6834(1)	32(1)
Si(1)	1056(2)	3647(1)	6818(1)	38(1)
Si(2)	808(2)	2355(1)	5973(1)	35(1)
C(1)	3005(7)	3637(3)	7223(3)	57(2)
C(2)	-58(9)	4143(2)	7254(3)	58(2)
C(3)	1080(8)	3899(3)	5917(3)	58(2)
C(4)	300(9)	1636(3)	6044(3)	58(2)
C(5)	-6(9)	2607(3)	5126(3)	63(2)
C(6)	2837(9)	2395(4)	5982(6)	102(3)
N(1)	-2525(4)	2511(1)	7913(2)	23(1)
O(1)	-38(3)	3098(1)	8400(2)	26(1)
O(2)	-584(3)	1728(1)	7600(1)	26(1)
O(3)	-265(3)	2103(1)	8928(1)	26(1)
C(7)	-2933(5)	3096(2)	7854(2)	28(1)
C(8)	-2407(5)	3446(2)	8462(2)	26(1)
C(9)	-930(5)	3439(2)	8716(2)	25(1)
C(10)	-391(5)	3770(2)	9266(2)	29(1)
C(11)	-1411(6)	4095(2)	9545(2)	31(1)
C(12)	-2883(6)	4112(2)	9309(2)	30(1)
C(13)	-3378(5)	3778(2)	8762(2)	29(1)
C(14)	-3911(6)	4477(2)	9653(3)	40(1)
C(15)	1209(6)	3742(2)	9586(2)	35(1)
C(16)	1548(7)	4182(3)	10119(3)	50(2)
C(17)	1430(8)	3193(3)	9943(4)	62(2)
C(18)	2287(7)	3805(3)	9047(3)	67(2)
C(19)	-3242(5)	2250(2)	7281(2)	30(1)
C(20)	-3076(6)	1644(2)	7244(2)	29(1)
C(21)	-1719(5)	1393(2)	7392(2)	29(1)
C(22)	-1558(6)	833(2)	7338(2)	34(1)
C(23)	-2838(7)	543(2)	7108(2)	45(1)
C(24)	-4181(7)	784(2)	6944(2)	42(1)
C(25)	-4292(6)	1334(2)	7027(2)	36(1)
C(26)	-5510(8)	446(3)	6681(3)	64(2)
C(27)	-156(7)	505(2)	7517(2)	42(1)
C(28)	-428(9)	84(3)	8075(3)	67(2)
C(29)	1186(7)	835(2)	7774(3)	52(2)
C(30)	209(8)	196(2)	6869(3)	50(2)
C(31)	-3159(5)	2293(2)	8537(2)	27(1)
C(32)	-2648(5)	1751(2)	8809(2)	28(1)
C(33)	-1186(5)	1701(2)	9077(2)	24(1)
C(34)	-736(6)	1259(2)	9503(2)	31(1)
C(35)	-1762(6)	846(2)	9530(2)	36(1)
C(36)	-3171(6)	861(2)	9201(2)	34(1)
C(37)	-3634(6)	1328(2)	8861(2)	30(1)
C(38)	-4187(7)	386(2)	9222(3)	52(2)
C(39)	743(6)	1243(2)	9950(2)	35(1)
C(40)	853(9)	1738(3)	10419(3)	68(2)
C(41)	874(11)	754(3)	10420(5)	102(4)
C(42)	2054(8)	1255(4)	9534(3)	76(2)

Anisotropic displacement parameters for **16a**:

Atom	U_{11}	U_{22}	U_{33}	U_{23}	U_{13}	U_{12}
Ta(1)	22(1)	20(1)	26(1)	1(1)	6(1)	-1(1)
Cl(1)	23(1)	46(1)	62(1)	9(1)	11(1)	4(1)
P(1)	44(1)	27(1)	26(1)	2(1)	9(1)	-5(1)
Si(1)	51(1)	30(1)	34(1)	7(1)	6(1)	-8(1)
Si(2)	36(1)	37(1)	35(1)	0(1)	13(1)	1(1)
C(1)	54(4)	60(4)	56(4)	8(3)	-2(3)	-23(3)
C(2)	93(6)	28(3)	53(3)	5(2)	14(3)	0(3)
C(3)	83(5)	46(4)	45(3)	20(3)	11(3)	-17(3)
C(4)	96(6)	46(4)	35(3)	-5(2)	16(3)	-2(3)
C(5)	102(6)	55(4)	35(3)	5(3)	21(3)	1(4)
C(6)	45(5)	117(8)	148(9)	-41(7)	29(5)	2(5)
N(1)	22(2)	17(2)	30(2)	1(1)	2(1)	-2(1)
O(1)	20(2)	26(2)	31(2)	-1(1)	1(1)	-1(1)
O(2)	31(2)	20(2)	29(2)	-2(1)	8(1)	1(1)
O(3)	29(2)	24(2)	26(1)	4(1)	5(1)	-1(1)
C(7)	26(3)	26(2)	31(2)	1(2)	-1(2)	-2(2)
C(8)	25(2)	19(2)	36(2)	-2(2)	0(2)	4(2)
C(9)	26(2)	23(2)	27(2)	4(2)	4(2)	-1(2)
C(10)	29(3)	26(2)	32(2)	-1(2)	2(2)	-3(2)
C(11)	39(3)	27(3)	28(2)	-6(2)	5(2)	-2(2)
C(12)	37(3)	22(2)	33(2)	-2(2)	11(2)	5(2)
C(13)	26(3)	25(2)	36(2)	0(2)	6(2)	4(2)
C(14)	43(3)	33(3)	47(3)	-9(2)	11(2)	5(2)
C(15)	29(3)	35(3)	40(3)	-7(2)	-3(2)	-4(2)
C(16)	47(4)	54(4)	47(3)	-19(3)	-12(2)	-1(3)
C(17)	54(4)	49(4)	75(4)	0(3)	-30(3)	2(3)
C(18)	35(4)	100(6)	68(4)	-28(4)	14(3)	-24(3)
C(19)	29(3)	30(3)	31(2)	-3(2)	1(2)	-2(2)
C(20)	38(3)	28(2)	22(2)	-2(2)	3(2)	-8(2)
C(21)	40(3)	24(2)	24(2)	-1(2)	8(2)	-8(2)
C(22)	54(3)	27(3)	22(2)	-2(2)	12(2)	-3(2)
C(23)	79(5)	24(3)	33(3)	-2(2)	11(3)	-15(3)
C(24)	60(4)	35(3)	31(2)	-3(2)	5(2)	-22(3)
C(25)	43(3)	38(3)	28(2)	-4(2)	4(2)	-12(2)
C(26)	73(5)	49(4)	67(4)	-2(3)	-5(3)	-35(3)
C(27)	75(4)	22(3)	30(2)	-4(2)	15(2)	8(2)
C(28)	111(7)	43(4)	54(4)	18(3)	39(4)	24(4)
C(29)	63(4)	42(3)	50(3)	-12(3)	-10(3)	15(3)
C(30)	74(5)	37(3)	44(3)	-14(2)	22(3)	-5(3)
C(31)	23(2)	29(3)	31(2)	-1(2)	7(2)	-1(2)
C(32)	32(3)	27(2)	26(2)	-2(2)	10(2)	-1(2)
C(33)	29(2)	22(2)	23(2)	-2(2)	10(2)	-1(2)
C(34)	37(3)	26(2)	31(2)	0(2)	10(2)	1(2)
C(35)	48(3)	27(3)	35(2)	5(2)	16(2)	1(2)
C(36)	48(3)	25(3)	32(2)	-1(2)	19(2)	-8(2)
C(37)	31(3)	32(3)	29(2)	-2(2)	12(2)	-11(2)
C(38)	55(4)	39(3)	65(4)	-2(3)	15(3)	-19(3)
C(39)	48(3)	31(3)	26(2)	7(2)	-1(2)	2(2)
C(40)	72(5)	75(5)	52(4)	-21(3)	-16(3)	11(4)
C(41)	101(7)	73(6)	119(7)	61(5)	-56(6)	-24(5)
C(42)	38(4)	145(8)	45(4)	-12(4)	-5(3)	16(4)

5.12 [L*Ta(Cl)As(SiMe₃)₂] (16b)

Crystallographic parameters and details of data collection and refinement for **16b**:

Empirical formula	C ₄₂ H ₆₆ AsClNO ₃ Si ₂ Ta
Formula weight	980.46
Crystal dimensions [mm]	0.10 x 0.06 x 0.01
Temperature [K]	203(2)
Wavelength [Å]	0.56087
Crystal system	monoclinic
Space group	<i>P</i> 2 ₁ / <i>n</i>
Unit cell dimensions	<i>a</i> = 9.2249(18) Å <i>b</i> = 24.833(5) Å <i>c</i> = 19.827(4) Å <i>β</i> = 96.08(3)°
Volume [Å ³]	4516.5(15)
<i>Z</i>	4
Calculated density [g/cm ³]	1.442
Absorption coefficient [mm ⁻¹]	1.772
F(000)	2000
Index ranges	-9 ≤ <i>h</i> ≤ 10, -25 ≤ <i>k</i> ≤ 28, -22 ≤ <i>l</i> ≤ 23
Θ range for data collection [°]	1.53 – 19.00
Reflections collected	12428
Independent reflections	5806 (<i>R</i> _{int} = 0.1981)
Completeness to Θ = 19.00°	78.4%
Absorption correction	numerical
Refinement method	full-matrix least squares on <i>F</i> ²
Data / restraints / parameters	5806 / 0 / 268
Goodness of fit on <i>F</i> ²	0.954
<i>R</i> ₁ / <i>wR</i> ₂ (<i>I</i> > 2σ(<i>I</i>))	0.0849, 0.1437
<i>R</i> ₁ / <i>wR</i> ₂ (all data)	0.2018, 0.1866
Largest difference peak and hole [e·Å ⁻³]	0.900, -1.325

Atomic coordinates and equivalent isotropic displacement parameters for **16b**:

Atom	<i>x</i>	<i>y</i>	<i>z</i>	<i>U</i> _{eq}
Ta(1)	-17(1)	2398(1)	8018(1)	30(1)
Cl(1)	2523(8)	2273(2)	8166(3)	53(2)
As(1)	-113(4)	2845(1)	6808(1)	42(1)
Si(1)	1046(11)	3680(3)	6816(4)	48(2)
Si(2)	825(8)	2351(3)	5960(3)	42(2)
C(1)	3060(40)	3651(13)	7240(15)	72(8)
C(2)	-30(40)	4151(12)	7259(14)	64(7)
C(3)	1180(40)	3922(11)	5946(12)	59(7)
C(4)	330(40)	1623(10)	6033(14)	56(7)
C(5)	20(40)	2572(13)	5110(12)	70(7)
C(6)	2760(50)	2402(18)	5994(18)	108(11)
N(1)	-2530(20)	2516(7)	7938(8)	34(6)
O(1)	-73(19)	3094(5)	8406(7)	35(5)
O(2)	-590(20)	1725(6)	7636(7)	35(5)
O(3)	-320(18)	2114(5)	8907(7)	30(5)
C(7)	-2990(30)	3108(9)	7848(11)	41(5)
C(8)	-2460(30)	3432(8)	8469(10)	32(5)
C(9)	-990(30)	3443(8)	8717(10)	31(5)
C(10)	-390(30)	3769(9)	9268(11)	36(5)
C(11)	-1450(30)	4087(8)	9535(11)	34(5)
C(12)	-2940(30)	4112(8)	9301(10)	31(5)
C(13)	-3390(30)	3774(9)	8752(10)	37(5)
C(14)	-3920(40)	4475(10)	9639(14)	54(6)
C(15)	1140(40)	3736(10)	9556(13)	51(6)
C(16)	1580(40)	4178(11)	10125(13)	58(7)
C(17)	1430(50)	3201(13)	9967(16)	87(9)
C(18)	2260(40)	3809(13)	9065(16)	80(9)
C(19)	-3280(30)	2230(8)	7314(10)	33(5)
C(20)	-3150(30)	1642(8)	7250(10)	30(4)
C(21)	-1790(30)	1403(8)	7383(9)	27(4)
C(22)	-1660(30)	826(9)	7320(11)	41(5)
C(23)	-2880(30)	546(10)	7087(11)	44(5)
C(24)	-4180(30)	777(10)	6958(12)	48(6)
C(25)	-4340(30)	1335(9)	7019(12)	46(6)
C(26)	-5530(40)	435(13)	6654(15)	78(9)
C(27)	-210(30)	500(10)	7519(11)	42(5)
C(28)	-420(40)	87(11)	8096(15)	70(8)
C(29)	1130(40)	810(12)	7767(15)	76(8)
C(30)	120(30)	185(9)	6872(11)	49(6)
C(31)	-3240(30)	2302(9)	8536(11)	45(5)
C(32)	-2690(30)	1750(9)	8798(11)	35(5)
C(33)	-1240(30)	1720(9)	9070(11)	36(5)
C(34)	-700(30)	1256(9)	9499(10)	34(5)
C(35)	-1800(30)	839(9)	9509(11)	38(5)
C(36)	-3160(30)	874(8)	9200(10)	33(5)
C(37)	-3710(30)	1338(8)	8850(10)	33(5)
C(38)	-4180(30)	393(10)	9215(12)	48(6)
C(39)	670(30)	1242(9)	9932(11)	41(5)
C(40)	770(50)	1754(12)	10394(15)	78(9)
C(41)	830(60)	771(16)	10428(19)	117(13)
C(42)	2160(40)	1282(13)	9593(16)	81(9)

Anisotropic displacement parameters for **16b**:

Atom	U_{11}	U_{22}	U_{33}	U_{23}	U_{13}	U_{12}
Ta(1)	31(1)	24(1)	36(1)	-1(1)	7(1)	-2(1)
Cl(1)	38(5)	54(5)	70(4)	1(3)	21(4)	1(3)
As(1)	58(2)	32(1)	38(1)	1(1)	13(2)	-7(1)
Si(1)	63(7)	30(4)	53(4)	9(3)	11(5)	-4(4)
Si(2)	44(5)	35(4)	49(3)	-2(3)	14(4)	-1(4)
N(1)	32(13)	40(14)	32(8)	13(8)	12(9)	-14(10)
O(1)	39(13)	27(9)	42(8)	-2(6)	12(9)	-6(8)
O(2)	36(13)	38(10)	31(7)	-14(6)	0(9)	12(8)
O(3)	39(12)	17(8)	38(8)	1(6)	18(9)	2(7)

5.13 [L*TaMe₂] (17)

Crystallographic parameters and details of data collection and refinement for **17**:

Empirical formula	C ₃₈ H ₅₄ NO ₃ Ta
Formula weight	753.77
Crystal dimensions [mm]	0.20 x 0.12 x 0.04
Temperature [K]	203(2)
Wavelength [Å]	0.56087
Crystal system	monoclinic
Space group	<i>P</i> 2 ₁ / <i>c</i>
Unit cell dimensions	<i>a</i> = 10.007(2) Å <i>b</i> = 19.679(4) Å <i>c</i> = 18.534(4) Å <i>β</i> = 90.45(3)°
Volume [Å ³]	3649.7(13)
<i>Z</i>	4
Calculated density [g/cm ³]	1.372
Absorption coefficient [mm ⁻¹]	1.642
<i>F</i> (000)	1544
Index ranges	-12 ≤ <i>h</i> ≤ 12, -25 ≤ <i>k</i> ≤ 24, -21 ≤ <i>l</i> ≤ 21
<i>θ</i> range for data collection [°]	1.19 – 20.89
Reflections collected	27357
Independent reflections	7479 (<i>R</i> _{int} = 0.0801)
Completeness to <i>θ</i> = 20.89°	95.1%
Absorption correction	numerical
Refinement method	full-matrix least squares on <i>F</i> ²
Data / restraints / parameters	7479 / 0 / 402
Goodness of fit on <i>F</i> ²	1.032
<i>R</i> ₁ / <i>wR</i> ₂ (<i>I</i> > 2σ(<i>I</i>))	0.0483, 0.1078
<i>R</i> ₁ / <i>wR</i> ₂ (all data)	0.0738, 0.1185
Largest difference peak and hole [e·Å ⁻³]	1.109, -1.383

Atomic coordinates and equivalent isotropic displacement parameters for **17**:

Atom	<i>x</i>	<i>y</i>	<i>z</i>	<i>U</i> _{eq}
Ta(1)	2340(1)	1665(1)	7031(1)	22(1)
O(1)	2283(4)	1802(2)	8068(3)	28(1)
O(2)	3125(4)	1564(2)	6104(3)	28(1)
O(3)	1670(4)	2578(2)	6875(3)	27(1)
N(1)	4362(5)	2345(3)	7141(3)	25(1)
C(1)	402(6)	1168(3)	6834(4)	23(1)
C(2)	3526(4)	692(2)	7313(3)	8(1)
C(3)	4568(6)	2591(3)	7896(4)	27(1)
C(4)	4484(7)	2062(3)	8485(4)	29(1)
C(5)	3249(6)	1729(3)	8595(3)	25(1)
C(6)	2981(7)	1360(3)	9229(4)	28(1)
C(7)	4079(7)	1273(4)	9691(4)	34(2)
C(8)	5360(7)	1554(4)	9572(4)	36(2)
C(9)	5509(7)	1960(4)	8974(4)	31(2)
C(10)	6500(9)	1420(5)	10085(5)	55(2)
C(11)	1580(8)	1069(4)	9417(4)	40(2)
C(12)	1201(12)	512(5)	8855(5)	71(3)
C(13)	570(9)	1641(5)	9405(6)	60(2)
C(14)	1566(9)	730(5)	10155(5)	53(2)
C(15)	5533(7)	1927(3)	6920(4)	31(1)
C(16)	5512(7)	1685(3)	6145(4)	32(1)
C(17)	4331(7)	1483(3)	5779(4)	29(1)
C(18)	4391(8)	1226(3)	5067(4)	34(2)
C(19)	5657(9)	1206(4)	4742(5)	43(2)
C(20)	6820(8)	1426(4)	5085(5)	41(2)
C(21)	6724(7)	1648(4)	5780(4)	39(2)
C(22)	8154(10)	1409(5)	4699(6)	69(3)
C(23)	3111(8)	979(4)	4674(4)	39(2)
C(24)	2370(9)	440(4)	5124(5)	52(2)
C(25)	2190(10)	1594(5)	4526(5)	57(2)
C(26)	3437(11)	653(6)	3935(5)	65(3)
C(27)	4292(7)	2957(3)	6653(4)	29(1)
C(28)	3251(6)	3471(3)	6853(4)	25(1)
C(29)	1925(6)	3248(3)	6961(3)	24(1)
C(30)	892(6)	3709(3)	7138(4)	27(1)
C(31)	1256(7)	4396(3)	7174(4)	29(1)
C(32)	2547(7)	4639(3)	7048(4)	31(2)
C(33)	3541(7)	4159(3)	6902(4)	30(1)
C(34)	2831(9)	5375(4)	7091(6)	49(2)
C(35)	-565(7)	3474(3)	7261(4)	31(2)
C(36)	-627(7)	2914(4)	7840(4)	37(2)
C(37)	-1455(8)	4050(4)	7497(6)	52(2)
C(38)	-1107(7)	3191(4)	6541(5)	44(2)

Anisotropic displacement parameters for **17**:

Atom	U_{11}	U_{22}	U_{33}	U_{23}	U_{13}	U_{12}
Ta(1)	21(1)	23(1)	21(1)	1(1)	0(1)	-3(1)
O(1)	26(2)	32(2)	25(3)	4(2)	-1(2)	-5(2)
O(2)	26(2)	32(2)	27(3)	-2(2)	0(2)	-2(2)
O(3)	26(2)	25(2)	30(3)	1(2)	0(2)	-1(2)
N(1)	20(3)	30(3)	26(3)	3(2)	1(2)	-5(2)
C(1)	13(3)	28(3)	28(4)	-2(2)	-3(2)	-10(2)
C(2)	5(2)	13(2)	5(2)	2(2)	-2(2)	6(2)
C(3)	24(3)	27(3)	29(4)	-1(3)	-1(2)	-4(2)
C(4)	30(3)	30(3)	26(4)	-5(3)	-4(3)	1(3)
C(5)	30(3)	26(3)	18(3)	-4(2)	4(2)	1(3)
C(6)	38(4)	29(3)	18(4)	0(2)	0(3)	-4(3)
C(7)	44(4)	39(4)	20(4)	-1(3)	-5(3)	5(3)
C(8)	31(4)	47(4)	29(4)	-4(3)	-10(3)	11(3)
C(9)	26(3)	41(4)	25(4)	-9(3)	-2(3)	-2(3)
C(10)	52(5)	78(6)	35(5)	12(4)	-14(4)	4(4)
C(11)	59(5)	43(4)	20(4)	8(3)	-3(3)	-20(4)
C(12)	104(9)	71(6)	37(6)	-10(4)	-1(5)	-59(6)
C(13)	42(5)	77(6)	60(6)	19(5)	23(4)	-8(5)
C(14)	57(5)	72(6)	30(5)	13(4)	3(4)	-23(5)
C(15)	31(4)	30(3)	30(4)	-2(3)	3(3)	-1(3)
C(16)	35(3)	27(3)	35(4)	0(3)	5(3)	0(3)
C(17)	32(3)	24(3)	32(4)	5(2)	9(3)	3(2)
C(18)	48(4)	21(3)	32(4)	0(3)	3(3)	4(3)
C(19)	58(5)	38(4)	33(5)	4(3)	21(4)	8(4)
C(20)	39(4)	37(4)	46(5)	-1(3)	21(4)	1(3)
C(21)	30(3)	35(4)	52(5)	2(3)	12(3)	2(3)
C(22)	55(6)	75(7)	78(8)	-3(5)	46(6)	1(5)
C(23)	50(5)	48(4)	19(4)	-5(3)	-1(3)	7(3)
C(24)	65(6)	39(4)	52(6)	-4(4)	-8(4)	-15(4)
C(25)	61(6)	63(6)	46(6)	5(4)	-8(4)	11(5)
C(26)	80(7)	83(7)	32(6)	-17(5)	8(5)	4(6)
C(27)	32(4)	31(3)	25(4)	3(3)	5(3)	1(3)
C(28)	28(3)	20(3)	26(4)	4(2)	-1(2)	-5(2)
C(29)	23(3)	28(3)	20(3)	4(2)	-2(2)	-3(2)
C(30)	25(3)	33(3)	21(4)	5(3)	-1(2)	-2(3)
C(31)	35(4)	22(3)	29(4)	-4(3)	-4(3)	2(3)
C(32)	33(4)	28(3)	32(4)	2(3)	-3(3)	-2(3)
C(33)	32(4)	30(3)	28(4)	6(3)	1(3)	-4(3)
C(34)	42(4)	29(4)	77(7)	-7(4)	-3(4)	-8(3)
C(35)	24(3)	31(4)	39(4)	6(3)	0(3)	2(3)
C(36)	29(4)	44(4)	38(5)	10(3)	5(3)	3(3)
C(37)	34(4)	44(5)	77(7)	10(4)	11(4)	10(3)
C(38)	26(4)	57(5)	50(5)	8(4)	-11(3)	-8(3)

5.14 [$\{\text{Cp}''\text{Ta}(\text{CO})_2(\mu, \eta^4: \eta^1: \eta^1: \eta^1\text{-P}_4)\}_6\{\text{CuCl}\}_8$] (**19a**)

Crystallographic parameters and details of data collection and refinement for **19a**·CH₂Cl₂:

Empirical formula	C ₉₁ H ₁₂₈ Cl ₁₀ Cu ₈ O ₁₂ P ₂₄ Ta ₆
Formula weight	4105.73
Crystal dimensions [mm]	0.08 x 0.08 x 0.04
Temperature [K]	150(1)
Wavelength [Å]	0.71073
Crystal system	trigonal
Space group	$R\bar{3}$
Unit cell dimensions	$a = 22.845(3)$ Å $c = 22.658(5)$ Å
Volume [Å ³]	10241(3)
Z	3
Calculated density [g/cm ³]	1.997
Absorption coefficient [mm ⁻¹]	6.526
F(000)	5910
Index ranges	$-25 \leq h \leq 27$, $-26 \leq k \leq 27$, $-26 \leq l \leq 26$
θ range for data collection [°]	1.78 – 24.99
Reflections collected	22248
Independent reflections	4007 ($R_{\text{int}} = 0.0756$)
Completeness to $\theta = 24.99^\circ$	100.0%
Absorption correction	empirical (SHELXA)
Refinement method	full-matrix least squares on F^2
Data / restraints / parameters	4007 / 14 / 250
Goodness of fit on F^2	1.022
R_1 / wR_2 ($I > 2\sigma(I)$)	0.0365, 0.0805
R_1 / wR_2 (all data)	0.0510, 0.0854
Largest difference peak and hole [e·Å ⁻³]	1.017, -3.340

Atomic coordinates and equivalent isotropic displacement parameters for **19a**·CH₂Cl₂:

Atom	<i>x</i>	<i>y</i>	<i>z</i>	<i>U</i> _{eq}
Ta(1)	6317(1)	5178(1)	6871(1)	17(1)
Cu(1)	6667	3333	6384(1)	46(1)
Cu(2)	4737(1)	3097(1)	7680(1)	19(1)
P(1)	6592(1)	4184(1)	6853(1)	20(1)
P(2)	7280(1)	5043(1)	7404(1)	19(1)
P(3)	6444(1)	4894(1)	7974(1)	19(1)
P(4)	5784(1)	4026(1)	7444(1)	21(1)
Cl(1)	6667	3333	5397(2)	58(1)
Cl(2)	3806(1)	3084(1)	7355(1)	28(1)
O(1)	7492(3)	5627(3)	5874(3)	36(1)
O(2)	7303(3)	6637(3)	7498(3)	34(1)
C(1)	5127(4)	4681(4)	6686(3)	24(2)
C(2)	5444(3)	4755(4)	6118(3)	23(2)
C(3)	5868(4)	5474(4)	6025(3)	24(2)
C(4)	5813(3)	5819(4)	6519(3)	23(2)
C(5)	5352(3)	5337(4)	6939(3)	23(2)
C(6)	5235(4)	4182(4)	5664(3)	24(2)
C(7)	5071(4)	3505(4)	5955(3)	28(2)
C(8)	5783(4)	4369(5)	5194(4)	38(2)
C(9)	4582(4)	4086(4)	5380(4)	38(2)
C(10)	5025(4)	5479(4)	7475(4)	30(2)
C(11)	4821(4)	4941(4)	7955(4)	35(2)
C(12)	5516(5)	6178(4)	7748(5)	51(3)
C(13)	4386(6)	5471(8)	7238(5)	68(4)
C(14)	7085(4)	5480(4)	6222(4)	27(2)
C(15)	6953(4)	6132(4)	7272(3)	26(2)
C(16)	6667	3333	3840(20)	114(14)
Cl(3)	6870(20)	3960(20)	4291(17)	180(16)
Cl(4)	7488(7)	3719(8)	3668(8)	57(4)

Anisotropic displacement parameters for **19a**·CH₂Cl₂:

Atom	U_{11}	U_{22}	U_{33}	U_{23}	U_{13}	U_{12}
Ta(1)	17(1)	16(1)	18(1)	2(1)	0(1)	8(1)
Cu(1)	47(1)	47(1)	45(1)	0	0	24(1)
Cu(2)	18(1)	20(1)	21(1)	0(1)	-1(1)	10(1)
P(1)	20(1)	19(1)	22(1)	0(1)	-1(1)	9(1)
P(2)	18(1)	20(1)	19(1)	1(1)	0(1)	9(1)
P(3)	19(1)	20(1)	18(1)	0(1)	0(1)	9(1)
P(4)	20(1)	18(1)	21(1)	1(1)	-1(1)	8(1)
Cl(1)	65(2)	65(2)	43(2)	0	0	32(1)
Cl(2)	19(1)	28(1)	36(1)	4(1)	-4(1)	11(1)
O(1)	32(3)	45(3)	33(3)	13(3)	13(3)	22(3)
O(2)	38(3)	22(3)	39(3)	-5(2)	-7(3)	12(3)
C(1)	16(3)	21(4)	34(4)	3(3)	-1(3)	10(3)
C(2)	16(3)	25(4)	26(4)	7(3)	1(3)	10(3)
C(3)	23(4)	22(4)	26(4)	8(3)	-7(3)	11(3)
C(4)	16(3)	22(4)	34(4)	4(3)	-3(3)	12(3)
C(5)	15(3)	22(4)	36(4)	-3(3)	-3(3)	13(3)
C(6)	24(4)	22(4)	17(3)	2(3)	-3(3)	5(3)
C(7)	29(4)	21(4)	29(4)	0(3)	-3(3)	10(3)
C(8)	38(5)	37(5)	25(4)	-8(3)	3(3)	9(4)
C(9)	37(5)	32(5)	37(5)	6(4)	-16(4)	11(4)
C(10)	26(4)	28(4)	42(5)	2(3)	7(3)	16(3)
C(11)	38(5)	30(4)	33(4)	-1(3)	10(4)	15(4)
C(12)	60(6)	22(4)	62(7)	-3(4)	33(5)	14(4)
C(13)	66(8)	108(10)	66(8)	12(7)	17(6)	70(8)
C(14)	28(4)	27(4)	32(4)	4(3)	-2(3)	18(3)
C(15)	31(4)	29(4)	25(4)	5(3)	2(3)	20(4)
C(16)	126(19)	126(19)	90(30)	0	0	63(9)
Cl(3)	180(30)	210(30)	120(20)	-30(20)	20(20)	70(30)
Cl(4)	52(8)	47(8)	60(9)	2(7)	4(7)	15(7)

5.15 [$\{\text{Cp}''\text{Ta}(\text{CO})_2(\mu, \eta^4: \eta^1: \eta^1: \eta^1\text{-P}_4)\}_6\{\text{CuBr}\}_8$] (**19b**)

Crystallographic parameters and details of data collection and refinement for **19b**·(CH₂Cl₂), crystallized from MeCN/CH₂Cl₂/DMF-*d*₇:

Empirical formula	C ₉₁ H ₁₂₈ Br ₈ ClCu ₈ N [*] O ₁₂ P ₂₄ Ta ₆
Formula weight	4446.02
Temperature [K]	153(2)
Wavelength [Å]	0.71073
Crystal system	trigonal
Space group	$R\bar{3}$
Unit cell dimensions	$a = 22.965(3)$ Å $c = 22.385(5)$ Å
Volume [Å ³]	10224(3)
Z	3
Calculated density [g/cm ³]	2.166
Absorption coefficient [mm ⁻¹]	8.706
F(000)	6330
Index ranges	$-21 \leq h \leq 29$, $-25 \leq k \leq 7$, $-28 \leq l \leq 27$
θ range for data collection [°]	2.09 – 27.08
Reflections collected	8610
Independent reflections	4785 ($R_{\text{int}} = 0.0515$)
Completeness to $\theta = 27.08^\circ$	95.5%
Absorption correction	numerical
Refinement method	full-matrix least squares on F^2
Data / restraints / parameters	4785 / 1 / 239
Goodness of fit on F^2	1.054
R_1 / wR_2 ($I > 2\sigma(I)$)	0.0478, 0.1299
R_1 / wR_2 (all data)	0.0535, 0.1350
Largest difference peak and hole [e·Å ⁻³]	1.341, -3.736

* The electron density at the center of the core of **19b** was assigned here as nitrogen (N), which yielded the best structural refinement values. The formula weight reflects the presence of the central N.

Atomic coordinates and equivalent isotropic displacement parameters for **19b**·(CH₂Cl₂), crystallized from MeCN/CH₂Cl₂/DMF-*d*₇:

Atom	<i>x</i>	<i>y</i>	<i>z</i>	<i>U</i> _{eq}
Ta(1)	1524(1)	4486(1)	197(1)	23(1)
Cu(1)	3596(1)	5022(1)	1013(1)	25(1)
Cu(2)	3333	6667	-311(1)	42(1)
Br(1)	3628(1)	4060(1)	710(1)	35(1)
Br(2)	3333	6667	-1347(1)	61(1)
P(1)	2665(1)	5100(1)	764(1)	25(1)
P(2)	2505(1)	5739(1)	170(1)	25(1)
P(3)	1663(1)	5576(1)	728(1)	25(1)
P(4)	1817(1)	4904(1)	1304(1)	25(1)
O(14)	92(3)	4015(3)	839(3)	41(2)
O(15)	1107(4)	5219(3)	-811(3)	42(2)
C(1)	2002(4)	3793(4)	7(3)	27(2)
C(2)	1930(4)	4032(4)	-554(3)	26(2)
C(3)	1229(4)	3754(4)	-651(3)	29(2)
C(4)	877(4)	3354(4)	-151(4)	29(2)
C(5)	1354(4)	3371(4)	269(4)	30(2)
C(6)	2501(4)	4386(4)	-1016(4)	33(2)
C(7)	2305(5)	4734(6)	-1506(4)	44(2)
C(8)	2586(5)	3818(5)	-1277(5)	43(2)
C(9)	3168(4)	4890(5)	-728(4)	36(2)
C(10)	1207(5)	2904(4)	801(4)	37(2)
C(11)	500(5)	2666(7)	1046(6)	61(3)
C(12)	1258(9)	2295(6)	562(6)	72(4)
C(13)	1725(5)	3238(5)	1298(4)	40(2)
C(14)	581(4)	4173(4)	607(4)	29(2)
C(15)	1240(4)	4951(4)	-459(4)	29(2)
N(1)*	3333	6667	1667	55(5)
C(17)	0	0	0	400(100)
Cl(1)	760(20)	350(20)	272(17)	124(11)

* Nitrogen assigned at center of the core of **19b**.

Anisotropic displacement parameters for **19b**·(CH₂Cl₂), crystallized from MeCN/CH₂Cl₂/DMF-*d*₇:

Atom	U_{11}	U_{22}	U_{33}	U_{23}	U_{13}	U_{12}
Ta(1)	20(1)	20(1)	28(1)	-2(1)	-2(1)	10(1)
Cu(1)	22(1)	22(1)	30(1)	-1(1)	-1(1)	11(1)
Cu(2)	40(1)	40(1)	46(1)	0	0	20(1)
Br(1)	33(1)	29(1)	49(1)	-10(1)	-6(1)	21(1)
Br(2)	69(1)	69(1)	45(1)	0	0	35(1)
P(1)	22(1)	23(1)	30(1)	-1(1)	-1(1)	11(1)
P(2)	23(1)	22(1)	30(1)	0(1)	0(1)	11(1)
P(3)	23(1)	23(1)	30(1)	0(1)	0(1)	12(1)
P(4)	24(1)	25(1)	28(1)	0(1)	1(1)	12(1)
O(14)	29(3)	38(3)	47(3)	-9(3)	3(3)	10(3)
O(15)	49(4)	36(3)	42(3)	-4(3)	-14(3)	23(3)
C(1)	23(4)	23(4)	35(4)	-7(3)	-7(3)	12(3)
C(2)	28(4)	21(4)	32(4)	-3(3)	-1(3)	14(3)
C(3)	30(4)	28(4)	30(4)	-10(3)	-9(3)	14(3)
C(4)	23(4)	25(4)	35(4)	-5(3)	-3(3)	9(3)
C(5)	30(4)	23(4)	37(4)	-5(3)	-6(3)	13(3)
C(6)	31(4)	37(4)	32(4)	-5(3)	-1(3)	16(4)
C(7)	42(5)	59(6)	39(5)	9(4)	6(4)	31(5)
C(8)	26(4)	45(5)	60(6)	-22(4)	0(4)	18(4)
C(9)	23(4)	39(5)	39(4)	-5(3)	-1(3)	11(4)
C(10)	41(5)	27(4)	42(5)	-3(3)	-2(4)	17(4)
C(11)	30(5)	70(8)	66(7)	28(6)	3(5)	11(5)
C(12)	125(12)	31(6)	67(7)	7(5)	2(7)	45(7)
C(13)	33(5)	43(5)	44(5)	8(4)	-4(4)	19(4)
C(14)	25(4)	23(4)	37(4)	0(3)	2(3)	11(3)
C(15)	28(4)	23(4)	32(4)	0(3)	-2(3)	9(3)
N(1)*	52(9)	52(9)	61(14)	0	0	26(4)

* Nitrogen assigned at center of the core of **19b**.

Crystallographic parameters and details of data collection and refinement for **19b**·(CH₂Cl₂), crystallized from MeCN/CH₂Cl₂ (no DMF-*d*₇):

Empirical formula	C ₉₀ H ₁₂₆ Br ₈ Cu ₈ O ₁₃ ^{**} P ₂₄ Ta ₆ , C _{0.44} Cl _{1.63}
Formula weight	4455.62
Crystal dimensions [mm]	0.09 x 0.08 x 0.06
Temperature [K]	123(1)
Wavelength [Å]	0.71073
Crystal system	trigonal
Space group	$R\bar{3}$
Unit cell dimensions	$a = 23.1232(15)$ Å $c = 22.5841(18)$ Å
Volume [Å ³]	10457.5(13)
Z	3
Calculated density [g/cm ³]	2.092
Absorption coefficient [mm ⁻¹]	8.492
F(000)	6240
Index ranges	$-25 \leq h \leq 29$, $-29 \leq k \leq 27$, $-28 \leq l \leq 28$
θ range for data collection [°]	2.07 – 26.86
Reflections collected	26985
Independent reflections	4986 ($R_{\text{int}} = 0.0613$)
Absorption correction	numerical
Refinement method	full-matrix least squares on F^2
Data / restraints / parameters	4986 / 0 / 233
Goodness of fit on F^2	0.994
R_1 / wR_2 ($I > 2\sigma(I)$)	0.0316, 0.0800
R_1 / wR_2 (all data)	0.0407, 0.0831
Largest difference peak and hole [e·Å ⁻³]	1.426, -2.827

^{**} The electron density at the center of the core of **19b** was assigned here as oxygen (O), which yielded the best structural refinement values. The formula weight reflects the presence of the central O.

Atomic coordinates and equivalent isotropic displacement parameters for **19b**·(CH₂Cl₂), crystallized from MeCN/CH₂Cl₂ (no DMF-*d*₇):

Atom	<i>x</i>	<i>y</i>	<i>z</i>	<i>U</i> _{eq}
Ta(1)	9628(1)	1807(1)	8534(1)	16(1)
Br(1)	10000	0	6997(1)	52(1)
Br(2)	12606(1)	2901(1)	9045(1)	29(1)
Cu(1)	10000	0	8027(1)	35(1)
Cu(2)	11645(1)	1907(1)	9348(1)	19(1)
P(1)	9901(1)	827(1)	8508(1)	19(1)
P(2)	10579(1)	1669(1)	9063(1)	18(1)
P(3)	9756(1)	1518(1)	9638(1)	19(1)
P(4)	9102(1)	668(1)	9101(1)	18(1)
O(1)	10593(2)	3241(2)	9176(2)	35(1)
O(2)	10778(2)	2229(2)	7527(2)	35(1)
C(1)	8765(3)	1401(3)	7783(2)	21(1)
C(2)	9192(3)	2101(3)	7689(2)	21(1)
C(3)	9144(3)	2453(3)	8184(2)	24(2)
C(4)	8682(3)	1977(3)	8604(2)	23(2)
C(5)	8551(3)	840(3)	7324(2)	26(2)
C(6)	8393(3)	166(3)	7609(2)	29(2)
C(7)	9088(3)	1022(3)	6840(3)	37(2)
C(8)	7897(3)	747(3)	7051(3)	34(2)
C(9)	8360(3)	2128(3)	9134(3)	30(2)
C(10)	8193(3)	1617(3)	9633(3)	37(2)
C(11)	7716(5)	2073(6)	8900(4)	64(4)
C(12)	8817(4)	2828(3)	9379(4)	51(3)
C(13)	10253(3)	2745(3)	8942(2)	23(2)
C(14)	10376(3)	2087(3)	7883(2)	23(2)
C(17)	8454(3)	1329(3)	8348(2)	22(1)
O(3)**	10000	0	10000	40(3)
Cl(1)	9627(12)	425(12)	5250(10)	158(11)
C(18)	10000	0	5410(30)	50(20)

** Oxygen assigned at center of the core of **19b**.

Anisotropic displacement parameters for **19b**·(CH₂Cl₂), crystallized from MeCN/CH₂Cl₂ (no DMF-*d*₇):

Atom	U_{11}	U_{22}	U_{33}	U_{23}	U_{13}	U_{12}
Ta(1)	15(1)	14(1)	19(1)	2(1)	0(1)	8(1)
Br(1)	61(1)	61(1)	33(1)	0	0	31(1)
Br(2)	25(1)	17(1)	40(1)	4(1)	10(1)	6(1)
Cu(1)	35(1)	35(1)	35(1)	0	0	18(1)
Cu(2)	17(1)	16(1)	21(1)	1(1)	1(1)	7(1)
P(1)	18(1)	17(1)	22(1)	0(1)	0(1)	9(1)
P(2)	16(1)	17(1)	21(1)	0(1)	-1(1)	8(1)
P(3)	19(1)	18(1)	19(1)	0(1)	1(1)	9(1)
P(4)	17(1)	16(1)	21(1)	2(1)	0(1)	7(1)
O(1)	38(2)	21(2)	42(2)	-3(2)	-7(2)	12(2)
O(2)	37(2)	40(2)	34(2)	15(2)	12(2)	24(2)
C(1)	20(2)	22(3)	23(2)	4(2)	-4(2)	12(2)
C(2)	17(2)	22(3)	24(2)	5(2)	-4(2)	9(2)
C(3)	21(3)	20(3)	30(3)	6(2)	-1(2)	10(2)
C(4)	20(3)	23(3)	29(3)	3(2)	-1(2)	14(2)
C(5)	25(3)	22(3)	26(2)	0(2)	-7(2)	7(2)
C(6)	35(3)	22(3)	27(3)	2(2)	-3(2)	12(2)
C(7)	37(3)	34(3)	29(3)	-2(2)	3(2)	9(3)
C(8)	28(3)	23(3)	44(3)	2(2)	-13(3)	7(2)
C(9)	28(3)	32(3)	39(3)	-2(2)	5(2)	21(3)
C(10)	40(4)	35(3)	35(3)	-1(3)	11(3)	19(3)
C(11)	53(5)	115(8)	56(5)	-3(5)	5(4)	65(6)
C(12)	64(5)	26(3)	59(5)	-1(3)	29(4)	20(3)
C(13)	26(3)	22(3)	25(2)	3(2)	-5(2)	14(2)
C(14)	24(3)	23(3)	24(2)	3(2)	0(2)	14(2)
C(17)	19(2)	18(2)	30(3)	3(2)	-3(2)	10(2)
O(3)**	41(4)	41(4)	36(6)	0	0	20(2)

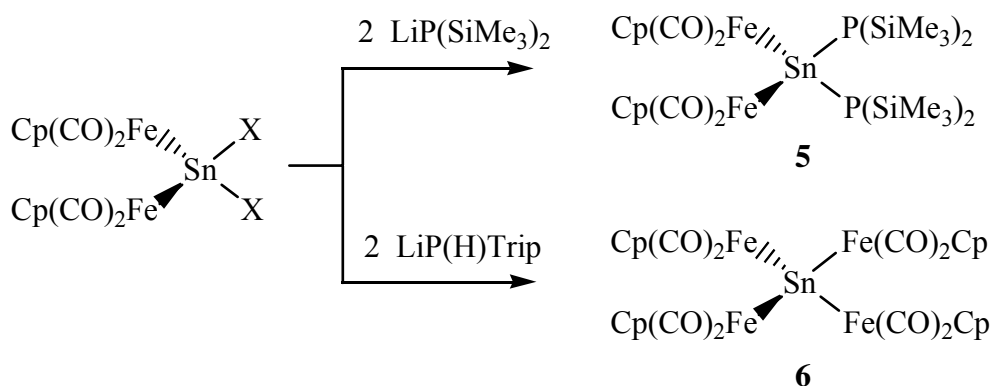
** Oxygen assigned at center of the core of **19b**.

Selected bond lengths [Å] and angles [°] in **19b** crystallized from MeCN/CH₂Cl₂ (no DMF-*d*₇):

P(1)-P(4)	2.160(2)	P(1)-P(2)	2.1837(18)
P(2)-P(3)	2.184(2)	P(3)-P(4)	2.1564(18)
Cu(1)-P(1)	2.3079(16)	Cu(2)-P(2)	2.3316(17)
Cu(1)-P(1)'	2.3079(18)	Cu(2)-P(3)'	2.3121(13)
Ta(1)-C _{Co} (13)	2.123(6)	Ta(1)-C _{Co} (14)	2.110(6)
Ta-C _{Cp} ''	2.409(7) ^a	Ta-P	2.6389(14) ^a
Cu(1)-Br(1)	2.3264(18)	Cu(2)-Br(2)	2.3624(9)
P(4)-P(1)-P(2)	88.14(7)	P(3)-P(2)-P(1)	91.09(8)
P(4)-P(3)-P(2)	88.23(7)	P(3)-P(4)-P(1)	92.48(7)
Br(1)-Cu(1)-P(1)	118.05(5)	Br(2)-Cu(2)-P(2)	121.27(4)
Br(1)-Cu(1)-P(1)'	118.05(5)	Br(1)-Cu(1)-P(1)''	118.05(5)
P(1)-Cu(1)-P(1)'	99.68(7)	P(2)-Cu(2)-P(3)'	114.69(5)
P(1)'-Cu(1)-P(1)''	99.68(7)	P(2)-Cu(2)-P(4)'	118.20(6)

^a Mean value is given

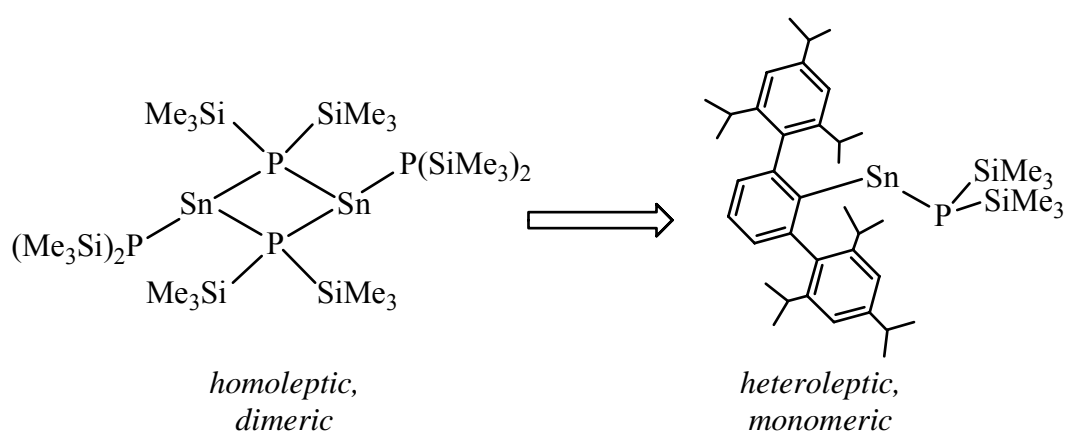
disproportionation of the Fp_2Sn fragment and formation of the homoleptic complex $[\text{Fp}_4\text{Sn}]$ (6).



Scheme 12: Reactivity of $[\text{Fp}_2\text{SnX}_2]$ with alkali-metal phosphanides.

6.2 Kinetically stabilized low-coordinate tin-phosphorus compounds

As an extension to the use of transition-metal fragments for the stabilization of tin-phosphorus compounds, the sterically encumbering terphenyl ligand, Ph^* , was used for the kinetic stabilization of low-coordinate tin-phosphorus compounds. Thus, while the bis(trimethylsilylphosphanyl) stannylene $[\text{Sn}\{\text{P}(\text{SiMe}_3)_2\}_2]_2$ is known as a bridged dimer, the terphenyl-stabilized $\text{Ph}^*\text{SnP}(\text{SiMe}_3)_2$ (**7**) could be isolated as the first heteroleptic stannylene phosphanide in monomeric form.

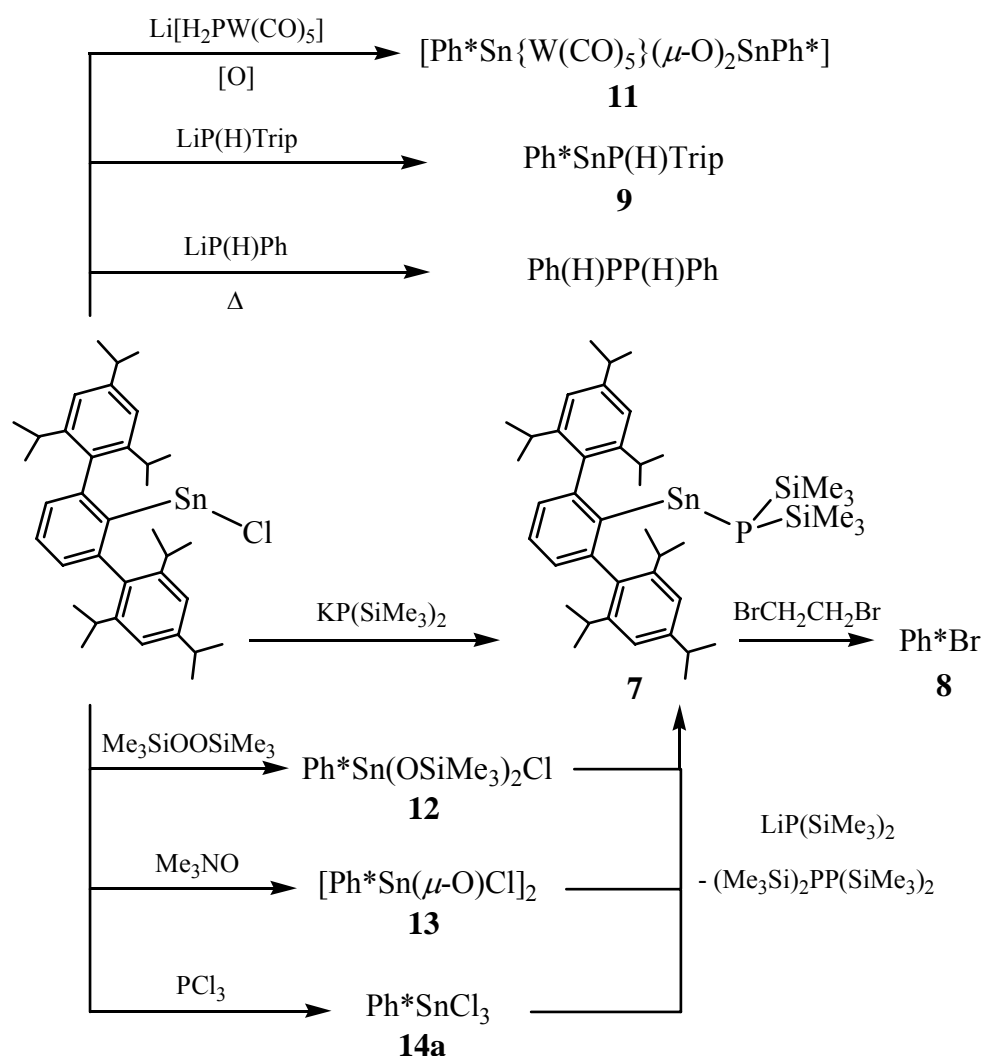


Scheme 13: Stabilization of heteroleptic stannylene phosphanide with a terphenyl group.

The reactivity of Ph^*SnCl was further explored in reactions with primary aryl phosphanides, from which the monomeric compound $\text{Ph}^*\text{SnP}(\text{H})\text{Trip}$ (**9**), featuring a reactive

P-bound proton, was observed. In addition, the anionic tin-phosphorous species $\text{Li}^+[\text{Ph}^*\text{SnP}(\text{H})\text{Trip}]^-$ (**10**) was detected, with the characteristics of its ^{31}P -NMR spectrum indicating tin-phosphorous multiple bonding; the nature of this bonding was considered by DFT calculations, and a case was made that anionic compound **10** represented an unprecedented mode of multiple tin-phosphorus bonding.

Furthermore, a series of terphenyl Sn(IV) compounds were synthesized and their potential as entry points into tin-phosphorus chemistry was surveyed in reactions with $\text{LiP}(\text{SiMe}_3)_2$. As shown in Scheme 14, the redox potential between stable Sn(II) and Sn(IV) forms plays a key role, whereby phosphorus reagents can exhibit a reducing or oxidizing effect on Ph^*Sn starting materials.



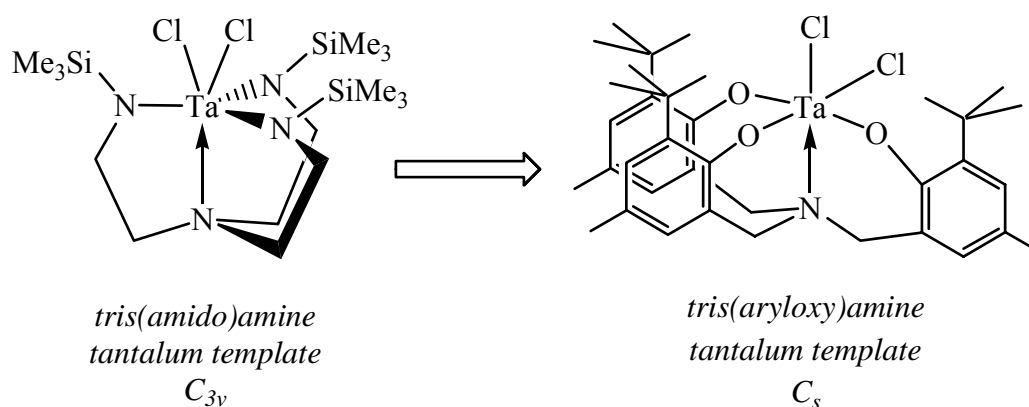
Scheme 14: Reactivity of $\text{Ph}^*\text{Sn}(\text{II})$ and $\text{Ph}^*\text{Sn}(\text{IV})$ templates with phosphanide reagents.

In reactions of Ph^*SnCl with alkali-metal phosphanides, the size of the substituents at phosphorus is decisive, as larger substituents allow cleaner reactions and formation of the monomeric terphenyl stannylene phosphanides **7** and **9**. An interesting avenue for further study would be the synthesis of stannylene phosphanide compounds in which the terphenyl group Ph^* is used at both the Sn and P atoms, thus offering considerable steric protection. In reactions of Ph^*SnCl with the smaller LiP(H)Ph reagent or in reactions of $\text{Ph}^*\text{Sn(IV)}$ starting materials with $\text{LiP(SiMe}_3)_2$, P–P bond formation pathways predominate. In order to circumvent reduction pathways on $\text{Ph}^*\text{Sn(IV)}$ reactants, the corresponding $\text{Ph}^*\text{Ge(IV)}$ compounds could potentially serve as interesting reagents for germanium-phosphorus chemistry, as the reduction potential for Ge is generally lower than that for Sn.

Despite the investigations directed at preparing $\text{Ph}^*\text{Sn}\equiv\text{P}$, the first compound with a $\text{Sn}\equiv\text{P}$ triple bond, no route to $\text{Ph}^*\text{Sn}\equiv\text{P}$ was developed in the current work. However, an entry point into low-coordinate heteroleptic Sn–P compounds has been developed, and this represents an initial step toward compounds of the type $\text{Ph}^*\text{Sn}\equiv\text{P}$.

6.3 Survey of a tris(aryloxy)amine tantalum platform

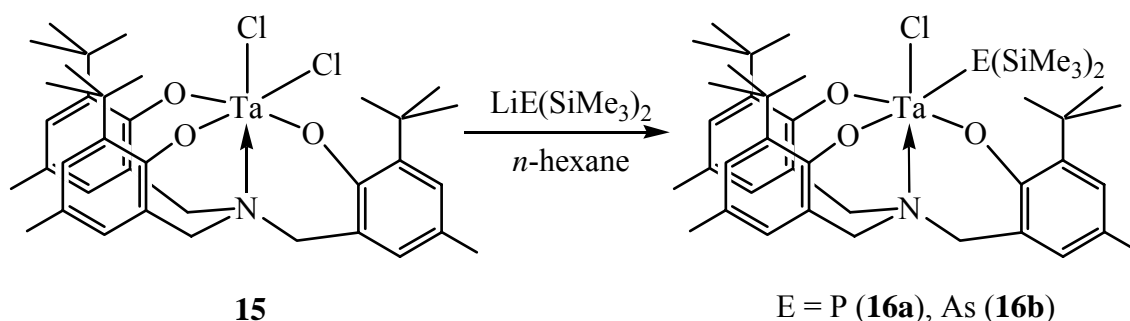
$[(\text{N}_3\text{N})\text{TaCl}_2]$ has previously been established as a viable entry point into Ta–P complexes with low-coordinate phosphorus ligands. It was postulated in this work that the tris(aryloxy)amine tantalum starting material $[\text{L}^*\text{TaCl}_2]$ (**15**) could be synthesized and would represent an alternative entry point into similar Ta–P chemistry.



Scheme 15: Symmetry comparison of the known $[(\text{N}_3\text{N})\text{TaCl}_2]$ complex and $[\text{L}^*\text{TaCl}_2]$ (**15**).

While the synthesis of $[\text{L}^*\text{TaCl}_2]$ was successful in this work, it displayed a C_s -symmetric geometry, in contrast to the C_{3v} -symmetric geometry exhibited by $[(\text{N}_3\text{N})\text{TaCl}_2]$, and revealed a reactivity pattern with alkali-metal trimethylsilyl phosphanide in which the resulting Ta–P bond was not stable. The mono-substituted Ta-phosphanide and -arsenide

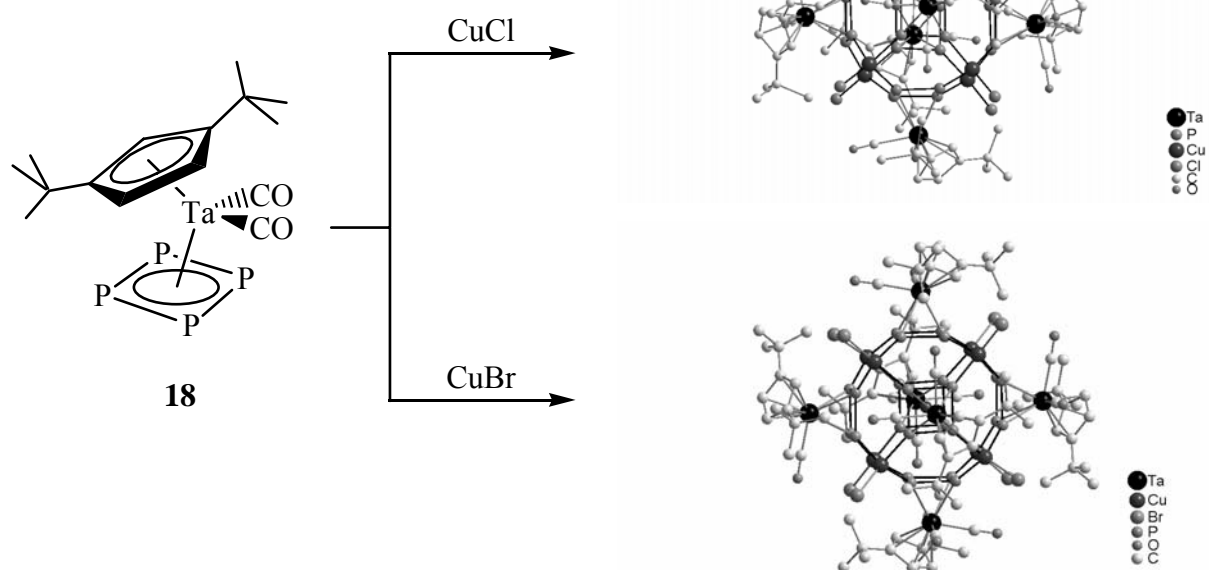
complexes $[L^*Ta(Cl)E(SiMe_3)_2]$ (**16a,b**) could be isolated with the pnictogenide ligand coordinated at the equatorial position.



However, attempts to synthesize the targeted tantalum phosphinidene complex $[L^*Ta=PSiMe_3]$ by reaction of $[L^*TaCl_2]$ with two equivalents $LiP(SiMe_3)_2$ or by halide/silane abstraction from $[L^*Ta(Cl)P(SiMe_3)_2]$ failed. The complexes **16a,b** were found to be unstable in solution at room temperature, and as a consequence, entry into tantalum-pnictinidene chemistry was determined unfeasible from $[L^*TaCl_2]$ by these routes. While the reactions of $[L^*TaCl_2]$ with $LiE(SiMe_3)_2$ exhibited only monosubstitution of the chloride ligands of **15**, reaction of $[L^*TaCl_2]$ with two equivalents of $MeLi$ afforded $[L^*TaMe_2]$ (**17**) and provided evidence that bis-substitution is indeed possible with a Ta(V) complex possessing a tris(aryloxy)amine ligand set.

6.4 Use of a *cyclo*-P₄ tantalum complex for synthesis of spherical molecules

In light of the previous synthesis of supramolecular assemblies of the type $[\{Cp^xFe(\mu, \eta^5: \eta^1: \eta^1: \eta^1: \eta^1: \eta^1-P_5)\}_{12}\{CuX\}_{10}\{Cu_2X_3\}_5\{Cu(CH_3CN)_2\}_5]$ ($X = Cl, Br$) with P₅-ligand complexes, investigations into preparing related assemblies with the P₄-ligand complex $[Cp''Ta(CO)_2(\eta^4-P_4)]$ (**18**) were carried out. In reactions of **18** with CuX ($X = Cl, Br, I$), spherical molecules of the type $[\{Cp''Ta(CO)_2(\mu, \eta^4: \eta^1: \eta^1: \eta^1: \eta^1-P_4)\}_6\{CuX\}_8]$ (**19a-c**) were isolated and structurally characterized for $X = Cl, Br$. The structures of **19a,b** reveal an exclusively inorganic inner P/Cu-core possessing 32 atoms. The inner cores of **19a,b** represent a fullerene-type geometry of alternating four- and six-membered rings and exhibit distorted O_h symmetry in the solid-state.



Scheme 16: Synthesis of spherical assemblies **19a,b** from $[\text{Cp}''\text{Ta}(\text{CO})_2(\eta^4\text{-P}_4)]$ and copper(I) halides.

These investigations have shown that $[\text{Cp}''\text{Ta}(\text{CO})_2(\eta^4\text{-P}_4)]$ can be employed in the coordination chemistry with copper(I) halides for the assembly of inorganic, spherical molecules, thus producing a novel 32-atom core. The use of the P_4 -ring ligands offers a stable source of four-membered rings for the formation of such structures where no precedence has been found for carbon in forming high-symmetry structures bearing four-membered rings. Initial investigations in this work have also shown evidence for the existence of $[\{\text{Cp}''\text{Ta}(\text{CO})_2(\mu, \eta^4: \eta^1: \eta^1: \eta^1: \eta^1\text{-P}_4)\}_6\{\text{CuI}\}_8]$ (**19c**), which would represent the first spherical P_n -ligand coordination assembly incorporating CuI.

7 Appendices

A.1 Directory of abbreviations

1D, 2D, 3D	One-, two-, three-dimensional	
Adogen 464	Methyltrialkyl(C ₈ -C ₁₀)ammonium chloride	
Aliquat 336	Methyltrialkyl(C ₈)ammonium chloride	
Ar	Aryl group	
ax	Axial position	
BAr ^F ₃	Tris(perfluorophenyl)borane	B(C ₆ F ₅) ₃
bpy	2,2'-Bipyridine	
<i>i</i> Bu	<i>iso</i> -Butyl	-CH ₂ CH(CH ₃) ₂
<i>n</i> Bu, Bu	<i>n</i> -Butyl	-CH ₂ CH ₂ CH ₂ CH ₃
<i>t</i> Bu	<i>tert</i> -Butyl	-C(CH ₃) ₃
Bz	Benzyl	-CH ₂ C ₆ H ₅
CN	Coordination number	
Cp	Cyclopentadienyl	η^5 -C ₅ H ₅
Cp'	<i>tert</i> -Butylcyclopentadienyl	η^5 - <i>t</i> BuC ₅ H ₄
Cp''	1,3-Di- <i>tert</i> -butylcyclopentadienyl	η^5 -1,3- <i>t</i> Bu ₂ C ₅ H ₃
Cp'''	1,2,4-Tri- <i>tert</i> -butylcyclopentadienyl	η^5 -1,2,4- <i>t</i> Bu ₃ C ₅ H ₂
Cp*	Pentamethylcyclopentadienyl	η^5 -C ₅ (CH ₃) ₅
Cp ^x	Any cyclopentadienyl ligand, as specified in text	
Cy	Cyclohexyl	-C ₆ H ₁₁
δ	Chemical shift	
Δv _{1/2}	Half-width	
DBU	1,8-Diazabicyclo[5.4.0]undec-7-ene	
DME	1,2-Dimethoxyethane	MeOCH ₂ CH ₂ OMe
DMF	Dimethylformamide	(CH ₃) ₂ NCHO
E	Main-group element, as specified in text	
EI-MS	Electron-ionization mass spectrometry	
ESI-MS	Electrospray ionization mass spectrometry	
Et	Ethyl	-CH ₂ CH ₃
eq	Equatorial position	
FD-MS	Field desorption mass spectrometry	

Fp	Dicarbonyl(η^5 -cyclopentadienyl)iron	$-(\text{CO})_2\text{CpFe}$
FT	Fourier transform	
HOMO	Highest occupied molecular orbital	
Hz	Hertz	
IR	Infrared	
J	Coupling constant	
L	Ligand	
L'H ₃	tris(2-hydroxy-3,5-dimethylbenzyl)amine	
L*H ₃	tris(2-hydroxy-3- <i>tert</i> -butyl-5-methylbenzyl)amine	
LUMO	Lowest unoccupied molecular orbital	
M	Metal atom	
Me	Methyl	$-\text{CH}_3$
Mes	Mesityl, 2,4,6-trimethylphenyl	$-2,4,6\text{-Me}_3\text{C}_6\text{H}_2$
Mes*	Supermesityl, 2,4,6-tri- <i>tert</i> -butylphenyl	$-2,4,6\text{-}t\text{Bu}_3\text{C}_6\text{H}_2$
ML _n	Transition-metal fragment	
$\tilde{\nu}_{\text{XY}}$	Infrared stretching frequency, between atoms X-Y	
NMR	Nuclear magnetic resonance	
N ₃ N	Tris(2-(trimethylsilylamido)ethylene)amine	$(\text{Me}_3\text{SiNCH}_2\text{CH}_2)_3\text{N}$
Np	Neopentyl	$-\text{CH}_2\text{C}(\text{CH}_3)_3$
OTf	Trifluoromethanesulfonate, triflate	$-\text{O}_3\text{SCF}_3$
Ph	Phenyl	$-\text{C}_6\text{H}_5$
Ph*	2,6-Bis-(2,4,6-tri- <i>iso</i> -propylphenyl)phenyl	$-2,6\text{-Trip}_2\text{-C}_6\text{H}_3$
PMDETA	Pentamethyldiethylenetriamine	$(\text{Me}_2\text{NCH}_2\text{CH}_2)_2\text{NMe}$
ppm	Parts per million	
<i>i</i> Pr	<i>iso</i> -Propyl	$-\text{CH}(\text{CH}_3)_2$
py	Pyridine	$\text{C}_5\text{H}_5\text{N}$
R	Organic group	
X	Halogen/halide or pseudohalide	
THF	Tetrahydrofuran	$\text{C}_4\text{H}_8\text{O}$
TM	Transition metal	
TMEDA	Tetramethylethylenediamine	$\text{Me}_2\text{NCH}_2\text{CH}_2\text{NMe}_2$
<i>p</i> -TsOH	<i>para</i> -Toluenesulfonic acid	$\text{C}_7\text{H}_7\text{SO}_3\text{H}$
TREN	Tris(2-amidoethylene)amine ligand set	$(\text{RNCH}_2\text{CH}_2)_3\text{N}$
Trip	2,4,6-Tri- <i>iso</i> -propylphenyl	$-2,4,6\text{-}i\text{Pr}_3\text{C}_6\text{H}_2$

A.1.1 NMR abbreviations

br	broad
s	singlet
d	doublet
t	triplet
q	quartet
sept	septet
m	multiplet

Combinations of multiplicity symbols are also used, such as “dt” for “doublet of triplets”

A.1.2 IR abbreviations

br	broad
w	weak
m	medium
s	strong
vs	very strong
sh	shoulder

A.2 Directory of compounds

- 1 $[\text{H}_3\text{PW}(\text{CO})_5]$
- 2 $[\text{H}(\text{Me}_3\text{Si})_2\text{PW}(\text{CO})_5]$
- 3 $[(\text{Me}_3\text{Si})_3\text{PW}(\text{CO})_5]$
- 4 $[\text{Fp}_2\text{Sn}\{\text{PH}_2\text{W}(\text{CO})_5\}_2]$
- 5 $[\text{Fp}_2\text{Sn}\{\text{P}(\text{SiMe}_3)_2\}_2]$
- 6 $[\text{Fp}_4\text{Sn}]$
- 7 $\text{Ph}^*\text{SnP}(\text{SiMe}_3)_2$
- 8 Ph^*Br
- 9 $\text{Ph}^*\text{SnP}(\text{H})\text{Trip}$
- 10 $\text{Li}^+[\text{Ph}^*\text{SnPTrip}]^-$
- 11 $[\text{Ph}^*\text{Sn}\{\text{W}(\text{CO})_5\}(\mu\text{-O})_2\text{SnPh}^*]$
- 12 $\text{Ph}^*\text{Sn}(\text{OSiMe}_3)_2\text{Cl}$
- 13 $[\text{Ph}^*\text{Sn}(\mu\text{-O})\text{Cl}]_2$

- 14a** Ph^*SnCl_3
14b Ph^*SnBr_3
15 $[\text{L}^*\text{TaCl}_2]$
16a $[\text{L}^*\text{Ta}(\text{Cl})\text{P}(\text{SiMe}_3)_2]$
16b $[\text{L}^*\text{Ta}(\text{Cl})\text{As}(\text{SiMe}_3)_2]$
17 $[\text{L}^*\text{TaMe}_2]$
18 $[\text{Cp}''\text{Ta}(\text{CO})_2(\eta^4\text{-P}_4)]$
19a $[\{\text{Cp}''\text{Ta}(\text{CO})_2(\mu, \eta^4: \eta^1: \eta^1: \eta^1: \eta^1\text{-P}_4)\}_6\{\text{CuCl}\}_8]$
19b $[\{\text{Cp}''\text{Ta}(\text{CO})_2(\mu, \eta^4: \eta^1: \eta^1: \eta^1: \eta^1\text{-P}_4)\}_6\{\text{CuBr}\}_8]$
19c $[\{\text{Cp}''\text{Ta}(\text{CO})_2(\mu, \eta^4: \eta^1: \eta^1: \eta^1: \eta^1\text{-P}_4)\}_6\{\text{CuI}\}_8]$

A.3 Literature Cited

- [1] M. Regitz, P. Binger, *Multiple Bonds and Low Coordination in Phosphorus Chemistry* (Eds. M. Regitz, O. J. Scherer), New York: Thieme, **1990**.
- [2] a) M. Scheer, *Coord. Chem. Rev.* **1997**, *163*, 271; b) B. P. Johnson, G. Balázs, M. Scheer, *Top. Curr. Chem.* **2004**, *232*, 1; c) B. P. Johnson, G. Balázs, M. Scheer, *Coord. Chem. Rev.* **2006**, in press.
- [3] a) O. J. Scherer, *Angew. Chem.* **1990**, *102*, 1137, *Angew. Chem. Int. Ed.* **1990**, *29*, 1104; b) K. H. Whitmire, *Adv. Organomet. Chem.* **1998**, *42*, 1.
- [4] O. J. Scherer, *Acc. Chem. Res.* **1999**, *32*, 751.
- [5] K. B. Dillon, F. Mathey, J. F. Nixon, *Phosphorus: The Carbon Copy*, New York: Wiley, **1998**.
- [6] S. Weinrich, H. Piotrowski, M. Vogt, A. Schulz, M. Westerhausen, *Inorg. Chem.* **2004**, *43*, 3756.
- [7] a) U. Vogel, Dissertation, Universität Karlsruhe, 2001; b) U. Vogel, A. Y. Timoshkin, M. Scheer, *Angew. Chem.* **2001**, *113*, 4541, *Angew. Chem. Int. Ed.* **2001**, *40*, 4409; c) U. Vogel, P. Hoemensch, K.-C. Schwan, A. Y. Timoshkin, M. Scheer, *Chem. Eur. J.* **2003**, *9*, 515; d) U. Vogel, K.-C. Schwan, M. Scheer, *Eur. J. Inorg. Chem.* **2004**, 2062.
- [8] M. Driess, C. Monsé, *Z. Anorg. Allg. Chem.* **2000**, *626*, 1091.
- [9] W.-W. du Mont, H. J. Kroth, *Angew. Chem.* **1977**, *89*, 832, *Angew. Chem. Int. Ed.* **1977**, *16*, 792; b) W.-W. du Mont, M. Grenz, *Chem. Ber.* **1985**, *118*, 1045.
- [10] A. M. Arif, A. H. Cowley, R. A. Jones, J. M. Power, *J. Chem. Soc., Chem. Commun.* **1986**, 1446.
- [11] A. H. Cowley, D. M. Giolando, R. A. Jones, C. M. Nunn, J. M. Power, W.-W. du Mont, *Polyhedron* **1988**, *7*, 1317.
- [12] R. W. Chorley, P. B. Hitchcock, B. S. Jolly, M. F. Lappert, G. A. Lawless, *J. Chem. Soc., Chem. Commun.* **1991**, 1302.
- [13] S. P. Constantine, G. M. De Lima, P. B. Hitchcock, J. M. Keates, G. A. Lawless, I. Marziano, *Organometallics* **1997**, *16*, 793.
- [14] S. C. Goel, M. Y. Chiang, W. E. Buhro, *J. Am. Chem. Soc.* **1990**, *112*, 5636.
- [15] S. C. Goel, M. A. Matchett, D. Cha, M. Y. Chiang, W. E. Buhro, *Phosphorus, Sulfur, and Silicon* **1993**, *76*, 289.
- [16] S. C. Goel, M. Y. Chiang, D. J. Rauscher, W. E. Buhro, *J. Am. Chem. Soc.* **1993**, *115*, 160.

- [17] M. Matchett, M. Y. Chiang, W. E. Buhro, *Inorg. Chem.* **1994**, 33, 1109.
- [18] M. Driess, R. Janoschek, H. Pritzkow, S. Rell, U. Winkler, *Angew. Chem.* **1995**, 107, 1746, *Angew. Chem. Int. Ed.* **1995**, 34, 1614.
- [19] M. Driess, S. Martin, K. Merz, V. Pintchouk, H. Pritzkow, H. Grützmacher, M. Kaupp, *Angew. Chem.* **1997**, 109, 1982, *Angew. Chem. Int. Ed.* **1997**, 36, 1894.
- [20] M. Westerhausen, M. Krofta, N. Wiberg, J. Knized, H. Nöth, A. Pfitzner, Z. *Naturforsch.* **1998**, 53b, 1489.
- [21] D. Nikolova, C. von Hänisch, A. Adolf, *Eur. J. Chem.* **2004**, 2321.
- [22] M. Westerhausen, W. Schwarz, Z. *Anorg. Allg. Chem.* **1996**, 622, 903.
- [23] R. E. Allen, M. A. Beswick, N. L. Cromhout, M. A. Paver, P. R. Raithby, M. Trevithick, D. S. Wright, *J. Chem. Soc., Chem. Commun.* **1996**, 1501.
- [24] A. D. Bond, A. Rothenberger, A. D. Woods, D. S. Wright, *J. Chem. Soc., Chem. Commun.* **2001**, 525.
- [25] P. Alvarez-Bercedo, A. D. Bond, R. Haigh, A. D. Hopkins, G. T. Lawson, M. McPartlin, D. Moncrieff, M. E. Gonzalez Mosquera, J. M. Rawson, A. D. Woods, D. S. Wright, *J. Chem. Soc., Chem. Commun.* **2003**, 1288.
- [26] M. McPartlin, A. D. Woods, C. M. Pask, T. Vogler, D. S. Wright, *J. Chem. Soc., Chem. Commun.* **2003**, 1524.
- [27] P. Jutzi, *Angew. Chem.* **1975**, 87, 269, *Angew. Chem. Int. Ed.* **1975**, 14, 232.
- [28] a) P. P. Power, *J. Chem. Soc., Dalton Trans.* **1998**, 18, 2939; b) P. P. Power, *Chem. Rev.* **1999**, 99, 3463.
- [29] G. Becker, Z. *Anorg. Allg. Chem.* **1976**, 423, 242.
- [30] G. Becker, G. Gutekunst, *Angew. Chem.* **1977**, 89, 477, *Angew. Chem. Int. Ed.* **1977**, 16, 463.
- [31] L. Weber, *Chem. Ber.* **1996**, 129, 367.
- [32] a) P. B. Hitchcock, C. Jones, J. F. Nixon, *Angew. Chem.* **1995**, 107, 522, *Angew. Chem. Int. Ed.* **1995**, 34, 492; b) C. Jones, J. W. Steed, R. C. Thomas, *J. Chem. Soc. Dalton Trans.* **1999**, 1541; c) J. Durkin, D. F. Hibbs, P. B. Hitchcock, M. B. Hursthouse, C. Jones, J. Jones, K. M. Malik, J. F. Nixon, G. Parry, *J. Chem. Soc. Dalton Trans.* **1996**, 3277; d) P. C. Andrews, C. L. Ratson, B. W. Skelton, A. H. White, *J. Chem. Soc., Chem. Commun.* **1997**, 1183; e) P. C. Andrews, J. E. McGrady, P. J. Nichols, *Organometallics* **2004**, 23, 446.
- [33] M. Driess, S. Rell, H. Pritzkow, *J. Chem. Soc., Chem. Commun.* **1995**, 253.

- [34] Some examples: a) A. M. Arif, A. Barron, A. H. Cowley, S. W. Hall, *J. Chem. Soc., Chem. Commun.* **1988**, 171; b) G. Becker, M. Bohringer, R. Gleiter, K.-H. Pfeifer, J. Grobe, D. LeVan, M. Hegemann, *Chem. Ber.* **1994**, 127, 1041; c) G. Becker, K. Hubler, *Z. Anorg. Allg. Chem.* **1994**, 620, 405; d) G. Becker, W. Schwarz, N. Seidler, M. Westerhausen, *Z. Anorg. Allg. Chem.* **1992**, 612, 72.
- [35] G. Märkl, H. Sejpka, *Angew. Chem.* **1986**, 98, 286, *Angew. Chem. Int. Ed.* **1986**, 25, 264.
- [36] M. Finze, E. Bernhardt, H. Willner, C. W. Lehmann, *Angew. Chem.* **2004**, 116, 4254; *Angew. Chem. Int. Ed.* **2004**, 43, 4160.
- [37] a) C. N. Smit, F. M. Lock, F. Bickelhaupt, *Tetrahedron Lett.* **1984**, 25, 3011; b) C. N. Smit, F. Bickelhaupt, *Organometallics* **1987**, 6, 1156; c) E. Niecke, E. Klein, M. Nieger, *Angew. Chem.* **1989**, 101, 792, *Angew. Chem. Int. Ed.* **1989**, 28, 751.
- [38] a) J. Escudié, C. Couret, J. Satgé, M. Andrianarison, J. D. Andriamizaka, *J. Am. Chem. Soc.* **1985**, 107, 3378; b) H. Ranaivonjatovo, J. Escudié, C. Couret, J. Satgé, M. Dräger, *New. J. Chem.* **1989**, 13, 389; c) H. Ranaivonjatovo, J. Escudié, C. Couret, J. Satgé, *J. Organometal. Chem.* **1991**, 415, 327.
- [39] a) M. Driess, *Angew. Chem.* **1991**, 103, 979, *Angew. Chem. Int. Ed.* **1991**, 30, 1022; b) M. Driess, U. Winkler, W. Imhof, L. Zsolnai, G. Huttner, *Chem. Ber.* **1994**, 127, 1031.
- [40] a) M. Driess, H. Pritzkow, S. Rell, U. Winkler, *Organometallics* **1996**, 15, 1845; b) M. Driess, R. Janoschek, *J. Mol. Struct. (Theochem.)* **1994**, 313, 129.
- [41] C. Couret, J. D. Andriamizaka, J. Escudié, J. Satgé, *J. Organomet. Chem.* **1981**, 208, C3.
- [42] C. Couret, J. Escudié, J. Satgé, A. Raharinirina, J. D. Andriamizaka, *J. Am. Chem. Soc.* **1985**, 107, 8280.
- [43] H. Ranaivonjatovo, J. Escudié, C. Couret, J. Satgé, *J. Chem. Soc., Chem. Commun.* **1992**, 1047.
- [44] a) J. Escudié, C. Couret, A. Raharinirina, *New. J. Chem.* **1987**, 11, 627; b) A. Kandri-Rodi, H. Ranaivonjatovo, J. Escudié, *Organometallics* **1994**, 13, 2787; c) A. Kandri-Rodi, J.-P. Declercq, A. Dubourg, H. Ranaivonjatovo, J. Escudié, *Organometallics* **1995**, 14, 1954.
- [45] A. S. Ionkin, W. J. Marshall, *Organometallics* **2003**, 22, 4136.
- [46] a) B. Twamley, P. P. Power, S. Haubrich, *Adv. Organomet. Chem.* **1999**, 44, 1; b) P. P. Power, *J. Organomet. Chem.* **2004**, 689, 3904.

- [47] T. Nguyen, A. D. Sutton, M. Brynda, J. C. Fettinger, G. J. Long, P. P. Power, *Science* **2005**, *310*, 844.
- [48] J. A. C. Clyburne, N. McMullen, *Coord. Chem. Rev.* **2000**, *210*, 73.
- [49] a) X.-W. Li, W. T. Pennington, G. H. Robinson, *J. Am. Chem. Soc.* **1995**, *117*, 7578; b) X.-W. Li, Y. Xie, P. R. Schreiner, K. D. Gripper, R. C. Crittendon, C. F. Campana, H. F. Schaefer, III, G. H. Robinson, *Organometallics* **1996**, *15*, 3798; c) J. Su, X.-W. Li, R. C. Crittendon, G. H. Robinson, *J. Am. Chem. Soc.* **1997**, *119*, 5471; d) Y. Xie, P. R. Schreiner, H. F. Schaefer, III, X.-W. Li, G. H. Robinson, *J. Am. Chem. Soc.* **1996**, *118*, 10635; e) Y. Xie, R. S. Grev, J. Gu, H. F. Schaefer, III, P. v. R. Schleyer, J. Su, X.-W. Li, G. H. Robinson, *J. Am. Chem. Soc.* **1998**, *120*, 3773; f) G. H. Robinson, *Acc. Chem. Res.* **1999**, *32*, 773.
- [50] a) R. J. Wehmschulte, P. P. Power, *Angew. Chem.* **1998**, *110*, 3344, *Angew. Chem. Int. Ed.* **1998**, *37*, 3152; b) B. Twamley, P. P. Power, *Angew. Chem.* **2000**, *112*, 3643, *Angew. Chem. Int. Ed.* **2000**, *39*, 3500; c) N. J. Hardman, R. J. Wright, A. D. Phillips, P. P. Power, *Angew. Chem.* **2002**, *114*, 2966, *Angew. Chem. Int. Ed.* **2002**, *41*, 2842; d) N. J. Hardman, R. J. Wright, A. D. Phillips, P. P. Power, *J. Am. Chem. Soc.* **2003**, *125*, 2667.
- [51] a) M. M. Olmstead, R. S. Simons, P. P. Power, *J. Am. Chem. Soc.* **1997**, *119*, 11705; b) L. Pu, M. O. Senge, M. M. Olmstead, P. P. Power, *J. Am. Chem. Soc.* **1998**, *120*, 12682; c) L. Pu, S. T. Haubrich, P. P. Power, *J. Organomet. Chem.* **1999**, *582*, 100; d) L. Pu, B. Twamley, P. P. Power, *J. Am. Chem. Soc.* **2000**, *122*, 3524; e) A. D. Phillips, R. J. Wright, M. M. Olmstead, P. P. Power, *J. Am. Chem. Soc.* **2002**, *124*, 5930; f) M. Stender, A. D. Phillips, R. J. Wright, P. P. Power, *Angew. Chem.* **2002**, *114*, 1863, *Angew. Chem. Int. Ed.* **2002**, *41*, 1785; g) P. P. Power, *J. Chem. Soc., Chem. Commun.* **2003**, 2091; h) L. Pu, A. D. Phillips, A. F. Richards, M. Stender, R. S. Simons, M. M. Olmstead, P. P. Power, *J. Am. Chem. Soc.* **2003**, *125*, 11626.
- [52] W. Setaka, K. Hirai, H. Tomioka, K. Sakamoto, M. Kira, *J. Am. Chem. Soc.* **2004**, *126*, 2696.
- [53] B. Twamley, P. P. Power, *J. Chem. Soc., Chem. Commun.* **1998**, 1979.
- [54] R. C. Smith, P. Gantzel, A. L. Rheingold, J. D. Protasiewicz, *J. Am. Chem. Soc.* **2003**, *125*, 40.
- [55] Y.-H. Hu, M.-D. Su, *Chem. Phys. Lett.* **2003**, *378*, 289.

- [56] a) S. Blaurock, E. Hey-Hawkins, *Z. Anorg. Allg. Chem.* **2002**, 628, 2515; b) T. Hocher, S. Blaurock, E. Hey-Hawkins, *Eur. J. Inorg. Chem.* **2002**, 1174; c) S. Chaudhury, S. Blaurock, E. Hey-Hawkins, *Eur. J. Inorg. Chem.* **2001**, 2587; d) U. Segerer, S. Blaurock, J. Sieler, E. Hey-Hawkins, *J. Organomet. Chem.* **2000**, 608, 21.
- [57] M Driess, J. Aust, K. Merz, *Eur. J. Inorg. Chem.* **2002**, 2961.
- [58] L Weber, U. Sonnerberg, *Chem. Ber.* **1991**, 124, 725.
- [59] a) H. Schäfer, W. Leske, *Z. Anorg. Allg. Chem.* **1987**, 552, 50; b) H. Schäfer, *Z. Anorg. Allg. Chem.* **1980**, 467, 105.
- [60] a) A. H. Cowley, A. R. Barron, *Acc. Chem. Res.* **1988**, 21, 81; b) A. H. Cowley, *Acc. Chem. Res.* **1997**, 30, 445.
- [61] a) P. B. Hitchcock, M. F. Lappert, W.-P. Leung, *J. Chem. Soc., Chem. Commun.* **1987**, 1282; b) P. Bohra, P. B. Hitchcock, M. F. Lappert, W.-P. Leung, *Polyhedron* **1989**, 8, 1184.
- [62] a) J. B. Bonanno, P. T. Wolczanski, E. B. Lobkovsky, *J. Am. Chem. Soc.* **1994**, 116, 11159; b) P. T. Wolczanski, *Polyhedron* **1995**, 14, 3335.
- [63] C. C. Cummins, R. R. Schrock, W. M. Davis, *Angew. Chem.* **1993**, 105, 758, *Angew. Chem. Int. Ed.* **1993**, 32, 756.
- [64] J. S. Freundlich, R. R. Schrock, W. M. Davis, *J. Am. Chem. Soc.* **1996**, 118, 3643.
- [65] a) M. Scheer, C. Troitzsch, P.G. Jones, *Angew. Chem.* **1992**, 104, 1395, *Angew. Chem. Int. Ed.* **1992**, 31, 1377; b) M. Scheer, C. Troitzsch, L. Hilfert, M. Dargatz, E. Kleinpeter, P.G. Jones, J. Sieler, *Chem. Ber.* **1995**, 128, 251; c) M. Scheer, U. Becker, M.H. Chisholm, J.C. Huffman, *J. Organomet. Chem.* **1993**, 461, C1.
- [66] M. Ehse, A. Romerosa, M. Peruzzini, *Top. Curr. Chem.* **2002**, 220, 107.
- [67] O. J. Scherer, H. Sitzmann, G. Wolmershäuser, *J. Organomet. Chem.* **1984**, 268, C9.
- [68] a) C. A. Ghilardi, S. Midollini, A. Orlandini, L. Sacconi, *Inorg. Chem.* **1980**, 19, 301; b) C. Bianchini, C. Mealli, A. Meli, L. Sacconi, *Inorg. Chim. Acta* **1979**, 37, L543.
- [69] O. J. Scherer, T. Brück, *Angew. Chem.* **1987**, 99, 59, *Angew. Chem. Int. Ed.* **1987**, 26, 59.
- [70] a) P. J. Stang, B. Olenyuk, *Acc. Chem. Res.* **1997**, 30, 502; b) D. Braga, F. Grepioni, G. R. Desiraju, *Chem. Rev.* **1998**, 98, 1375; c) O. M. Yaghi, H. Li, C. Davis, D. Richardson, T. L. Groy, *Acc. Chem. Res.* **1998**, 31, 474; d) P. F. H. Schwab, M. D. Levin, J. Michl, *Chem. Rev.* **1999**, 99, 1863; e) S. Leininger, B. Olenyuk, P. J. Stang, *Chem. Rev.* **2000**, 100, 853.

- [71] a) M. Di Vaira, M. P. Ehses, M. Peruzzini, P. Stoppioni, *Polyhedron* **1999**, 18, 2331;
b) M. Di Vaira, P. Stoppioni, M. Peruzzini, *J. Chem. Soc., Dalton Trans.* **1990**, 109.
- [72] M. F. Cecconi, C. A. Ghilardi, S. Midollini, A. Orlandini, *J. Chem. Soc., Chem. Commun.* **1982**, 229.
- [73] a) J. Bai, E. Leiner, M. Scheer, *Angew. Chem.* **2002**, 114, 820, *Angew. Chem. Int. Ed.* **2002**, 41, 783; M. Scheer, L. Gregoriades, J. Bai, M. Sierka, G. Brunklaus, H. Eckert, *Chem. Eur. J.* **2005**, 11, 2163.
- [74] J. Bai, A. V. Virovets, M. Scheer, *Angew. Chem.* **2002**, 114, 1808, *Angew. Chem. Int. Ed.* **2002**, 41, 1737.
- [75] J. Bai, A. V. Virovets, M. Scheer, *Science* **2003**, 300, 781.
- [76] M. Scheer, J. Bai, B. P. Johnson, R. Merkle, A. V. Virovets, C. E. Anson, *Eur. J. Inorg. Chem.* **2005**, 4023.
- [77] a) A. Marinetti, S. Bauer, L. Ricard, F. Mathey, *Organometallics* **1990**, 9, 793; b) F. Mercier, F. Mathey, C. Afiong-Akpan, J. Nixon, *J. Organomet. Chem.* **1988**, 348, 361; c) F. Mercier, F. Mathey, *Tetrahedron Lett.* **1986**, 27, 1323; d) F. Mercier, F. Mathey, *Tetrahedron Lett.* **1985**, 26, 1717; e) F. Mercier, F. Mathey, *J. Chem. Soc., Chem. Commun.* **1984**, 782; f) B. Deschamps, F. Mathey, *Phosphorus and Sulfur* **1983**, 17, 317.
- [78] F. Nief, F. Mercier, F. Mathey, *J. Organomet. Chem.* **1987**, 328, 349.
- [79] S. J. Archer, K. R. Koch, S. Schmidt, *Inorg. Chim. Acta* **1987**, 126, 209.
- [80] a) W.-W. du Mont, *J. Organomet. Chem.* **1977**, 131, C37; b) W.-W. du Mont, B. Neudert, *Chem. Ber.* **1978**, 111, 2267; c) W.-W. du Mont, J. L. Lefferts, J. J. Zuckerman, *J. Organomet. Chem.* **1979**, 166, 347.
- [81] a) W.-W. du Mont, *J. Organomet. Chem.* **1978**, 153, C11; b) W.-W. du Mont, H. J. Kroth, *Z. Naturforsch.* **1980**, 35b, 700.
- [82] W. Uhlig, A. Tzschach, *Z. Anorg. Allg. Chem.* **1989**, 576, 281.
- [83] H. Schäfer, H.; W. Leske, *Z. Anorg. Allg. Chem.* **1987**, 550, 57.
- [84] a) H. Schumann, L. Rösch, H.-J. Kroth, J. Pickardt, H. Neumann, B. Neudert, *Z. Anorg. Allg. Chem.* **1977**, 430, 51; b) H. Schumann, O. Stelzer, J. Kuhlmei, U. Niederreuther, *Chem. Ber.* **1971**, 104, 993.
- [85] M. J. Aroney, I. E. Buys, M. S. Davies, T. W. Hambley, *J. Chem. Soc., Dalton Trans.* **1994**, 2827.
- [86] U. Vogel, M. Scheer, *Z. Anorg. Allg. Chem.* **2001**, 627, 1593.

- [87] Some examples: a) D. Dakternieks, C. L. Rolls, *Inorg. Chim. Acta* **1989**, 161, 105; b) D. Hänssgen, E. Stahlhut, H. Aldenhoven, A. Dörr, *J. Organomet. Chem.* **1992**, 425, 19; c) R. Martens, W.-W. du Mont, J. Jeske, P. G. Jones, W. Saak, S. Pohl, *J. Organomet. Chem.* **1995**, 501, 251.
- [88] D. Hänssgen, H. Aldenhoven, *Chem. Ber.* **1990**, 123, 1833.
- [89] D. Hänssgen, H. Aldenhoven, M. Nieger, *Chem. Ber.* **1990**, 123, 1837.
- [90] Isotope abundances for NMR active tungsten and tin nuclei: ^{183}W (14.3%), ^{119}Sn (8.6%), ^{117}Sn (7.7%); *CRC Handbook of Chemistry and Physics*, 79th Ed. (Ed. D. R. Lide), CRC Press: Boca Raton, FL, 1998.
- [91] H. Schumann, H.-J. Kroth, *Z. Naturforsch.* **1977**, 32b, 876.
- [92] A. K. Rodi, H. Ranaivonjatovo, J. Escudié, A. Kerbal, *Phosphorus, Sulfur, and Silicon* **1997**, 126, 157.
- [93] M. J. Hampden-Smith, D. Lei, E. Duesler, *J. Chem. Soc., Dalton Trans.* **1990**, 2953.
- [94] J. E. O'Connor, E. R. Corey, *Inorg. Chem.* **1967**, 6, 968.
- [95] Only one example resulted from multiple SciFinder searches: C. Jones, A. F. Richards, *J. Chem. Soc., Dalton Trans.* **2000**, 3233.
- [96] H. Schumann, H.-J. Kroth, *Z. Naturforsch.* **1977**, 32b, 513.
- [97] F. Lindenberg, E. Hey-Hawkins, *J. Organomet. Chem.* **1992**, 435, 291.
- [98] E. Hey-Hawkins, F. Lindenberg, *Organometallics* **1994**, 13, 4643.
- [99] K. Merzweiler, L. Weisse, *Z. Naturforsch.* **1990**, 45b, 971.
- [100] M. Moll, H. Behrens, P. Merbach, K. Görting, G. Liehr, R. Böhme, *Z. Naturforsch.* **1980**, 35b, 1115.
- [101] a) J. R. Chipperfield, S. Clark, D. E. Webster, H. Yusof, *J. Organomet. Chem.* **1991**, 421, 205; b) D. J. Patmore, W. A. G. Graham, *Inorg. Chem.* **1966**, 5, 2222.
- [102] P. B. Hitchcock, M. F. Lappert, M. J. McGeary, *Organometallics* **1990**, 9, 884.
- [103] a) J. R. Chipperfield, D. E. Webster, H. Yusof, *J. Organomet. Chem.* **1992**, 434, 53; b) D. J. Patmore, W. A. G. Graham, *Inorg. Chem.* **1968**, 7, 771.
- [104] P. Hackett, A. R. Manning, *J. Chem. Soc., Dalton Trans.* **1974**, 20, 2257.
- [105] G. Schmid, G. Etzrodt, *J. Organomet. Chem.* **1977**, 131, 477.
- [106] R. Karl-Bernhard, S. Pellegrini, A. Mortreux, E. Monflier, *J. Organomet. Chem.* **1995**, 486, 123.

- [107] Reviews of synthetic approaches to Ge=E multiple bonds (E = CR, NR, O, S, Se, Te):
a) J. Escudié, C. Couret, H. Ranaivonjatovo, J. Satgé, *Coord. Chem. Rev.* **1994**, *130*, 427; b) J. Barrau, G. Rima, *Coord. Chem. Rev.* **1998**, *178–180*, 593.
- [108] G. Ossig, A. Meller, S. Freitag, R. Herbst-Irmer, *J. Chem. Soc., Chem. Commun.* **1993**, 497.
- [109] B. E. Eichler, L. Pu, M. Stender, P. P. Power, *Polyhedron* **2001**, *20*, 551.
- [110] M. Weidenbruch, *J. Organomet. Chem.* **2002**, *646*, 39.
- [111] B. Schiemenz, P. P. Power, *Organometallics* **1996**, *15*, 958.
- [112] C.-J. F. Du, H. Hart, K.-K. D. Ng, *J. Org. Chem.* **1986**, *51*, 3162.
- [113] R. Bolton, J. P. B. Sandall, *J. Chem. Soc., Perkin Trans. 2* **1977**, 278.
- [114] B. E. Eichler, B. L. Phillips, P. P. Power, M. P. Augustine, *Inorg. Chem.* **2000**, *39*, 5450.
- [115] L. Pu, M. M. Olmstead, P. P. Power, *Organometallics* **1998**, *17*, 5602.
- [116] B. E. Eichler, P. P. Power, *Inorg. Chem.* **2000**, *39*, 5444.
- [117] B. E. Eichler, A. D. Phillips, S. T. Haubrich, B. V. Mork, P. P. Power, *Organometallics* **2002**, *21*, 5622.
- [118] B. E. Eichler, A. D. Phillips, P. P. Power, *Organometallics* **2003**, *22*, 5423.
- [119] P. Kircher, G. Huttner, K. Heinze, *J. Organomet. Chem.* **1998**, *562*, 217.
- [120] M. Regitz, P. Binger, *Angew. Chem.* **1988**, *100*, 1541, *Angew. Chem. Int. Ed.* **1988**, *27*, 1484.
- [121] M. F. Lappert, P. P. Power, *J. Chem. Soc. Dalton Trans.* **1985**, 51.
- [122] M. F. Lappert, M. C. Misra, M. Onyszchuk, R. S. Rowe, P. P. Power, M. J. Slade, *J. Organomet. Chem.* **1987**, *330*, 31.
- [123] P. B. Hitchcock, H. A. Jasim, M. F. Lappert, W.-P. Leung, A. K. Rai, R. E. Taylor, *Polyhedron* **1991**, *10*, 1203.
- [124] B. Twamley, N. J. Hardman, P. P. Power, *Acta Cryst.* **2000**, *C56*, E514.
- [125] N.C. Zanetti, R.R. Schrock, W.M. Davis, *Angew. Chem.* **1995**, *107*, 2184, *Angew. Chem. Int. Ed.* **1995**, *34*, 2044.
- [126] N.C. Mösch-Zanetti, R.R. Schrock, W.M. Davis, K. Wanninger, S.W. Seidel, M.B. O'Donoghue, *J. Am. Chem. Soc.* **1997**, *119*, 11037.
- [127] a) M. Baudler, B. Carlsohn, D. Koch, P. K. Medda, *Chem. Ber.* **1978**, *111*, 1210; b) J.-P. Albrand, J.-B. Robert, *J. Chem. Soc., Chem. Commun.* **1976**, 876.

- [128] T. Koch, S. Blaurock, F. B. Somoza Jr., A. Voigt, R. Kirmse, E. Hey-Hawkins, *Organometallics* **2000**, *19*, 2556.
- [129] R. Felsberg, S. Blaurock, P. C. Junk, R. Kirmse, A. Voigt, E. Hey-Hawkins, *Z. Anorg. Allg. Chem.* **2004**, *630*, 806.
- [130] a) M. Driess, *Chemie in unserer Zeit* **1993**, *27*, 141; b) M. Yoshifuji, I. Shima, N. Inamoto, K. Hirotsu, T. Higuchi, *J. Am. Chem. Soc.* **1981**, *103*, 4587; c) A. H. Cowley, *Polyhedron* **1984**, *3*, 389; d) L. Weber, *Coord. Chem. Rev.* **1992**, *92*, 1839; e) N. C. Norman, *Polyhedron* **1993**, *12*, 2431; f) A. H. Cowley, J. G. Lasch, N. C. Norman, M. Pakulski, *J. Am. Chem. Soc.* **1983**, *105*, 5506; g) C. Couret, J. Escudie, Y. Madaule, H. Ranaivonjatovo, J.-G. Wolf, *Tetrahedron Lett.* **1983**, *24*, 2769; h) N. Tokitoh, Y. Arai, T. Sasamori, R. Okazaki, S. Nagase, H. Uekusa, Y. Ohashi, *J. Am. Chem. Soc.* **1998**, *120*, 443; i) N. Tokitoh, Y. Arai, R. Okazaki, S. Nagase, *Science* **1997**, *277*, 78.
- [131] Gaussian 03, Revision B.01, M. J. Frisch, G. W. Trucks, H. B. Schlegel, G. E. Scuseria, M. A. Robb, J. R. Cheeseman, J. A. Montgomery, Jr., T. Vreven, K. N. Kudin, J. C. Burant, J. M. Millam, S. S. Iyengar, J. Tomasi, V. Barone, B. Mennucci, M. Cossi, G. Scalmani, N. Rega, G. A. Petersson, H. Nakatsuji, M. Hada, M. Ehara, K. Toyota, R. Fukuda, J. Hasegawa, M. Ishida, T. Nakajima, Y. Honda, O. Kitao, H. Nakai, M. Klene, X. Li, J. E. Knox, H. P. Hratchian, J. B. Cross, C. Adamo, J. Jaramillo, R. Gomperts, R. E. Stratmann, O. Yazyev, A. J. Austin, R. Cammi, C. Pomelli, J. W. Ochterski, P. Y. Ayala, K. Morokuma, G. A. Voth, P. Salvador, J. J. Dannenberg, V. G. Zakrzewski, S. Dapprich, A. D. Daniels, M. C. Strain, O. Farkas, D. K. Malick, A. D. Rabuck, K. Raghavachari, J. B. Foresman, J. V. Ortiz, Q. Cui, A. G. Baboul, S. Clifford, J. Cioslowski, B. B. Stefanov, G. Liu, A. Liashenko, P. Piskorz, I. Komaromi, R. L. Martin, D. J. Fox, T. Keith, M. A. Al-Laham, C. Y. Peng, A. Nanayakkara, M. Challacombe, P. M. W. Gill, B. Johnson, W. Chen, M. W. Wong, C. Gonzalez, J. A. Pople, Gaussian, Inc., Pittsburgh PA, **2003**. For a current listing of basis sets and ECPs, see <http://www.gaussian.com>.
- [132] D. Agustin, G. Rima, H. Gornitzka, J. Barrau, *Eur. J. Inorg. Chem.* **2000**, 693.
- [133] A. L. Balch, M. M. Olmstead, D. P. Oram, *Inorg. Chem.* **1988**, *27*, 4309.
- [134] M. Weidenbruch, A. Stilter, J. Schlaefke, K. Peters, H. G. von Schnering, *J. Organomet. Chem.* **1995**, *501*, 67.

- [135] J. Beckmann, K. Jurkschat, S. Rabe, M. Schürmann, *Z. Anorg. Allg. Chem.* **2001**, 627, 2413.
- [136] M. Veith, M. Grosser, V. Huch, *Z. Anorg. Allg. Chem.* **1984**, 513, 89.
- [137] M. Veith, M. Gouygou, A. Detemple, *Phosphorus, Sulfur, and Silicon* **1993**, 75, 183.
- [138] P. Jutzi, U. Meyer, B. Krebs, M. Dartmann, *Angew. Chem.* **1986**, 98, 894, *Angew. Chem. Int. Ed.* **1986**, 25, 919.
- [139] M. Veith, V. Huch, J. P. Majoral, G. Bertrand, G. Manuel, *Tetrahedron Lett.* **1983**, 24, 4219.
- [140] For usage of $\text{Me}_3\text{SiOOSiMe}_3$ as a mild, non-radical oxidation agent, see: a) D. Brandes, A. Blaschette, *J. Organomet. Chem.* **1974**, 73, 217; b) D. Brandes, A. Blaschette, *J. Organomet. Chem.* **1973**, 49, C6; for similar oxidation of Sn(II) with benzoyl peroxide, see: c) A. Tzschach, M. Scheer, K. Jurkschat, *Z. Anorg. Allg. Chem.* **1984**, 508, 73.
- [141] L. Pu, N. J. Hardman, P. P. Power, *Organometallics* **2001**, 20, 5105.
- [142] M. A. Edelman, P. B. Hitchcock, M. F. Lappert, *J. Chem. Soc., Chem. Commun.* **1990**, 1116.
- [143] H. Puff, R. Gattermayer, R. Hundt, R. Zimmer, *Angew. Chem.* **1977**, 89, 556, *Angew. Chem. Int. Ed.* **1977**, 16, 547.
- [144] P. Brown, M. F. Mahon, K. C. Molloy, *J. Chem. Soc., Chem. Commun.* **1989**, 1621.
- [145] J. Janssen, J. Magull, H. W. Roesky, *Angew. Chem.* **2002**, 114, 1425, *Angew. Chem. Int. Ed.* **2002**, 41, 1365.
- [146] R. Pietschnig, R. West, D. R. Powell, *Organometallics* **2000**, 19, 2724.
- [147] R. S. Simons, S. T. Haubrich, B. V. Mork, M. Niemeyer, P. P. Power, *Main Group Chem.* **1998**, 2, 275.
- [148] C. H. Yoder, L. A. Margolis, J. M. Horne, *J. Organomet. Chem.* **2001**, 633, 33.
- [149] R. Colton, D. Dakternieks, *Inorg. Chim. Acta* **1988**, 143, 151.
- [150] P. Brown, M. F. Mahon, K. C. Molloy, *J. Organomet. Chem.* **1992**, 435, 265.
- [151] a) T. Allspach, M. Regitz, G. Becker, W. Becker, *Synthesis* **1986**, 31; b) M. Regitz, P. Binger, *Angew. Chem.* **1988**, 100, 1541, *Angew. Chem. Int. Ed.* **1988**, 27, 1484; c) M. Regitz, *Chem. Rev.* **1990**, 90, 191.
- [152] H. Schumann, R. Fischer, *J. Organomet. Chem.* **1975**, 88, C13.
- [153] M. Scheer, P. Kramkowski, K. Schuster, *Organometallics* **1999**, 18, 2874.

- [154] P. Kramkowski, G. Baum, U. Radius, M. Kaupp, M. Scheer, *Chem. Eur. J.* **1999**, *5*, 2890.
- [155] N. V. Timosheva, A. Chandrasekaran, R. O. Day, R. R. Holmes, *Organometallics* **2001**, *20*, 2331.
- [156] L. R. Chamberlain, I. P. Rothwell, J. C. Huffman, *Inorg. Chem.* **1984**, *23*, 2575.
- [157] a) G. Becker, H. Schmidt, W. Uhl, *Inorg. Synth.* **1990**, *27*, 243; b) G. Becker, A. Münch, G. Witthauer, *Z. Anorg. Allg. Chem.* **1982**, *492*, 15; c) G. Becker, C. Witthauer, *Z. Anorg. Allg. Chem.* **1982**, *492*, 28; d) O. Mundt, G. Becker, M. Rössler, C. Witthauer, *Z. Anorg. Allg. Chem.* **1983**, *506*, 42; G. Becker, H. Freudenblum, O. Mundt, M. Reti, M. Sachs, in *Synthetic Methods of Organometallic and Inorganic Chemistry*, Vol. 3 (Eds. W. A. Herrmann, H. H. Karsch), Stuttgart: Thieme Verlag, **1996**, p. 193 ff.
- [158] a) M. Scheer, J. Müller, M. Häser, *Angew. Chem.* **1996**, *108*, 2637, *Angew. Chem. Int. Ed.* **1996**, *35*, 2492; b) M. Scheer, J. Müller, G. Baum, M. Häser, *J. Chem. Soc., Chem. Commun.* **1998**, 2505; c) M. Scheer, J. Müller, M. Schiffer, G. Baum, R. Winter, *Chem. Eur. J.* **2000**, *6*, 1252.
- [159] V. Christou, J. Arnold, *Angew. Chem.* **1993**, *105*, 1551, *Angew. Chem. Int. Ed.* **1993**, *32*, 1450.
- [160] M. B. Dinger, M. L. Scott, *Inorg. Chem.* **2000**, *39*, 1238.
- [161] J. R. Clark, A. L. Pulvirenti, P. E. Fanwick, M. Sigalas, O. Eisenstein, I. P. Rothwell, *Inorg. Chem.* **1997**, *36*, 3623.
- [162] S. Groysman, S. Segal, M. Shamis, I. Goldberg, M. Kol, Z. Goldschmidt, E. Hayut-Salant, *J. Chem. Soc., Dalton Trans.* **2002**, 3425.
- [163] Y. Kim, P. N. Kapoor, J. G. Verkade, *Inorg. Chem.* **2002**, *41*, 4834.
- [164] S. Groysman, I. Goldberg, M. Kol, Z. Goldschmidt, *Organometallics* **2003**, *22*, 3793.
- [165] N. Govindaswamy, D. A. Quarless, Jr., S. A. Koch, *J. Am. Chem. Soc.* **1995**, *117*, 8468.
- [166] J.-W. Hwang, K. Govindaswamy, S. A. Koch, *J. Chem. Soc., Chem. Commun.* **1998**, 1667.
- [167] M. Kol, M. Shamis, I. Goldberg, Z. Goldschmidt, S. Alfi, E. Hayut-Salant, *Inorg. Chem. Commun.* **2001**, *4*, 177.
- [168] J. S. Freundlich, R. R. Schrock, W. M. Davis, *Organometallics* **1996**, *15*, 2777.

- [169] J. S. Freundlich, R. R. Schrock, C. C. Cummins, W. M. Davis, *J. Am. Chem. Soc.* **1994**, *116*, 6476.
- [170] S. Blaurock, E. Hey-Hawkins, *Eur. J. Inorg. Chem.* **2002**, 2975.
- [171] R. W. Chesnut, L. D. Durfee, P. E. Fanwick, I. P. Rothwell, K. Folting, J. C. Huffman, *Polyhedron* **1987**, *6*, 2019.
- [172] a) R. W. Chesnut, B. D. Steffey, I. P. Rothwell, J. H. Huffman, *Polyhedron* **1988**, *7*, 753; b) R. W. Chesnut, J. S. Yu, P. E. Fanwick, I. P. Rothwell, *Polyhedron* **1990**, *9*, 1051.
- [173] O. J. Scherer, J. Vondung, G. Wolmershäuser, *Angew. Chem.* **1989**, *101*, 1395, *Angew. Chem. Int. Ed.* **1989**, *28*, 1355.
- [174] R. Winter, Dissertation, Universität Kaiserslauten, **1993**.
- [175] O. J. Scherer, R. Winter, G. Wolmershäuser, *Z. Anorg. Allg. Chem.* **1993**, *619*, 827.
- [176] R. Riemschneider, *Z. Naturforsch.* **1963**, *18b*, 641.
- [177] S. Schonholzer, M. Slongo, C. Rentsch, M. Neuenschwander, *Makromol. Chem.* **1980**, *181*, 37.
- [178] C. G. Venier, E. W. Casserly, *J. Am. Chem. Soc.* **1990**, *112*, 2808.
- [179] E. V. Dehmlow, C. Bollmann, *Z. Naturforsch.* **1993**, *48b*, 457.
- [180] E. V. Dehmlow, C. Bollmann, *Tetrahedron Lett.* **1991**, *32*, 5773.
- [181] A. C. Reddy, E. D. Jemmis, O. J. Scherer, R. Winter, G. Heckmann, G. Wolmershäuser, *Organometallics* **1992**, *11*, 3894.
- [182] R. Winter, personal communication.
- [183] J. T. Gill, J. J. Mayerle, P. S. Welcker, D. F. Lewis, D. A. Ucko, D. J. Barton, D. Stowens, S. J. Lippard, *Inorg. Chem.* **1976**, *15*, 1155.
- [184] P. G. Jones, *Acta Cryst.* **1992**, *C48*, 1307.
- [185] H. W. Kroto, *Nature* **1987**, *329*, 529.
- [186] Y. D. Gao, W. C. Herndon, *J. Am. Chem. Soc.* **1993**, *115*, 8459.
- [187] For *ab initio* calculations on C₃₂ (O_h), see: F. L. Gu, Q. S. Li, A. Q. Tang, *Ac. Chim. Sin.* **1995**, *53*, 942.
- [188] A. Y. Timoshkin, *Inorg. Chem. Comm.* **2002**, *6*, 274.
- [189] A. Y. Timoshkin, H. F. Schaefer III, *J. Am. Chem. Soc.* **2004**, *126*, 12141.
- [190] A. Y. Timoshkin, H. F. Schaefer III, *Inorg. Chem.* **2005**, *44*, 843.
- [191] F. Uhlig, S. Gremler, M. Dargatz, M. Scheer, E. Herrmann, *Z. Anorg. Allg. Chem.* **1991**, *606*, 105.

- [192] G. Fritz, W. Hölderlin, *Z. Anorg. Allg. Chem.* **1976**, 422, 104.
- [193] F. Uhlig, R. Hummeltenberg, *J. Organomet. Chem.* **1993**, 452, C9.
- [194] G. Becker, G. Gutekunst, H.-J. Wessely, *Z. Anorg. Allg. Chem.* **1980**, 462, 113.
- [195] a) A. Adolf, Diplomarbeit, Universität Karlsruhe, **2003**; b) D. C. Bradley, M. B. Hursthouse, M. Motevalli, D. H. Zheng, *J. Chem. Soc., Chem. Commun.* **1991**, 7.
- [196] N. Auner, in *Synthetic Methods of Organometallic and Inorganic Chemistry*, Vol. 2 (Eds. N. Auner, U. Klingebiel), Stuttgart: Thieme Verlag, **1996**, p. 280.
- [197] A. L. Balch, D. E. Oram, *Organometallics* **1988**, 7, 155.
- [198] C. C. Hsu, R. A. Geanangel, *Inorg. Chem.* **1980**, 19, 110.
- [199] S. J. Archer, K. R. Koch, S. Schmidt, *Inorg. Chim. Acta* **1987**, 126, 209.
- [200] W. A. Herrmann, C. Zybille, in *Synthetic Methods of Organometallic and Inorganic Chemistry*, Vol. 1 (Eds. W. A. Herrmann, A. Salzer), Stuttgart: Thieme Verlag, **1996**, p. 137.
- [201] A. A. Pasynskii, Y. V. Torubaev, F. S. Denisov, A. N. Grechkin, K. A. Lyssenko, S. E. Nefedov, V. M. Novotortsev, Zh. V. Dobrokhotova, *Russ. Chem. Bull.* **1999**, 48, 1744.
- [202] D. J. Patmore, W. A. G. Graham, *Inorg. Chem.* **1966**, 5, 1405.
- [203] P. Kölle, G. Linti, H. Nöth, G. L. Wood, C. K. Narula, R. T. Paine, *Chem. Ber.* **1988**, 121, 871.
- [204] Y. van den Winkel, H. M. M. Bastiaans, F. Bickelhaupt, *J. Organomet. Chem.* **1991**, 405, 183.
- [205] K. Bourumeau, A.-C. Gaumont, J.-M. Denis, *J. Organomet. Chem.* **1997**, 529, 205.
- [206] C. Frenzel, E. Hey-Hawkins, *Phosphorus, Sulfur, Silicon Relat. Elem.* **1998**, 143, 1.
- [207] a) F. X. Kohl, P. Jutzi, *Organomet. Synth.* **1986**, 3, 489; b) D. Feitler, G. M. Whitesides, *Inorg. Chem.* **1976**, 15, 466.
- [208] O. T. Beachley, R. Blom, M. R. Churchill, K. Faegri, J. C. Fetting, J. C. Pazik, L. Victoriano, *Organometallics* **1989**, 8, 346.
- [209] P. Jutzi, H. Saleske, *Chem. Ber.* **1984**, 117, 222.
- [210] G. M. Sheldrick, *SHELXS-97*, University of Göttingen, **1997**.
- [211] G. M. Sheldrick, *SHELXL-97*, University of Göttingen, **1997**.
- [212] E. Keller, *SCHAKAL-97*, A Fortran Program for Graphical Representation of Molecular and Crystallographic Models, Universität Freiburg, **1997**.

- [213] K. Brandenburg, M. Berndt, *DIAMOND 2.0*, Visual Crystal Structure Information System, Bonn, **1998**.

Acknowledgments

I would like to express my gratitude to the following people:

Prof. Dr. Manfred Scheer for intellectual and professional guidance, for the opportunity to work in an exciting research group, for involving me in the preparation of many manuscripts, and especially for allowing me a large degree of independence and creative freedom to explore a wide range of synthetic aspirations.

Prof. Dr. Henri Brunner and Dr. Joachim Wachter for the infrastructure and guidance at the University of Regensburg.

Karin Kilgert and Anette Baust for administrative assistance.

Fabian Dielmann for synthetic collaboration and theoretical calculations, which all provided a substantial impetus for the later stages of the preparation of this work.

Gábor Balázs, Laurence Gregoriades, Sergej Konchenko, Florian Kraus, Thomas Roßmeier, Rajiv Trivedi, and Ulf Vogel, who, whether directly or indirectly, made significant intellectual contributions to this work in the form of advice, observations, and encouragement.

Manfred “Musch” Muschiol for assistance with the autoclave reactions and preparation of Ph*I.

Roger Merkle, who selflessly and quite meticulously coordinated the group’s move from Karlsruhe to Regensburg.

Daniela Riesterer and Kathrin Bratz for assistance with the preparation of numerous starting materials.

Shining Deng for encouraging discussions during daily trips to the Mensa.

Prof. Dr. Hellmut Eckert and co-workers, Universität Münster, for solid-state ^{31}P -MAS-NMR spectra.

Dr. Marek Sierka, Humboldt-Universität zu Berlin, for discussions and DFT calculations.

Michael Bräu for assistance with the powder diffraction data.

All staff and co-workers of the NMR, MS, elemental-analysis, X-ray diffraction, stockroom, glass-blowing, and mechanical facilities at the University of Karlsruhe and the University of Regensburg as well as all lab assistants in the Scheer group at the University of Regensburg.

All co-workers who made for a stimulating and convivial working environment – Alex, Andy, Anton, Ari, Barbara, the other Brian, Christian E., Christian K., Christof, Conny, Dani, Daniel, Eva, Fabian, Florian, Gábor, Hannes, Johann, Junfeng, Kalle, Kathrin, Frau Kilgert, Laurence, Lisi, Miriam, Musch, Naziha, Nikolai, Petra, Rajiv, Roger, Schotti, Sergej, Shining, Shouzhong, Thomas, Ulf, Dr. Wachter, and Walter.

Dani, Kathrin, Christian, and Fabian for the pleasant lab atmosphere.

Martina... for long-distance support, personal inspiration, and so much more.

Curriculum Vitae

Personal Data

Address	Schäffnerstr. 21 D-93047 Regensburg	Date of Birth	January 18, 1976
Marital Status	single	Place of Birth	Gallatin, Tennessee
		Citizenship	USA

Secondary and Post-Secondary Education/ Research

Franklin-Simpson Elementary/High Schools, Franklin, Kentucky, USA	Aug. 1981 – May 1994
Commencement of chemistry studies	Aug. 1994
<i>Visiting Research Scholar</i> , Organic Chemistry University of California, Santa Barbara , Santa Barbara, USA Supervisor: Fred Wudl, Institute for Polymers and Organic Solids	Summer 1996
<i>Undergraduate Research Assistant</i> , Analytical Chemistry Rhodes College , Memphis, Tennessee, USA Supervisor: Bradford Pendley, Department of Chemistry	Aug. 1996 – May 1997
<i>Visiting Research Scholar</i> , Surface Chemistry University of Southern California , Los Angeles, USA Supervisor: Bruce Koel, Laboratory for Molecular Robotics	Summer 1997
<i>Bachelor of Science</i> , Chemistry/German, <i>magna cum laude</i> Rhodes College , Memphis, Tennessee, USA	Aug. 1994 – May 1998
<i>Summer Internship</i> , Polymer Chemistry Procter & Gamble , Cincinnati, Ohio, USA Supervisor: Steve Smith, Miami Valley Laboratories	Summer 1998
<i>Fulbright Grantee</i> , Organometallic Chemistry Universität Karlsruhe , Karlsruhe, Germany Supervisor: Manfred Scheer, Institute for Inorganic Chemistry	Oct. 1998 – July 1999
<i>Master of Science</i> , Chemistry California Institute of Technology , Pasadena, California, USA Thesis Supervisors: Thomas J. Meade and Scott E. Fraser, Divisions of Chemistry and Biology	Sept. 1999 – Aug. 2001
<i>Ph.D. Candidate</i> , Inorganic Chemistry Universität Karlsruhe , Karlsruhe, Germany Thesis Supervisor: Manfred Scheer, Institute for Inorganic Chemistry	Sept. 2001 – March 2004
<i>Ph.D. Candidate</i> , Inorganic Chemistry Universität Regensburg , Regensburg, Germany Thesis Supervisor: Manfred Scheer, Institute for Inorganic Chemistry	April 2004 – January 2006
Ph.D. Exam Date (anticipated)	January 11, 2006

Publications

Spherical Cluster Comprising a Four- and Six-Membered Ring Motif

B. P. Johnson, F. Dielmann, G. Balázs, M. Sierka, M. Scheer

Angewandte Chemie **2006**, *Angewandte Chemie, International Edition* **2006**, in press.

Low-Coordinate E₁ Ligand Complexes of Group 15 Elements – A Developing Area

B. P. Johnson, G. Balázs, M. Scheer

Coordination Chemistry Reviews **2006**, in press.

Fullerene-Like Nanoballs formed by Pentaphosphaferrocene and CuBr

M. Scheer, J. Bai, B. P. Johnson, R. Merkle, A. V. Virovets, C. Anson

European Journal of Inorganic Chemistry **2005**, 4023.

Complexes with a Metal-Phosphorus Triple Bond

B. P. Johnson, G. Balázs, M. Scheer

Topics in Current Chemistry **2004**, 232 (New Aspects in Phosphorus Chemistry IV), 1.

Book Review: “Phosphorus-Carbon Heterocyclic Chemistry: The Rise of a New Domain” Edited by François Mathey

B. P. Johnson

Angewandte Chemie **2003**, 115(9), 1000, *Angewandte Chemie, International Edition* **2003**, 42(9), 970.

Complexes with a Metal-Phosphorus Triple Bond as Versatile Building Blocks in Coordination and Organometallic Chemistry

M. Scheer, M. Schiffer, E. Leiner, B. P. Johnson, C. Haindl, S. Umbarkar

Phosphorus, Sulfur and Silicon and the Related Elements **2002**, 177(6-7), 1617.

Complexes with a Metal Phosphorus Triple Bond - A Novel Class of Highly Reactive Compounds

M. Scheer, P. Kramkowski, M. Schiffer, B. P. Johnson, E. Leiner

Phosphorus, Sulfur and Silicon and the Related Elements **2001**, 168-169, 179.

Untersuchungen zur Darstellung von [Cp^xSb{M(CO)₅}₂] (Cp^x = Cp, Cp*; M = Cr, W)

M. Schiffer, B. P. Johnson, M. Scheer

Zeitschrift für Anorganische und Allgemeine Chemie **2000**, 626, 2498.

Novel Approach to Intermediates Containing a Tungsten-Arsenic Triple Bond

B. P. Johnson, M. Schiffer, M. Scheer

Organometallics **2000**, 19, 3404.

Scientific Meetings

Kugelförmige Moleküle auf Basis von P_n -Ligand Komplexen
und Cu(I) Halogeniden

B. P. Johnson, F. Dielmann, R. Merkle, M. Scheer
Poster Presentation, GDCh Annual Meeting (Jahrestagung)

September 2005
Düsseldorf, Germany

Spherical Molecules Formed by Coordination of P_n -Ligand Complexes
with Copper(I) Salts

B. P. Johnson, F. Dielmann, R. Merkle, M. Scheer
Poster Presentation, 230th ACS National Meeting

August 2005
Washington, DC, USA

Monomeric Tin(II)-Phosphanides Stabilized by Bulky Terphenyl Ligands

B. P. Johnson, M. Scheer
Poster Presentation, 7th Young Scientists' Conference on Chemistry

April 2005
Berlin, Germany

Stabilization of Unusual Main-Group Moieties by Organometallic Fragments

M. Scheer, K.-C. Schwan, B. P. Johnson, U. Vogel
21st International Conference on Organometallic Chemistry

July 2004
Vancouver, Canada

P_n -Ligand Complexes as Linking Units for the Formation of Novel Polymeric
Networks and Inorganic Fullerene-like Molecules

M. Scheer, J. Bai, B. P. Johnson, L. Gregoriades, A. V. Virovets
225th ACS National Meeting

March 2003
New Orleans, Louisiana, USA

Multifunctional Conjugates for Fluorescence and Magnetic Resonance Imaging

B. P. Johnson, T. J. Meade
Poster Presentation, 10th International Conference on Bioinorganic Chemistry

August 2001
Florence, Italy

Bifunctional Agents for Fluorescence and Magnetic Resonance Imaging

B. P. Johnson, T. J. Meade
Poster Presentation, 221st ACS National Meeting

April 2001
San Diego, California, USA

Novel Approach to Intermediates Containing Tungsten-Arsenic Triple Bonds

B. P. Johnson, M. Schiffer, M. Scheer
Oral Presentation, Scientific Colloquium for the Universities of
Hannover, Karlsruhe, Leipzig, Marburg, and Tübingen

July 2000
Hirschegg, Austria

Synthetic Approach to Metal-Complex Intermediates Possessing
Heavier Pnictogenido Ligands

B. P. Johnson, M. Schiffer, M. Scheer
Oral Presentation, 218th ACS National Meeting

August 1999
New Orleans, Louisiana, USA